THE UNIVERSITY OF NEW SOUTH WALES
KENSINGTON, NSW AUSTRALIA 2033

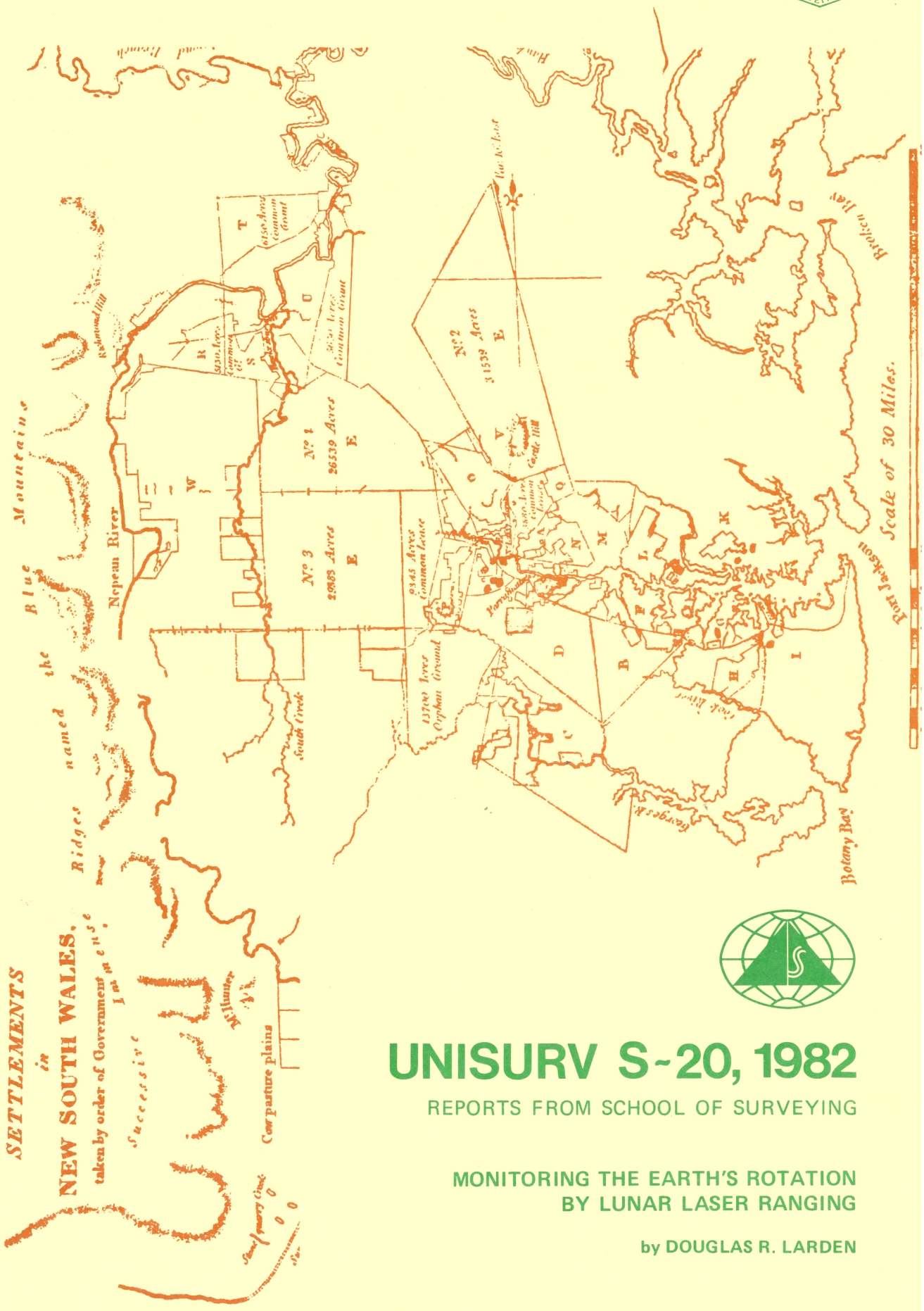

UNISURV S-20, 1982

REPORTS FROM SCHOOL OF SURVEYING

MONITORING THE EARTH'S ROTATION BY LUNAR LASER RANGING

by DOUGLAS R. LARDEN

UNISURV REPORT NO. 20, 1982

MONITORING THE EARTH'S ROTATION BY LUNAR LASER RANGING

by

DOUGLAS R. LARDEN

Received March, 1982

SCHOOL OF SURVEYING
THE UNIVERSITY OF NEW SOUTH WALES
P.O. BOX 1
KENSINGTON, N.S.W. 2033
AUSTRALIA

National Library of Australia
Card No. and ISBN
0 85839 029 9

ABSTRACT

The thesis investigates the potentialities and problems of measuring the Earth's polar motion and Universal time by Lunar Laser Ranging (LLR). Theoretical developments and concepts are presented within the framework of a review on the Earth's rotation and a comprehensive summary of the LLR technique. Aspects of the Earth's rotation which are considered include; the basic modes of rotation, the reference frames and measurement systems used to monitor these modes, and the causes of the many features which contribute to the rotation spectrum.

The description of the LLR technique is divided into four categories. The algorithms required to model the physical processes which cause time variations in the measured range are outlined. Also discussed are the scientific achievements and future objectives of the experiment, the coordinate systems and procedures used to estimate the predicted range, the method of parameter refinement, and the operational status of the network.

To study the feasibility of accurately monitoring the Earth's polar motion and Universal time by LLR, a simplified model of the distance between an earth-bound observatory and a lunar retroreflector is developed. The conventional approach is used, in which each effective range observation is assumed to be constructed in accordance with the 'normal point' concept and is treated in the analysis as a single entity. Estimable parameters are identified and the model assumptions clearly documented. There is also a brief discussion on the difficulties of extracting Earth rotation information from single station data.

The model is used to carry out studies designed to examine the dependence of the results on network constituency, station geometry, lunar declination, averaging interval, measurement uncertainties, hour angle coverage, and data loss due to weather, sun-moon angle and zenith distance constraints. The most significant conclusion is that the present five-station LLR network, ranging with measurement uncertainties of 3 cm, should be able to provide a high percentage

of two-day values for polar motion and Universal time to better than 5 cm and that additional southern hemisphere stations will be needed if daily values are desired on a continuous basis at this level of resolution. The effect of systematic errors is also discussed briefly.

Anticipating that the new space ranging methods will achieve accuracies of 2-3 cm, further studies are undertaken to explore the effects of two geophysical mechanisms which now have the potential to contaminate the results from earth rotation and geodetic experiments. First, the changes in LLR station coordinates produced by lithospheric plate motion are considered and their effects on polar motion and Universal time results are computed. Estimates of these station drifts are calculated from plate velocity models and then used as input to determine the time it takes plate motion effects to become significant. Results for selected LLR network combinations are tabulated and discussed in detail.

Seasonal variations in the geometrical shape of the earth's surface and the position of the geocentre will also be detected by space ranging measurements. One contribution to these variations is that due to atmospheric and groundwater loading. Global atmospheric pressure data, values of groundwater storage and load deformation theory are, therefore, used to estimate the crustal response at strategic geodetic locations. This response is represented using conventional load Love numbers. The results, which are marginally significant at the 2-3 cm accuracy level, are depicted on a series of world contour maps. Particular emphasis is given to regions where the displacements are largest and to the results at sites where lunar, satellite and interferometric geodesy is, or is likely to be,conducted. Only the radial displacements need to be considered. The accompanying motion of the geocentre is also estimated but is found to be almost negligible.

TABLE OF CONTENTS

GLOSSARY OF ACRONYMS AND ABBREVIATIONS

ALSEP	Apollo Lunar Surface Experiment Package
BIH	Bureau International de l'Heure
CERGA	Centre d'Etudes et Recherches Geodynamics et Astronomiques, Grasse, FRANCE
CIO	Conventional International Origin
COSPAR	ICSU Committee on Space Research
CW	Chandler Wobble
DMA	Defence Mapping Agency
DPMS	Dahlgren Polar Monitoring Service
EROLD	Earth Rotation by Lunar Distance
ET	Ephemeris Time
EW	Eulerian Wobble
FDPM	Forced Diurnal Polar Motion
FGGE	First GARP Global Experiment
GARP	Global Atmospheric Research Programme
GAST	Greenwich Apparent Sidereal Time
GEOS-3	Geodynamics Experimental Ocean Satellite
GP	General Precession
GPS	Global Positioning System
GSFC	Goddard Space Flight Centre
H.M.S.O.	Her Majesty's Stationery Office
IAT	International Atomic Time
IAU	International Astronomical Union
ICSU	International Council of Scientific Unions
ILS	International Latitude Service
IPMS	International Polar Motion Service
IUGG	International Union of Geodesy and Geophysics
JPL	Jet Propulsion Laboratory
LAGEOS	Laser Geodynamics Satellite
LLB 5	Lunar Libration Model No. 5
LLR	Lunar Laser Ranging
l.o.d.	Length of Day
LP	Lunisolar Precession

M_2	Semi-Diurnal Ocean Tide Constituent
MESA	Maximum Entropy Spectral Analysis
MIT	Massachusetts Institute of Technology
MJD	Modified Julian Day
NASA	National Aeronautics and Space Administration
NDFN	Nearly Diurnal Free Nutation
NDPM	Nearly Diurnal Polar Motion
PCN	Principal Core Nutation
PFN	Principal Forced Nutation
POLARIS	Polar Motion Analysis by Radio Interferometric Surveying
PP	Planetary Precession
PZT	Photographic Zenith Tube
rms	Root Mean Square
SLR	Satellite Laser Ranging
SPM	Secular Polar Motion
TLRS	Transportable Laser Ranging Station
UNESCO	United Nations Education, Scientific and Cultural Organization
UT	Universal Time
UT0	Observatory dependent measurements of UT
UT1	UT0 corrected for polar motion
UTC	Universal Coordinated Time
VLBI	Very Long Baseline Interferometry
VZT	Visual Zenith Telescope

NOTATION AND CONVENTIONS

SYMBOL	
A,C	principal moments of inertia for a spheriodal Earth; A also denotes the amplitude of annual radial deformation
[A]	design matrix; matrix of coefficients $\partial\rho/\partial P_n$ for parametric corrections to distance model
a,b	probability factors in weather model; a also denotes the Earth's radius
a_o, b_o	constants of integration (2.16)
a_0^0	fraction of the Earth covered by oceans
[B]	vector of constant terms in system of normal equations
C_{nm}, S_{nm}	spherical harmonic coefficients of degree n and order m
c	velocity of light in vacuo; also denotes correlation coefficient in weather model
c_{ij}	correlation between i-th and j-th parameter of distance model
D	mutual separation of Moon and Sun (= L-L')
d_{MJD}	time of observation in Modified Julian Days*
$\vec{d}$	displacement vector due to loading
$\vec{d}_r$	radial displacement due to loading, $d_r = \lvert\vec{d}_r\rvert$
$\vec{d}_t$	tangential displacement due to loading, $d_t = \lvert\vec{d}_t\rvert$
dx/dt	derivative of x with respect to time; also denoted by $\dot{x}$
E	eccentric anomaly of the Earth-Moon centre of mass in its orbit about the barycentre (3.6); also denotes elevation angle
e_i	independent random variable
e_{ijk}	alternating tensor
F	argument of lunar latitude
F_i	Bernoulli random variable of two-state Markov chain
f	laser frequency
f_k	body force (e.g. due to gravitational attraction)

* Further subscription and/or superscription may be used for purposes of clarification. A notation used in one section only is defined locally.

SYMBOL	
G	universal gravitational constant
$[G]$	inverse of variance-covariance matrix for observations
g	local acceleration due to gravity at the surface of the Earth*
$\bar{g}$	value of g averaged over the surface of the Earth
H	geocentric hour angle of lunar reflector
H_i	absolute angular momentum
$[H]$	coefficient matrix in theory of surface loading
h_i	relative angular momentum*
h_n, k_n, ℓ_n	Love numbers of degree n (load Love numbers if primed)
$\bar{h}$	mean elevation above sea-level
I_{ij}	inertia tensor
i_{ij}	perturbations in inertia tensor I_{ij}
$\vec{i}$	unit vector*
k	modification factor (5.27)
$\vec{k}$	vector, selenocentre to lunar reflector
L	lunar mean longitude* (solar if primed)
L_i	torque
$[L]$	lunar libration matrix $\{= R_3(-\psi_m')R_1(\Theta_m')R_3(-\phi_m')\}$
M	mean anomaly of the Earth-Moon centre of mass in its orbit about the barycentre (3.6); also denotes mass of the Earth*
M_m	mass of the Moon
$\vec{M}$	vector, barycentre to selenocentre
m	January-July surface load difference
m'	April-October surface load difference
m_b	mass of a disturbing body (e.g. sun)
m_i	direction cosines of the Earth's spin vector (2.10, 2.18)
$\vec{m}$	vector, geocentre to selenocentre

SYMBOL	
$[N]$	normal matrix $\{= [A]^T[G][A]\}$ nutation matrix $\{= R_1(-\varepsilon)R_3(\Delta\psi)R_1(\varepsilon)\}$
n	lunar sidereal mean motion
n_i	outwardly directed normal to surface element, dS
P	atmospheric pressure*
P_n	n-th parameter in distance model; also denotes n-th lithospheric plate in global tectonic model
$P_n(\cos\psi)$	Legendre polynomial of degree n in terms of $\cos\psi$
$[P]$	precession matrix $\{= R_3(\zeta_0)R_2(\Theta)R_3(z)\}$
P_{ij}	stress tensor (including non-hydrostatic contribution T_{ij})
Q	quality factor*
$[Q]$	variance-covariance matrix of adjusted parameters
q	surface load*, in grams cm^{-2}
R	gas constant
$R_i(\phi)$	counterclockwise rotation about the i-th axis through an angle ϕ
$\vec{R}$	vector, barycentre to geocentre
$\vec{R}_{em}$	vector, barycentre to Earth-Moon centre of mass
$\vec{R}_g$	vector, geocentre to centre of mass of disturbing body
r_s	distance from geocentre to observatory
r_r	distance from geocentre to lunar reflector
$\vec{r}$	vector, geocentre to observing station* (geocentric station vector)
$\vec{r}'$	$\vec{r}$ corrected for polar motion
$\vec{r}''$	$\vec{r}$ transformed to barycentric system
$\vec{r}_r$	vector, geocentre to lunar reflector
S	surface of the Earth; dS' surface element; $dS = \cos\phi d\phi d\lambda$ is a surface element on a unit sphere

SYMBOL	
S_n	surface spherical harmonic of degree n
[S]	sidereal matrix {= $R_3(-\theta)$}
T	temperature*
T_{ij}	non-hydrostatic stress tensor
[T]	vector of residuals; also denotes transition probability matrix
t	time* (UT1, UTC, ET or IAT as required)
U	perturbation U_1 in ambient gravitational potential due to deformation plus the potential U_2 of any applied mass load*
U_n	potential U of degree n
u_i	velocity vector relative to x_i system
V	volume; dV volume element
$V_n(r)$, $W_n(r)$	radially dependent functions defining radial and tangential displacements, respectively
[v]	vector of corrections to observations
$\vec{v}(r)$	velocity vector of point r located on lithospheric plate P_n* (= $\vec{w}_n \times \vec{r}_n$)
W	tide producing potential
W_2	tide producing potential of degree 2
W1, W2, W3	indicators of observability
w_i	angular velocity*
X_i	space-fixed reference system (1950.0)
x,y	coordinates for pole of spin axis in BIH system*
x_i	earth-fixed reference system (rotating frame)
x_{i_m}	lunar-fixed reference system (rotating frame)
[Y]	vector of six parameters in theory of surface loading
Z	zenith distance*
α	right ascension of lunar reflector*; also denotes the longitude of the Sun on April 15
α_i	transformation angles
β	phase of annual radial deformation; also denotes lunar moment of inertia parameter
β_m	ecliptic latitude of the Moon

SYMBOL	
$\vec{\beta}$	vector, barycentre to observatory
γ	Eddington-Robertson relativistic parameter lunar moment of inertia parameter mean temperature gradient
Δ_1	one-way travel time correction for curvature of photon path (3.22)
Δ_2	one-way travel time correction for atmospheric retardation
$[\Delta P]$	vector of parametric correction
ΔT	relativistic clock correction* (3.6)
Δx_i	Cartesian components of position of geocentre with respect to system located at centre of mass of the earth plus load
$\Delta\varepsilon$	nutation in obliquity*
$\Delta\rho$	one-way distance equivalent for $\Delta\tau$
$\Delta\tau$	time delay residual
$\Delta\psi$	nutation in ecliptic longitude*
δ	declination of lunar reflector
δ_c	time interval between IAT and ET
δ_{ij}	Kronecker delta
$\delta\vec{r}$	change in $\vec{r}$ due to tidal and loading effects
δ_T	phase angle of earth-tidal bulge
δUT1	tidally-induced change in UT1
$\delta x, \delta y$	components of forced diurnal polar motion
ε	instantaneous obliquity of ecliptic
$\bar{\varepsilon}$	mean obliquity of ecliptic*
ζ_0, Θ, z	precession angles
Θ_m, ϕ_m, ψ_m	lunar libration angles with respect to mean equatorial system of 1950.0 (if primed they refer to the mean ecliptic system of date)
θ	Greenwich apparent sidereal time*
$\bar{\theta}$	Greenwich mean sidereal time
λ	geocentric longitude of observatory* (positive eastward from Greenwich); also denotes Lamé parameter
λ_m	ecliptic longitude of the Moon

SYMBOL	
$\partial\rho/\partial P_n$	derivative of ρ with respect to n-th parameter in distance model*
μ	gravitational constant of the solar system probability factor in weather model Lamé parameter
ξ	change in sea-level
ℓ	lunar mean anomaly (solar if primed)
ρ	distance from observatory to lunar reflector* density of matter*
$\vec{\rho}$	vector, observatory to lunar reflector*
σ	frequency of oscillation*; also denotes perpendicular distance from observatory to the Earth's spin axis
σ_i	uncertainty of i-th observation
σ_i^2	variance of i-th observation
$\vec{\sigma}_m$	vector, barycentre to lunar reflector
σ_p	random error contribution to uncertainty in p-th parameter of distance model
σ_p^2	variance of p-th parameter in distance model*
σ_p^s	systematic error contribution to uncertainty in p-th parameter of distance model
σ_r	frequency of the Eulerian wobble
τ	two-way time delay*
ϕ	geocentric latitude of observatory*
ψ	geocentric angle between a point on the Earth's surface and a load on the Earth's surface
$\psi_i(t)$	excitation functions for a rigid Earth
ψ_{sm}	Sun-Moon angle
Ω	nominal value for the Earth's diurnal spin rate*; also denotes ecliptic longitude of ascending node of the lunar orbit
ω	coupling parameter in Brans-Dicke theory
$\|x\|$	absolute value of x
$\langle x \rangle$	expected value of x
θ	longitude of the Sun measured from the beginning of the year

CONVENTIONS

A vector $\vec{X}$ is represented in the form

$$\vec{X} = X_i \vec{i}$$

where X_i are the vector components along the rectangular coordinate axes defined by the unit vectors $\vec{1}$, $\vec{2}$, $\vec{3}$.

The scalar product of two vectors is given by

$$\vec{X} \cdot \vec{Y} = X_1 Y_1 + X_2 Y_2 + X_3 Y_3$$

while the vector product is defined as

$$\vec{X}\vec{Y} = \vec{X} \times \vec{Y} = (X_2 Y_3 - X_3 Y_2)\vec{1} + (X_3 Y_1 - X_1 Y_3)\vec{2} + (X_1 Y_2 - X_2 Y_1)\vec{3} \ .$$

The operator $\vec{\nabla}$ is defined as

$$\vec{\nabla} = \frac{\partial}{\partial x_i} \vec{i}$$

Thus,

$$\vec{\nabla} U = \frac{\partial U}{\partial x_i} \vec{i}$$

INDEX OF FIGURES

INDEX OF TABLES

ACKNOWLEDGEMENTS

I would like to express my sincere appreciation to Dr. A. Stolz for his supervision, encouragement, patience and assistance throughout the preparation of this thesis. I have greatly profited from our association.

Thanks is extended to the various members of staff and post-graduate students of the School of Surveying, University of New South Wales for the time spent discussing some of the problems encountered during this work. In particular, I wish to record my appreciation to the late Associate Professor R. S. Mather who, by example, was a constant source of encouragement and inspiration. Thanks is also extended to Professor P. V. Angus-Leppan for his interest and comments on the manuscript. Computing assistance given by W. Kent and B. Hirsch during the early stages of this work is acknowledged. I would especially like to thank D. Bowring for his help in digitizing and preparing the groundwater data in a suitable format for analysis.

The author greatly appreciates the cooperation from Dr. P. J. Morgan of the Division of National Mapping who made possible several visits to the Orroral LLR site.

Financial support during this project was obtained from a Commonwealth Postgraduate Research Award and a part-time teaching assistantship at the School of Surveying, University of New South Wales. This project was completed while the author held a Fulbright Travel Grant administered in Australia by the Australian-American Education Foundation and in the United States by the Institute for International Education. Special thanks is extended to Dr. P. L. Bender of the Joint Institute for Laboratory Astrophysics and the National Bureau of Standards, University of Colorado for making this period of overseas study possible, for the many valuable discussions which helped clarify many of the conceptual issues that arose during the course of this work and for his comments on the manuscript. I would like to thank G. Romey and L. Haas for their excellent typing of the final draft and tables.

Finally, I extend to all my family and friends my upmost appreciation

for their encouragement and support during these years of postgraduate study. A special word of thanks goes to my brother Arnold, who unselfishly drafted the global contour maps. To my wife, Margaret, I express my sincere thanks and deep appreciation for her unfailing love, patience, support and confidence in knowing I would complete this dissertation. Her contribution has been immeasurable.

CHAPTER 1

INTRODUCTION

Observations of the earth's rotation have long been an important asset for studying the physics and dynamics of the earth. The surge of interest in this field during the late nineteenth century led to many research papers by distinguished scientists. In more recent times, the diversity of the subject inspired Munk and MacDonald (1960) and Lambeck (1980) to write extensive monographs dealing with the geophysical aspects of the problem. A substantial amount of the earth rotation data discussed in these latter studies were obtained by classical techniques employing optical and photographic instruments. While the accuracy of such data is adequate to explain many of the rotational phenomena, there are still several unresolved areas that require the rotational motions to be measured with an accuracy about an order of magnitude better.

A solution to this predicament comes with the development of the space ranging techniques. For example, precise tracking of artificial satellites for studying the earth's gravity field, laser ranging to lunar retroreflectors to further understand the dynamics of the lunar orbit and rotation and the application of radio interferometric techniques for locating the position of quasars all require accurate monitoring of the earth's rotation. This prerequisite is also of fundamental importance to the geodesist who wants to use the space techniques to coordinate points on the earth's surface at the 5 cm level or better.

One particular consequence of these technological advances will be the improved observation of the earth's polar motion and angular position in space (UT1). Polar motion and UT1 contribute to changes in the spatial and geographical location of satellite tracking stations. They also contain valuable information on the meteorological and geophysical phenomena affecting the earth's rotation (e.g., winds, earthquakes) and, for these reasons, need to be monitored regularly as well as accurately. All space ranging techniques have the potential to

achieve this goal. However, it is the purpose of this study to investigate specifically the feasibility of using fixed lunar laser ranging observatories to provide this information. An assessment is also made of the significance of some pertinent geophysical mechanisms that hitherto have been regarded as observational noise sources in the space ranging techniques but, in the future, could produce detectable effects at the expected 1 to 3 cm measurement accuracy level.

Since the main body of this study deals with the problems and potentialities of monitoring the earth's rotation by lunar laser ranging, it is important that the concepts and fundamental principles of both the earth's rotation and the lunar laser ranging technique be understood. Chapter 2 is devoted to the earth's rotation and although the review is unavoidably lengthy, it gives the reader an appreciation of the diversity of the subject. The basic modes of the earth's rotational motions are identified within the framework of rigid-body theory using the well-known Euler equations. The equations of motion are extended, in accordance with Liouville's development, to incorporate the rotational response of a deformable earth. Systems for determining the earth's rotation are discussed in Section 2.3 together with the basic merits and limitations of each method. Section 2.4 summarizes the main geophysical processes that perturb the rotation of the earth from its rigid-body state and highlights the contentious areas where sustained research effort is still needed. The chapter concludes with a brief perspective on the main criteria governing the establishment of a future earth rotation service and the role each technique is likely to play.

In Chapter 3, the discussion focusses immediately on the lunar laser ranging experiment. The reference coordinate systems used in the reduction of LLR data are defined and a complete description of the precise time-delay modelling procedures and formulation of the observation equation is given. This outline is essentially a review and more comprehensive account of the description given by Stolz (1979). Attempts are made to clearly define the sign convention used throughout the mathematical formulation. The chapter continues with a summary of

the past and present scientific achievements from LLR, together with an outline of the method used for parameter improvement. Finally, the status of the LLR network is discussed in Section 3.4 as a means of selecting realistic LLR network combinations for use in the numerical analysis.

Because of the nature of the earth-moon geometry, several assumptions can be invoked to simplify the observation equation. The derivation of the distance and observation equation for single ranges using the simplified approach is outlined in Chapter 4. The estimable parameters are identified and particular attention is given to the problems of parameter separability as implied by the mathematical structure of the observation equation. It is assumed that each observation has been formed according to the 'normal point' concept (Abbot et al. 1973) and since the primary object of the study is to examine how well LLR can determine polar motion and UT1 and not the lunar motion, it was decided not to parameterize the lunar orbital and librational motions separately. In fact, for the majority of the numerical experiments carried out here, the lunar ephemeris is assumed to be perfectly known. All parameters that constitute the mathematical model are assumed constant over the specified analysis interval.

The mathematical formulation developed in Chapter 4 is used in Chapter 5 to perform a series of variance studies to investigate the potentialities of LLR for monitoring polar motion and UT1. This approach is chosen out of necessity because of a lack of real observations from a network of LLR stations. Consideration is given to the dependency of the results on the network constituency, station geometry, lunar declination, the analysis interval, hour angle coverage, the loss of data caused by the weather, the sun-moon angle condition and the zenith distance restriction. Creating a realistic observational environment is indeed one of the more critical aspects of this study. The conditions of observability and the justification for their adoption are summarized in Section 5.2. In particular, a detailed theoretical development of the weather model is presented since meteorological factors result in the greatest loss of range data. This summary precedes a

general description of the earth rotation analyses undertaken in this work. The results and their significance are discussed in the remaining two sections of Chapter 5.

The need to investigate the effect of geophysical and meteorological processes on geodetic observations and experiments conducted at the 1 to 3 cm accuracy level is clearly obvious. Chapters 6 and 7 explore the geodetic consequences of two phenomena, namely, lithospheric plate motion and seasonal atmospheric-groundwater loading, respectively. The sixth chapter deals specifically with plate motion effects on earth rotation results from LLR. Firstly, a brief review of the global plate tectonics concept is given. Estimates of the expected rates of change in the coordinates of the LLR stations, based on a suite of absolute plate velocity models, are used as input to determine the degree to which polar motion and UT1 results would be contaminated if such movements are not accounted for in high-precision experiments. Plate models that give results which are in good agreement are identified.

Seasonal variations in atmospheric pressure and groundwater storage may also produce measurable effects. These will appear primarily as radial surface deformations and as a movement of the geocentre. Included in Chapter 7 are the basic theory needed to calculate the crustal deformations caused by surface loading and the motion of the geocentre, a description of the data used, the results for the seasonal departures in radial position due to atmospheric-groundwater loading on a global scale and at individual geodetic observatories, the calculated motion of the geocentre, and a discussion on the significance and accuracy of the results.

The overall conclusions and recommendations for this work are documented in Chapter 8.

CHAPTER 2

THE EARTH'S ROTATION: A STATUS REPORT

2.1 Introduction

The rotation of the earth with its theoretical and experimental aspects is the basis of fundamental astronomy. Although problems involving rotation have been investigated by many prominent scientists, ongoing research activities still produce several challenging questions of geodynamic interest. One major factor which complicates our understanding of why the earth rotates the way it does is that the earth is not a rigid body. For example, to study the rotational consequences of wind and ocean circulation, air-mass and groundwater variations, and sea-level fluctuations requires some speculation about the internal physical processes that can also produce similar effects (e.g. earthquakes, core motions and plate tectonic activity).

Recent improvements in instrumentation and the development of geodetic space ranging techniques (Smith et al. 1972, MacDoran 1973, Bender et al. 1973, Anderle 1973), however, have opened up new avenues for the solution to many of these outstanding problems. Features of the earth's rotation which need to be studied or explained in more detail include: (a) the short-period diurnal, fortnightly and monthly terms; (b) the sudden irregular changes; (c) the damping of the Chandler wobble; (d) the character of secular polar motion and its associated long-period variations, and; (e) the precession and nutation.

This chapter is devoted to reviewing the numerous aspects of the earth's rotation. As a point of departure, the basic concepts and theory are presented in Section 2.2. In Section 2.3 a brief account of the methods for determining the earth's rotation is given, together with the basic limitations of each method. This precedes a summary in Section 2.4 of the numerous features which constitute the rotation

spectrum. The remaining section comments briefly on the future role each technique is likely to play.

2.2 Theoretical Concepts

2.2.1 Preamble

If the earth were rigid, spherical and rotated uniformly about a fixed axis, its rotation would not be the subject of great interest. On the contrary, complex variations in the rate of rotation and orientation of the spin axis with respect to the earth and to space have stimulated numerous scientific discussions during the past century.

Despite the realization of the earth's non-conformity to structural and geometrical homogeneity, its rotation can still be investigated by applying the basic laws of dynamics. However, no attempt has been made to rigorously compute the rotation because any achievement made in mathematical rigor is lost due to a lack of accurate information on the earth's variable density distribution. At best, computations of the rotation can only be obtained by constructing realistic models of the earth's physical properties. These theoretical results are then compared with results obtained by observation. Such attempts, which usually require recourse to geophysical data and theory, have been realized and are discussed in Section 2.4.

The rotation of the earth about its centre of mass, the geocentre, can be represented mathematically in several different ways. The following development is based on the well-known Euler-Liouville equations. In providing a framework for review, the dynamic equations of motion are solved for a rigid spheroidal earth and then extended to account for a deformable body. This approach introduces a useful mathematical foundation that relates the earth's rotational response to geophysical occurrences. Alternate approaches (see e.g. Grafarend 1977) give essentially the same result.

2.2.2 Earth Rotation Dynamics

An established dynamic principle which evolved from the application of Newtonian mechanics to rotating bodies states that the torque acting on a body is equal to the rate of change in its angular momentum. The

implementation of this principle requires the definition of two reference systems; one fixed in space, the other fixed to the earth and, therefore, moving with it. Neglecting the practical realization and definition of these systems for the moment, let each be denoted by a rectangular Cartesian coordinate system such that X_i $i = 1,2,3$ and x_i represent the space and earth-fixed systems, respectively. The geocentre is located at the origin of both reference systems.

The equations of motion in the space-fixed system can be expressed by the vector equation

$$\left(\frac{d\vec{H}}{dt}\right)_{X_i} = \vec{L} \qquad (2.1)$$

which equates the time derivative of the angular momentum $\vec{H}$ about the geocentre with the vector $\vec{L}$ representing the applied torque. If the x_i system is rotating with an angular velocity w_i relative to the X_i system then equation (2.1) can be transformed and written as (Munk and MacDonald 1960)

$$\frac{dH_i}{dt} + e_{ijk}w_jH_k = L_i \quad . \qquad (2.2)$$

L_i are the components of the torque exerted on the earth, H_i are the components of the angular momentum and w_i are the components of the rotation vector, with respect to the x_i system. The alternating tensor e_{ijk} equals 0 if any two subscripts are equal, equals 1 if any subscripts are in even order and equals -1 if any subscripts are in odd order. By the usual convention for summation any term containing a repeated suffix is given all possible values for that suffix and the results then added. Equation (2.2) is quite general and can, therefore, be applied to a deformable earth.

The angular momentum H of the system is comprised of the following components: (a) a contribution due to rotation, and; (b) a component designating relative angular momentum due to a motion of particles u_i relative to the x_i system. A third component is introduced if the geocentre moves relative to the x_i system. It does not appear if the geocentre coincides with the origin at all times. Nevertheless, the

consequences of geocentre motion need to be investigated in view of the expected geodetic accuracy goals. This aspect is dealt with in Chapter 7.

The components h_{1i} of the rotational contribution h_1 have the form

$$h_{1i} = I_{ij} w_j \tag{2.3}$$

where I_{ij} is the second order inertia tensor for matter contained in a volume V. Elements of I_{ij} are defined as

$$I_{ij} = \int_V \rho(x_k x_k \delta_{ij} - x_i x_j) dV \quad . \tag{2.4}$$

δ_{ij} is the Kronecker delta with the properties that if $i = j$, $\delta_{ij} = 1$, and if $i \neq j$ then $\delta_{ij} = 0$ and the density of matter contained in an elemental volume dV is denoted by ρ.

The individual components of the relative angular momentum are given by the relation

$$h_{2i} = \int_V \rho e_{ijk} u_k x_j dV \quad . \tag{2.5}$$

Combining equations (2.3) and (2.5) algebraically gives

$$H_i = I_{ij} w_j + h_{2i} \quad . \tag{2.6}$$

2.2.2.1 Reference Frames

The choice of reference frame for the rotating x_i system and the space-fixed X_i system is altogether arbitrary. For example, Smith (1974) adopts a rotating frame of constant angular velocity such that all the deviations of a rotating earth from its equilibrium state of uniform rotation appear explicitly. In the case of the rotating frame x_i being earth-fixed, as applies here, w_i represents the components of the earth's instantaneous angular velocity.

In practice, it is common to choose a reference system which facilitates maximum simplification of the equations of motion. Of the options available, the principal (or figure) and geographic axes are chosen for their conceptual and practical significance, respectively.

The principal axes are most useful for studying the dynamics of a rigid body. By aligning the x_i system with the principal axes, the form of equation (2.2) is greatly simplified because the products of inertia vanish. In addition, there is no relative angular momentum in a rigid body which means that the term h_{2i} drops out of equation (2.6).

The selection of a suitable reference frame for describing the rotation of a deformable earth should be related in some way to the observatories. The system used at present is shown in figure 2.1 and is often called the "geographic" frame (Munk and MacDonald 1960). It is defined such that: (a) the origin lies as close as possible to the geocentre; (b) the x_3 axis is directed towards the Conventional International Origin (CIO) which corresponds very nearly to the mean terrestrial position of the spin axis as observed during the period 1900 to 1905 by the International Latitude Service (ILS), and; (c) the x_1 axis passes through the point of zero longitude as defined by the Bureau International de l'Heure (BIH) (see e.g. Guinot et al. 1971). The x_2 axis is directed towards longitude 90°E to form a right-handed system.

It must be remembered, however, that the geographic system is not a true earth-fixed system because the observatory coordinates, which essentially define the system, are undergoing geographic and geocentric variations that are induced, for example, by tectonic plate motions. Attempts have been made to determine these motions from astronomical evidence (see e.g. Proverbio and Poma 1976). Changes of this nature will contaminate the results of earth rotation experiments and so it is desirable to either model or estimate the significance of these systematic effects. Once again, these aspects are considered in more detail in Chapters 6 and 7.

With the precision of geodetic measurements approaching the centimetre level, the geographic reference system can only be considered earth-fixed for periods not exceeding a few years. Indeed, further refinements in the space ranging techniques will soon make a total reappraisal of the reference frame problem necessary. For instance, Stolz and Larden (1977) have shown that the effect of plate tectonic motion becomes significant in earth rotation studies after three months if a lunar laser ranging network provides measurements with uncertainties of 3 cm.

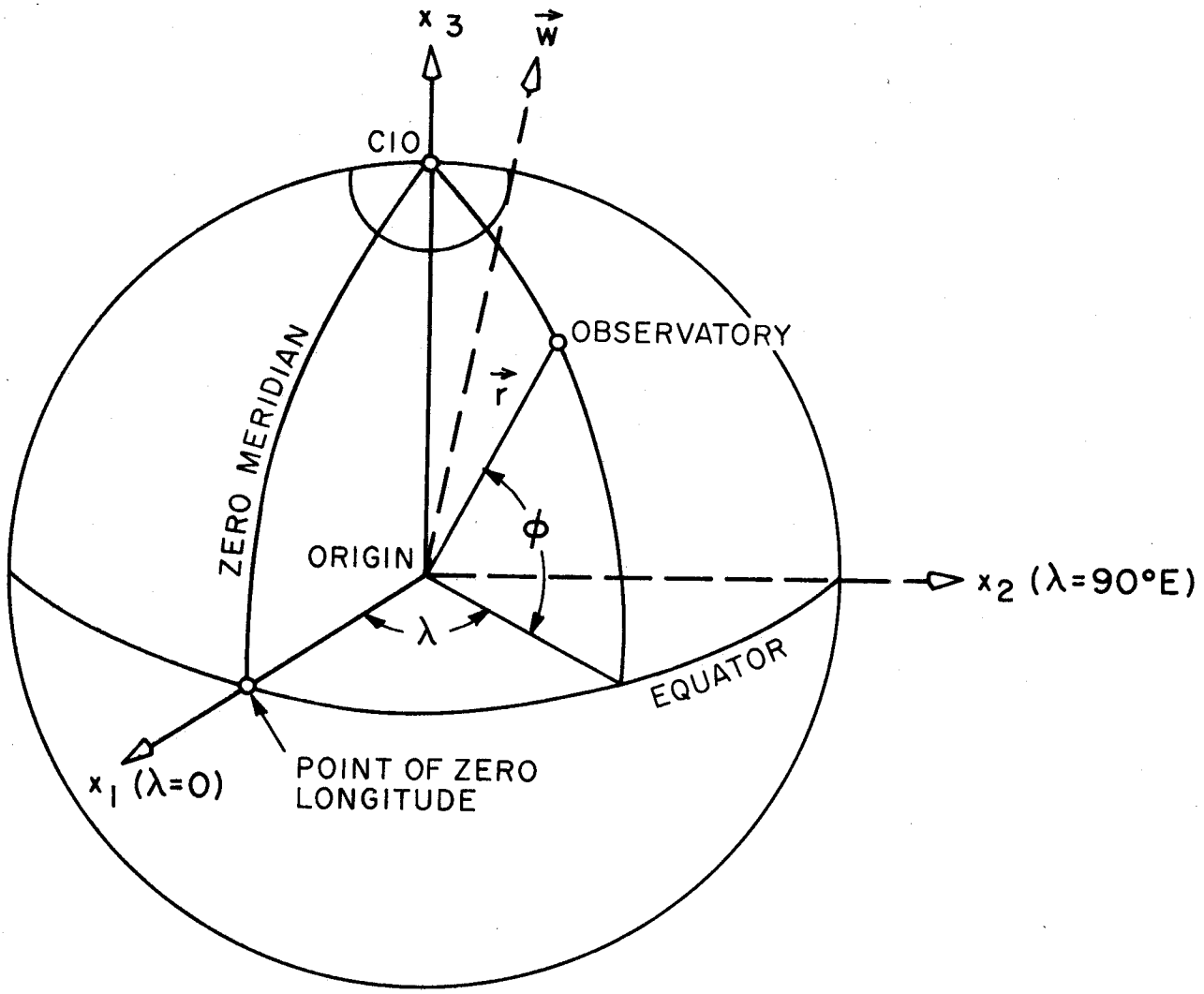

Figure 2.1 Geographic Reference System

To measure the earth's orientation in space the X_i system must be defined. One common choice is the mean equinox-ecliptic frame for the epoch 1950.0 (see, e.g. Explanatory Supplement 1961). In this system, the X_3 axis coincides with the north pole of the mean ecliptic for the epoch of 1950.0 and the X_1 axis coincides with the direction towards the mean equinox of 1950.0. The X_2 axis forms a right-handed Cartesian coordinate system. It is important to recognize here that the equinoctial point may not be the same for different ephemerides (Mulholland 1975).

In 1974 a colloquium was organized to initiate some thought on the complex subject of defining a reference frame for geodynamic studies. The feasibility of defining a system accurate to 5×10^{-9} radians in orientation and 1 cm in position was considered but only the basic requirements were established (Kolaczek and Weiffenbach 1975).

2.2.2.2 Rigid Earth Theory

To describe the basic modes of rotation for a rigid spheroidal earth, equation (2.2) is developed further. Let A and C be the principal moments of inertia, such that $A = I_{11} = I_{22}$ and $C = I_{33}$. For a rigid earth, only the rotation contributes to the total angular momentum. If the principal axes are used for the x_i system then equation (2.2) is expressed as

$$I_{ij} \frac{dw_j}{dt} + e_{ijk} w_j (I_{kl} w_l) = L_i \quad . \tag{2.7}$$

Expanding equation (2.7) as components along the base vectors x_i and rewriting in terms of A and C gives

$$\begin{aligned} A \frac{dw_1}{dt} + (C-A) w_2 w_3 &= L_1 \\ A \frac{dw_2}{dt} - (C-A) w_1 w_3 &= L_2 \\ C \frac{dw_3}{dt} &= L_3 \quad . \end{aligned} \tag{2.8}$$

Equation (2.8) defines the classical Eulerian motion for a rigid spheroidal earth. Specific forms of solution are considered in Section 2.2.3.

2.2.2.3 Deformable Earth Theory

The hypothesis of rigidity is always useful for describing the fundamental concepts of rotation. The implications underlying this assumption are that (a) all the mass particles maintain a constant relative position and (b) the inertia tensor is time invariant. Moreover, this assumption is only one of convenience because the earth is far from rigid. Departures from rigidity not only distort what one may consider to be idealized motions but also create new spectral features in the rotation.

Investigating these effects properly requires a more sophisticated model. In 1858 Liouville extended Euler's work by (a) assuming the inertia tensor varied with time and (b) assigning to the total angular momentum contributions from rotation and relative angular momentum. Substituting equation (2.6) into equation (2.2) and differentiating with respect to time yields

$$\frac{d}{dt}(I_{ij}w_j + h_{2i}) + e_{ijk}w_j(I_{kl}w_l + h_{2k}) = L_i \quad . \tag{2.9}$$

An accurate linearization of equation (2.9) is obtained by using the following perturbation scheme (Munk and MacDonald 1960)

$$\begin{aligned} I_{11}(t) &= A + i_{11}(t) \quad & I_{12} &= i_{12} \quad & w_1 &= \Omega m_1 \\ I_{22}(t) &= A + i_{22}(t) \quad & I_{13} &= i_{13} \quad & w_2 &= \Omega m_2 \\ I_{33}(t) &= C + i_{33}(t) \quad & I_{23} &= i_{23} \quad & w_3 &= \Omega(1+m_3) \quad . \end{aligned} \tag{2.10}$$

Ω is a nominal value of the earth's spin rate, i_{ij} are small perturbations in the inertia tensor, m_1 and m_2 are the direction cosines of the spin axis with respect to the earth-fixed x_i system and Ωm_3 is the difference between the instantaneous spin rate and the nominal value Ω. The scheme is only valid if the figure and spin axes stay in close proximity to the x_3 reference axis. The quantities, $i_{ij}C^{-1}$, m_i and $h_{2i}(C\Omega)^{-1}$ are small so their squares and products can be omitted from the development for most studies. However, for certain investigations (e.g. wobble ellipticity) it is necessary to retain some of these smaller terms (Lambeck 1980). After substitution of equation (2.10) into (2.9) and neglecting 2nd order terms one can write (2.9) as

$$\sigma_r^{-1}\frac{dm_2}{dt} - m_1 = -\psi_1(t)$$

$$\sigma_r^{-1}\frac{dm_1}{dt} + m_2 = \psi_2(t) \qquad (2.11)$$

$$\frac{dm_3}{dt} = \frac{d\psi_3(t)}{dt}$$

where σ_r and $\psi_i(t)$, $i = 1,2,3$ are defined as

$$\sigma_r = (C-A)A^{-1}\Omega \qquad (2.12)$$

and

$$\psi_1(t) = \left(i_{13} + \frac{di_{23}}{dt}\Omega^{-1} - L_2\Omega^{-2} + h_{21}\Omega^{-1} + \frac{dh_{22}}{dt}\Omega^{-2}\right)(C-A)^{-1}$$

$$\psi_2(t) = \left(i_{23} + \frac{di_{13}}{dt}\Omega^{-1} + L_1\Omega^{-2} + h_{22}\Omega^{-1} - \frac{dh_{21}}{dt}\Omega^{-2}\right)(C-A)^{-1} \qquad (2.13)$$

$$\psi_3(t) = \left(-i_{33} + \Omega^{-1}\int_0^t L_3 dt - h_{23}\Omega^{-1}\right)C^{-1} \quad .$$

Equation (2.11) gives the mathematical relations needed to explore the irregularities in the earth's rotation. An exact solution demands complete knowledge of all the excitation processes that can cause changes in the inertia tensor I_{ij}, the relative angular momentum h_{2i} and the torque L_i.

The unique characteristic of the Liouville equation is its provision for a direct comparison between geophysically calculated variations in the rotation and the observed variations. The left-hand sides of equation (2.11) are determined from classical and modern measurements whereas the right-hand sides are calculated from geophysical data. The dimensionless excitation functions $\psi_i(t)$ represent all the known geophysical effects that influence the rotation. The research carried out in this work is oriented towards estimating how much lunar laser ranging data can improve the frequency and accuracy of the quantities m_1, m_2 and m_3 or more specifically, their earth rotation counterparts x, y and UT1 (see later sections for explanation of notations). Techniques for evaluating equation (2.11) are given in Munk and MacDonald (1960) and Lambeck (1980).

2.2.3 Rotational Characteristics

2.2.3.1 Basic Modes

The following outline of the basic modes of rotation is limited to the theory governing a torque-free rigid body and a descriptive summary of the torque-induced modes. The theory of rotation for a torque-free rigid body was formulated by Euler in 1765. In this case, the total angular momentum remains constant, that is, $d\vec{H}/dt = \vec{L} = 0$. Equation (2.8) reduces to

$$\begin{aligned} \frac{dw_1}{dt} + \sigma_r w_2 &= 0 \\ \frac{dw_2}{dt} - \sigma_r w_1 &= 0 \\ C\frac{dw_3}{dt} &= 0 \end{aligned} \qquad (2.14)$$

where

$$\sigma_r = (C-A)A^{-1}w_3 \quad . \qquad (2.15)$$

Equation (2.15) follows directly from equations (2.10) and (2.12) for $m_3 = 0$. The solutions to equation (2.14) are straightforward and can be handled by standard mathematical techniques. They are (Lambeck 1980, p. 31)

$$\begin{aligned} w_1 &= a_o \cos \sigma_r t + b_o \sin \sigma_r t \\ w_2 &= a_o \sin \sigma_r t - b_o \cos \sigma_r t \\ w_3 &= \text{constant} = \Omega \quad . \end{aligned} \qquad (2.16)$$

Equation (2.16) is an example of harmonic motion with angular frequency σ_r and constants of integration a_o, b_o and Ω. For values of A, C and Ω that are appropriate to the Earth, $\sigma_r \simeq 1/306$ revolutions per day.

To an observer standing on the earth's surface, equation (2.16) implies that (a) the angular velocity component w_3, is constant and (b) the spin axis w, describes a circle about the figure axis x_3 at an angular frequency of σ_r. If this motion is viewed from space the situation changes slightly. The concepts are best illustrated using the classical

Poinsot diagram of Figure 2.2. Provided there is no slippage between the two cones, the basic features are (1) the direction of the angular momentum vector $\vec{H}$ remains fixed in space ($L_i = 0$) and, therefore, constitutes an invariable axis, (2) the figure axis traces out a cone, in space, about the angular momentum vector in a prograde manner and (3) the spin axis generates two cones, one with respect to the figure axis and a much smaller space cone about the angular momentum vector. To an astronaut on the moon, the earth would appear to wobble about its spin axis but if he were back on the earth's surface the spin axis would appear to move relative to the surface.

The terminology used in the literature to define these motions can at times be confusing (Rochester 1970). Throughout this work the general term given to describe the movement of the earth's surface relative to the spin axis is polar motion. The components of polar motion are either referred to as wobble or by some other descriptive term that unambiguously defines the motion. For the spatial motion of the spin axis, the terms precession and nutation are used for the secular and periodic components, respectively. The term secular is used only in a geodetic sense since over geological timescales precession is in fact a periodic motion.

While polar motion and nutation are different in principle, the laws of dynamics governing the conservation of angular momentum require that when one occurs it must be accompanied by the other, even though the relative amplitudes may be very different. The terms 'forced' and 'free' are used occasionally to distinguish between motions that are induced by torque action and those that are not.

Within this context, the torque-free motion of a rigid spheroidal earth relative to its spin axis is called Eulerian wobble (EW). Euler predicted that if the spin and figure axes of the earth were not in coincidence, the earth would wobble about its spin axis with an amplitude no greater than 0.3 arcsecs with a period of approximately 306 days. The associated motion of the spin axis in space has a small amplitude of about 0.001 arcsecs, a nearly diurnal period (Woolard 1953, p. 32) and is referred to as nearly diurnal free nutation (NDFN). The earth's

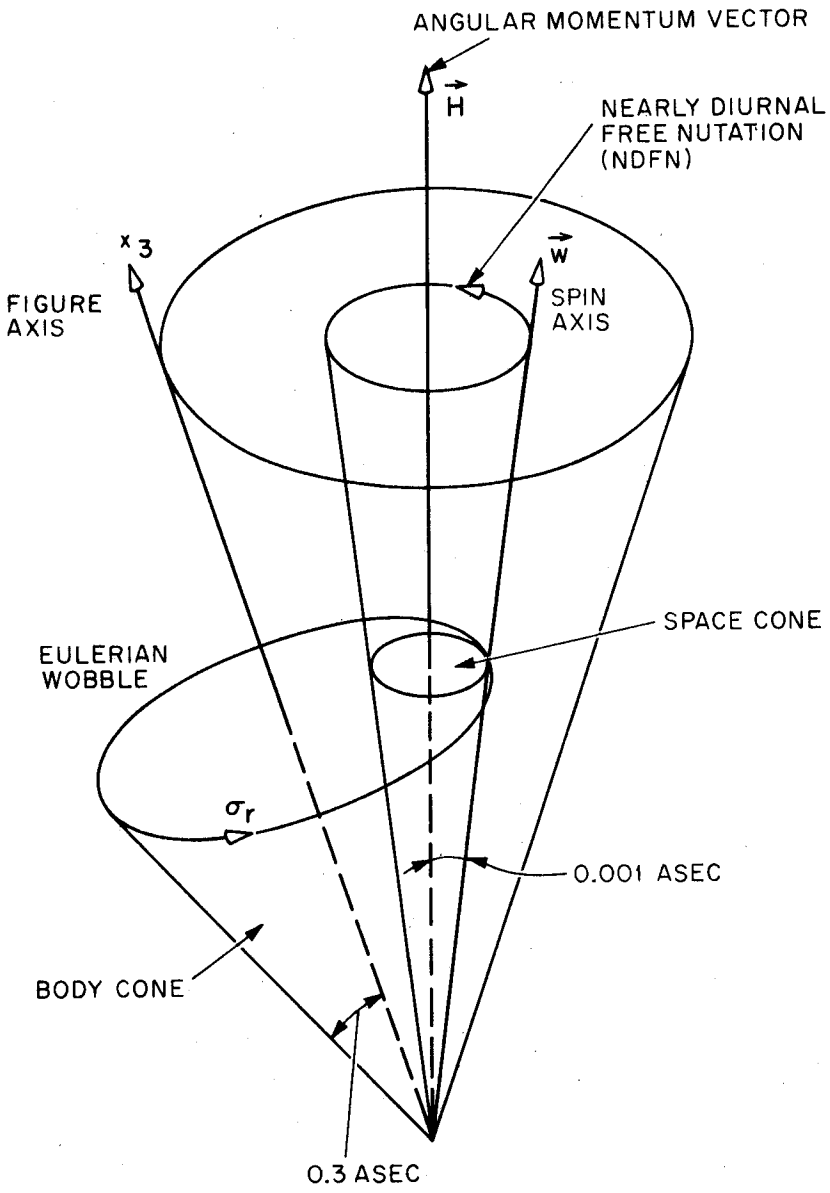

Figure 2.2 Poinsot Construction for a Rigid Earth

angular velocity w will hereafter be called the spin rate. Various forms of this particular mode are discussed in Section 2.2.3.2.

A second group of rotation modes arise when the torque components in equation (2.8) are not equal to zero ($L_i \neq 0$). The components L_i are generally written as the sum of two terms (Munk and MacDonald 1960)

$$L_i = \int_V \rho e_{ijk} x_j f_k dV + \int_S e_{ijk} x_j p_{km} n_m dS' \quad . \tag{2.17}$$

The first integral accounts for the effect of a body force f_k (e.g. the luni-solar and planetary gravitational attraction) acting on the equatorial bulge. The second integral accounts for the surface stress p_{km} acting in a direction k on a surface element dS'. n_m is the outwardly directed normal to the surface element. Surface stresses that cause radial deformation only do not produce a torque. The evaluation of equation (2.17) is outside the scope of this study but has been done elsewhere (see e.g. McClure 1973, Wahr 1979). Instead, the discussion which follows deals only with the modes that are generated by the gravitational attraction on the equatorial bulge. Section 2.4 is devoted to the more diverse subject of the rotational spectra for a deformable earth with fluid core.

The major gravitational contribution comes from the sun and the moon and to a lesser extent the planets. These forces cause the plane of the earth's orbit around the sun (ecliptic) and the earth's equator to constantly change their orientation in space. The gravitational attraction of the other planets, for example, causes the ecliptic to slowly change its position in space and although this so-called planetary precession (PP) has no direct influence on the position of the spin axis in space it does cause the space-fixed reference system X_i to move slowly with time. This phenomenon causes the obliquity of the ecliptic (angle subtended by the ecliptic and equatorial planes) to decrease at a rate of about 47 arcseconds per century (asecs cy^{-1}). It also causes the equinox (the point where the ecliptic and equatorial planes intersect) to move in a westerly direction along the earth's equator at a rate of about 13 asecs cy^{-1}.

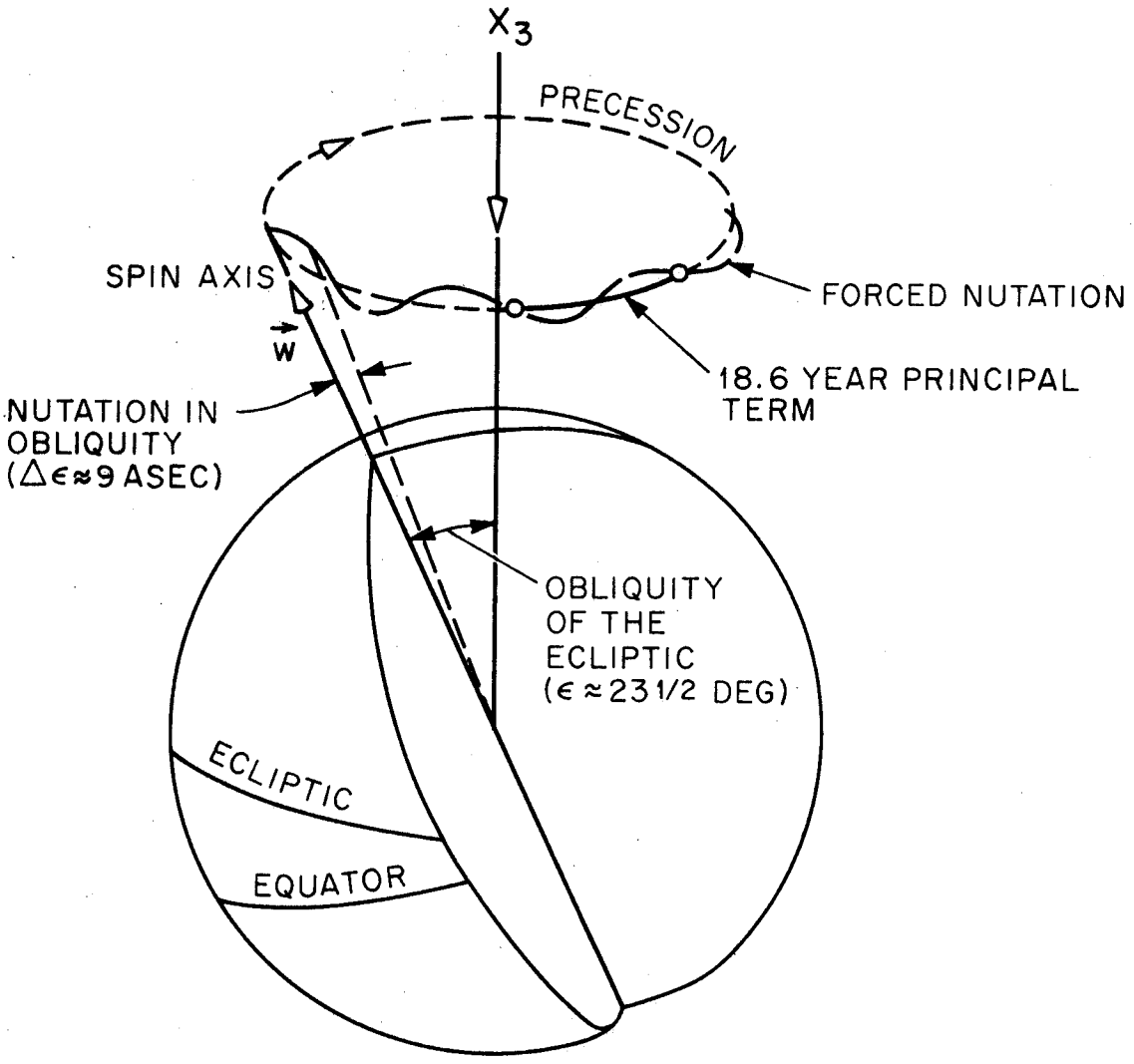

Figure 2.3 Precession and Nutation (taken from Rochester 1973)

The movement of the spin axis in space is a consequence of the complex interaction between the lunisolar gravitational potential and the earth's equatorial bulge. The 'secular' component of the motion is called the lunisolar precession (LP). The spin axis moves around the ecliptic pole tracing out a cone in space with an apex angle of about 47 degrees every 26,000 years. The corresponding 'secular' displacement of the equinox along the ecliptic plane occurs at a rate of about 5037 asecs cy^{-1}. The compounded motion of the lunisolar and planetary precessions is called general precession (GP).

Superimposed on the GP are the forced nutations whose periodicities are functions of the orbital period of the earth around the sun and the moon around the earth. The major term is known as the principal forced nutation (PFN). It has an amplitude, in obliquity, of about 9 asecs, a period of 18.6 years and is a consequence of the regression of the nodal line for the lunar orbit. These basic motions are illustrated in Figure 2.3.

As well as producing the precession and nutation, the lunisolar attraction also generates another mode called forced diurnal polar motion (FDPM). Theoretical aspects of this mode were studied long ago (see e.g. Klein and Sommerfeld 1903). Although referred to as FDPM, this mode is really the difference between the nutations for the spin and figure axes. The nature of this motion is shown in Figure 2.4 and if viewed in an earth-fixed coordinate system appears as a retrograde diurnal movement of the spin axis. The amplitude of FDPM varies from about 0.001 to about 0.02 asecs. Failure to correctly model FDPM in latitude observing programs will cause so-called 'dynamical' variations to appear (Atkinson 1973,1975). This phenomenon is discussed in more detail in Section 2.4.

With the theoretical foundations of the earth's rotation having been established, astronomers began the awesome task of matching observation with theory.

2.2.3.2 Observational History

Compared to the free modes, the forced modes of the earth's rotation are well understood. The precessional motions have been studied by astronomers for thousands of years. Early values for the precession

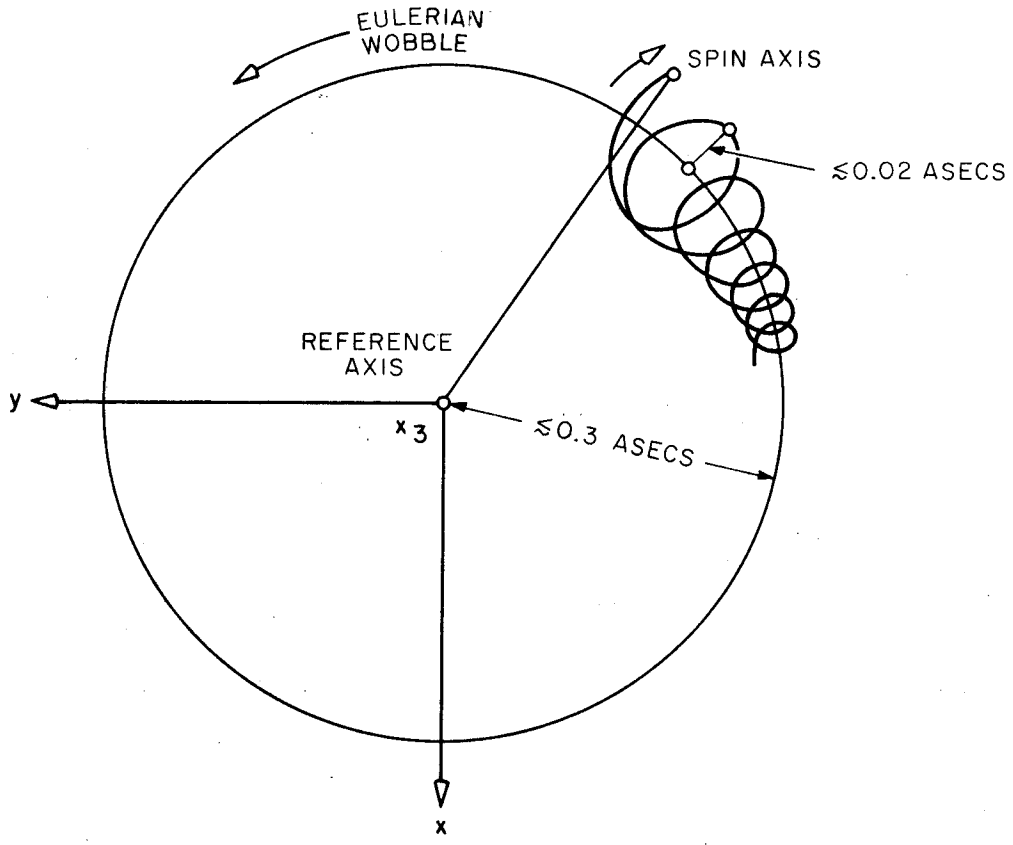

Figure 2.4 Forced Diurnal Polar Motion in a Rigid Earth

were derived by Bessel at the beginning of the nineteenth century but in recent work, Newcomb's (1897) values based on sun observations during the period 1756 to 1869, have been widely used. Woolard (1953) was the first to give an exhaustive treatment on the theory of nutation and although his results were only applicable for a rigid earth they were sufficient for use in classical applications.

Nevertheless, there is now considerable evidence to show that the results from early work do not conform too well with present-day observations (Melchior 1971, Fricke 1971). The discrepancies are mainly caused by (a) liquid core effects, (b) the earth's elasticity and (c) outdated astronomical constants (see Sec. 2.4 for further discussion).

Astronomical records of the spin rate also span a time interval of some thousand years, although short-period variations have only been detected since 1930. The spin rate is very important because it gives a measure of the true rotational position of the earth-fixed coordinate system x_i relative to the space-fixed system X_i.

Historically, astronomers have observed meridian star transits in order to establish local sidereal time (Mulholland 1972). Using an almost linear relation, sidereal time is converted to Universal time to establish a scale suitable for measuring the rotational position of the earth in space. Measurements of Universal time (UT) that are observatory dependent are designated UT0. Such measures are contaminated by polar motion which causes the observatory meridian to move with respect to the spin axis. Correcting UT0 for polar motion gives UT1, that is, a measure of the spin of the earth as a whole. Analyses of UT1 measurements reveal secular, periodic and irregular variations. Their causes are summarized in Section 2.4.

Since 1955, a uniform time scale has been provided by atomic frequency standards. This scale, called International Atomic Time (IAT), is used along with its sister time scale Universal Coordinated Time (UTC) to measure the time variations in m_3. UTC itself is a hybrid time scale; the rate is defined relative to the atomic clock rate and the epoch defined relative to UT (Mulholland 1972). Until the introduction of IAT, the uniform time scale was based on the observed motions of the sun, moon

and planets. The relationship between these various scales is given in Chapter 3 where the precise modelling of the lunar range observations is discussed.

Determinations of polar motion are obtained by observing variations in latitude. The suggestion by Euler in 1765 that the spin axis may move with respect to the earth's surface aroused sufficient interest for astronomers to begin searching for his predicted 306-day variation. By 1880, however, considerable skepticism prevailed because the results were much smaller than expected.

Research tests on the aberration constant of light, by Küstner in 1884, rekindled what appeared to be a dying interest in the search for polar motion. The results of his experiment were very discouraging because they were neither internally consistent nor compatible with the findings of his contemporaries. Indeed, they suggested the aberration constant was variable. Having extensively examined all possible sources of error, Küstner concluded that the variation he was observing should have been attributed to a variation in latitude of 0.2 asecs rather than an aberration. This discovery was supported in time by additional observations from the Potsdam, Berlin and Waikiki astronomical observatories. However, nothing definite was said about the exact period of the motion, except that it was quasi-annual.

Around this time, S. C. Chandler was analyzing latitude data that he had accumulated from the preceding 200 years. He found that in addition to an annual term there existed another component, hereafter called the Chandler wobble (CW), with a period of 428 days (Chandler 1891). The discrepancy between the period observed by Chandler and that predicted by Euler's theory was entirely unexpected and raised doubts about the validity of Chandler's results. A year later, Newcomb argued that Euler's theory needed modification to account for the earth's elasticity and demonstrated intuitively how the yielding of the solid earth and the presence of the oceans would increase the EW period by 40 percent. Lambert et al. (1931) have documented a detailed and interesting historical account of these discoveries for the inquisitive reader.

2.3 Systems for Determining the Earth's Rotation

2.3.1 Established Methods

2.3.1.1 Classical Astronomy

A direct and timely consequence of these early latitude studies was the establishment of the International Latitude Service (ILS) in 1899. Latitude observations made by an initial network of six stations have provided continuous information on polar motion to this present day. The approximate location of these stations on the 39th parallel of latitude was prescribed so that systematic errors in star positions, proper motions and the ephemeris would be eliminated by observing the same stars and using the same reduction constants (Markowitz 1968). By 1946, the network constituency stabilized and the stations which now remain are Carloforte, Gaithersburg, Kitab, Mizusawa and Ukiah.

In 1962 the ILS continued its operation under the auspices of the International Polar Motion Service (IPMS). There are now approximately 80 stations contributing data to the IPMS. The IPMS publish jointly, a pole path derived from the 5 ILS stations and a determination from all the collaborating stations (Yumi 1978).

A request for real-time information on polar motion and spin rate led to the formation of the Bureau International de l'Heure (BIH) in 1955. The BIH has about 80 stations that measure latitude variations and UT0 in order to simultaneously compute the position of the spin axis and UT1. Although both services publish values of the pole, they do work independently. The main difference is in how the services endeavour to preserve their systems so the results are not dependent on the total number of observatories contributing to any particular solution (see e.g. BIH 1978).

There is no significant disparity between the magnitude of the instrumental errors associated with the instruments used by these agencies. The standard deviation for a single PZT observation is 0.2 asecs and this compares favourably with recent estimates for the VZT (Kolaczek 1977). The corresponding precision of a latitude and time determination from a night of observations is of the order 0.02 to 0.03 asecs and 2 to 3 milliseconds (msecs), respectively.

Table 2.1. Quoted Precision for Polar Motion and Universal Time (taken from Kolaczek 1977)

Service	Polar Motion x,y; asecs	Universal Time UT1; msecs	Averaging Time days
ILS	0.03	---	14
IPMS	0.01-0.02	---	14
BIH	0.01	1	5

Errors for the published values of polar motion and UT1 are listed in Table 2.1 for each agency. The values for polar motion are denoted by the parameters x and y. In the geographic frame of Figure 2.1, x represents the offset of the spin axis from the CIO as measured along the zero meridian being reckoned positive towards the point of zero longitude and y is the offset perpendicular to the zero meridian reckoned positive towards longitude 270°E. The difference between the IPMS and BIH pole paths can sometimes amount to 0.1 asecs although usually the departures don't exceed 0.03 asecs. Discrepancies between the pole paths can be due to errors caused by refraction, local variations in gravity, ephemeris errors and differing data reduction methods. To separate different systematic effects is very difficult and the importance of studying the local meteorological and geophysical biases has been stressed many times (see e.g. Wells and Chinnery 1973). Studies by Thurm in 1960 indicate that the percentage contribution to the total error of a VZT observation caused by refraction, instrumental and ephemeris errors is 40%, 40% and 15%, respectively.

The error budget of Table 2.1 clearly summarizes the precision of the classical techniques. For a complete account of the classical methods and how they are used to obtain earth rotation information, the text by Mueller (1969) is recommended. The data reduction procedures are listed in the annual reports of the BIH and the IPMS.

2.3.1.2 Satellite Doppler Tracking

One major development during recent times has been the application of the Doppler principle as a method for tracking artificial earth satellites to obtain geodetic and earth rotation information. The following discussion only deals with the basics of the technique since the exact method has been documented in numerous research papers (see e.g. Anderle 1973).

Data gathered from the U.S. Navy navigation satellites by a network of about 20 Tranet stations are analyzed to provide polar motion information. The stations record data from 5 or 6 satellites in polar orbits at altitudes of about 1000 kilometers (km).

The basic observable is the phase change, or Doppler shift, of a continuous wave signal generated by an oscillator located on the satellite. The phase change over a given time interval is proportional to the change in the distance from the station to the satellite. If the satellite orbit is known, then the 'along-track' station component can be determined when the Doppler shift is zero. This occurs when the satellite occupies a position such that its velocity vector is perpendicular to the line of sight from the station. For satellites in polar orbit, the station and satellite latitudes are nearly equal when the Doppler shift is zero and residuals in the along-track position of the satellite can, therefore, be analyzed to improve the meridian component of polar motion at the tracking station. From a well-distributed station network the x and y coordinates of the spin axis are easily obtained.

The analysis of along-track residuals was first reported by Anderle and Beuglass (1970). Limited computations were performed prior to 1969 but the results were too scattered to enable definite conclusions to be drawn. Since 1971, the spin axis position has been determined simultaneously with the orbital parameters of the satellite (Anderle 1976). The computations were originally carried out at the Dahlgren Laboratory of the Naval Surface Weapons Centre and the spin axis position was published as 2 day values by the Dahlgren Polar Monitoring Service (DPMS). However, since 1975 the computations have been performed by the Defence Mapping Agency (DMA).

To evaluate the accuracy of the Doppler technique from individual station accuracies is difficult because numerous stations and satellites are involved in the determination. Nevertheless, analyses undertaken during early 1976 show that the average root mean square (rms) error for a spin axis position determination from 48 hours tracking to one satellite is approximately 0.003 asecs in each coordinate. This estimate of precision, which only includes observational errors, has also been reproduced in subsequent years (Anderle 1977). Unfortunately, uncertainties in the earth's gravity field and the model for atmospheric drag produce orbital errors which continue to cause problems. For example, the standard deviation of an individual two-day determination with respect to a five-day mean sometimes exceeds 0.02 asecs while the standard

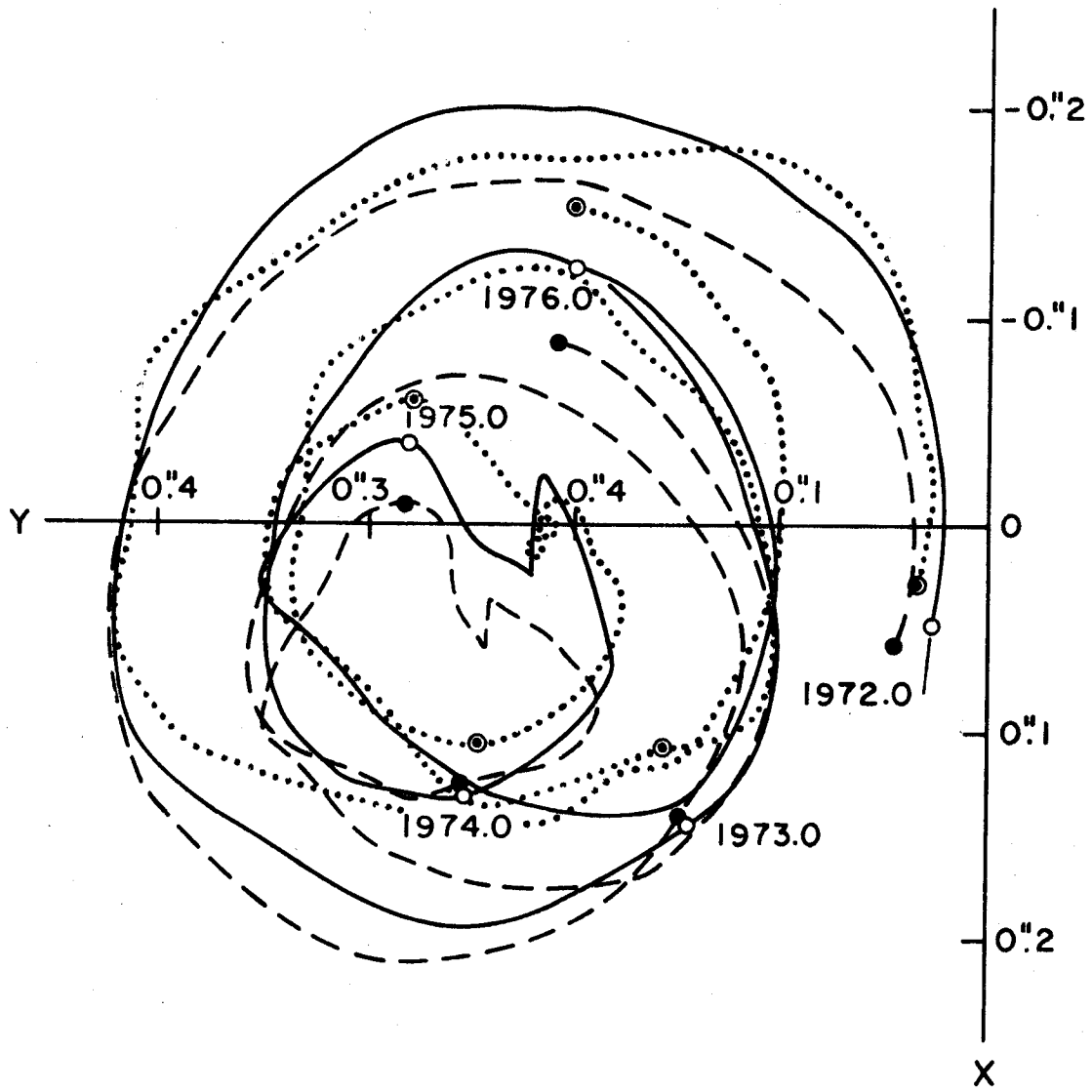

Figure 2.5 Pole Paths from 1972.0 to 1976.0. Solid line - BIH Vondrak smoothed values; broken line - IPMS 0.05 yearly values; dotted line - DMA Gaussian smoothed values (taken from Larden 1981)

deviation of a five-day mean (standard error) based on observations from two satellites is 0.01 arcsecs (Anderle 1976, Oesterwinter 1979). These estimates are essentially the same as those obtained by classical techniques (Graber 1976).

Doppler data have also been incorporated into BIH solutions (see e.g. BIH 1978). Figure 2.5 shows the pole path curves obtained from DMA, BIH and ILS data for the period 1972 to 1976. The rms deviation between the DMA and BIH results is of the order 0.02 and 0.01 asecs for the x and y coordinates, respectively. Slightly larger discrepancies are evident between these results and the ILS values. Preliminary determinations of UT1 from Doppler data have been reported by R. Anderle but have not been documented on a regular basis.

Despite the advantage of being an all-weather, all-day system it is still not clear how much of an improvement can be made by the Doppler technique over the classical method. One of the limitations of the Doppler technique is the well-known problem of having to analyze radio signals which are travelling through the earth's ionosphere.

2.3.2 Procedures Under Development

During the last decade three new methods for measuring the earth's rotation have been developed. They are, laser ranging to artificial satellites (SLR), lunar laser ranging (LLR) and very long baseline interferometry (VLBI). Each technique has the potential to provide earth rotation information on a daily basis with 5 cm accuracy. An intuitive assessment of these methods shows that all have specific attributes for measuring the earth's rotation. However, for a program requiring (a) homogeneous data (b) continuity of results and (c) economy of operation, a combination of resources may be required.

The following discussion does not intend to advocate any single technique, but merely describes the observational methods, summarizes the experimental results to date and comments generally on the obvious limitations of each method.

2.3.2.1 Satellite Laser Tracking

Since the fitting of corner-cube retroreflectors to the Beacon Explorer satellites and their subsequent launching in the 1960's, the technological advances in satellite laser ranging systems can only be described as revolutionary and their application for geodetic studies a formality. Presently, there are about twenty satellite ranging systems in operation. Collectively, they form a worldwide network which includes stations in the U.S.A., Japan, France, Australia, Germany, South America and Hawaii.

The details of a typical laser system have been described by Johnson (1977). Design and instrumentation improvements over the past decade have led to a five-fold reduction in the noise level of the observations. Currently, most laser systems are achieving a precision of about 10 cm with the ultimate goal being 1-2 cm (see e.g. NASA 1979).

The main problem with using low-orbit satellites, like the Beacon Explorer series, for measuring the earth's rotation stems once again from an inadequate knowledge of the earth's gravity field. However, the orbit of the Laser Geodynamics Satellite (LAGEOS) is designed to overcome this very aspect. It is almost circular, has an inclination of 110 degrees and a semi-major axis of approximately two earth radii. This geometry not only reduces the orbit perturbations due to the gravity field but also allows simultaneous tracking of the spacecraft from widely separated sites.

The basic measurement consists of the time it takes a laser pulse to complete the transmitter-satellite-receiver distance. Corrections to this time interval are usually made for (a) circuit calibrations (b) pulse shape effects and (c) the distance from the reflector to the centre of mass of the satellite (Smith et al. 1973). For very short-pulse laser systems (see e.g. Wilson et al. 1978) the correction at (b) can generally be ignored.

Sufficient satellite laser observations are now available to permit determinations of the earth's rotation over extended periods of time. Recently reported are polar motion and UT1 values derived from LAGEOS observations for the period 1976 to 1981 (see e.g. Tapley et al. 1981).

The first attempt to extract latitude variations from laser tracking data was by Smith et al. (1972). In short, fluctuations in the inclination of a satellite orbit can be analyzed for improved values of the instantaneous latitude of the tracking station. To obtain values for polar motion and UT1, two or more stations have to track the satellite. Smith used tracking data from the Greenbelt laser to the Beacon Explorer-C satellite and confined the analysis to times when the satellite occupied the northern apex of its orbit. This configuration ensures accurate determinations of the inclination. For the five-month period between July and November 1970 the rms difference between the satellite laser and BIH latitude values at Greenbelt was slightly less than 1 metre.

In a more recent study, Dunn et al. (1977) re-analyzed a three-week period of the 1970 data by fitting, in the first instance, a reference orbit to the data and then adjusting the station coordinates to best fit the reference orbit on thirteen individual days. On each day values for the station latitude and UT0 were obtained and their rms difference with corresponding BIH values was 0.025 asecs and 0.81 msecs, respectively.

Polar motion results from a multi-station network were reported recently by Smith et al. (1979). Observations were gathered from a total of seven LAGEOS tracking stations; four in the U.S.A., two in South America and one in Australia. Five-day values for polar motion were obtained from three interlocking 30-day reference orbits covering the period October to December 1976. The formal errors for the x and y components were 0.003 and 0.002 asecs, respectively but the authors believe an accuracy of somewhere between 0.01 and 0.02 asecs is more realistic. From this experience and previous simulations (Kolenkiewics et al. 1977) it is expected that daily pole positions to about 0.002 asecs and UT1 values to about 0.2 msecs, consistent over 2 to 3 months, are feasible.

Schutz et al. (1979) reported pole positions obtained by laser measurements to the GEOS-3 satellite. Data from three NASA/GSFC stations located at Greenbelt, Bermuda and Grand Turk were used in the analysis. The small longitude dispersion between the three stations

prevented a good determination of the x component for polar motion and although the results were not as impressive as those obtained by Smith et al. (1979) they do indicate that meaningful information on the earth's rotation is possible from a regional station network.

The three main hurdles to overcome when determining the earth's rotation by satellite methods are (Bender 1975) (1) the satellite orbit uncertainty, (2) the effect of atmospheric refraction on the laser measurement, and (3) the statistical and systematic measurement errors. Of the three, the main source of error at present lies in the orbit. Nevertheless, once the lower degree harmonics of the earth's gravitational field are improved and the effects of the earth's albedo radiation pressure on the satellite are correctly modeled there should not be too many remaining problems. If a sufficient number of well-distributed tracking stations are available then the orbit uncertainty should not be substantially worse than the limitations mentioned in (2) and (3). Both of these are expected to be modeled at the one centimetre level.

Comparatively speaking, laser ranging is more precise than Doppler tracking. The LAGEOS satellite is also far more stable to track than any low-altitude spacecraft and even though the laser ranging technique is dependent on fine weather for observational success, recent simulation studies indicate this not to be a significant drawback for future geodynamical applications (see e.g. Bender and Goad 1979).

2.3.2.2 Very Long Baseline Interferometry

The beginnings of radio interferometry date back to the third decade of this century. Experiments were limited to short baselines because it was felt that the two antennae should be connected by a coaxial cable in order to properly compare the reception times of the radio signal. The realization that very long baseline interferometry (VLBI) could be used as a powerful tool for accurately measuring the earth's rotation (Gold 1967) coincided with the discovery that atomic frequency standards were stable enough to record the arrival time of the signal at each site independently. This discovery allowed baseline lengths to increase to intercontinental proportions.

To extract earth rotation information from VLBI data is a complex and laborious process (see, e.g. Counselman 1976 for a general review). The basic observables are radio signals emitted by distant quasars or transmitters on artificial satellites and the moon. Quantities which can be measured include; the instantaneous difference in phase of the signal as it arrives at each end of the baseline, its time derivative and also its derivative with respect to the observed radio frequency. These quantities are often referred to as fringe phase, fringe rate and group-delay measurements, respectively. All three are sensitive to variations in the earth's rotation but the latter two are more suitable because they skirt the phase ambiguity question inherent in the fringe phase measurements (Rogers 1970).

Groups at the Massachusetts Institute of Technology (MIT), Jet Propulsion Laboratory (JPL) and the Goddard Space Flight Centre (GSFC) are involved in the majority of the analyses. In fact, it has been these studies which have provided the main impetus for improved determinations of the positions of radio sources and the compilation of a fundamental source catalogue for a global geodynamics program. The most accurate source coordinates are known to about 0.01 asecs.

Since the introduction of VLBI in geodesy, most experiments have dealt with the measurement of baseline lengths (see e.g. Ong et al. 1976, Robertson et al. 1979, Niell et al. 1979). For example, the first measurement of the Haystack-Greenbank baseline had a precision of 2 metres (Hinteregger et al. 1972) and agreed with the land survey at the same level. One of the most impressive length determinations by the interferometric technique so far is for the short 1.24 km Haystack-Westford baseline. From October 1974 to December 1976, 11 independent measurements of the vertical and two horizontal components had rms scatters of 7, 5 and 3 mm about each respective mean (Rogers et al. 1978). The corresponding rms variation for the baseline length was 3 mm. The mean results agreed to 6 mm or better with the values obtained from the conventional land survey (Carter et al. 1980).

Experiments designed to carry out measurements of the earth's rotation have been few in number. One of the first was conducted by

J. L. Fanselow on the Goldstone-Madrid baseline where on five separate occasions during the latter part of 1971 values of UT1 were obtained. Each had a formal error of about 2 msecs and the rms difference with BIH Circular D results was at the 1 msec level. The average observation period for each experiment lasted about 15 hours. During the period 1973 to 1977 inclusive, 12 additional single-day UT1 values were obtained; the result of the last experiment having a formal error of 0.6 msecs (Fanselow et al. 1979).

In general, baselines parallel to the earth's equatorial plane are more suitable for measuring UT1 variations and baselines perpendicular to this plane are more sensitive to variations in polar motion (Williams 1970). Shapiro et al. (1974) present the results of nine separate VLBI experiments during 1972 and 1973 to determine the length and variations in the direction of the 3900 km baseline vector between Haystack and Goldstone. The rms scatter of the length determinations was less than 20 cm, or 5 parts in 10^8. Changes in the direction of the baseline were interpreted as changes in UT1 and polar motion; the rms scatter between these results and the BIH Circular D values was 2.9 msecs and 0.042 asecs, respectively. Although the Haystack-Goldstone baseline is essentially parallel to the equator, there is sufficient latitude separation to obtain the x component of polar motion. A detailed account of these and several other experiments is given by Robertson (1975).

In a more recent study by Robertson et al. (1980), comparisons were made between VLBI estimates of the x-component of the pole and UT1 and the corresponding ones from lunar laser ranging, satellite laser ranging, satellite Doppler and the classical techniques for the period September 1976 to May 1978. In particular, the comparison between the lunar laser ranging and VLBI determinations of UT1 suggests that the rms of the uncertainties in each set are below 1 msec.

A distinct advantage of the VLBI method is its all-weather capability but this has been offset, in the past, by the difficulties in measuring the amount of water vapour along the path of the signal. With the use of water radiometers and surface meteorological readings, modelling of this critical parameter should be achieved at the centimetre level

very soon (see e.g. Wu 1979, Resch and Claflin 1980). In the future, very accurate measurements of polar motion and UT1 are anticipated when project POLARIS becomes fully operational (Carter 1980).

2.3.2.3 Lunar Laser Ranging

The technique of laser ranging to reflectors located on the moon was first suggested back in the early 1960's (Bender et al. 1973). Since then numerous scientific objectives have been pursued with improved determinations of the earth's rotation being a prominent one. Because the primary concern of this investigation is to see how well the earth's rotation can be monitored by LLR, the discussion in this section will be limited to the more general aspects of the experiment. Technical details are left until the following chapters.

The prospect and benefit of obtaining high-accuracy laser range measurements of the earth-moon distance soon became evident after the sustained research which took place in the field of laser technology during the early 1960's. Extending the technique beyond the realm of an artificial satellite to include the moon depended on three important considerations. They were (1) the development of a high-powered ruby laser capable of sending a pulse of light over twice the earth-moon distance, (2) the design of reflector arrays which could avoid serious diffraction problems and be used during full moon and (3) the deployment of these arrays to the lunar surface by either manned or unmanned spacecraft.

Considerations (1) and (2) were achieved by 1966 but it was only by chance that (3) was fulfilled. Due to problems of work overload on the Apollo 11 spaceflight in 1969, the disposition of simple experiments including an array on the lunar surface took precedence over the Apollo Lunar Surface Experiment Package (ALSEP). By 1973, five arrays had been placed at different locations on the lunar surface. Included were three American designed arrays sent on Apollo missions 11, 14 and 15 and two French designed packages mounted on the Lunakhod 1 and 2 exploration vehicles sent by the U.S.S.R. on Luna flights 17 and 21, respectively. All of these arrays, with the exception of Lunakhod 1, have reflected signals

consistently during the ensuing years. With VLBI measurements using the ALSEP transmitters on the lunar surface, direct comparisons between the LLR and VLBI techniques can be made (Counselman et al. 1973, King et al. 1976).

Several countries have displayed an active interest in the numerous scientific objectives offered by LLR. Some of the stations which have already ranged to the moon are situated at Ft. Davis, Texas; Haleakala, Hawaiian Is.; Orroral, Canberra and Crimea, U.S.S.R. Plans are underway to range from Wettzel, Germany; Calern, France and Dodaira, Japan. Further details on the early history of the experiment can be found in Bender et al. (1973) and Mulholland (1980).

The basic range measurement is the time it takes a laser pulse to travel from a transmitting telescope on earth to a reflector on the moon and back to a photo-multiplier unit. The systems at Ft. Davis, Texas and Orroral, Canberra need only one telescope to transmit and receive the laser pulse while the system at Haleakala uses separate facilities to accomplish these tasks (Carter et al. 1977). Listed in Table 2.2 are the basic attributes of the present systems at McDonald Observatory, Texas and Orroral, Canberra.

Descriptions of the LLR observation process (see, e.g. Abbot et al. 1973, Silverberg 1974, Shelus 1978) and the calculation of the journey time (Calame 1976, Mulholland 1977, Stolz 1979) are readily available. The measurements consist of two separate sets of data. Firstly, an integral number of 50 nanosecond (nsec) intervals which occur between the initial firing of the laser pulse and its subsequent detection by the photomultiplier is determined and recorded. The second consists of an accurate determination of the fractional time between (1) the start pulse generated by the outgoing laser pulse and the first clock pulse (50 nsec interval) encountered after the laser is fired and (2) the stop pulse generated when detection occurs and the next clock pulse. These data are combined with circuit calibration and accurate clock information to produce the measured journey time (see e.g. Shelus 1978).

Table 2.2 Basic System Characteristics for the Orroral and McDonald LLR Tracking Stations

Item	McDonald	Orroral
Telescope Diameter	2.7 metres	1.5 metres
Pulse		
(i) Length	3 nsecs	6 nsecs
(ii) Energy	1.2 Joules	1 Joule
(iii) Repetition Rate	20 shots/min.	12 shots/min.
Normal Point Uncertainty	1 nsec	$\simeq$ 1 nsec
Beam Divergence	1.5 arcsecs	4 arcsecs
Information Source	Silverberg (1974)	P.J. Morgan (1981, private communication)

In the early stages of the LLR experiment, the separation of signal from noise was accomplished using a 'residual bin' system (Abbot et al, 1973) but these days, a far more sophisticated method of filtering is used (see e.g. Shelus (1978) for a summary). Real returns are usually detected after an accumulation of approximately 50 to 300 shots over a 5 to 30 minute period and are distinguishable if the distribution is statistically compatible with Poisson's probability law. A good knowledge of the calculated journey time helps reduce the noise level of the observations.

After recognizing the success of an observing sequence, the individual returns are reduced to a common time by means of linear function fitting. The condensed construct is called a 'normal point', containing without degradation, all the information of the individual returns. Its precision is determined by the length of the laser pulse and the number of the returned signal pulses observed.

The main limitations which must be overcome in order to use LLR as a technique to monitor the earth's rotation can be categorized as (a) operational, (b) model and (c) geometrical. Silverberg (1974) summarizes the main operational limitations to include (1) transparency effects due to cloud cover and atmospheric water vapour content, (2) atmospheric visibility effects on telescopic guidance and beam collimation, (3) image contrast problems during daytime observing particularly around new moon, (4) equipment malfunctions and precautionary air traffic restrictions and (5) time sharing conflicts.

Recent improvements in modelling the lunar orbit and librations have allowed limited studies of the earth's rotation using single station data (see e.g. Stolz et al. 1976, King et al. 1978, Calame and Guinot 1979). However, even if the orbital and libration motions were perfectly known there are still more fundamental factors that ultimately will control the frequency and limit the accuracy of earth rotation results obtained by LLR. Factors which need consideration include (a) the effects of weather and time scheduling, (b) the observation uncertainty, (c) the network constituency and (d) the geometric limitations related mainly to station location, lunar declination and hour angle coverage.

The significance of these factors is examined in this work. In the next section, the main features of the earth's rotation are reviewed in order to establish a realistic yardstick for assessing the significance of the simulated results.

2.4 Spectrum of the Earth's Rotation

2.4.1 Variational Causes

Changes in the earth's rotation are usually described in terms of the terrestrial and spatial movements of the spin axis (i.e. polar motion and precession-nutation) and irregularities in the spin rate. Such changes are caused by phenomena which broadly divide into three classes: those which change the total angular momentum of the earth (e.g. the lunisolar torque, ocean tidal dissipation, solar wind torque); those which change the mass distribution of the earth (e.g. earthquakes, lithospheric plate motions, deglaciation) and those which involve a redistribution of angular momentum but not an overall change (e.g. core-mantle coupling).

Studies on the complexities of the earth's rotation date well back into the last century. Lambeck (1980) summarizes the more recent developments to include (a) the role of core-mantle interactions, (b) the correlation of earthquake activity with irregular changes in polar motion and spin rate, (c) the determination of improved CW parameters, (d) the effect of ocean tidal dissipation on the earth's secular acceleration and (e) the contribution of atmospheric circulation to changes in the earth's spin rate.

In particular, the role played by the earth's liquid outer core on the rotation of the mantle has stimulated much research during the last three decades. A theoretical understanding of the problem was sought near the turn of the century (see e.g. Poincaré 1910) and this work was later extended independently by Jeffreys and Vincente (1957a,b) and Molodensky (1961) to account for the elasticity of the mantle.

Two of the most recent and comprehensive studies on this subject have been published by Smith (1977) and Wahr (1979). The first deals with the effect of liquid core stratification on the CW and NDFN while

the latter study gives the best solution to date for the forced nutations of a rotating, elliptical, elastic and oceanless earth. The results of these studies are discussed later on in this section.

With regard to the remaining items (b)-(e), the amount of available literature on these subjects since Munk and McDonald's (1960) historic geophysical discussion is both extensive and diversified (see e.g. Rochester 1973, Smylie 1977, Lambeck 1980). The summary which follows here is neither authoritarian nor complete, however, it does give some perspective on the areas that should be further investigated once data from the new space ranging methods are consistently acquired.

2.4.2 Space Motions

2.4.2.1 Precession

In present day geodetic studies it is customary to represent the precessional motion of the earth by mathematical expressions derived by Simon Newcomb (see e.g. Mueller 1969, p. 62-68). For periods less than one century, polynomial series are quite sufficient (Laubscher 1972) but if the computations are needed over longer periods, say for paleoclimatological applications, a trigonometric series is more expedient (Berger 1977).

The bases of the precession model are the fundamental astronomical constants which define the precession rates. A collation of numerous optical determinations made during the period 1925-60 (Böhme and Fricke 1965) and the more recent analyses by Fricke (1972), Laubscher (1976) and Asteriadis (1977) all indicate conclusively that Newcomb's lunisolar precession (LP) rate of 5037.1 asecs cy^{-1} for 1900.0 is too small by about 1 asec cy^{-1}. Another correction of about 1.4 asecs cy^{-1} is also required to account for errors in Newcomb's value for the planetary precession (PP) rate and non-precessional motion of the equinox (Asteriadis 1977). The error in the PP rate only amounts to 0.03 asecs cy^{-1} (Laubscher 1972).

Measurements of the precession by space ranging methods are few in number. VLBI and Doppler tracking of interplanetary space probes are the techniques which appear to offer the most promise (see e.g. Walter 1974).

The first VLBI determination of the GP, consistent with the current value obtained by classical methods, was reported by Robertson (1975). The quoted uncertainty for this result is 0.05 arcseconds per year (asecs yr^{-1}) which agrees exactly with Elmore's (1976) error estimate based on a hypothetical experiment. Pease (1977) notes in his analysis of Doppler data from interplanetary space probe missions that he can conveniently remove an apparent right ascension drift of -1.1 ± 0.3 asecs cy^{-1} by adopting Fricke's LP correction of 1.1 asecs cy^{-1}.

The precession mode has little to offer in regard to understanding more about the earth's interior. Toomre (1966) has shown that inertial coupling and viscous friction are capable of balancing any difference in the torque on the core and the mantle during precession (see also Rochester 1974).

2.4.2.2 Nutation

The numerical series listed in the Explanatory Supplement of Astronomical Ephemeris and Nautical Almanac (Explanatory Supplement 1961) was derived by Woolard (1953). Independent rigid-body results which take into account Eckert et al.'s (1966) improvements to Brown's lunar theory and the higher degree harmonics of the earth's gravitational potential have also been published (Kinoshita 1977) but as discussed later these theories are not the best available.

Woolard's treatment gives the nutations for three major dynamical axes, that is, the spin, figure and angular momentum axes. His mathematical approach involves, in the first instance, the numerical integration of Poisson's equations to derive the nutations for the angular momentum vector (Woolard 1953, p. 124). The nutations for the spin and figure axes are obtained by adding to the solution of Poisson's equations several forced periodic terms plus a correction for the NDFN (see Section 2.2.3.1). The latter correction, however, is only marginally significant at the level of truncation adopted by Woolard. Woolard also uses the Oppolzer terms to calculate the difference between the nutations of the spin and figure axes (Woolard 1953, p. 159). The characteristic periods of these terms when viewed in a space-fixed frame are

two weeks or more but when viewed in an earth-fixed frame they combine to produce the FDPM (see Figure 2.4 and also McClure 1973).

Several modifications must be made to Woolard's rigid-body theory to account for the effect of elasticity and a liquid core (see e.g. Jeffreys and Vicente 1957a,b; Molodensky 1961, Shen and Mansinha 1976, Sasao et al. 1980). The most significant changes include, (a) a reduction in the amplitude of the PFN from its rigid-body value of about 9.21 asecs to approximately 9.20 asecs, (b) corrections of about 0.006 and 0.02 asecs to the rigid-body annual and semiannual terms, respectively due mainly to liquid core effects (see also Melchior 1971) and (c) a correction of about 0.002 asecs to the fortnightly nutation terms due mainly to elasticity (McClure 1973).

Of all the nutation theories formulated to date, the most recent, comprehensive and thorough treatment is by Wahr (1979). This theory, based on the scalar equations and normal mode algorithm scheme presented by Smith (1974,1976,1977), takes into account all the tidally induced motions of the earth, that is, deformation, nutation and changes in spin rate. The computation systematically includes the effect of rotation and ellipticity throughout the core and mantle without artificially separating one from the other and considers the stratification of the material in each major layer. These results, along with several others are listed in Table 2.3 for the dominant nutations of the mean figure axis for the mantle. Observational results are also given for comparison. It is clear from this tabulation that the observations for the principal and semi-annual terms agree best with the models for an elastic earth with liquid core (Models 4-7, Table 2.3).

The choice of reference axis for the nutation series has become a major discussion point during the past few years. Fedorov (1963) suggests the angular momentum vector because its nutations are virtually independent of the earth model but Woolard (1953) believed as Oppolzer (1880) did that the nutations should be given for the spin axis and this opinion is still held by many today. Nevertheless, astronomers involved in latitude work were puzzled by the appearance of a periodic term in the results that was identical to the theoretical fortnightly Oppolzer

Table 2.3 Summary of the Theoretical and Observed Nutation Amplitudes for Various Earth Models

Model Reference	Nutation Period, Days				Source
	6800	365	183	14	
	$\Delta\varepsilon$, $-\Delta\psi \sin\varepsilon$: arcsecs				
1	9.228,6.874	0.000,-0.050	0.553,0.508	0.095,0.088	Kinoshita et al. (1979)
2	9.210,6.858	0.000,-0.050	0.552,0.506	0.094,0.081	Woolard (1953)
3	9.210,6.858	0.000,-0.050	0.552,0.506	0.092,0.079	McClure (1973)
4	9.204,6.844	0.005,-0.056	0.572,0.523	0.097,0.090	Mblodensky (1961)
5	9.197,6.833	--- , ---	0.577,0.527	0.097,0.090	Shen and Mansinha (1976)
6	9.202,6.841	0.005,-0.057	0.574,0.525	0.098,0.090	Sasao et al. (1980)
7	9.203,6.842	0.005,-0.057	0.574,0.525	0.098,0.091	Wahr (1979)
Astronomical Observations*	9.205,6.841	--- , ---	0.578,0.533	0.091,0.086	McCarthy et al. (1980)

*Mean values taken from McCarthy's paper. Observed values of annual term not listed.

term that contributed to the FDPM. Atkinson (1973) describes this phenomenon as a 'dynamical' variation of latitude and points out that there would be other periodic variations were it not for the obscuring nature of the observing procedure and the accuracy of the results. Atkinson (1973,1975) recognized the connection between this fortnightly variation and the Oppolzer term of similar period and proved that observations made from the earth's surface were sensitive to the nutations of the mean figure axis and not the spin axis. Atkinson's results and recommendations refer only to the rigid earth case and, therefore, need slight modification to account for non-rigid effects.

Wahr (1979) computes the nutation for the mean figure axis of the outer crustal portion of the earth because, strictly speaking, this is the surface from which the observations are performed. The nutations for this axis are, for all practical purposes, identical to the nutations for the mean figure axis of the mantle (ibid. 1979); the latter having been used by others. The mean figure axis is chosen for non-rigid calculations in order to avoid using the instantaneous figure axis which undergoes large tidally-induced diurnal variations. This distinction is not needed in rigid-earth theory because the figure axis remains fixed relative to the body.

The IAU (1980) have finally decided to adopt the mean figure axis of the mantle as the reference axis for the nutations. Molodensky's (1961) work was chosen ahead of the far more sophisticated work of Wahr (1979) but a review of this decision has been recommended by the IUGG (1980). The historical and experimental aspects of the earth's nutations are discussed in Fedorov et al. (1980).

2.4.2.3 Variations in Obliquity

In addition to displacing the equinox at a rate of about 13 asecs cy^{-1}, the planetary precession causes the obliquity of the ecliptic to oscillate with a mean period of about 40,000 years. Over geodetic timescales this oscillation is not apparent. Observers merely see a 'secular' decrease in the obliquity at a rate of about 47 asecs cy^{-1}.

As usual, the observed rate does not agree with theory. Early attempts to explain the difference, which observations suggest could range

anywhere between 0.1 and 0.3 arcsecs cy^{-1} (Duncombe 1958, Fricke 1972), appeared quite successful. The theoretical results of Aoki and Kakuta (1971) indicated that electromagnetic coupling at the core-mantle boundary could explain a 0.1 arcsec cy^{-1} discrepancy but Rochester (1973) had reservations about their approach and emphasized the complexity of the problem and the need for more sophisticated levels of geophysical modelling.

In a subsequent paper (Rochester 1976), specific flaws in Aoki's work were mentioned, the principal one being the neglect of inertial fluid coupling between the core and mantle. Rochester showed that the combined effect of inertial and frictional coupling made only a minor, if not negligible, contribution of 0.0004 asecs cy^{-1} towards explaining any real discrepancy. It has also been pointed out that deficiencies in the planetary theories are not responsible either (Krasinsky 1975).

A more recent study of observational data by Duncombe and Van Flandern (1976) has reduced the discrepancy between observation and theory to 0.01 ± 0.05 asecs cy^{-1} indicating that there may not be a large error after all. If the new space ranging methods are capable of determining variations in the obliquity to within 0.01 asecs from one year of data (see e.g. Kaula 1973) then a discrepancy as large as that observed by Duncombe (1958) and Fricke (1972) would be detected after about 10 years of continuous observation.

2.4.3 Polar Motion

2.4.3.1 Chandler Wobble

To assert that the CW has been the most studied spectral feature of all the earth's 'free' rotation modes is probably an understatement. Astronomers and geophysicists alike have explored the nature of this wobble in an effort to learn more about the hidden properties of the earth's interior and the oceans.

Approximately 80 years of monitoring polar motion has enabled the CW period to be determined with an uncertainty of approximately one percent (see e.g. Wilson 1979). Theoretical explanations for the difference between the EW and CW period have also been successful within the bounds

of the observational uncertainty and the effects of elasticity, fluid core and oceans now seem well understood. Smith (1977), for example, has calculated 403.6 days for the period of a realistic oceanless, elastic earth model, which includes a neutrally stable fluid core, and has shown that the result is insensitive to the earth model.

Equilibrium theories for the ocean tidal response to the CW have been formulated (see e.g. Dahlen 1976). According to Dahlen, the equilibrium pole tide lengthens the period of Smith's (1977) model by 27.6 days, while realistic non-equilibrium considerations do not change this result significantly (Lambeck 1980). Including the effect of mantle anelasticity brings the predicted CW period to about 434 days (ibid. 1980), compared with 431 ± 4 days from observations (Wilson 1979).

Most analysts are reluctant to specify an exact period because the spectral peak is typically broad. A broad peak can indicate two possibilities (1) the data are noisy and (2) the wobble is undergoing excitation and damping. The variable excitation and damping also prompts related questions on energy dissipation and the nature of the excitation mechanisms which obviously have maintained the wobble for such a long time.

A convenient measure of the energy lost in an oscillating system which is randomly excited and then damped is the quality factor Q (see e.g. Merriam and Lambeck 1979, Anderson and Minster 1979). Low values of Q indicate high levels of dissipation, thus making the search for an energy sink difficult (Jeffreys 1956). Q estimates for the earth at the CW frequency (Q_{cw}) are derived from astronomical data and generally range from 30 to 100 (see e.g. Yatskiv and Sasao 1975, Wilson 1979), although substantially larger values have also been reported (see e.g. Graber 1976, Ooe 1978, Wilson and Vicente 1980).

In the past, energy sinks have been sought outside the mantle because the majority of Q_{cw} estimates for the earth were less than those determined at seismic frequencies for the mantle. In an extensive review of the problem, Smith and Dahlen (1981) investigated whether the difference between the observed Q_{cw} for the Chandler wobble and the Q for the mantle observed at frequencies in the seismic band might be due

to variations of the Q for the mantle with frequency. This possibility had been suggested previously by others (see e.g. Jeffreys 1978, Anderson and Minster 1979). Using CW, tidal and free oscillation data, Anderson and Minster (1979) conclude that the variation of Q for the mantle is proportional to the cube root of the frequency; a result which they note is consistent with laboratory measurements of the transient creep and internal friction of solids at high temperature. However, the implication for mantle rheology of a transient creep model inferred from this result is not consistent with post-glacial rebound data (Peltier et al. 1980). On the other hand,some evidence presented by Smith and Dahlen (1981) suggests the possibility that there may not be any variation of Q for the mantle with frequency. If this is the case, then the question of mantle dissipation of wobble energy is still very much open and energy sinks will have to be sought elsewhere. The role of the core in these considerations appears to be minimal since core-mantle coupling is weak during wobble (Rochester 1974), however, the oceans cannot be ruled out (Wunsch 1974).

The pole tide is the ocean tide induced by the CW. The response is generally assumed to follow equilibrium laws, in which case, the tidal amplitude is about 1/2 cm. If this assumption is correct then wobble energy cannot be dissipated in the oceans. However, characteristics of the pole tide have been observed at a sprinkling of sites around the globe and there is some evidence which suggests the response actually departs from equilibrium at least regionally in both phase and amplitude (see e.g. Dickman 1979a for a recent summary). Such departures could play a significant role in the damping of the CW.

In his examination of the problem, Dickman (1979a) theoretically models a wide variety of non-equilibrium situations that may occur on a global basis and also in the North and Baltic seas. The models encompass order of magnitude changes in the equilibrium amplitude and phase lags up to 120°. The time taken for these tides to damp the CW and their corresponding impact on the period of the CW were calculated. For the models considered, the results show a non-equilibrium contribution to the CW period ranging from -57 to 200 days and an ocean capacity to

damp the CW amplitude in accordance with the observed Q_{cw} values. Nevertheless, in order for the validity of the less plausible tidal models to hold, unrealistic changes in present core models are necessary to allow overall agreement with observation. Smith (1977) considered a suite of stable and moderately stable stratified core models and found the effect on the CW period to vary by only a few days at the most.

The real question that must be answered is 'How strong is the observational evidence for a non-equilibrium pole tide?' At the moment, there is only weak support for the existence of a non-equilibrium global pole tide (Haubrich and Munk 1959, Miller and Wunsch 1973) and it seems mere conjecture to state otherwise when the two most important parameters in the problem are not well defined. The observed amplitude and phase varies appreciably from site to site (see e.g. Currie 1975, Hosoyama et al. 1976, Naito 1977, Daillet 1979) and may also depend on record length (Hosoyama et al. 1976). The latter authors also suggest qualitatively that non-equilibrium features at low and high latitudes tend to cancel causing the overall effect on the CW to vanish. Until these aspects and the large scatter in Q_{cw} values are cleared up the dissipation question will remain unresolved.

An attractive alternative to the above problem is to argue that two distinct periods exist within the CW spectral peak. This model has already been proposed by some researchers as a means of surpassing the dissipation problem (see e.g. Gaposhkin 1972). Alternatively, Pedersen and Rochester (1972) stress that a homogeneous data set of length much greater than eighty years must be available and the analysis methods be closely scrutinized before splitting of the Chandler peak is seriously considered.

The search for CW excitation mechanisms has also been difficult. At present there are two possibilities; namely, the sideband effects associated with the annual redistribution of atmospheric mass and the mass redistribution accompanying large earthquakes. Munk and Hassan (1961) originally dismissed atmospheric excitation, claiming that the sidebands did not contain enough power to sustain the CW. Wilson and

Haubrich (1976) revived the issue, but could only attribute 25% of the CW variability to the atmosphere. Lambeck (1980) believes that part of the missing power could be a result of the inadequate coverage of surface pressure data over Central Asia and observational uncertainty. The basis of this suggestion is the noticeable difference in the results by Wilson and Haubrich, Siderenkov (1973) and Jochmann (1976) for the annual atmospheric excitation function. All studies are based on different data sets. Ooe (1979) has compared the irregular fluctuations of the atmospheric excitation function given by Kikuchi (1975) with the irregular fluctuations in the IPMS polar motion data. The comparison is accomplished by subtracting off the seasonal and long-period terms from each respective data set. The correlation between the two curves, however, is quite poor and only reaffirms Lambeck's suspicions about the data.

The suggestion that earthquakes could play a role in CW excitation was first given this century by Milne (1906). The earthquake excitation hypothesis was dismissed by Munk and McDonald (1960) but later revived by Mansinha and Smylie (1967) after they realized the significance of the pioneer work done by Press (1965) on earthquake displacement fields. Since then a variety of solutions to the problem have been formulated (see e.g. Smylie and Mansinha 1971, Dahlen 1973). Initially, the theoretical diversity of each approach generated much debate on the extent to which the CW could be excited by a large earthquake but a recent study by Mansinha et al. (1979) suggests that most of the differences appear to have been resolved.

The theoretical study by Smith (1977) shows that the coseismic displacements during the 1960 Chilean earthquake could have shifted the figure axis by 0.65 metres and that there could have been an additional motion of 0.86 metres if the precursory motion suggested by Kanamori and Cipar (1974) is correct. O'Connell and Dziewonski (1976) have evaluated the cumulative seismic excitation function from 234 large earthquakes ($M > 7.8$) that occurred between 1901 and 1970 to yield a synthetic curve that resembles the observed CW during the same period. They conclude that earthquakes provide about 50% of the energy needed to explain the CW

variance but Wilson and Haubrich (1977) believe the estimate is too large by a factor of 2.

Haubrich (1970) and Dahlen (1971) have argued previously that attempts to correlate changes in the pole path with earthquake occurrences will remain inconclusive so long as the noise levels in the astronomical data stay at their existing levels (see also Smylie et al. 1973). The situation is unclear to say the least and although it is tempting to suggest that a combination of atmospheric and seismic processes may produce the necessary energy for excitation the fact is the combined excitation function is not much better than either contribution alone (Lambeck 1980). Space ranging data will be a most welcome asset in this area.

2.4.3.2 Annual Term

Superimposed on the CW is a forced seasonal variation which is generally attributed to meteorological effects. For analysis purposes, it is desirable to separate this term from the Chandler component. This is usually accomplished by either a least-squares harmonic approach if long data series are available (see e.g. Yumi 1970) or a non-linear technique like MESA if the record length is short (see e.g. Wells and Chinnery 1973).

It is difficult to separate these components because it is likely that the respective amplitudes for both have a time dependency. As well as CW damping and excitation, there is now observational evidence (see e.g. Chollet and Debarbat 1972) which indicates that year-to-year variations in global weather patterns could affect the constancy of the annual amplitude. Their study shows the annual term in the latitude of the Paris observatory varying between 0.04 and 0.10 asecs in amplitude over a period of 14 years. Wells and Chinnery (1973) find a significant inconsistency between the observed amplitude and phase of the annual component at individual stations and stress the importance of determining the local and regional biases in the latitude measurements. Lambeck (1980) also notes the significance of these factors and suggests they may be partially responsible for the discrepancy between the observed annual amplitude and that derived from geophysical data.

To first order, the amplitude of the annual component can be accounted for by the seasonal redistribution of atmospheric mass. The earliest evaluation was undertaken by Spitaler (1897) and since then Munk and Hassan (1961), Siderenkov and Chvykov (1973), Jochmann (1976), Wilson and Haubrich (1976) and many others have estimated this contribution. A precise computation must account for the response of the oceans to pressure variations over and above the mean pressure. In the work reported to date, the calculations agree reasonably well for zero ocean response but not for an inverted barometer response (Lambeck 1980).

The groundwater contribution (i.e. water stored in the water table, as snow, in lakes and vegetation) and the seasonal ocean variations are also very important for comparing the observed and calculated phase of the annual term (Jeffreys 1972). For a given area, the groundwater storage is a function of the precipitation, runoff, evaporation and transpiration rates (Manabe 1969). At the moment only limited computations can be undertaken because (1) accurate rates of runoff are extremely difficult to obtain on a global basis and (2) data for essential effects (e.g. radiation rates, air humidity and wind velocity), which are needed to compute the rates of evaporation and transpiration, are generally not available (Lambeck 1980). Instead, empirical relations have to be used to estimate the global water balance (see e.g. van Hylckama 1956,1970).

The seasonal changes in sea-level are caused mainly by (1) wind stress, (2) temperature and salinity changes, (3) atmospheric pressure effects and (4) ocean tidal excitation, but not all these factors will contribute. In particular, changes in temperature and salinity will alter the specific volume of water but not the mass. These so-called steric changes do not load the Earth and therefore will not contribute to the annual excitation function. Seasonal ocean currents and winds are further possibilities although they are mainly controlled by geostrophic forces. The effects of such forces on polar motion would vanish when integrated over the entire earth if there were no land areas (Munk and MacDonald 1960). Sanchez (1979) has investigated the effect of ocean tidal excitation on polar motion and has shown that the annual component of the

potential displaces the spin axis by 0.012 asecs, a contribution which amounts to about 10% of the observed variation.

Other short-period terms are also evident in the polar motion spectrum. A semi-annual term has been observed in the Kimura z term but its amplitude is close to the noise level of the observations. Although the astronomical evidence is not really convincing at the moment, there could be sufficient meteorological excitation at the semi-annual frequency to generate a semi-annual wobble (Lambeck 1980). Ocean tidal excitation can also play a dominant role in this regard. Sanchez (1979) computes wobble amplitudes due to the ocean tides of 0.01 and 0.002 arcsecs at the semi-annual and monthly periods, respectively. These have yet to be confirmed by observation. Additional terms with periods ranging from 19 to 34 months have also been reported by Sugawa et al. (1973) but their origin is still uncertain. Sasao (1978) discusses ways in which the earth tides can induce small wobbles. These effects, like the FDPM, should be removed before the actual observations are used to determine the CW and annual terms.

2.4.3.3 Long Period and Secular Trends

Analyses of the ILS and BIH astronomical data have shown that the polar motion records contain a secular variation (see e.g. Poma and Proverbio 1976). Often called secular polar motion (SPM) or polar wandering, this feature still has an uncertain origin but can be explained two ways.

The first involves the dynamical principle which equates the geographical movement of the mean spin axis with shifts in the figure axis that are caused by mass transfer mechanisms (see e.g. Goldreich and Toomre 1969). Since the spin axis is dynamically constrained to cycle closely about the figure axis then a change in the position of the mean spin axis reflects a displacement of the figure axis provided the observations are free from systematic error. If errors of this type are present they will cause an 'apparent' secular trend in the polar motion spectrum. Changes in station coordinates due to continental drift (see e.g. Dickman 1977) and errors in star catalogues (Guinot and Feissel 1968) are just two phenomena that can produce apparent effects.

The concept of SPM is by no means novel. Discussions on the subject are found in the classic work by Darwin (1877) and later on by Inglis (1957) but understanding the origin and extent of the trend has not been easy. To date, researchers have used paleomagnetic and astronomical data in their pursuits. Paleomagnetic evidence indicates that the spin axis could have moved, over the past 115 million years, at an average rate of about 0.1 milliarcsecs per year in a direction approximately 220°E of Greenwich (van der Voo 1978). However, these estimates have uncertainties which are the same order of magnitude as the measured rate. Van der Voo (1978) and Jurdy (1981) also note that the direction of the motion is quite variable and depends, to a large extent, on the data used to reconstruct the plates.

Many attempts have been made to estimate the secular trend from astronomical evidence since Lambert's (1922) analysis of the first 18 years of ILS data. Table 2.4, taken from Poma and Proverbio (1976), summarizes the numerous determinations since 1922. In all cases, the ILS data were used to deduce the annual rate and its direction. The general rate is about 0.003 asecs yr^{-1} in a direction 290°E of Greenwich and is in good agreement with recent results obtained from BIH data (ibid. 1976).

At present, the results from paleomagnetic and astronomical evidence disagree,with the rate deduced from the astronomical evidence being about an order of magnitude larger. The discrepancy may be due to a number of factors including (1) systematic errors in each data set and (2) different record lengths. However, since the astronomical data only span a period which in geological terms is very short, it is likely that the observed astronomical trend is merely a transient one. The results from paleomagnetic evidence are based on rock samples whose ages are greater than 10^5 years. It seems probable that during this length of time the spin axis could have moved at rates similar to those inferred from ILS and BIH data, but that on the average such motions have cancelled out.

Table 2.4 Rates and Direction of Secular Polar Motion (taken from Poma and Proverbio (1976)

Author	Year	Angular Velocity	Direction (longitude E)	Period of Observations
Lambert, W. D.	1922	0".0066/yr	277	1900-1918
Kimura, H.	1924	58	293	1900-1924
Wanach, B.	1927	47	318	1900-1925
Wanach, B. and Mahnkopf, N.	1932	63	276	1900-1911
Wanach, B. and Mahnkopf, N.	1932	51	298	1900-1923
Hattori, T.	1947	45	287	1900-1939
Hattori, T.	1959	359	294.8	1900-1947
Markowitz, W.	1960	32	300	1900-1959
Yumi, S. and Wako, Y.	1966	296	287.1	1933-1966
Stoyko, A.	1967	32	290.2	1890-1966
Proverbio, E. et al.	1971	294	294.4	1900-1962
Proverbio, E. et al.	1972	277	299.3	1900-1962
Proverbio, E. and Quesada, V.	1973	307	290.4	1900-1969

One common source of systematic error in the paleomagnetic and astronomical data is that introduced by continental drift. Jurdy and van der Voo (1974), realizing the significance of lithospheric plate motions in their interpretation of paleomagnetic data, have used a least-squares algorithm to separate the absolute term due to SPM from the observed displacement field. Similar methods have also been used in the interpretation of SPM results based on astronomical data. Soler and Mueller (1978) and Dickman (1977) have calculated the secular changes in the station coordinates of the ILS and IPMS networks using the plate velocity models of Solomon et al. (1975) in order to see whether SPM is simply an artifact which appears when such changes are not taken into account. Their results are in close agreement and indicate that only 10 to 20% of the observed shift can be explained by station drift. Uncertainties in the stellar proper motions have also been ruled out as an important source of error (Guinot and Feissel 1968).

The suggestion and theory which relates a gradual mass redistribution occurring on or within the earth's surface to secular perturbations in the earth's inertia tensor and rotation was first put forward by Darwin (1877). Since then numerous investigations on the subject have been undertaken. Current opinion favors the effect of a redistribution of mass between the Greenland ice regions and the oceans as the most probable cause of the observed secular trend (Lambeck 1980). The contribution from plate tectonic mass transfer appears to be small.

Munk and MacDonald (1960), Cazenave (1975), Dickman (1979b) and Nagiboglu and Lambeck (1980) have all considered the effect of deglaciation and the associated rise in sea-level on the long-term secular behaviour of the earth's rotation. Although this phenomenon appears significant to first order, the gravitational and viscoelastic interactions between the melting ice, rising sea-level and the elastic earth need to be known on a global basis before an accurate calculation can be made (Farrell and Clark 1976). The geophysical data are just too sparse, at present, to enable a complete calculation.

The same predicament occurs when modelling and calculating the rotational consequence of plate tectonic mass transfer. Different types of

mechanisms have been investigated but the reliability of the models is still questionable. Several assumptions can be invoked when modelling these mechanisms. One is to assume that mass is merely being displaced in active seismic zones while the second assumes that mass is accumulating temporarily in subduction zones and dispersing from spreading zones (Mather and Larden 1978). Over geological timescales ($>10^5$ years) the displacement model is clearly the most plausible. Mass accumulation and dispersion are conceivable over shorter periods (possibly $<10^2$ years) but isostatic processes must dominate over longer periods.

Soler and Mueller (1978) have calculated the changes in the inertia tensor using a model that only incorporates the crustal portion of the earth. The corresponding secular motion of the spin axis was calculated and found to be negligible, almost zero, compared with the observed trend. However, the model they formulated failed to take into account the density changes that occur when (1) the lithospheric material in subduction zones moves underneath the continental plate into the underlying asthenosphere (see e.g. Isacks et al. 1968) and (2) the rotational part of the earth's equatorial bulge moves to conform with the new position of the figure axis (Goldreich and Toomre 1969). Both these factors must be taken into account in the formulation of future geological models for plate tectonic mass transfer.

Mantle convection (Takeuchi and Sugi 1972) and the destruction and generation of crustal material along plate boundaries (Liu et al. 1974) are further phenomena that can cause SPM. However, the assumptions made in both these studies need further clarification before the conclusions are taken seriously. Earthquakes (see e.g. Mansinha and Smylie 1967, Smith 1977) also appear significant. Since the possibility that the astronomical data are reflecting a transient secular feature in polar motion cannot be ruled out, this would suggest that both the astronomical and paleomagnetic results may indeed be compatible. Moreover, if future studies verify deglaciation as the major contributor, then more sophisticated models for the mass redistribution occurring in regions of extreme seismic activity may not be needed for this purpose.

The only other appreciable long-term variation in polar motion that appears in the astronomical data has a period of about 30 years (see e.g. Vicente and Currie 1976). Busse (1970) suggests that this decade scale mode is associated with movements of the solid inner core but this would only be valid if large density contrasts existed in the region of the outer core. Recent seismic data indicates that this is not likely to be the case. Lambeck (1980) has differenced the BIH and ILS data and shows evidence to suggest that the decade wobble may simply be a consequence of the observing or reduction process and not a real excitation at all. Further study is needed.

2.4.3.4 Diurnal Polar Motion

Probably the most controversial feature associated with the liquid core is the torque-free nearly diurnal polar motion (NDPM). Referred to by Rochester (1973) as the nearly diurnal free wobble, the motion appears as a homogeneous term in the solution of the equations of motion and, therefore, its amplitude and phase can only be determined by observation. Hough (1895) and Sludskii (1896) first predicted the NDPM as a retrograde cyclic movement of the spin axis relative to the earth's surface with a period approximately 3 minutes short of a sidereal day. NDPM must not be confused with FDPM or the NDFN because the latter motions are not of core origin (see Secs. 2.2.3.1 and 2.4.2.2). If the NDPM is viewed in a space-fixed system it appears as a free nutation with a period of several hundred days. Toomre (1974) calls this mode the principal core nutation (PCN).

The kinematical relation which connects the NDPM with the PCN is very similar to the relation connecting the CW with the NDFN (see Rochester et al. 1974 for respective mathematical developments). Earth models chosen by Jeffreys and Vicente (1957a,b) indicate the PCN/NDPM ratio for both amplitude and period to be about 460. Values based on models used by Molodensky (1961) are quite different. One is in close agreement with 460, the other being 204. Other estimates discussed by Jeffreys (1980) are equally discrepant and this illustrates the importance of choosing good models for mantle and core structure when studying this mode.

It might be thought that the diversity of these theoretical results pointed to measurements of the PCN as being a useful constraint for modelling the earth's structure. However, Wahr (1979) has shown this not to be the case. Using three of the latest most heavily constrained models based on seismic data, he obtained PCN/NDPM ratios all within 1% of 458.

Previous attempts to observe either the PCN or the NDPM have been treated with skepticism. Early analysts (see e.g. Popov 1963) were more interested in observing the NDPM, yielding values of the order 0.01-0.02 asecs. Toomre (1974) stressed, however, that these results were inconclusive because they suggested the PCN had an amplitude about 460 times larger. The existence of a nutation term this large with a period of several hundred days clearly was refuted by observational evidence.

Rochester et al. (1974) reconsidered the problem and from an analysis of declination data gathered at the Loomis observatory, established an upper limit of 0.12-0.26 asecs for the PCN amplitude in the frequency domain of 0-4 cycles per year (c yr^{-1}). Adopting a ratio of 460, the corresponding upper limit for the NDPM amplitude was 0.0003-0.0006 asecs. This estimate is clearly more realistic in view of the current observational evidence.

Ooe and Sasao (1974) and Yatskiv et al. (1975) sought an explanation for Popov's (1963) extremely high value for the NDPM amplitude and, after examining his method of analysis, realized that he had observed a combined variation in polar motion and nutation. This implies that Popov's estimate actually refers to the PCN amplitude. The situation is still uncertain and further research is needed. Data from the lunar laser ranging experiment are presently being analyzed for this specific purpose. Preliminary results indicate that the PCN amplitude does not exceed 0.005 asecs and perhaps may be even smaller (Wahr and Larden 1981).

2.4.3.5 Irregular Fluctuations

From time to time irregular fluctuations occur in polar motion that are very difficult to explain. For example, a sudden change was observed by the BIH, IPMS and DMA during the period May to December 1974 (BIH 1975). The extent of the irregularity is shown in Figure 2.5.

The rationale for the existence of these fluctuations can have either an observational or geophysical basis. From an observational standpoint, such trends could be the result of systematic errors. For example, Alley and Bender (1968) have shown that a 1×10^{-8} per km gradient in the index of refraction at a PZT station produces a 0.02 asec deflection in vertical observations. If similar conditions were to exist over the Eurasian continent with a periodic signature of six months then a trend similar to the one observed during 1974 is feasible.

Geophysical bases for the appearance of these fluctuations have been discussed in Section 2.4.3.1 If the sudden changes are real they should correlate well with times when mass redistribution occurs. Earthquakes are certainly capable of producing short-period variations in polar motion (Smith 1977) but considerable research effort is needed to see whether the atmosphere or the core has sufficient power at periods less than one year to produce short-period fluctuations. Larden (1981) has made an effort to verify the 1974 irregularity using LLR data. Results of the analysis indicate the trend may be real, however, the data over two critical lunations appear seriously affected by systematic errors. This prevents definite conclusions to be drawn. The verification of wobble excitation times is most important if excitation mechanisms are to be identified. Clearly, the space ranging methods will be the leading contributors in the future.

2.4.4 Spin Rate

Aspects of the Earth's variable rate of rotation, or spin rate, and their geophysical causes have been recently investigated and reviewed by Lambeck (1980). From equation (2.10) it is easy to show that a change in the spin rate, or equivalently, length of day (l.o.d.) and Universal Time are related to m_3 according to (Munk and MacDonald 1960)

$$m_3 = \frac{w_3 - \Omega}{\Omega} = - \frac{\Delta(\text{l.o.d.})}{\text{l.o.d.}} = \frac{d(\text{UT1-IAT})}{dt} \quad . \qquad (2.18)$$

As mentioned previously in Section 2.2.3.2 the observed quantity is not

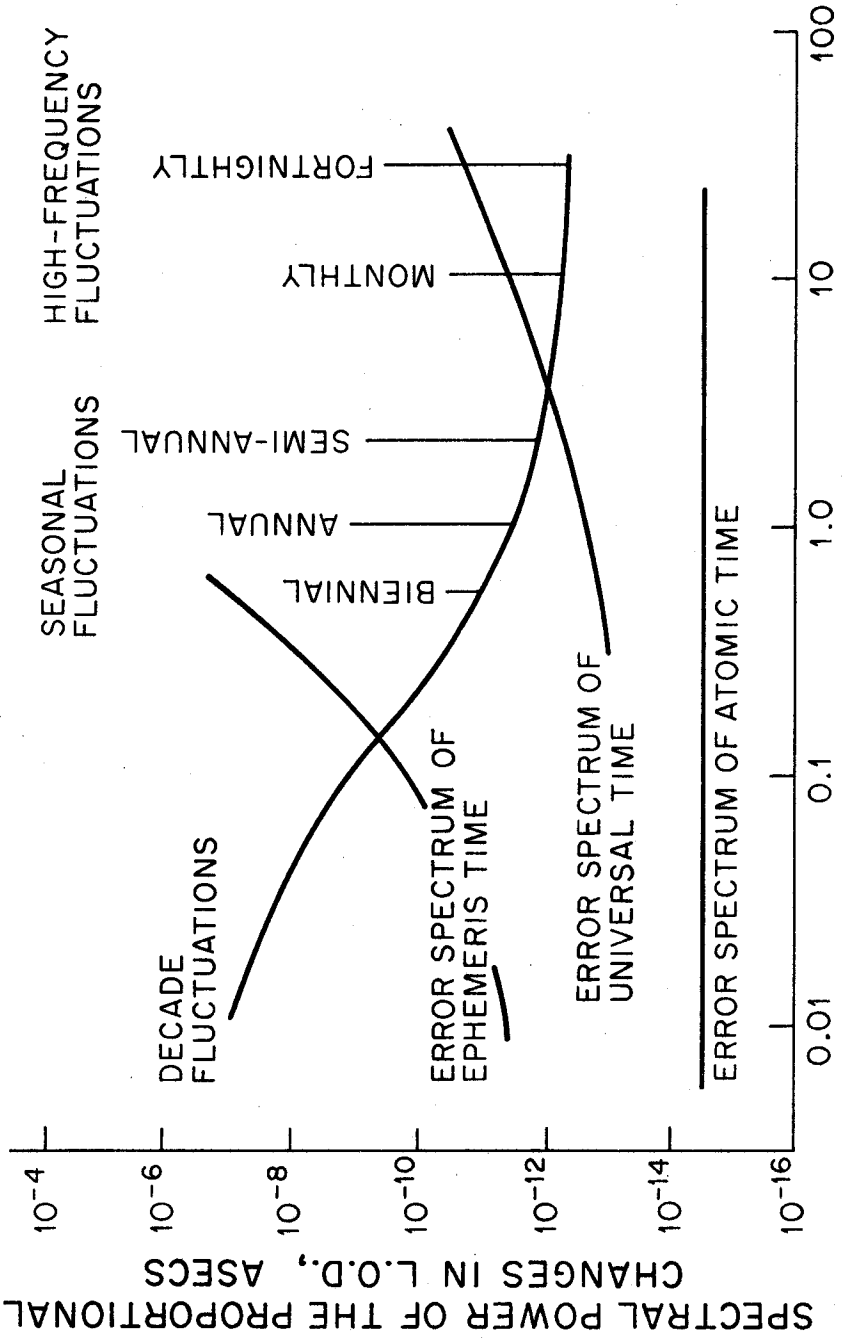

Figure 2.6 Schematic Power Spectrum of the Proportional Changes in the Length of Day

really the m_3 but the integrated amount by which the earth is slow or fast after a certain elapsed time interval with respect to a uniform spin rate.

Often regarded as the richest spectrum of all, the earth's spin rate contains many observable features of geophysical and astronomical origin. Figure 2.6, after Lambeck (1980), is a schematic of the power spectrum for the proportional changes in the l.o.d. The discussion which follows here serves only to summarize the main features of this spectrum, their causes, and those areas where space ranging measurements can make important contributions. Pertinent information has been extracted from recent articles by Lambeck and Cazenave (1974,1977), Rochester's (1973) review paper and Lambeck (1980).

2.4.4.1 Long Period and Secular Trends

Prior to the development of atomic clocks, only long-period fluctuations and the secular deceleration of the earth's spin rate $\dot{\Omega}$ could be measured. Dissipation of tidal energy has long been considered the most suitable explanation for the secular deceleration or increase in l.o.d. (Munk and MacDonald 1960). Figure 2.7 illustrates the principle behind this phenomenon. Due to frictional processes, a portion of the tidal energy is absorbed by the solid earth and oceans and this causes a lag in the tidal response. The phase lag, in effect, is the angle (δ_T) between the line of maximum bulge and the direction to the tide-producing body. Since the two are misaligned, a net torque is exerted on the bulge by the tide-producing body causing a slowing of the earth's spin rate.

The lunar torque is the main contributor, being about 4 to 5 times larger than its solar counterpart (Rochester 1973). Minor contributions come from non-tidal sources. Those suggested are (1) gradual changes in the earth's mass distribution from post-glacial isostatic rebound and (2) torques within the earth, for example, electromagnetic coupling between the core and mantle (Lambeck 1980).

Astronomical observations give a direct measure of $\dot{\Omega}$ but cannot distinguish between the steady retardation due to tidal friction $\dot{\Omega}_{(T)}$

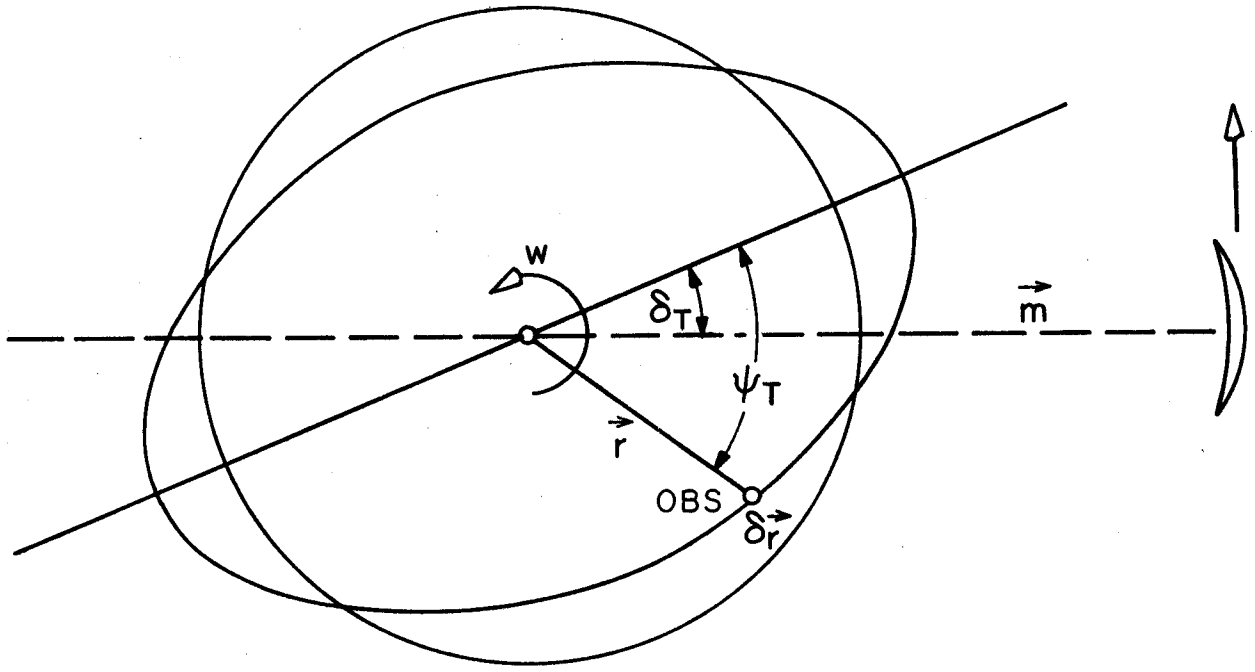

Figure 2.7 Frictional Tide Response. If there is no dissipation, then $\delta_T = 0$. The notations are added to enable further referencing from Chap. 3 and thus avoid duplication.

and the non-tidal contributions $\dot{\Omega}_{(NT)}$. However, separation can be accomplished by observing the associated orbital deceleration of the moon (Munk and MacDonald 1960). In the case of the moon, the angular momentum lost by the earth due to the action of the lunar torque is transferred to the lunar orbit. Assuming Kepler's third law and the conservation of angular momentum within the earth-moon system, one observes an increase in the mean earth-moon distance and a decrease in the lunar mean motion $\dot{n}$ (see Stacey 1977 for a discussion). Once $\dot{n}$ is known the lunar contribution to the earth's tidal deceleration can be directly evaluated. The solar contribution is less significant but once both are known estimates of $\dot{\Omega}_{(NT)}$ can then be made.

Lambeck (1979) outlines two indirect ways of measuring $\dot{n}$ and hence $\dot{\Omega}$. They are (1) the evaluation of the tidal energy dissipated in the oceans using ocean tide models and (2) the use of satellite derived second degree harmonics of the ocean tide potential to calculate the rate of work done on the ocean surface by the lunisolar potential. Astronomical observations, on the other hand, generally place estimates of $\dot{n}$ in the range -20 to -30 asecs cy^{-2} (see e.g. Morrison and Ward 1975, Muller 1976). Data from the lunar ranging experiment has also been used to determine $\dot{n}$. Williams et al. (1978) deduce a value for $\dot{n}$ of 23.8 $\pm$ 4 asecs cy^{-2} which has since been re-estimated, without significant change, by Dickey et al. (1980) using data through May 1980. Calame and Mulholland (1978) also give similar values. This indicates that LLR is a good source of information on $\dot{n}$. Lambeck (1977) documents the theory that permits an evaluation of $\dot{n}$ from satellite-derived ocean tide parameters. Application of the theory by Felsentreger et al. (1978 ,1979) and Goad and Douglas (1978) to data from various low-altitude satellites gives values of $\dot{n}$ that also fall within the domain determined by lunar laser ranging.

Observed values of $\dot{\Omega}$ are about 50 times larger than $\dot{n}$ while the non-tidal contribution to $\dot{\Omega}$ is about a factor of 10 larger than $\dot{n}$ but of opposite sign (see Lambeck 1977,1979). These rates imply that energy is being dissipated at a rate approximately equal to 4×10^{19} ergs/sec (Lambeck 1977).

Estimates of $\dot{\Omega}$ and $\dot{n}$ have also been obtained from paleontological data (Scrutten 1978). Recent results are in good agreement with astronomical, satellite and lunar ranging results (Lambeck 1980).

In addition to the earth's deceleration, there are several long-period fluctuations in the l.o.d. Figure 2.8, after Lambeck and Cazenave (1977), illustrates the periodic nature of the variations that occurred between 1820 and 1940. The maximum change in the l.o.d. occurred during the period 1870 to 1900 and corresponds to about 1 part in 10^7 or 9 msecs. Once again, electromagnetic coupling of core motions to the mantle or possibly topographic coupling seem to be the most plausible excitation mechanisms for these variations (see e.g. Hide 1977).

Lambeck and Cazenave (1976) have looked at the long-period spectral features of the atmospheric and oceanic mass redistributions and find that the relevant components can, at the most, explain only 20% of the observed changes between 1820 to 1940. The meteorological excitation function also lags the observed variations by about 10 to 15 years indicating that the two seemingly correlated phenomena may have a common origin. Recently, Currie (1980,1981) suggested that solar activity may be responsible for an 11-year signal in the l.o.d. A similar signal has also been found in surface air temperature (Currie 1979) and sea-level (Currie 1976) records but whether these effects are real remains to be seen. Some additional information may come from the FGGE program (see e.g. Hide et al. 1980).

2.4.4.2 Seasonal Variations

The improvement in time standards led to the detection of several periodic variations in the earth's spin rate. Discussed in this section are the annual, semi-annual and quasi-biennial terms, all owing their existence to some extent to the change in the earth's angular momentum produced by the zonal wind circulation (see e.g. Lambeck 1980).

The annual term, having by far the largest amplitude (approximately 20-25 msecs) of the three, is sustained by the variable solar energy received by the atmosphere as the earth orbits the sun. Munk and Miller (1950) were the first to interpret the annual change to be of wind

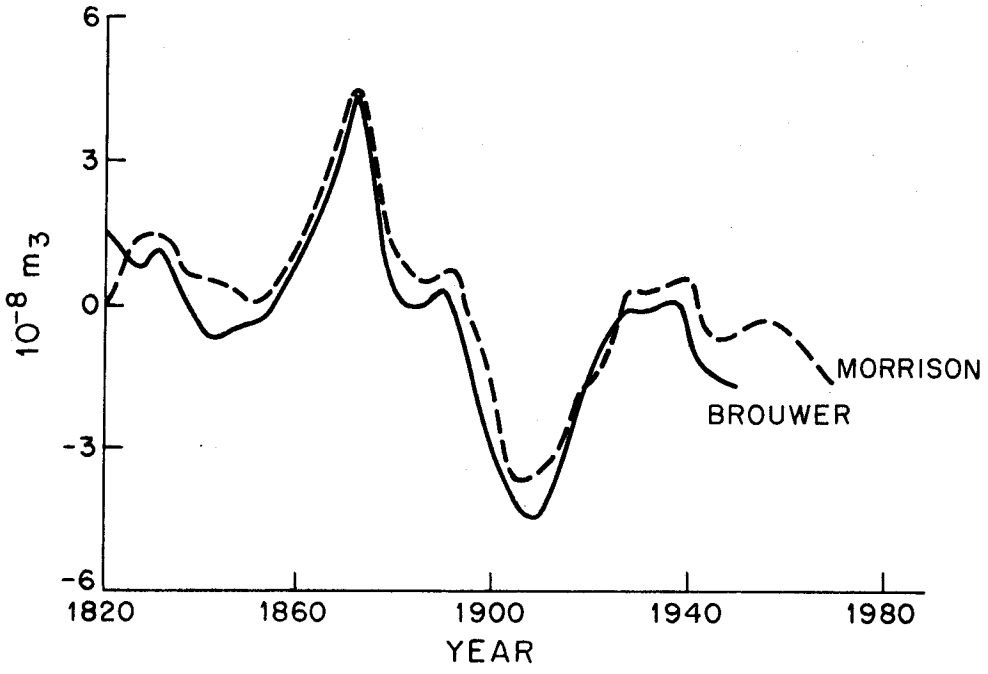

Figure 2.8 Long-Period Variations in m_3 since 1820 (taken from Lambeck and Cazenave 1977)

origin and when Munk and MacDonald (1960) recomputed the excitation function with additional data they found that 60% of the annual variation could be explained by this mechanism. Lambeck and Cazenave (1973) reconsidered the problem when they discovered that no attempt had been made to re-evaluate the new wind data that had become available since then. Their results were very instructive, showing that 96% of the annual variation in the l.o.d. during the period 1958 to 1961 could be explained by the zonal wind circulation.

Another related and important aspect of the annual term is its time variation. Year-to-year fluctuations in amplitude and phase are evident in the astronomical data but uncertainties in this data do not permit an adequate evaluation at present (Lambeck 1980). However, attempts are being made to resolve some of the issues using newer and independent data (see e.g. Lambeck and Hopgood 1979).

With regard to the semi-annual term, about 50% of the observed amplitude of about 9 msecs is attributed to the solar-induced earth tide. Seventy-six percent of the remaining non-tidal contribution can be explained by the zonal wind circulation (Lambeck and Cazenave 1973) but there are potentially important gaps in the wind data at high latitudes which, if filled, could provide better agreement (Lambeck 1980). Atmospheric, oceanic and groundwater variations make negligible contributions at the semi-annual frequency (Munk and MacDonald 1960).

The possibility that relativistic effects could cause annual and semi-annual changes in the l.o.d. was recently pointed out by Nordtvedt and Will (1972). This possibility arises because of a prediction from gravitational theory that the Cavendish constant may change as the earth orbits the sun. In response to this change, the earth's self-gravitational pull should change causing the earth to "breathe" inwards and outwards (Misner et al. 1973). As a result, there will be a corresponding change in the earth's moments of inertia which will give rise to small annual and semi-annual variations in the l.o.d.

Rochester and Smylie (1974) suggest that these effects may be observable if the meteorological excitation functions are known with precision.

Quasi-biennial variations in the l.o.d. were first reported by Iijima and Okazaki (1966). Their results revealed a term with a 26-month period but Markowitz (1970) later observed a term near 24 months and pointed out that it was not strictly periodic. An earlier analysis of the tropical zonal wind data uncovered a quasi-biennial oscillation which varied between about 20 and 30 months (Dartt and Belmont 1964). Lambeck and Cazenave (1973) have also examined the biennial oscillation and established quantitatively a relation between the biennial wind circulation and the rather irregular quasi-biennial oscillation in the l.o.d. The amplitudes of the excitation and observed functions agree to within 8% and the phases to within 5 degrees. Their results highlight the biennial oscillation as a non-stationary phenomenon; a fact supported by harmonic analysis of the BIH astronomical data which shows spectral lines near 2 to 3 years.

It is clear that tremendous progress has been made in understanding the seasonal variations in the l.o.d. The possibility of using astronomical and space ranging data to formulate boundary conditions for future global wind circulation models must be contemplated (Lambeck 1977).

2.4.4.3 High Frequency Perturbations

Apart from the seasonal, biennial, long-period and secular variations, the l.o.d. spectrum also exhibits considerable power at higher frequencies. Harmonic analysis of the BIH astronomical data shows several peaks in the frequency range 0.3 and 36 cycles/year (Lambeck and Cazenave 1974). Munk and MacDonald (1960) suspected irregularities in the zonal wind and ocean circulation as the cause of these anomalous fluctuations but noted, of course, that features with periods near one month and two weeks were of tidal origin.

Lambeck and Cazenave (1974) have shown quantitatively that all the irregular variations in spin rate in the frequency domain of 0.3 to 6 cycles/year are of zonal wind origin. Order of magnitude estimates by

these same authors also show zonal winds playing a dominant role in explaining l.o.d. variations with frequencies higher than 6 cycles/year. However, this is not entirely unexpected since the global atmospheric circulation exhibits a broad continuum from about 8 months down to a few days (Mitchell 1976).

Large and rapid variations of a non-periodic nature also occur from time to time in the l.o.d. One of these was reported by Guinot (1970) as a 10 msec jump in Universal Time over a five-day interval during April 1968. This anomaly has been investigated by Lambeck and Cazenave (1974) but it is still not clear whether this is a real fluctuation caused by the rapid propagation in latitude of the zonal westerlies in the northern hemisphere or just unusual noise in the BIH results. In a subsequent review paper, Lambeck and Cazenave (1977) stress the importance of determining the meteorological contribution to such changes before making any related geophysical interpretations.

2.5 Future Perspective

The main criteria to be met by any measuring system with a potential for monitoring the earth's rotation are: (a) the system must provide information at a frequency compatible with the desired sampling interval and (b) the quality of the data must satisfy a standard which allows current ambiguities between observation and theory to be resolved.

Establishing a desired sampling interval and accuracy standard can be accomplished jointly, by simply examining the observed and theoretical aspects of the earth's rotation and assessing the criteria in this fashion. This review chapter was written specifically for this purpose. In particular, the discussion of Section 2.4 clearly shows that observational discrepancies, differences in theoretical treatments and differences between theory and observation are still prevalent; some issues requiring resolution at the 5 cm level. Detection of sudden changes in the earth's spin rate is also very important and, therefore, makes the acquisition of daily information imperative.

Past history has shown, however, that the established techniques described in Section 2.3.1 cannot meet the requirements set out in the preceding paragraph. Moreover, if VLBI measurements succeed in providing frequent earth rotation information then the only outstanding question for those concerned about the future monitoring of the earth's rotation is the role of the laser ranging techniques.

Overall success at monitoring the earth's rotation by LAGEOS ranging will depend on whether the short-period perturbations in the satellite orbit are small enough to enable short-period fluctuations to be identified (Bender and Goad 1979). For LLR, the errors in the orbit and librations have periods greater than fourteen days and so the detection of short-period changes by this technique should be possible if there is sufficient data.

LAGEOS, on the other hand, can be tracked more frequently than the moon, thereby indicating the capability of the system to provide all the necessary information on polar motion. In contrast to this, LLR is more suitable for measuring long-term variations in the earth's spin rate because the lunar orbit is very stable over these time intervals. It is partially for these reasons that Silverberg (1979) suggests a pooling of both LAGEOS and LLR resources as the most cost-effective approach.

Nevertheless, before deciding on the future role of the laser ranging techniques, important questions still have to be answered. One concerns the extent to which the LLR technique can provide daily information on the earth's rotation at the 5 cm accuracy level. The numerical work in Chapter 5 has been carried out to answer this question. As a means of introducing this work, the important aspects of the LLR experiment are discussed in the next chapter. These include the precise modelling of the range measurements, improvements in the parameters of the earth-moon system and finally the status of the LLR network. The mathematical models discussed in Chapter 3 are then simplified in Chapter 4 to a form more suitable for the variance studies of Chapter 5.

CHAPTER 3

THE LUNAR RANGING EXPERIMENT

3.1 Introduction

The acquisition of high-accuracy distance measurements between the earth and the moon has opened the way for a vast improvement in our understanding of the dynamics within this system. Since 1969 over 2500 normal points, representing about 24000 photon returns, have been obtained at the McDonald Observatory. At present, the typical measurement uncertainty is 10 to 15 cm. In the future, it is hoped an accuracy of 2 to 3 cm will be obtained from a worldwide network of stations, however, recent progress towards this objective has been slow.

Nevertheless, numerous scientific objectives have already been accomplished through the analysis of the data gathered thus far. They include (a) improved determinations of the lunar orbit, the selenodetic coordinates of the reflectors, the geodetic position of McDonald and the earth-to-moon mass ratio (b) accurate values of the fractional moments of inertia and several low degree and order harmonics of the lunar gravity field from measurements of the physical librations (c) an accurate check on gravitational theories, in particular, the Nordtvedt effect, and (d) studies of the earth's rotation and its irregularities.

The basic models used for the analysis of LLR observations are (a) the orbital motions and space orientations of the earth and moon (b) the observatory coordinates and their time variations due to solid-body tides and polar motion (c) the coordinates of the retroreflectors and (d) the relativistic and refractive effects on the photon path. In the following section a detailed description of the time-delay computation is given together with the formulation of the range residual. A summary of the improvements in the model parameters over the past decade is then given and the present status of the experiment examined.

3.2 Precise Modeling of the Time Delay

The analysis of lunar laser ranging data not only requires observations of the earth-moon distance but also a physical model that enables the distance to be predicted mathematically. Differences between these two quantities, that is, the residuals, can be analyzed to improve the parameters occuring in the prediction model. The model must take into account the basic physical laws which govern the passage of light through the medium which separates the earth and moon as well the orbits and rotations of these two bodies. Since the travel path of the photon through the solar gravitational field is subject to relativistic effects and the accelerations of the earth and moon in space are not the same, it is necessary to formulate the prediction model in a space-fixed system because the abovementioned effects would be obscured in a purely geocentric calculation (Mulholland 1977). A barycentric coordinate system is chosen together with an appropriate theory of relativity. Formulation of the mathematical model in a geocentric frame is only permissible when acceleration effects and possible relativistic effects are corrected for. This approach is followed in Chapter 4 where a more simplified model is discussed and developed for the variance studies carried out in Chapter 5.

Another consideration worthwhile noting before embarking on an outline of the prediction process concerns the use of the term 'distance'. Mulholland (1975, 1977) emphasizes that measurements to the moon are not measurements of distance in the true sense of the word even though it is convenient to think of them as such. The observation is really a time-delay because the times of photon transmission, reflection and detection do not occur simultaneously. Nevertheless, it is a good approximation to treat the process as if the distance were measured instantaneously; the mind seems to rest easier if it can visualize an observation in terms of distance rather than time. An appropriate value for the speed of light c, serves as the intermediary constant which relates both quantities.

The following outline of the precise time-delay computation is based primarily on information documented by Mulholland (1977) and Stolz (1979).

3.2.1 Time Scales, Coordinate Systems and Basic Concepts

As discussed earlier in Section 2.2.3.2, three major time scales enter into the reduction process of lunar range data. They are (1) Universal time (2) Dynamical time and (3) International atomic time. Universal time, or more specifically UT1, is needed because it is a direct measure of the earth's diurnal rotation in space. Dynamical time is the time argument in the ephemeridies of the planets, the earth-moon mass centre and the moon. In Newtonian applications, dynamical time is often referred to as Ephemeris time while for relativistic applications, the term Coordinate time is sometimes preferred. However, to avoid confusion and remain consistent with previous documentations of the time-delay computation the term Ephemeris time (ET) will be used throughout this work in place of Dynamical time. Ephemeris time, therefore, refers to the time argument in the ephemeris which incorporates the theory of general relativity. The third scale, International atomic time, is the best approximation to uniform time currently available and, as such, should define the unit of time in applications of this type (Mulholland 1972). As the discussion proceeds, the role of these time scales becomes more obvious.

The three coordinate systems employed in the time-delay computation are (1) the 1950.0 barycentric mean equatorial system, (2) the earth-fixed system described in Section 2.2.2.1 and (3) a selenocentric lunar-fixed system. The barycentric frame is assumed to be fixed in space and has its origin at the centre of mass of the solar system (≡ barycentre). It differs, in two respects, from the ecliptic frame (see Section 2.2.2.1) which can be used to monitor the earth's rotation in space. Firstly, the reference plane of the barycentric system is the mean equator of 1950.0 instead of the mean ecliptic and secondly, the origin is no longer at the geocentre. Reasons for the change in origin are given above. It is a routine matter to calculate the transformation

parameters that relate these two systems. Standard formulae are given, for example, in the Explanatory Supplement.

In the usual development of the equations of motion, the lunar-fixed reference system coincides with the principal axes of inertia, however, to define these axes accurately one needs recourse to observations and a theory for the lunar rotation. The rotation is generally described by three Euler angles which are derived according to Cassini's laws of synchronous motion and departures therefrom. In some developments, these angles are given with respect to the mean ecliptic of date (see e.g. Mulholland 1977) in which case additional transformations are needed if the 1950.0 mean equatorial system is chosen as the inertial frame (see Section 3.2.3). Since the rotation is a function of the fractional momenta of inertia and the low degree harmonics of the lunar gravity field, partial derivatives must be derived in order to locate the principal axes in a position which best fits the observations in a least squares sense (see Section 3.3.1).

The lunar-fixed reference system is defined such that the x_{1_m} axis coincides with the axis of greatest moment of inertia. This axis points roughly in the mean direction of the earth as a result of the moon's synchronous and librational motions. The x_{3_m} axis coincides with the axis of least moment of inertia. It points roughly in the direction of the moon's spin axis. The system is right handed and the subscript m distinguishes the lunar-fixed system from the earth-fixed system.

Apart from the optical librations, which are computed directly from Cassini's laws, most of the remaining librational motion is produced by the torque exerted on the moon by the earth as the former moves through the earth's gravitational field. These are called the physical librations and are discussed in more detail in Section 3.3.2. Integration constants also appear in the equations of motion and these terms constitute the 'free' librations. As in the case of polar motion, the amplitude and phase of the 'free' librations can only be determined by observation although their periods can be predicted from theory (see section 3.3.2).

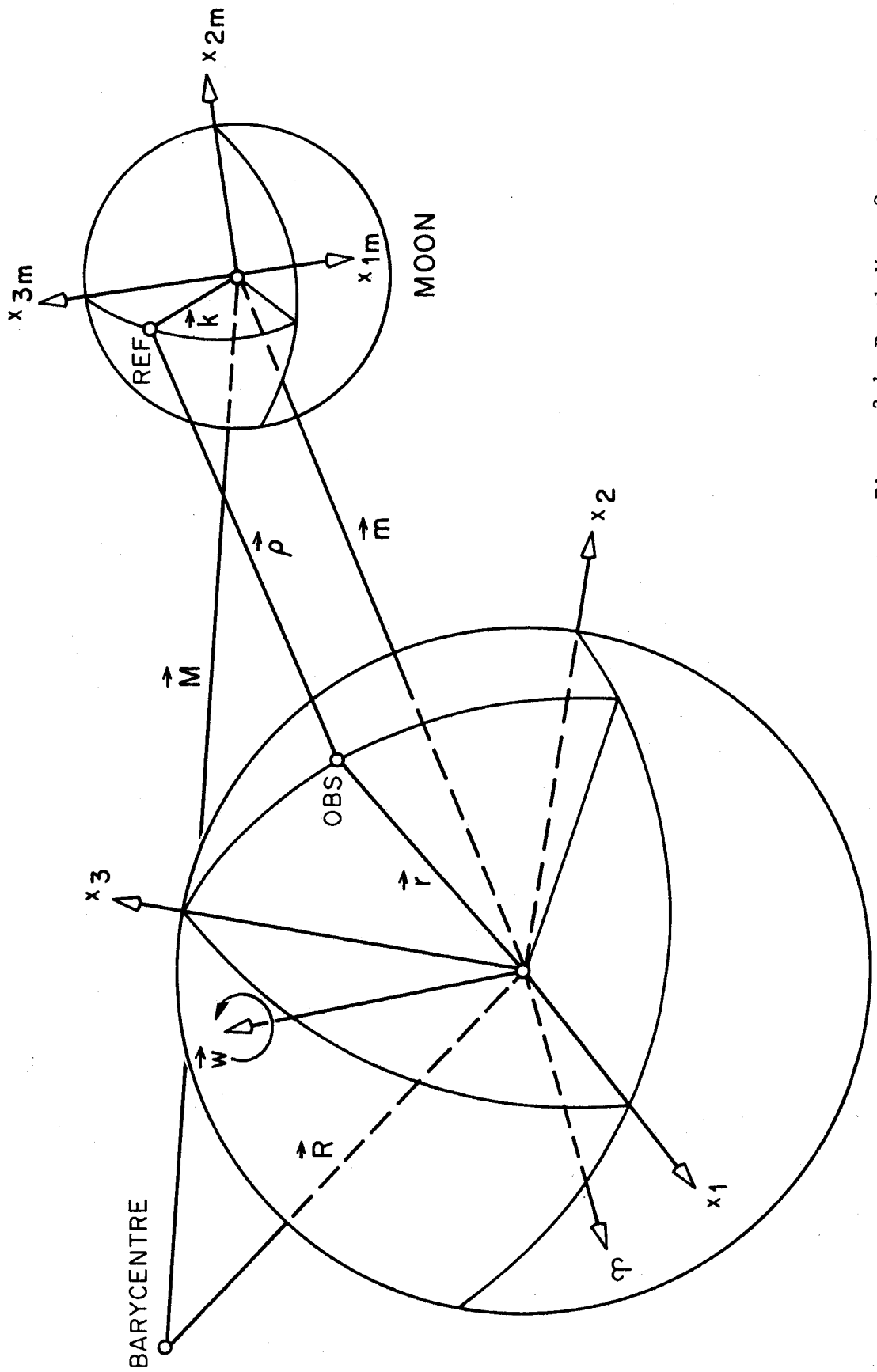

Figure 3.1 Earth-Moon Geometry

All quantities which enter into the time-delay computation have to be expressed in the same coordinate system. The 1950.0 barycentric mean equatorial system is chosen for the ephemeris and needed for a solution are the ephemeris coordinates of (a) the telescope at the time of transmission (b) the reflector at the time of reflection and (c) the telescope at the time of detection. Figure 3.1 gives a basic illustration of the geometry of the earth-moon system. The orbits of the earth and moon are denoted by the vectors $\vec{R}$ and $\vec{M}$ respectively, the vector $\vec{r}$ denotes the telescope position in the earth-fixed system x_i and $\delta\vec{r}$ its time variations due to tidal and loading effects, the vector $\vec{m}$ gives the components of the earth-moon distance in the barycentric frame and $\vec{k}$ the reflector position in the lunar-fixed system x_{i_m}.

The ephemeris coordinates of the telescope are obtained by modelling the sidereal, polar, nutational and precessional motions of the vector $\vec{r}$ (see Chapter 2), transforming the vector $\vec{r}$ back into the 1950.0 barycentric system in accordance with these motions, and adding to the result the ephemeris coordinates for $\vec{R}$. The ephemeris coordinates for the reflector are obtained in a similar, but not identical, fashion once the ephemeris coordinates for $\vec{M}$ and the libration angles have been determined.

Corrections for relativistic, refractive and instrumental effects are introduced to ensure all measurable quantities are not omitted. Carrying out the prediction in the framework of Einstein's general relativity, as opposed to the Newtonian model, ensures that (1) the orbital accelerations of the earth and moon, (2) the behaviour of the observatory clock as it moves through the gravitational field of the solar system and (3) the curvature of the photon path are all taken into account. Atmospheric refraction also causes curvature in the photon path and must be included along with an instrumental calibration constant.

In the next three Sections 3.2.2, 3.2.3 and 3.2.4 a step-by-step description of the prediction calculation is presented. Vector and

matrix notation are used to simplify the presentation. More specific aspects are referenced where appropriate.

3.2.2 Ephemeris Position of Telescope at Transmission Time

Calculating the ephemeris coordinates of the telescope involves a series of transformations to account for the earth's rotational motions, corrections for the earth tide effects and a conversion from Universal time to Ephemeris time. The spin axis is arbitrarily chosen as the reference axis for the transformations (Mulholland 1977) even though any one of the dynamical axes previously mentioned in Chapter 2 could have been adopted.

Since the earth-fixed system x_i moves with respect to the spin axis as a result of polar motion, it is obvious that during a series of measurements to the moon, the telescope vector $\vec{r}$ will continually change its orientation relative to this axis. This movement is measured as a function of UTC (see Section 2.2.3.2) which is always defined in terms of IAT. If t_t(UTC) denotes a photon transmission time and one assumes the spin axis passes through the geocentre then the instantaneous position $\vec{r}'(t_t)$, of the vector $\vec{r}$ relative to the spin axis and the instantaneous equator (plane orthogonal to the spin axis and passing through the geocentre) is

$$\vec{r}'(t_t) = R_1[y]R_2[x]\vec{r} \quad . \tag{3.1}$$

x and y define the spin axis position as measured in a plane which is tangential to the x_3 reference pole of the earth-fixed frame x_i (see BIH 1978). $R_i[\phi]$ is a 3 x 3 matrix representing a counter clockwise rotation of the coordinate system through an angle ϕ about the ith axis as viewed down the positive direction. It is consistent in form and convention with the rules adopted by Kaula (1966, p. 14) and Goldstein (1950, p. 99) for a right-handed system. Although the BIH and other services adopt a left-handed system for publishing x and y (see Section 2.3.1.1), equation (3.1) has been formulated in such a way to maintain the convention of the BIH system and still allow the use of Kaula's (1966) rotation scheme. Mulholland (1977) and Stolz (1979) do not

elaborate on the sign convention adopted for their developments so their equations must only be considered in general terms.

Several data sets of x and y are available (see Section 2.3). The BIH publish in their annual reports various sets including raw (unsmoothed), combination (Doppler plus BIH), Vondrak smoothed and now recent values deduced from LAGEOS (BIH 1978). LLR analysts opt for another BIH set, the 5-day Circular D smoothed values, which are readily available every month. However, these values contain the annoying 'dynamical' variations of latitude (FDPM) because the BIH reduction program uses the nutations of the spin axis instead of the mean figure axis of the mantle (see Sections 2.2.3.1 and 2.4.2.2 for further comments). Williams (1974) adopts McClure's (1973) elastic earth calculations and corrects the BIH values by

$$\begin{aligned}\delta x = {} & 0.0087 \sin\theta - 0.0065 \sin\{\theta-2(F+\Omega)\} - 0.0029 \sin\{\theta-2(F-D+\Omega)\} \\ & - 0.0013 \sin\{\theta-\ell-2(F+\Omega)\} - 0.0012 \sin\{\theta-2F-\Omega\} \\ & + 0.0012 \sin\{\theta-\Omega\} + 0.0005 \sin\{\theta-\ell\} + 0.0005 \sin\{\theta+\ell\} \end{aligned} \tag{3.2a}$$

$$\begin{aligned}\delta y = {} & -0.0087 \cos\theta + 0.0065 \cos\{\theta-2(F+\Omega)\} + 0.0029 \cos\{\theta-2(F-D+\Omega)\} \\ & +0.0013 \cos\{\theta-\ell-2(F+\Omega)\} + 0.0012 \cos\{\theta-2F+\Omega\} \\ & -0.0012 \cos\{\theta-\Omega\} - 0.0005 \cos\{\theta-\ell\} - 0.0005 \cos\{\theta+\ell\} \end{aligned} \tag{3.2b}$$

The corrections δx and δy are expressed in units of arcseconds and must be added to the Circular D values $x_{\text{circ D}}$ and $y_{\text{circ D}}$. θ is the angular equivalent of Greenwich sidereal time and ℓ, F, D and Ω are the fundamental arguments from Brown's lunar theory. Substituting equations (3.2a,b) into (3.1) and rewritting in terms of $x_{\text{circ D}}$ and $y_{\text{circ D}}$ gives

$$\vec{r}'(t_t) = R_1\left[y_{\text{circ D}}+\delta y\right] R_2\left[x_{\text{circ D}}+\delta x\right]\vec{r}' \tag{3.3}$$

In addition to the rotations described by equation (3.3), the vector $\vec{r}$ has to be corrected for earth tide distortions and variations due to ocean, atmospheric and groundwater loading. At present, no attempt is made to correct the measurements made at McDonald observatory for loading distortions since these variations are not significant at

the 10 cm measurement precision level. This assumption is examined more closely in Chapter 7 in view of the expected laser ranging accuracy goals of 1-3 cm. The radial distortions due to earth tides, however, can be as large as 50 cm peak-to-peak, but like the spin axis coordinates x and y, this correction does not vary significantly during the 2.5 second return journey time of the photon. In other words, if t_d(UTC) denotes the detection time of the photon then $\vec{r}'(t_t)$ will equal $\vec{r}'(t_d)$ to well within the computation accuracy. It is, therefore, accepted practice to leave this correction until a later stage of the computation (see equations 3.27-3.28).

Having transformed the vector $\vec{r}$ from the earth-fixed system x_i to a frame defined by the instantaneous equator and spin axis it now follows to transform $\vec{r}'(t_t)$ into the 1950.0 barycentric system X_i. This is accomplished via the Greenwich apparent sidereal time GAST, the nutation matrix [N] and the precession matrix [P]. The quantities which enter into the transformations include (figure 3.2), (1) the nutation in ecliptic longitude $\Delta\psi$, (2) the nutation in obliquity $\Delta\varepsilon$, (3) the mean obliquity $\bar{\varepsilon}$, (4) the precession angles z, Θ and ζ_0, (5) the earth's angular position in space UT1, (6) the expression α_s, which defines the right ascension of the fiducial point to which UT is referred (see Explanatory Supplement 1961) and (7) the ephemeris time appropriate to the transmission time t_t(UTC), that is, t_t(ET).

One may start by computing the nutation parameters $\Delta\psi$ and $\Delta\varepsilon$ for the spin axis since these quantities, along with UT1, $\bar{\varepsilon}$, and α_s, are needed to calculate the GAST. At the moment, Melchior's (1971) corrections based on Molodensky's (1961) Earth Model 2 are added to Woolard's (1953) rigid earth values to account for elastic and liquid core effects (Williams 1974). Denoting Woolard's values as $\Delta\psi_r$ and $\Delta\varepsilon_r$ then $\Delta\psi$ and $\Delta\varepsilon$, expressed in arcseconds, are given as

$$\Delta\psi = \Delta\psi_r - 0.0043\ \sin\{2(F+\Omega)\} - 0.0411\ \sin\{2(F-D+\Omega)\} + 0.0193\ \sin\ell'$$
$$+ 0.0441\ \sin\Omega - 0.0017\ \sin\{\ell'+2(F-D+\Omega)\} + 0.0036\ \sin\ell$$
$$- 0.0003\ \sin\{\ell+2(F+D)\} \qquad (3.4a)$$

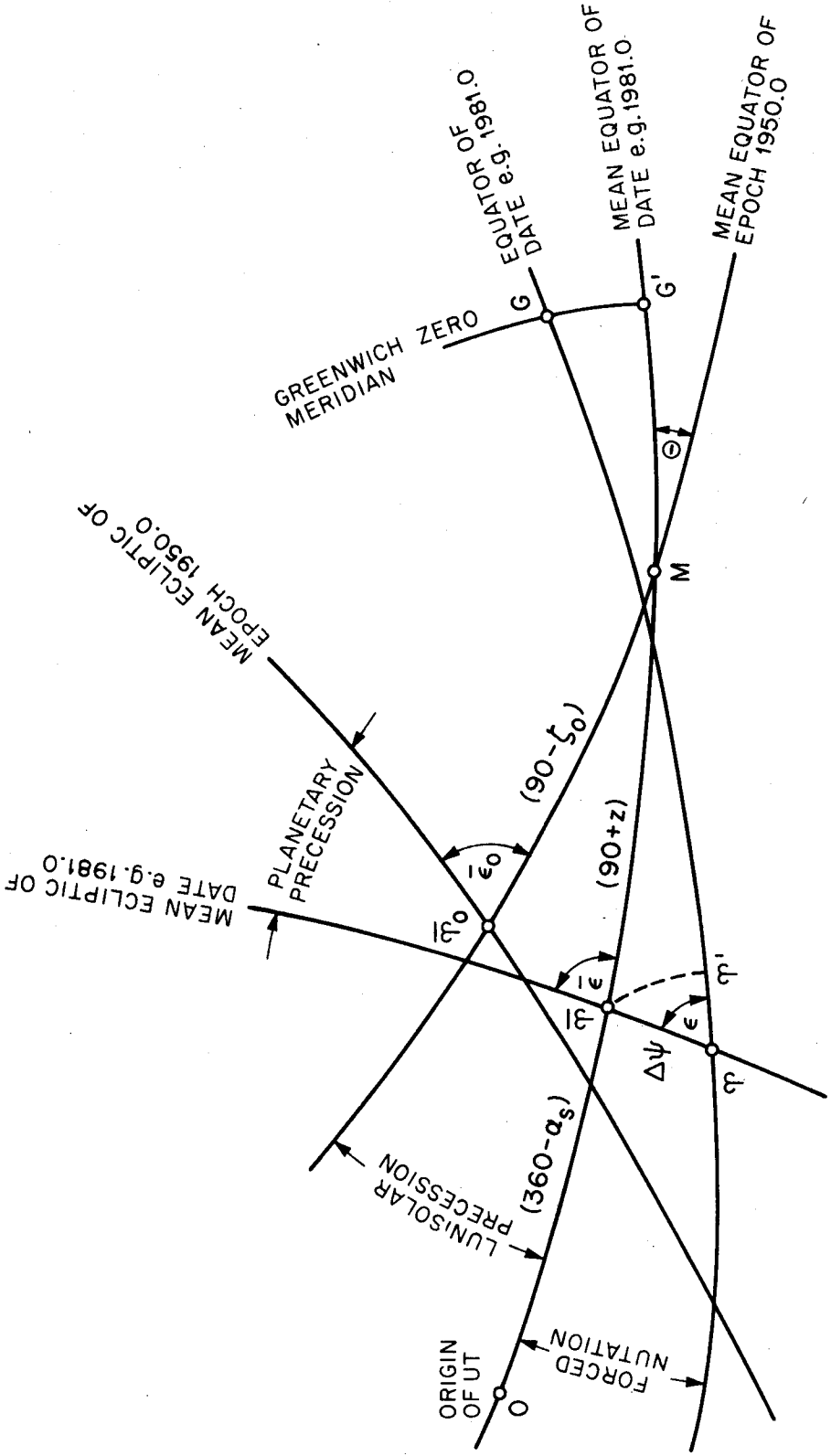

Figure 3.2 Precession, Nutation and Sidereal Angles

Schedule for Figure 3.2

Notation	Description
$\bar{\gamma}_0$	Mean Equinox of Epoch 1950.0
$\bar{\varepsilon}_0$	Mean Obliquity of Epoch 1950.0
$\bar{\gamma}$	Mean Equinox of Date e.g. 1981.0
$\bar{\varepsilon}$	Mean Obliquity of Date e.g. 1981.0
γ	Instantaneous Equinox of Date e.g. 1981.0
ε	Instantaneous Obliquity of Date e.g. 1981.0 $\varepsilon = \bar{\varepsilon} + \Delta\varepsilon$
$\Delta\psi$	Nutation in Ecliptic Longitude
$\Delta\varepsilon$	Nutation in Obliquity
θ, z, ζ_0	Precession Angles
OG'	$\equiv$ UT1
γG	$\equiv$ GAST = θ
$\gamma\gamma'$	$\Delta\psi \cos\varepsilon$

$$\Delta\varepsilon = \Delta\varepsilon_r + 0.0022\ \cos\{2(F+D)\} + 0.0202\ \cos\{2(F-D+\Omega)\} + 0.0056\ \cos\ell'$$
$$- 0.0086\ \cos\Omega + 0.0008\ \cos\{\ell'+2(F-D+\Omega)\} + 0.0004\ \cos\ell$$
$$+ 0.0002\ \cos\{\ell+2(F+\Omega)\} \qquad (3.4b)$$

The solar mean anomaly ℓ', together with the lunar parameters ℓ, F, D and Ω constitute the five fundamental arguments of the nutation theory. As the demand on computational accuracy increases in the future, it would seem imperative to consider Wahr's (1979) values for $\Delta\psi$ and $\Delta\varepsilon$ since these are based on realistic earth models such as that of Gilbert and Dziewonski (1975) and avoid the ad hoc computational approach used by others (see discussion in Section 2.4.2.2 for further comments).

Polynomial expressions for $\bar{\varepsilon}$ and α_s, as well as the precession angles z, Θ and ζ_0, are given in the Explanatory Supplement (1961). To evaluate $\Delta\psi$, $\Delta\varepsilon$, $\bar{\varepsilon}$, α_s, z, Θ and ζ_0 at the time of photon transmission, t_t(UTC) must be converted to ephemeris time t_t(ET) according to

$$t_t(ET) = t_t(UTC) + (IAT-UTC) + \delta_c + \Delta T(t_t) \qquad (3.5)$$

IAT-UTC relates UTC to IAT and allows for the constant adjustments which are made to UTC in order to keep the difference between UTC and UT1 reasonably small. It is an integer number of seconds defined by international convention. For example, during 1980 the value for IAT-UTC was exactly 19 seconds. The third term δ_c is basically an integration constant which accounts for the difference in the origins of IAT and ET at the initial epoch of IAT. The value for δ_c used by LLR analysts at JPL is 32.1843817 secs. ΔT_t includes periodic relativistic corrections which account for the behaviour of the observatory clock as it moves through the gravitational field of the solar system, or to express it differently, the periodic corrections to the observatory clock reading that would give the corresponding reading if the clock were co-moving with the solar system barycentre. For Newtonian applications, $\Delta T_t = 0$. However, within the framework of Einstein's theory of general relativity the expression developed by Moyer (1976) is the most recent and up-to-date. Expressing ΔT_t as a function of the first six major contributing terms gives

$$\Delta T(t_t) = 1.658 \times 10^{-3} \sin E + 3.17679 \times 10^{-10} \sigma \sin(UT+\lambda)$$
$$+ 5.312 \times 10^{-12} \sigma \sin(UT+\lambda-M) - 1.3677 \times 10^{-11} \sigma \sin(UT+\lambda+2L')$$
$$+ 1.548 \times 10^{-6} \sin D + 20.73 \times 10^{-6} \sin(L'-L_J) + ... \quad (3.6)$$

where $\Delta T(t_t)$ is in seconds, M and E are the mean and eccentric anomalies of the earth-moon mass centre in its orbit about the barycentre, respectively, σ is the spin axis distance to the observatory clock in km, λ the longitude of the clock measured eastward from Greenwich, L' the mean solar longitude, and L_J the heliocentric mean longitude of Jupiter.

The time argument UT, which appears in the second, third and fourth terms of equation (3.6) has, up until now, been loosely defined as a measure of the earth's rotational position in space with only an occasional passing reference to its precise definition (see above and Section 2.2.3.2). The origin of UT is, by definition, a fiducial point whose right ascension α_s, as measured on the mean equator to date (see Figure 3.2), has an identical time dependent motion to that of the 'fictituous' mean sun. A second order polynomial is used to describe the motion and the time argument is counted in UT (Explanatory Supplement 1961). UT is simply the hour angle of the fiducial point with respect to the Greenwich zero meridian plus 12 hours.

In practice, UT1 (UT corrected for polar motion) is used to evaluate ΔT_t (Moyer 1976). Values of UT1 are also published by the BIH in Circular D smoothed format as 5-day averages of the difference UT1-UTC. However, the smoothing process removes several tidally-induced variations in UT1, which for LLR applications, must be taken into account. Williams (1974) corrects the interpolated BIH value of UT1 at the transmission time t_t(UTC) according to the expression (Woolard 1959)

$$\delta UT1 = -k_2 \{2.47 \sin(2F+2\Omega)$$
$$+ 1.02 \sin(2F+\Omega) + 2.63 \sin\ell + 0.58 \sin(2D-\ell)\} \quad (3.7)$$

Only terms with period one month or less, that is, periods less than the BIH smoothing interval, and amplitude greater than 0.5 milliseconds are

included. δUT1 is given in milliseconds with 0.29 being a typical value for the Love number k_2 of degree 2. UT1 at the time of transmission t_t(UTC) can be written as

$$t_t(\text{UT1}) = t_t(\text{UTC}) + \text{UT1} - \text{UTC} + \delta\text{UT1} \tag{3.8}$$

Equation (3.8) thus defines the 'true' rotational position of the earth in space. It is true, not in an error-free sense, but only so far as the effects of polar motion are removed.

The point has now been reached where a series of rotations can be applied to the vector $\vec{r}'(t_t)$ to determine its components in the 1950.0 mean equatorial system at time t_t. The first step is to compute the Greenwich apparent sidereal time θ. The GAST can be expressed as

$$\theta = \bar{\theta}(t_t) + \Delta\psi \cos\varepsilon \tag{3.9}$$

where $\bar{\theta}(t_t) = t_t(\text{UT1}) + \alpha_s + 12^h$ is the Greenwich mean sidereal time. $\Delta\psi \cos\varepsilon$ accounts, to first order, for the motion of the instantaneous equinox of date relative to the mean equinox of date as measured along the instantaneous equator (see Figure 3.2). The rotation matrix for the GAST is simply

$$[S] = R_3[-\theta] \quad . \tag{3.10}$$

The negative sign denotes a clockwise rotation consistent with Kaula's (1966) convention. To continue the transformation of the vector $\vec{r}'(t_t)$ from the instantaneous equator of date to the 1950.0 mean equatorial system the nutation [N] and precession [P] matrices are needed. The nutation matrix is

$$[N] = R_1(-\bar{\varepsilon})R_3(\Delta\psi)R_1(\varepsilon) \tag{3.11}$$

where $\varepsilon = \bar{\varepsilon} + \Delta\varepsilon$ is the instantaneous obliquity of date, $\Delta\psi$ and $\Delta\varepsilon$ are computed from equations (3.4a,b) and the expression for $\bar{\varepsilon}$ is given in the Explanatory Supplement. The precession matrix consists of three rotations given by

$$[P] = R_3(\zeta_0)R_2(-\theta)R_3(z) \tag{3.12}$$

Once again, equations (3.11) and (3.12) are completely consistent and must be evaluated using Kaula's (1966) sign convention and the rotation angles as listed in the Explanatory Supplement. If $\vec{r}''(t_t)$ denotes the vector equivalent of $\vec{r}'(t_t)$ in the 1950.0 mean equatorial system then

$$\vec{r}''(t_t) = [P][N][S]\vec{r}'(t_t) \tag{3.13}$$

All that remains to complete the transformation is the computation of the barycentric coordinates $\vec{R}(t_t)$ for the centre of mass of the earth. These are extracted from the earth-moon ephemeris using the time argument $t_t(ET)$ from equation (3.5). Quantities tabulated in the present ephemeris include the barycentric position of the earth-moon centre of mass $\vec{R}_{em}(t_t)$ as well as the component of the earth-moon vector $\vec{m}$. The data are represented as coefficients of Chebyshev polynomials and are interpolated accordingly (Stolz 1979). In order to calculate $\vec{R}(t_t)$ the earth-moon mass ratio must be known. A constant $v = 1/(1+M_e/M_m)$, where M_e and M_m are the masses of the earth and moon respectively, is used to calculate the quantity $v\vec{m}$ which is subtracted from $\vec{R}_{em}(t_t)$ to deduce $\vec{R}(t_t)$, that is

$$\vec{R}(t_t) = \vec{R}_{em}(t_t) - v\vec{m} \tag{3.14}$$

The telescope coordinates in the barycentric mean equatorial system of 1950.0 are simply

$$\vec{\beta}(t_t) = \vec{r}''(t_t) + \vec{R}(t_t) \tag{3.15}$$

3.2.3 Ephemeris Position of Reflector at Reflection Time

With the conditions of the photon departure having been determined, the next step is to compute the barycentric coordinates of the reflector at the time $t_r(ET)$ when reflection occurs. The process is obviously an iterative one since the exact time of reflection is not known. As a first approximation, however, the reflection time can be estimated by

$$t_r(ET) = t_t(ET) + \tau_0/2 \tag{3.16}$$

where τ_0 is the observed time delay. A first approximation to the ephemeris position of the reflector can be obtained by interpolating the barycentric coordinates of the selenocentre $\vec{m}(t_r)$ and the Eulerian (libration) angles $\psi_m(t_r)$, $\Theta_m(t_r)$ and $\phi_m(t_r)$ of the lunar-fixed system x_{im} at time $t_r(ET)$. The lunar ephemeris used at JPL lists these quantities with respect to the mean equatorial system of 1950.0 (Williams, private communication 1980). The corresponding approximate ephemeris position $\vec{\sigma}_m(t_r)$ of the reflector whose lunar-fixed position is expressed by the vector $\vec{k}$ is

$$\vec{\sigma}_m(t_r) = R_3(-\psi_m)R_1(\Theta_m)R_3(-\phi_m)\vec{k} + \vec{M}(t_r) \tag{3.17}$$

However, in some applications (see e.g. Melbourne et al. 1968, Eckhardt 1973) the libration angles are given with respect to the mean ecliptic of date (Mulholland 1977). Denoting the Euler angles relative to the mean ecliptic of date, e.g. 1981.0, as $\psi'_m(t_r)$, $\Theta'_m(t_r)$ and $\phi'_m(t_r)$ (see figure 3.3) permits one to write the transformation of the vector $\vec{k}$ to the mean equatorial system of 1950.0 as

$$\vec{\sigma}_m(t_r) = [P]R_1(-\bar{\varepsilon})[L]\vec{k} + \vec{M}(t_r) \tag{3.18}$$

where

$$[L] = R_3(-\psi'_m)R_1(\Theta'_m)R_3(-\phi'_m) \tag{3.19}$$

is the libration rotation matrix. Equating equations (3.17) and (3.18) gives

$$R_3(-\psi_m)R_1(\Theta_m)R_3(-\phi_m) = [P]R_1(-\bar{\varepsilon})[L] \tag{3.20}$$

The evaluation of equation (3.17) or (3.18) together with the velocity of light c permits a second approximation to the reflection time

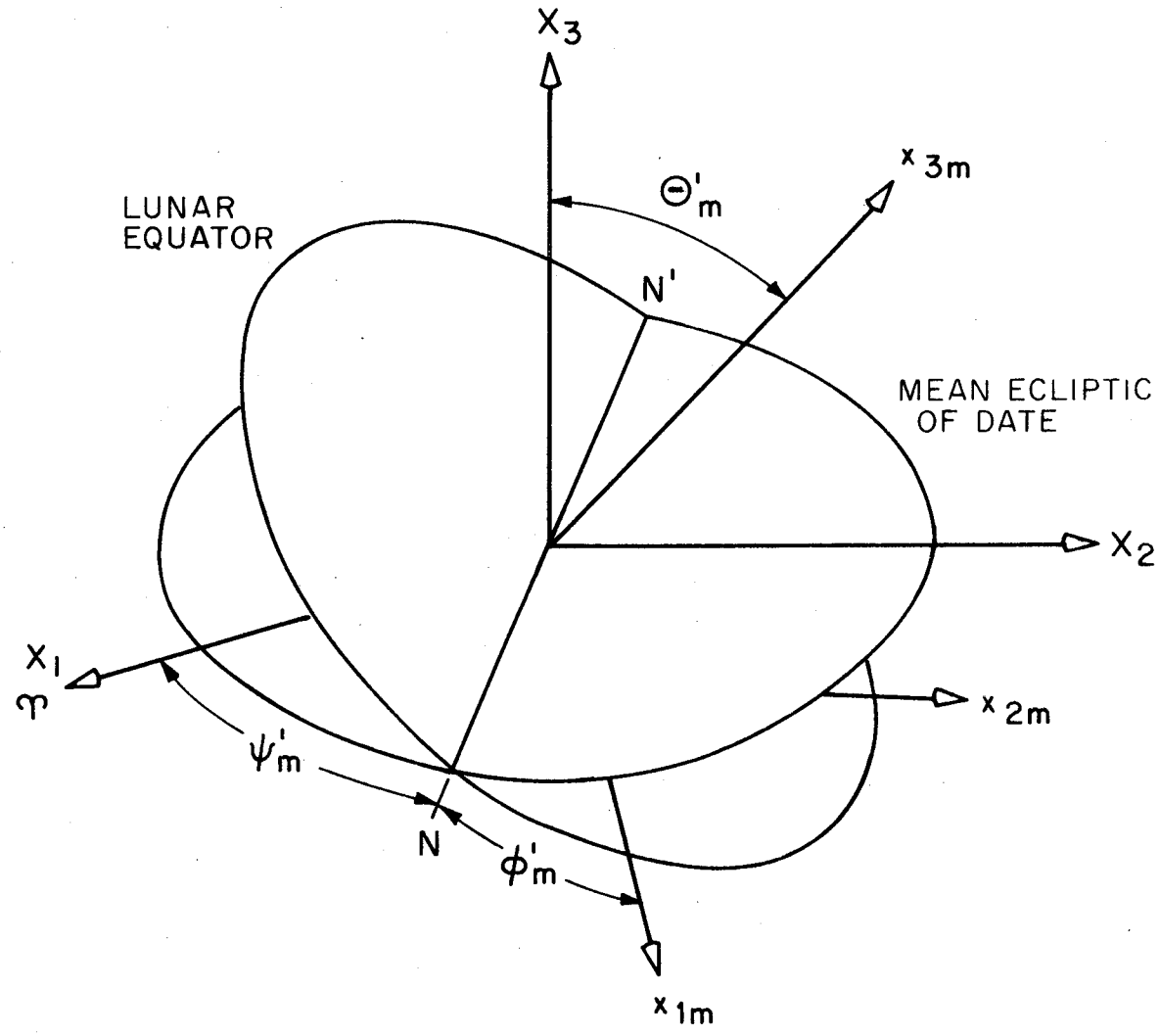

Figure 3.3 Orientation of the Lunar-fixed System with Respect to the Mean Ecliptic

$$t_r(ET) = t_t(ET) + c^{-1}|\vec{\sigma}_m(t_r) - \vec{\beta}(t_t)| \tag{3.21}$$

to be calculated. Unfortunately, the subtraction of $\vec{\sigma}_m(t_r)$ from $\vec{\beta}(t_t)$ will not give the exact one-way time delay to the reflector because the photon path through the gravitational field of the solar system and the earth's atmosphere is curved. These effects are of order 10^{-7} in the one-way time delay and, therefore, small enough to neglect temporarily during the iteration cycle between equations (3.17) and (3.21). However, once the difference to successive approximations $t_r(ET)$ is no longer significant the iteration for $\vec{\sigma}_m(t_r)$ is terminated and the curvature corrections made. About three orders of magnitude are gained for each iterative cycle if the Newton-Raphson method is used (Stolz 1979).

The time-delay of the photon path produced by the gravitational field of the solar system is deduced from Einstein's theory of general relativity. These equations have been solved exactly by Schwarzschild for a massless particle moving in the gravitational field of a single, spherically symmetric, massive body located at the origin of a non-rotating coordinate system. The particle trajectory is a geodesic curve and the increment in the one-way travel time over the Euclidean straight-line value is (Holdridge 1967)

$$\Delta_1 = \frac{(1+\gamma)\mu}{c^3} \ln a \tag{3.22}$$

where

$$a = \{\vec{\beta}(t_t) + \vec{\sigma}_m(t_r) + \vec{\rho}_c\}\cdot\{\vec{\beta}(t_t) + \vec{\sigma}_m(t_r) - \vec{\rho}_c\}^{-1}$$

and $\vec{\rho}_c = |\vec{\sigma}_m(t_r) - \vec{\beta}(t_t)|$ is the calculated vector joining the telescope and reflector. The Eddington-Robertson parameter γ, which describes the curvature of the photon path, is equal to unity for general relativity and μ denotes the gravitational constant of the solar system. Further details are given in Misner et al. (1973). Again, it is noted that Δ_1 will equal zero for Newtonian applications. The earth's atmosphere will

also increase the photon travel time over its Euclidean equivalent but this can be modelled very accurately by a linear function of the atmospheric surface pressure at the time of photon transmission (see e.g. Hopfield 1976). At the McDonald Observatory in Texas the correction applied is (Stolz 1979)

$$\Delta_2 = \frac{0.9869\{2.3835+0.00476(f^2-18.643)\}P}{299.7925\{\sin E + 0.00143\ \cos E(\sin E+0.0445\ \cos E)^{-1}\}} \tag{3.23}$$

where Δ_2 is in nanosecs, P is the atmospheric pressure in millibars, f is the laser frequency in 10^{14} Hz and E is the elevation angle. Adding Δ_1 and Δ_2 to the iterated value of $t_r(ET)$ and maintaining appropriate units gives the final estimate of the reflection time $t_r'(ET)$ as

$$t_r'(ET) = t_r(ET) + \Delta_1 + \Delta_2 \tag{3.24}$$

3.2.4 Ephemeris Position of Telescope at Detection Time

The procedure for estimating the detection time of the photon return again requires an iterative calculation because the arrival time is a function of the ephemeris position of the telescope, which is a function of the unknown time. Similarly, an initial approximation is made based on the assumption that reflection occurred at the midpoint of the total time-delay, that is

$$t_d(ET) = 2t_r(ET) - t_t(ET) \tag{3.25}$$

Following the steps outlined in Section 3.2.2, a first approximation to the ephemeris position of the telescope $\vec{\beta}(t_d)$ at the approximate time of detection is made using the time argument $t_d(ET)$. If the transmitting and receiving telescopes are identical then only equations (3.4a,b) and (3.8)-(3.15) need to be evaluated because the changes in the telescope coordinates relative to the spin axis (eq. [3.1]-[3.3]) and the tidal variations in UT1 (eq. [3.7]) are not significant during the return journey time. The second approximation to $t_d(ET)$ takes the form (see eq. [3.21])

$$t_d(ET) = t_r'(ET) + c^{-1}|\vec{\sigma}_m(t_r)-\vec{\beta}(t_d)| \tag{3.25a}$$

with the iterative cycle continuing until the value of $t_d(ET)$ agrees sufficiently well with the previous approximation. If $\hat{\Delta}_1$ and $\hat{\Delta}_2$ denote the re-evaluation of equations (3.22) and (3.23) at the time of detection, then adding these quantities to the iterated value of $t_d(ET)$ for the final detection time $t_d'(ET)$ gives

$$t_d'(ET) = t_d(ET) + \hat{\Delta}_1 + \hat{\Delta}_2 \tag{3.26}$$

In practice, $\Delta_1 = \hat{\Delta}_1$ and $\Delta_2 = \hat{\Delta}_2$ over the period of the return journey time.

3.2.5 Calculated Time-Delay and the Time-Delay Residual

To complete the calculation of the time-delay τ_c, the components of the earth's tidal deformation vector $\vec{\delta r}$ must be estimated. An adequate representation of the tidal distortion due to the disturbing bodies (in this case, the sun and moon) in terms of the tidal potential W_2, is (Stolz 1979)

$$a_1 = \frac{\ell_2}{g \sin\psi_T} \frac{\partial W_2}{\partial \psi_T} = -\frac{3\ell_2}{g} \cos\psi_T \tag{3.27a}$$

$$a_2 = \frac{h_2}{g} W_2 + a_1 \cos\psi_T \tag{3.27b}$$

where

$$W_2 = \frac{1}{2} G m_b r^2 R_g^{-3} (3 \cos^2 \psi_T - 1) \quad . \tag{3.27c}$$

a_1 and a_2 are the horizontal and vertical amplitudes of displacement, respectively; G is the universal gravitational constant, m_b is the mass of the disturbing body, ψ_T is the angle between the telescope vector $\vec{r}$ and the tidal bulge which is phase-shifted by an angle δ_T relative to the transit of the disturbing body (see e.g. fig. 2.7), ℓ_2 and h_2 are the Shida and Love numbers of degree 2, respectively and $R_g = |\vec{R}_g|$ is the geocentric distance to the centre of the disturbing body. For the

sun, $\vec{R}_g = \vec{R}(t_d)$ and for the moon $\vec{R}_g = \vec{m}(t_d)$. The earth-tidal deformation vector is

$$\delta\vec{r} = -a_1 R_3(-\delta_T) \frac{\vec{R}_g}{R_g} + a_2 \frac{\vec{r}''}{r} \tag{3.28}$$

where the lunar and solar contributions are determined separately and combined to produce $\delta\vec{r}$.

The calculated time-delay τ_c can be written as

$$\tau_c(\text{IAT}) = t_d'(\text{ET}) - t_t(\text{ET}) + \frac{2}{c} \vec{\rho}^* \cdot \delta\vec{r} + \Delta t(t_t) - \Delta t(t_d) \tag{3.29}$$

where τ_c is expressed in atomic time for comparison with the observed time-delay $\tau_0(\text{IAT})$, as determined by the observatory clock (see Mulholland 1977 for discussion). Using respective time arguments, the relativistic corrections $\Delta T(t_t)$ and $\Delta T(t_d)$ are evaluated from equation (3.6) while the tidal deformation vector $\delta\vec{r}$ contributes to τ_c by way of the dot product with the unit vector $\vec{\rho}^*$ between the telescope and the reflector. The result is divided by the velocity of light c to convert the units from distance to time and a factor 2 is included because the correction must be made twice for the two-way time delay computation.

Computing the time-delay residual $\Delta\tau$, is accomplished simply by the following subtraction

$$\Delta\tau(\text{IAT}) = \tau_c(\text{IAT}) - \tau_0(\text{IAT}) \tag{3.30}$$

The quantity, $\Delta\tau$ provides a basis for improving the parameters which are used to derive the calculated estimate of the time delay. The standard adjustment procedure is outlined in the next section together with a review of the improvements in the physical parameters of the earth-moon system.

3.3 Parameter Improvement and Scientific Achievements

Over the last ten years, the LLR data have yielded important scientific results in astronomy, selenophysics, geodesy and cosmology. Early results from the experiment have been described by Bender et al.

(1973) and so the purpose of this section is to summarize more recent results and differentiate between the parameters that are solved for and those that are modelled. The summary draws heavily on information documented in a recent review by Mulholland (1980). Before proceeding further, however, a brief outline of the method of parameter improvement is given.

3.3.1 Parameter Estimation by Least Squares

A frequently employed technique to obtain reliable functional representation of the earth-moon distance is the method of Least Squares. In the discussion that follows it is assumed that equation (3.30) has been converted to its one-way distance equivalent. Removing the time argument from equation (3.30) for generality gives

$$\Delta\rho = \rho_c - \rho_0 \tag{3.31}$$

where $\Delta\rho = c\Delta\tau/2$, $\rho_0 = c\tau_0/2$ and $\rho_c = c\tau_c/2$. Equation (3.31), in the classical least squares problem, contributes to an observation equation in which the residual $\Delta\rho$ is the computed minus observed term. For every observation i, a value $\Delta\rho_i$ is formed and the procedure of the differential correction is used to determine the corrections v_i to the observed range ρ_0 and corrections ΔP to the approximate values P_b for the parameters of the prediction model ρ_c. Noting with care the definition of $\Delta\rho$ as given above, the resulting system of equations to be solved is

$$\sum_n \frac{\partial\rho_{ci}}{\partial P_n} \cdot \Delta P_n + \Delta\rho_i = v_i \tag{3.32}$$

or in matrix format

$$\underset{i\times n}{[A]}\ \underset{n\times 1}{[\Delta P]} + \underset{i\times 1}{[T]} = \underset{i\times 1}{[v]} \tag{3.33}$$

where

$$T = \Delta\rho = \rho_c - \rho_0 \tag{3.34}$$

Equations (3.32) and (3.33) express the computational model in a

linearized form. The partial derivatives $\partial\rho_{ci}/\partial P_n$ are in fact first-order terms in a Taylor series expansion of ρ_c about the approximate values for the parameters P_n. Together they represent the coefficients of the design matrix [A] in equation (3.33).

The desired computational quantities are the corrections ΔP_n which yield improved estimates for the parameters that constitute the prediction model (see Section 3.2). In practice, $i > n$ and so a solution constraint must be applied in order to obtain a unique set of corrections. Known as the least squares principle, this constraint states that the sum of the weighted squares of the observation corrections v_i is a minimum, or

$$m = [v]^T[G][v] \tag{3.35}$$

where [G] is a square matrix of order i whose elements are the weight coefficients of the observations. For uncorrelated observation errors, [G] becomes a diagonal matrix with (Kaula 1966)

$$g_{ii} = (\sigma_i^2)^{-1} \; ; \qquad g_{ij} = 0 \quad \text{for} \quad i \neq j$$

where σ_i^2 is the variance of the observation. The weight matrix [G] is simply the inverse of the variance-covariance matrix for the observations. Observations with large variance, therefore, will contribute less to the solution. When real data are available, standard statistical techniques can be used to see if the a priori estimate of the [G] matrix used in the adjustment is a reliable estimate of reality. These algorithms are not given here since this study only demands a knowledge of optimization procedures. Readers are referred to texts on adjustment theory for further information.

To minimize the function m, equation (3.35) is differentiated with respect to v and the result set to zero. Taking equation (3.33) into account yields a system of normal equations of the form

$$\underset{n\times n}{[N]}\ \underset{n\times 1}{[\Delta P]} + \underset{n\times 1}{[B]} = 0 \tag{3.36}$$

where

$$[N] = [A]^T[G][A] \text{ and } [B] = [A]^T[G][T] \tag{3.37}$$

Of particular importance to this study is the inverse of the normal matrix [N] because this is an estimate of the variance-covariance [Q] for the adjusted parameters P_n, that is

$$[Q] = [N]^{-1} \tag{3.38}$$

The least squares estimate for the corrections ΔP to approximate values for the parameters P is given by

$$[\Delta P] = -[N]^{-1}[B] \tag{3.39}$$

At present, only a small amount of geodynamical information has come from the LLR experiment because a network of stations must be ranging in order to properly evaluate equation (3.36) for the desired corrections. This is particularly true for polar motion (x,y) and Universal Time (UT1) where observations from at least two stations are needed to separate these three components. If, however, hypothetical observations are simulated under realistic conditions then equation (3.38) can be evaluated to find out how well the LLR technique can determine the sought parameters. This is possible because the evaluation does not require a knowledge of the observed distance, just the times of observation, the positions of the telescope and reflector, the observation uncertainty and the partial derivatives.

The main reasons for the difference between the calculated and observed distance, as shown in equation (3.31), are (a) errors in the model used to predict the distance, (b) systematic observational effects due to instrumental, atmospheric and timing system anomalies and (c) random effects. Systematic errors are always a problem and no matter how many observations are available the method of least squares will not eliminate this type of error. The adjustment procedure just described only acknowledges the existence of random observational errors. Unlike previous studies (see e.g. Hauser 1974), no attempt has been made to include long-term correlations between the

observation errors. Readers are also referred to Kaula (1966) for the development of a more general covariance analysis which includes both random and systematic effects.

3.3.2 Lunar Orbit and Rotation, Selenodetic and Gravitational Information

Two of the foremost tasks in the early stages of the LLR experiment were the construction of an improved lunar ephemeris and physical libration theory. Both were an absolute necessity because the lunar ranging data were two to three orders of magnitude better than the classical optical data. While the early theories for the lunar orbit (see e.g. Brown 1908) and librations (see e.g. Koziel 1948) were sufficient for classical applications they did not have the accuracy that was required to regulate the range gate at the level suitable for photon detection.

The conventional version of Brown's theory was known to include errors equivalent to 2 km in distance that were largely due to uncertainties in the astronomical constants. Even the use of updated astronomical constants did not improve the situation very much because the level of truncation in Brown's work gave rise to errors on the order of 500 m. Integrating the orbit numerically to avoid the truncation problem and adjusting the lunar moment of inertia parameters β and γ, the reflector coordinates $\vec{k}$ and the geocentric longitude λ_m at McDonald reduced the rms value of the residuals $\Delta\rho_i$ to about 50 metres by 1970 (Bender et al. 1973).

Similarly, the theory for the physical librations in vogue at the beginning of the experiment was also limited in its application because of the level of truncation (Eckhardt 1965). However, by 1970 the theory included improvements to the second degree terms of the lunar gravitational field (Eckhardt 1970) and, together with the ephemeris based on the techniques described in Garthwaite et al. (1970), was used to obtain the results through 1970 reported by Bender et al. (1973).

Even though rapid progress was made in the initial stages of the experiment it was still apparent that considerable work had to be done on the orbital and librational theories. For example, it was noted that

the third degree harmonics of the lunar gravity field played a significant part in the libration theory (see e.g., Kaula and Baxa 1973) and that to fully exploit the LLR data an ephemeris based on a complete 2nd-order theory of general relativity had to be implemented (Mulholland 1980). Including these effects and continuing to solve for the lunar moment of inertia parameters β and γ brought the rms residual down to the metre level by 1974. A typical value for β in units of 10^{-6} can range from 631.26 to 631.69 while for γ the range is 227.18 to 228.02 (Mulholland 1980).

Nowadays, most LLR solutions have a rms residual of about 40 cm (see e.g. Williams 1977) and if one of the solution parameters is UTO the rms residual drops even further to about 25 cm. Among the parameters and phenomena improved in these adjustments are the telescope and observatory coordinates as contained in the vectors $\vec{r}$ and $\vec{k}$, the mass of the earth-moon system, the Keplerian elements of the lunar orbit as contained in the vector $\vec{M}$ and their initial values, tidal friction effects on the lunar orbit (see Section 2.4.4.1), the Nordtvedt effect, the initial conditions for the librations, the lunar moment of inertia ratios β and γ, some of the third degree harmonics of the lunar gravitational field, several long-period and tidal terms in Universal time and the lunar dissipation factor.

A discussion of the geodetic and earth rotation parameters and those of geophysical interest is left until the next two sections. The remaining part of this section summarizes the current status of the models for the lunar orbit and physical librations and the contributions of LLR to gravitational theory and selenodetic control.

There has been no serious attempt to discuss the significance of the adjusted Keplerian elements from an orbit integration since comparisons between individual integrations indicate they are highly model-dependent (Mulholland 1980). This reduces their effectiveness as a source of physical information. One physical quantity which enters into Kepler's third law of satellite motion and can be determined from LLR observations, in restricted form, is the combined mass of earth-moon system. What is in fact determined from LLR is the ratio of the solar mass to

the combined mass of the earth and moon. The most recent value is 328900.54 ± 0.02 (Ferrari et al. 1980).

As was intimated previously, although not directly stated, the orbit of the moon around the earth cannot be considered a point-mass problem as is commonly the case with artificial satellites. Both the earth and the moon are sufficiently non-spherical and large enough to effect the lunar orbit and its rotation. In present-day analyses, zonal harmonics through degree 4 are used to model the shape of the earth and a combination of 3rd-degree zonal and tesseral harmonics as well as the 2nd-degree terms are used for the moon (Williams 1977). A more recent solution, however, includes some 4th-degree terms for the moon as well (Williams, private communication 1980).

One of the main reasons for improving the model of the lunar figure was to overcome the inadequacies in the earlier theories for the physical librations. The physical librations are merely the small perturbations on the larger apparent oscillations (optical librations) associated with the Cassini motion (see e.g. Mulholland 1980). Both the optical and physical librations are represented by the Euler angles which describe the lunar rotation (see Section 3.2.3).

There are three standard techniques for determining the physical librations, the analytic, semi-analytic and the numerical. A series of semi-analytic solutions (see e.g. Eckhardt 1973) have been formulated in which the perturbing forces are described by a Fourier series whose arguments are linear combinations of the fundamental parameters of the lunar theory but whose coefficients are purely numerical. The main problem associated with the semi-analytic theory is the completeness with which the perturbing forces are represented, particularly the effects of the other planets. Similar problems are encountered using the analytic approach (see e.g. Migus 1980). Although sustained research effort is still needed in this area, an extensive set of 'additive and planetary' terms is now being used by the LLR analysts to supplement the analytic and semi-analytical theories (see Mulholland 1980 for further details).

The advantage of the numerical approach (see e.g. Cappallo 1980) is that the forced terms can be represented to virtually any level of precision. One readily available solution, designed JPL LLR5, incorporates all planetary effects and lunar gravity coefficients through degree 3 (Williams 1977). Two of the main drawbacks with the numerical approach are (1) the calculations can only be made for a finite time span and (2) the numerical solution admits homogeneous terms which the computer cannot distinguish from the forced terms. In any numerical integration procedure, free oscillations are always implicit in the starting conditions and errors in these conditions can generate large periodic terms that are completely spurious in terms of the physical problem (Mulholland 1980). The approach used at JPL to help minimize such effects is to adjust the integrations to fit as closely as possible to a semi-analytic theory.

The search for homogeneous terms, or 'free' librations as they are more commonly called, in the lunar rotation has been the subject of a series of papers by Odile Calame. From an inspection of the equations of motion and knowing the values for the lunar gravity field parameters (see Table 3.1), it can be shown that these terms have three permissible periods. The modes most readily determinable from the LLR data are the libration in longitude with an amplitude of about 2 asecs and period of 2.9 years and one in latitude with an amplitude of about 3 asecs and a synodic period of 27 days (see e.g. Calame 1977). Another component in latitude is not well-determined; the solution amplitude is very model-dependent and usually less than 0.5 asecs.

Until now, only meteoroid impacts have been considered as the excitation mechanism of the free librations (see e.g. Peale 1975, 1976) but both these theoretical studies suggest that the free libration amplitudes should be much smaller than the values determined by Calame. To resolve this issue, a deeper understanding of the processes governing the dissipation of lunar rotational energy and lunar deformation is needed (see Kovalevsky 1977 and Mulholland 1980 for further discussion). Nevertheless, one clear message from the work of Peale and Calame is

Table 3.1 Typical Values for the Harmonic Coefficients of the Lunar Gravity Field through Degree 3 (taken from Williams 1977). The reference frame is chosen such that C_{00}, C_{10}, C_{11}, S_{11}, C_{21} and S_{21} are all equal to zero. Terms of the form S_{n0} do not exist in the spherical harmonic expansion. The coefficients are in units of 10^{-6}.

Degree and Order (n m)		Harmonic Coefficient C_{nm}	S_{nm}
2	0	-202.72	---
2	2	22.3	0
3	0	-10.4	---
3	1	28.6	8.8
3	2	4.8	1.7
3	3	2.7	-1.1

that an earlier observation of the free libration in longitude by Koziel (1967) is about an order of magnitude too large.

As mentioned previously in Section 2.4.4.1, one of the major features of the lunar orbit is the decrease in the lunar mean motion $\dot{n}$. The details of that discussion will not be repeated here except to say that interpreting the geophysical significance of $\dot{n}$ is difficult, particularly if the gravitational constant G is varying as well (Mulholland 1980). So far, LLR has established an upper limit for $|\dot{G}/G|$ of 3×10^{-11} yr^{-1} (Williams et al. 1978) which is in good agreement with the limit determined by other techniques (see e.g. Shapiro et al. 1971).

Testing for the time variation of G is not the only study of cosmological interest that can be made with LLR. Nordtvedt (1973) showed that a departure from unity of the inertial to gravitational mass ratio for astronomical bodies would cause the earth and moon to "fall" towards the sun at different rates. The main variation in the earth-moon distance occurs with a period of 29.53 days and has an amplitude which is model-dependent. For general relativity the amplitude is zero but for the Brans-Dicke theory (Brans and Dicke 1961) the amplitude is 1 m if the coupling parameter ω is equal to 6. Analyses of the LLR data (Shapiro et al. 1976, Williams et al. 1976), however, verify the equivalence principle to 7 parts in 10^{12} and this corresponds to ω being greater than 29 in the Brans-Dicke theory. This result is consistent with zero amplitude for the Nordtvedt term and with the results obtained by Reasenberg et al. (1979) using data from the Viking relativity experiment.

LLR contributions to selenodetic control are best described in terms of the reflector coordinates and the problems associated with their determination. In an absolute sense, the reflector coordinates have little significance since their values are clearly dependent on the model chosen for the physical librations (Bender et al. 1973, Mulholland 1980). Expressed differently, any error in the physical libration model will be partly absorbed in the adjustment as corrections to the reflector coordinates. A clear example of this is shown in Table 3.2 where the Cartesian coordinates of 4 of the 5 reflector arrays currently

Table 3.2 Rectangular Cartesian Coordinates for the Reflector Arrays in the Principal Axis System

Cartesian coordinate*	Largest discrepancy	Reference Source		
		Williams (1977)	Ferrari et al. (1980)	Mulholland (1980)
$\begin{bmatrix} x_1 \\ x_2 \\ x_3 \end{bmatrix}_0$	(0.476)	1592.490	1592.014	1592.486
	(1.089)	689.522	690.606	689.517
	(0.036)	21.036	21.048	21.012
$\begin{bmatrix} x_1 \\ x_2 \\ x_3 \end{bmatrix}_2$	(0.351)	1652.319	1652.668	1652.317
	(1.116)	-522.205	-521.097	-522.213
	(0.076)	-109.755	-109.685	-109.761
$\begin{bmatrix} x_1 \\ x_2 \\ x_3 \end{bmatrix}_3$	(0.092)	1554.763	1554.671	1554.762
	(1.078)	96.924	98.002	96.932
	(0.032)	765.038	765.046	765.014
$\begin{bmatrix} x_1 \\ x_2 \\ x_3 \end{bmatrix}_4$	(0.575)	1339.973	1339.398	1339.962
	(0.920)	800.871	801.791	800.871
	(0.015)	756.390	756.393	756.378

*All values are in kilometres.

on the lunar surface are listed. The values are shown for three different solutions and are given with respect to the principal axes. The subscripts 0, 2, 3, 4 refer to the reflector packages left by the Apollo 11, 14, 15 and Lunakhod 2 missions, respectively.

The most striking aspect of this table is the 1 km displacement in the x_2 coordinate of each reflector as determined by Ferrari et al. (1980) compared to the other two solutions. Discrepancies ranging from 0.1 to 0.6 km also exist in the x_1 coordinates and this suggests that the physical libration model used by Ferrari et al. is displacing the principal axes by these amounts. The results of Williams (1977) and Mulholland (1980) agree quite well.

Computations of the baseline lengths between respective reflector arrays agree much better for all solutions. The average difference is on the order of 15 m (Mulholland 1980). This clearly indicates that selenodetic control and mapping can be achieved to higher accuracy on a relative basis and that there is still more room for improvement in the physical libration model. For a range accuracy of 2 to 3 cm, terms in the physical libration model with amplitudes ranging from 0.007 to 0.01 asecs must be retained (see e.g. Breedlove 1977).

3.3.3 Geodetic and Earth Rotation Parameters

The ability to use LLR data for geodetic and earth rotation purposes was recognized quite early during the experiment (see e.g. Chollet 1970, Faller et al. 1972). However, since that time, the full potential of the LLR has never been utilized in these areas because of the numerous problems that have prevented the completion of a global network of high-accuracy ranging stations. While the measurement uncertainty at McDonald Observatory is typically 10 to 15 cm, this is not the case for the other stations which have ranged to the moon; the measurement uncertainties at the Crimean and Orroral observatories are at the metre level (see e.g. Calame 1975, Shelus et al. 1979). Until substantial improvement is made in shortening the pulse length and reducing the calibration uncertainties at these stations no useful tectonic information will be forthcoming (Mulholland 1980).

Analyses of the data for earth rotation information are more prevalent but since McDonald is the only station producing high quality data, determinations are limited to station values of UT0 and $\Delta\phi$. Most studies have concentrated specifically on extracting UT0 information (see e.g. Stolz et al. 1976, Harris and Williams 1977, King et al. 1978 , Calame and Guinot 1979). All these studies indicate the capability of LLR to accurately determine this parameter by at least a factor of 3 better than that achieved by the classical techniques. Several periodic trends are also evident in the UT0 results but the cause of these effects is still an open question (Mulholland 1980). It is customary to solve for these terms before daily UT0 values are determined.

To this author's knowledge only three attempts have been made to extract information on the variation of latitude ($\Delta\phi$) at McDonald. The first of these was by Shelus et al. (1977) who analyzed an extensive set of LLR data acquired during October 1975. No effort was made to pre-select observations that were geometrically favorable for the determination of the McDonald latitude and as a consequence the results at northern declination were far from impressive. The sensitivity of the range measurement to the latitude variation of a northern hemisphere station diminishes when the moon occupies the northern apex of its orbit.

Larden (1981), on the other hand, set out to verify a rather large excursion in the polar motion curve which occurred during 1974. BIH, IPMS and Doppler values of polar motion were used to derive the variation in latitude at McDonald. Interpolated values were then obtained and compared at appropriate times with LLR determinations in order to verify the trend. In this case, analysis was confined to times when the range was most sensitive to latitude variations, that is, when the moon was at southern declination. Although serious attempts were made to assess the systematic effect of lunar orbital and librational errors on the outcome of the study, it was learned later that the LLR data during a critical period of the analysis had been contamin-

ated by calibration errors. This prevented a definite conclusion to be drawn about the reality or otherwise of the 1974 irregularity.

Langley et al. (1981) have undertaken a detailed analysis of the data and solved for monthly values of the McDonald latitude simultaneously along with all other relevant parameters in the problem. Current indications are that the rms range residual is reduced to about 15 cm if the latitude parameter is included in the adjustment.

There have been many different theoretical studies on just how well LLR can determine the polar motion coordinates x, y and Universal time UT1 (Fajemirokun 1971, Kaula 1973, Stolz and Larden 1977, Leick 1980). All studies differ widely in their basic assumptions, parameterization of the earth's rotation, the method of dealing with the individual ranges and the analysis interval for the simulation.

One of the major reasons why it is difficult to draw conclusions about the accuracy with which earth rotation information can be obtained by LLR from Fajemirokun's study is the severe limitations placed on the observation schedule. At most, only one range is assumed from a given station to a given reflector per day. This not only eliminates much of the earth rotation information which is contained in the diurnal signature of the range residual but also aliases it with the lunar parameters. Kaula includes four frequencies from the polar motion and UT1 spectra. The frequencies chosen were higher than or equal to 1 cycle/month because the time span of his analysis was generally only 437 days. This clearly prevented a realistic solution for the semi-annual, annual and Chandler terms. Both Fajemirokun and Kaula conduct their simulations with a network of three stations but this is where the similarity ends. Unlike Kaula, Fajemirokun models the rotation of the earth by three Euler angles and their rates at epoch and makes no attempt to include the effect of weather or systematic biases on the observation variances. Kaula allows 3 observations per day from any given station and thereby recognizes the significant role that the diurnal variation in the range residual has in separating out the earth rotation information contained in the range measurement.

As stated by Mulholland (1980), the most comprehensive theoretical study to date on how well one might obtain earth rotation information from LLR data was that carried out by Stolz and Larden (1977). Since the work presented here reports the details of that study and the research carried out since then, a complete account of the work is left until Chapters 5 and 6.

Finally, a different approach for the analysis of the LLR data has been proposed by Leick (1980). Following the theoretical work of Arnold (1974), Leick carried out several numerical experiments to see whether daily values of the earth's rotation could be obtained to the measurement accuracy if simultaneous range measurements were differenced. Although the results indicate that this is possible when a sufficient number of observations are available, no attempt was made in the study to assess the effect of the weather on the results. This clearly is an important omission if the continuity of results is to be considered. While range differencing may be useful when searching for fluctuations in the earth's rotation with periods less than one day, there is no evidence to suggest this approach is more advantageous than the single range method.

In the next section, the status of the LLR network is reviewed briefly in order to justify the selection of the station locations chosen for the numerical studies described in Chapter 5.

3.4 LLR Network Status

Although most of the observations have come from McDonald Observatory, there have been reports of ranging from eight other locations as well (Mulholland 1980). These are the Lick Observatory (California USA), Catalina Station (Arizona USA), Observatoire de Pic du Midi (France), Crimean Astrophysical Observatory (Crimea USSR), Dodaira Station (Japan), Agassiz Station (Massachusetts USA), Mt. Haleakala Observatory (Hawaii USA) and the Orroral Station (Australia).

Of these nine, only five remain. The Lick and Agassiz facilities were intended to be temporary and, therefore, are no longer in operation. The Catalina and Orroral units are one and the same; the former

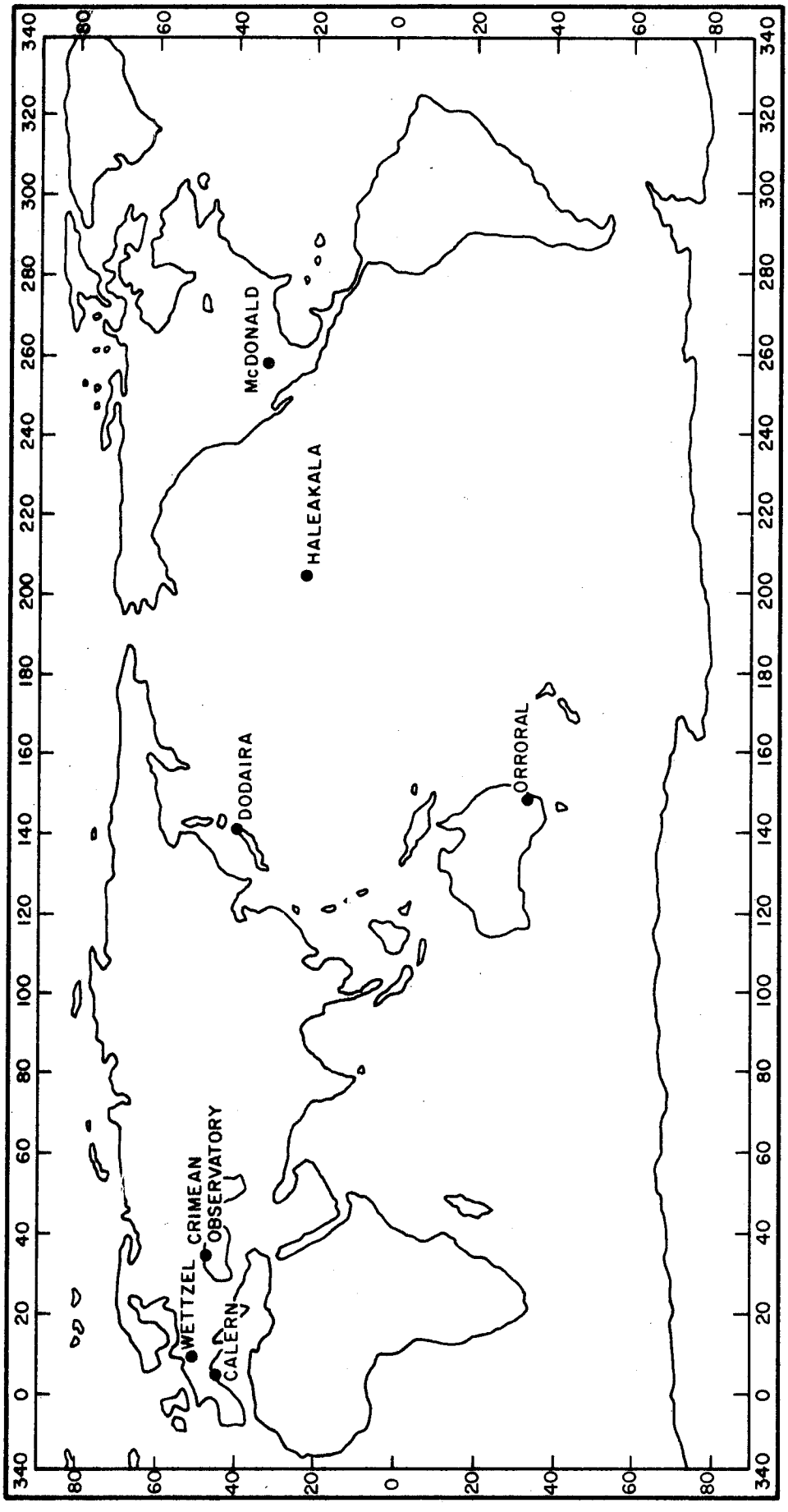

Figure 3.4 Location of Stations Capable of Ranging to the Moon

having been transferred to the Orroral site in the early 1970's. The laser system from Pic du Midi is now relocated at the CERGA Observatory in Calern, France where it is now being tested with a new optical and electronic system. Plans are also underway to range to the moon from a station situated at Wettzel, Germany.

Thus the full complement of stations capable of ranging to the moon presently stands at seven. Their locations are shown in Figure 3.4. Of these, the systems at Dodaira, Calern and Wettzel are still in various stages of testing and the data from the Crimean Observatory has very restricted availability outside the Soviet team. For this study, the LLR network consists of a maximum of five stations. They are McDonald, Mt Haleakala, Orroral, Calern and Dodaira. At the time these experiments began, the author was not aware of the plans to range from the Wettzel station and so it was not included. The Crimean Observatory was not considered because its contribution to earth rotation experiments would probably be small if data availability was limited.

CHAPTER 4

SIMPLIFIED MODELING OF LUNAR RANGE MEASURES

4.1 Preamble

One of the more advantageous aspects of LLR sensitivity studies of the type undertaken here is that several useful and valid approximations can be implemented that reduce the distance equation discussed in Chapter 3 to a more workable form. In this chapter, the distance equation is simplified and expressed in terms of the spherical coordinates of the observing station and lunar reflector. The geographic reference frame, previously defined in Section 2.2.2.1, is used throughout the formulation. The development is then extended in order to derive the trigonometric functions for the coefficients $\partial\rho_{ci}/\partial P_n$ of the observation equations (see eqs. 3.32 and 3.33) for single ranges. The estimable parameters, particularly those related to the earth's rotation, are identified and a discussion then follows on the structure of the observation equation and the degree to which the parameters can be separated. This will provide some insight into their individual determination before carrying out the numerical experiments. The mathematical formulation of the distance equation for simultaneous observations has been given elsewhere (see e.g. Chollet 1970, Arnold 1974, Stolz 1975, Leick 1980) and will not be discussed here.

4.2 Derivation of the Distance Equation

4.2.1 Coordinate System Definition

While it is necessary to use three coordinate systems to calculate the precise time delay, this is not the case when the intention is merely to investigate how well the geodynamical parameters in the problem can be determined (see e.g. Chollet 1970, Faller et al. 1972). For the case of single measurements, it is convenient to express both the coordinates of the observing station and the lunar reflector in the geographic reference system whose origin is at the geocentre (see Figure 2.1). The geocentre is defined specifically in this study as the centre

of mass of the solid earth plus core. In the author's opinion, this definition aides in the understanding of the concept of geocentre motion in relation to the surface mass loading problem (see Chapter 7 for further discussion).

Figure 4.1 depicts the simplified geometry of the Earth-Moon system. The position of the observatory in the geographic system x_i is given by three parameters r_s, ϕ and λ which denote the geocentric distance, latitude and east longitude of the observatory, respectively. It follows that

$$\vec{r}_s = \begin{bmatrix} x_1 \\ x_2 \\ x_3 \end{bmatrix}_{obs} = r_s \begin{bmatrix} \cos\phi \cos\lambda \\ \cos\phi \sin\lambda \\ \sin\phi \end{bmatrix} \quad . \tag{4.1}$$

When the spherical coordinates of the reflector, that is, r_r, δ and α are given in the space-fixed frame X_i, as implied by Figure 4.1, then it is necessary to transform these quantities into the x_i system by a simple rotation through θ. Here r_r, δ and α are the geocentric distance, declination and right ascension of the reflector, respectively and θ is the Greenwich sidereal time. Therefore, if $\vec{r}_r$ denotes the position vector of the reflector in the x_i system, then

$$\vec{r}_r = \begin{bmatrix} x_1 \\ x_2 \\ x_3 \end{bmatrix}_{ref} = r_r \begin{bmatrix} \cos\delta \cos(\alpha-\theta) \\ \cos\delta \sin(\alpha-\theta) \\ \sin\delta \end{bmatrix} = \vec{m} + \vec{k} \quad . \tag{4.2}$$

The position vector of the distance, $\vec{\rho}$ is simply obtained by differencing equations (4.1) and (4.2), that is,

$$\vec{\rho} = \vec{r}_r - \vec{r}_s \quad . \tag{4.3}$$

Equation (4.3) expresses the distance between an earth-based observatory and a lunar reflector in vector format. It is completely general and can be evaluated for any epoch of observation. However, it is desirable for both a conceptual and practical reason to expand equation (4.3) in

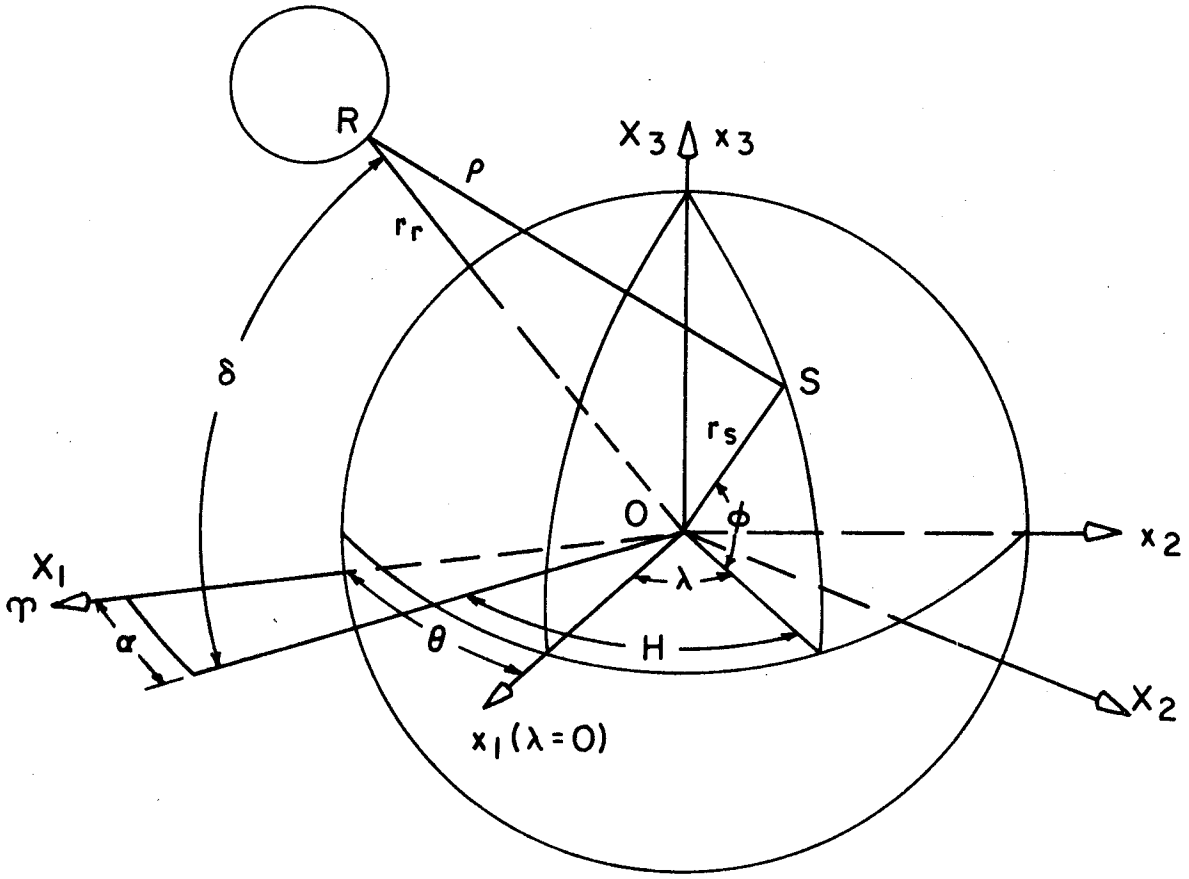

Figure 4.1 Simplified Geometry of the Earth-Moon System

terms of the previously defined spherical coordinates of the observatory and the reflector. This approach will help give a better understanding of how well the parameters of the problem can be separated from one another.

4.2.2 Distance Equation

The form of equation (4.3) is very convenient because the problem has now been divided into two parts, that is, the dynamics of the earth and the moon. For example, the dependence of the distance on the lunar orbit and rotation, and the lunar tides is contained in the vector $\vec{r}_r$ while the vector $\vec{r}_s$ contains information on the earth's rotation, the earth tides, surface deformation due to loading and changes in station position due to the tectonic plate motions. Both $\vec{r}_r$ and $\vec{r}_s$ contain information on the motion of the geocentre (see Chapter 7).

To investigate the dependence of the distance on the parameters which define the earth's rotation in more detail, it is also necessary to express equation (4.3) in terms of the equivalent distance ρ, rather than the "equivalent distance vector" $\vec{\rho}$. Substituting equation (4.1) and (4.2) into equation (4.3) gives

$$\rho = |\vec{\rho}| = \{(r_r \cos\phi\cos(\alpha-\theta) - r_s \cos\phi\cos\lambda)^2 + (r_r \sin\delta - r_s\sin\phi)^2$$

$$+ (r_r \cos\delta\sin(\alpha-\theta) - r_s \cos\phi\sin\lambda)^2\}^{1/2} \quad . \qquad (4.4)$$

After some elementary trigonometric manipulation, equation (4.4) reduces to

$$\rho = \{r_s^2 + r_r^2 - 2r_r r_s(\cos\phi \cos\delta \cos H + \sin\phi \sin\delta)\}^{1/2} \qquad (4.5)$$

where H, the geocentric hour angle of the reflector, is given by

$$H = \lambda + \theta - \alpha \quad . \qquad (4.6)$$

H is zero when the reflector crosses the observatory meridian, is -60° about 4 hours earlier, and is +60° about 4 hours later when the reflector is to the west of the observatory meridian.

Equation (4.5), in its present form, contains only five parameters. They are determinable only if the corresponding design matrix [A] (see eqs. 3.32 and 3.33) is non-singular. In this case, the parameter list P (see Section 3.3.1) can be expressed generally as

$$P = f(r_s, r_r, \phi, \delta, H) \tag{4.7}$$

Accordingly, in the least squares adjustment process, these parameters become the parameters for refinement.

It is important to realize, however, that each parameter of this list can also be expressed as a function of many other parameters. For example, the declination of the reflector δ can be expressed as a function of Brown's fundamental arguments of the lunar theory (see e.g. Appendix D, Hauser 1974) and so it is possible to reformulate the distance equation (4.5) in terms of any desired parameter which can influence the range measurement. In the next section, the basic observation equation is developed. Consideration is given specifically to the parameters that are used to define polar motion and the earth's angular position in space (UT1).

4.3 Basic Observation Equation for Parameter Refinement

In order to perform a sensitivity study it is necessary to calculate what effect small variations in the parameters have on the distance ρ between the observatory and the reflector. Together with the difference between the observed and predicted values of the distance, these partial derivatives are used to correct the approximate values of the parameters. It is assumed here that the measured distances have been corrected for all instrumental and other systematic errors (e.g. calibration constants and atmospheric refraction). This assumption eliminates the need to introduce a systematic error model into the observation equation (see e.g. Hauser 1974 for the treatment of such effects). Nevertheless, an attempt is made in Chapter 5 to treat the effect of systematic errors in a subjective way.

Given equation (4.7), the mathematical structure of the distance equation (4.5) in a least squares sense can be expressed as

$$\rho_a = f(P_a) \tag{4.8}$$

where ρ_a is the vector of adjusted values for the observed distance ρ_0, and P_a is the vector of the adjusted parameters. Using the notation of Section 3.3.1,

$$\rho_{a_i} = \rho_{o_i} + v_i \tag{4.9}$$

and

$$P_a = P_b + \Delta P \quad . \tag{4.10}$$

In equation (4.10), P_b is the vector of approximate values used to compute the predicted distance ρ_c. Unless real observations are available, equations (4.9) and (4.10) cannot be evaluated. The main concern here is the structure of the design matrix [A]. Its formulation requires the partial differentiation of equation (4.5).

4.3.1 Partial Derivatives

In practice, care must be exercised when calculating the partial derivatives. The procedure, as described by Stolz (1979), is (a) to split the predicted distance (see Section 3.2) into its upward and downward leg components and (b) then partially differentiate the expressions so obtained with respect to the parameters that are to be improved. This level of sophistication, however, it not necessary for sensitivity studies of the type undertaken here(see e.g. Silverberg et al. 1976, Leick 1980). As a first approximation, equation (4.5) is differentiated on the basis that the amount by which the earth rotates during the travel time of the pulse is negligible. The elements of the design matrix [A] are

$$A^{il}_{r_s} = \frac{\partial \rho}{\partial r_s} = \rho^{-1}(r_s - r_r \cos\phi\cos\delta\cos H - r_r \sin\phi\sin\delta)_i$$

$$A^{i2}_{r_r} = \frac{\partial \rho}{\partial r_r} = \rho^{-1}(r_r - r_s\cos\phi\cos\delta\cos H - r_s\sin\phi\sin\delta)_i$$

$$A^{i3}_{\phi} = \frac{\partial \rho}{\partial \phi} = \rho^{-1}(r_r r_s\sin\phi\cos\delta\cos H - r_r r_s\cos\phi\sin\delta)_i$$

$$A^{i4}_{\delta} = \frac{\partial \rho}{\partial \delta} = \rho^{-1}(r_r r_s\cos\phi\sin\delta\cos H - r_r r_s\sin\phi\cos\delta)_i$$

$$A^{i5}_{H} = \frac{\partial \rho}{\partial H} = \rho^{-1}(r_r r_s\cos\phi\cos\delta\sin H)_i \quad . \tag{4.11}$$

Substituting equation (4.11) into equation (3.32) gives the basic observation equation

$$v_i = \Delta\rho_i + \rho^{-1}\{(r_s - r_r\cos\phi\cos\delta\cos H - r_r\sin\phi\sin\delta)_i\Delta r_s + (r_r - r_s\cos\phi\cos\delta\cos H - r_s\sin\phi\sin\delta)_i\Delta r_r + (r_r r_s\sin\phi\cos\delta\cos H - r_r r_s\cos\phi\sin\delta)_i\Delta\phi + (r_r r_s\cos\phi\sin\delta\cos H - r_r r_s\sin\phi\cos\delta)_i\Delta\delta + (r_r r_s\cos\phi\cos\delta\sin H)_i\Delta H\} \quad . \tag{4.12}$$

Note also that

$$\Delta H = \Delta\lambda + \Delta\theta - \Delta\alpha \quad . \tag{4.13}$$

The symbol i indicates that for every measured distance, ρ_{oi} an observation equation must be formed. The ith row of the design matrix [A] consists of the values for the coefficients that are enclosed by the subscripted parentheses. The coefficients must be evaluated at each measurement time. According to equation (4.12) the design matrix will have five columns. The values for the coefficients may be placed in any order so long as consistency is maintained throughout the least squares procedure.

There is still yet another approximation that can be introduced without seriously affecting the results of the error analysis. Omitting terms of order r_s/ρ in equation (4.12) is equivalent to neglecting

quantities of magnitude less than 2% because r_s/ρ for the Earth-Moon system $\cong 1/60$. Without serious degradation, equation (4.12) can be rewritten as

$$v_i = \Delta\rho_i - (\cos\phi\cos\delta\cos H+\sin\phi\sin\delta)_i \Delta r_s + \Delta r_r + r_s(\sin\phi\cos\delta\cos H-\cos\phi\sin\delta)_i\Delta\phi$$
$$+ r_s(\cos\phi\sin\delta\cos H-\sin\phi\cos\delta)_i\Delta\delta + (r_s\cos\phi\cos\delta\sin H)_i\Delta H \quad . \qquad (4.14)$$

Rearranging terms slightly gives

$$v_i = \Delta\rho_i - \{\cos(\phi-\delta)-\cos\phi\cos\delta(1-\cos H)\}_i \Delta r_s + \Delta r_r$$
$$+ r_s\{\sin(\phi-\delta) - \sin\phi\cos\delta(1-\cos H)\}_i\Delta\phi + \{r_s\cos\phi\cos\delta\sin H\}_i\Delta H$$
$$- r_s\{\sin(\phi-\delta) + \cos\phi\sin\delta(1-\cos H)\}_i\Delta\delta \quad . \qquad (4.15)$$

As mentioned previously, the corrections Δr_s, Δr_r, $\Delta\phi$, ΔH and $\Delta\delta$ are not only introduced to take into account the errors in the initial values for these respective parameters. For example, the corrections $\Delta\phi$ to the latitude and ΔH to the hour angle of the reflector may also contain a contribution attributable to errors in the models used for polar motion and plate motion. Thus, one can write generally

$$\Delta\phi = \Delta\phi_{init} + \Delta\phi_{pole} + \Delta\phi_{plate} + \ldots\ldots \qquad (4.16)$$

$$\Delta H = \Delta H_{init} + \Delta H_{pole} + \Delta H_{plate} + \Delta H_{UT1} + \ldots\ldots \quad . \qquad (4.17)$$

To express equation (4.15) merely as a function of the corrections to the parameters for polar motion (x,y) and the earth's angular position (UT1) the well-known equations of conditions are introduced, that is (see e.g. Guinot et al. 1971)

$$\Delta\phi = \Delta\phi_{pole} = \Delta x\cos\lambda - \Delta y\sin\lambda \qquad (4.18)$$

$$\Delta H = \Delta H_{UT0} = \Delta H_{pole} + \Delta H_{UT1} = \tan\phi(\Delta x\sin\lambda+\Delta y\cos\lambda) + \Delta UT1 \quad . \qquad (4.19)$$

Equation (4.18) simply relates the corresponding correction that should be applied to an observers latitude if the coordinates of the spin axis

(x,y), as defined according to BIH convention (see Section 2.3.1.1), are corrected by amounts Δx and Δy, respectively. It is assumed here that the forced diurnal variations in x and y have been removed by using an appropriate nutation theory for the mean figure axis (see Section 2.4). The combined effect of polar motion and a change in UT1 on the hour angle of the reflector is given by equation (4.19). Substituting (4.18) and (4.19) into (4.15) and assuming that the initial station coordinates, the lunar ephemeris and all other influences on the range are perfectly known gives (Stolz and Larden 1977)

$$v_i = \Delta\rho_i + r_s\left[\{\sin\phi\cos\delta\cos(\lambda-H) - \cos\lambda\sin\delta\cos\phi\}_i\,\Delta x\right.$$
$$- \{\sin\phi\cos\delta\sin(\lambda-H) - \sin\lambda\sin\delta\cos\phi\}_i\,\Delta y$$
$$\left. + \{\cos\phi\cos\delta\sin H\}_i\,\Delta UT1\right] \quad . \qquad (4.20)$$

Obviously, the equations (4.18, 4.19) of conditions imply that a minimum of two stations either well separated in latitude or longitude must be ranging in order to determine Δx, Δy and $\Delta UT1$ uniquely. Equation (4.20) is the basic observation equation used throughout this work. Such simple modelling demands that an accurate reference frame adjustment has been carried out and a good lunar orbit and libration model are available. In this case, the design matrix [A] has only three columns. With i observations, equations (3.37) and (3.38) can be applied to determine the resulting uncertainties in Δx, Δy and $\Delta UT1$ given a suitable set of observational assumptions (see Chapter 5). Expressions similar to equation (4.20) have been derived by Wahr and Larden (1981) to analyze the LLR data for information on the earth's nutation.

Additional parameters, or a reliable geophysical model, must be included in equation (4.20) if the stations are undergoing substantial displacements due to plate motion. If not, the variations in station coordinates due to plate motion will be absorbed as corrections to the earth rotation parameters and thus contaminate the results. Over short intervals ($\lesssim$1 year) these effects will not be distinguisable if the range uncertainties remain at 10 to 15 cm. This would not be the case, however, if 3 cm range accuracies are obtained (see Chapter 6). It is

also important to note that space ranging techniques like LLR are not capable of determining plate motions in an absolute sense. For example, any east-west crustal motion $\dot{\lambda}_c$, common to all stations in the LLR network, cannot be separated from a secular change $\dot{\theta}$ in the earth's angular position or a drift $\dot{\alpha}$ in the right ascension of the reflector. The linear dependence of these three parameters is clearly evident in equations (3.9) and (4.6).

4.3.2 Evaluation of the Coefficients

To evaluate the coefficients of equation (4.20), expressions have to be derived for α, δ, θ, ϕ and λ. Fortunately, ϕ and λ do not vary significantly and so for sensitivity-type studies it is quite acceptable to adopt constant values for these parameters to evaluate the coefficients. Given the approximations made thus far, values for ϕ and λ that are correct to within 0.2 degrees are more than sufficient. Typical values of ϕ and λ for stations of the LLR network are listed in Table 5.1.

In contrast, the quantities θ, α and δ change dramatically with time. θ and α complete full cycles in one day and one month, respectively, while the declination δ can change from -28° to 28° in 14 days. The Greenwich sidereal time θ is computed using the expression (Kaula 1966, p. 85-86)

$$\theta = 1.72218613 + 6.300388098\ (d_{MJD} - 36933.0) \qquad (4.21)$$

where d_{MJD} is the time of observation in Modified Julian Days and θ is in radians. To an accuracy sufficient for this study, α and δ can be computed from the well-known expressions (Explanatory Supplement 1961, p. 26)

$$\begin{aligned} \cos\delta\cos\alpha &= \cos\beta_m\cos\lambda_m \\ \cos\delta\sin\alpha &= \cos\beta_m\sin\lambda_m\cos\varepsilon - \sin\beta_m\sin\varepsilon \\ \sin\delta &= \cos\beta_m\sin\lambda_m\sin\varepsilon - \sin\beta_m\cos\varepsilon \end{aligned} \qquad (4.22)$$

In the above expressions β_m, λ_m and ε are the ecliptic latitude and

longitude of the moon and the obliquity of the ecliptic, respectively. To an accuracy that is consistent or better than that needed for this study (Hauser 1974)

$$\sin(\lambda_m - L) = 0.10976 \sin\ell - 0.0223 \sin(\ell - 2D) + 0.01149 \sin 2D + 0.00373 \sin 2\ell - 0.00324 \sin\ell' - 0.00200 \sin 2F - 0.00103 \sin(2\ell - 2D) - 0.00100 \sin(\ell' + \ell - 2D) + 0.00093 \sin(\ell + 2D) - 0.00080 \sin(\ell' - 2D) + 0.00072 \sin(\ell - \ell') - 0.0061 \sin D - 0.00053 \sin(\ell + \ell') \quad (4.23)$$

and

$$\sin \beta_m = 0.08950 \sin F + 0.00490 \sin(\ell + F) - 0.00485 \sin(F - \ell) - 0.00303 \sin(F - 2D) \quad . \quad (4.24)$$

Expressions for the fundamental arguments ℓ, ℓ' F and D of Brown's theory, the mean longitude of the Moon L, and ε are given in the Explanatory Supplement (1961). They are to first order in d_{MJD}

$$\varepsilon = 23^\circ.452294 - 0^\circ.0000003563(d_{MJD} - 15019.5) \quad (4.25)$$

$$L = 270^\circ.436586 - 13^\circ.1763965268(d_{MJD} - 15019.5) \quad (4.26)$$

$$\ell = 296^\circ.104608 + 13^\circ.0649924465(d_{MJD} - 15019.5) \quad (4.27)$$

$$\ell' = 358^\circ.475833 + 0^\circ.9856002669(d_{MJD} - 15019.5) \quad (4.28)$$

$$F = 11^\circ.250889 + 13^\circ.2293504490(d_{MJD} - 15019.5) \quad (4.29)$$

$$D = 350^\circ.737486 + 12^\circ.1907491914(d_{MJD} - 15019.5) \quad (4.30)$$

The arguments ℓ, ℓ', F and D refer to the lunar mean anomaly, the solar mean anomaly, the argument of lunar latitude and the mean lunar-solar

difference in longitude, respectively with the coefficients in units of degrees.

Therefore, given the time of observation d_{MJD} equations (4.21) to (4.30) are all that are needed to evaluate the coefficients in equations (4.20). All observatories are assumed to lie on the surface of a sphere with radius r_s = 6371 km. The computational procedure for the simulations is discussed in more detail in the following chapter. In the next section, the degree to which the parameters can be separated is discussed.

4.4 Comments on Parameter Separation

In order to separate out the earth rotation information contained in the correction terms $\Delta\phi$ and ΔH from information on the lunar orbit and rotation, it is important that H has a nearly diurnal period (≈25 hours) compared to the monthly cycle for the lunar declination δ and right ascension α. A close inspection of equation (4.15) also indicates that it is particularly desirable to schedule the off-meridian observations so that they are symmetric about the time when the moon crosses the meridian of the observatory and cover a period of at least six hours, preferably eight. This criterion ensures a good determination of the sinH and cosH signatures and hence, the earth rotation parameters in equation (4.15).

Consider for example, the "single-station" solution parameter ΔUT0. As described in Sections (2.3.1) and (2.4.4) it is the version of UT that has not been corrected for polar motion and as such is the only form of UT that can be derived from single station data (single station data cannot separate the component of polar motion perpendicular to the observer's meridian from UT1). ΔUT0 can be expressed alternatively as the apparent variation in the observer's longitude and thus its derivative is identical with that for the hour angle of the reflector (see eqs. 4.12 and 4.13). So to order r_s/ρ

$$\frac{\partial\rho}{\partial_{UT0}} \approx r_s \cos\phi\cos\delta\sin H \quad . \tag{4.31}$$

If the basic analysis interval covers only one day or even just a few

days, then it is clear that r_r, α and δ are practically constant since the shortest periodic variation of significance in these parameters is a libration term of 13.6 days. As a result, the first terms of the coefficients for Δr_s, $\Delta\phi$ and $\Delta\delta$ in equation (4.15) are also approximately constant and thus will have a similar effect as the coefficient for the Δr_r term. This leaves just the cosH and sinH signatures as well as a constant term to be filtered out from data that are analyzed for short-period (<a few days) information.

Equation (4.31) shows that an error in UT0 will produce a range residual that varies during the course of a day's ranging as the sine of the hour angle of the reflector. No other error source of similar magnitude is expected to introduce such a rapid variation in the range residuals and so this signature should yield an unambiguous estimate of UT0. It should also be pointed out that since H is zero at meridian transit and sinH varies quite rapidly during a normal observing period it is not essential for the hour angle coverage to be anywhere near 6 to 8 hours for an accurate determination of the sine curve. In this particular instance, a spacing of 3 hours between the first and last observations of the day is all that is needed for a good determination of UT0 (see e.g. Stolz et al. 1976). If the observations are perfectly symmetric about the meridian then UT0 is rigorously decoupled from the other parameters.

The preceding discussion illustrates the potential of the LLR technique for studying the short-period changes in the earth's spin rate. Problems such as locating the origin of the lunar right ascension in a space-fixed frame defined by a stellar catalogue or the effect of long-period errors in the lunar orbit are not significant if the object of the analysis is to search for the occasional abrupt changes that may occur in UT0 over a period of a few days or less.

For longer period studies the situation is less clear (Mulholland 1980). Obviously, the variation in the lunar parameters cannot be considered constant and so the amplitude of the errors in these terms at the critical frequencies must be studied carefully. For example, when the LLR data are analyzed for the subtle year-to-year fluctuations in the

annual term of the earth's spin rate efforts must be made to ensure that there are no errors in the lunar right ascension at frequencies that can possibly beat together to produce a similar effect.

The determination of the latitude ϕ of an LLR station and its variation requires more stringent scheduling of the observations in hour angle. Writing the derivative to order r_s/ρ as

$$\frac{\partial \rho}{\partial \phi} \approx r_s\{\sin(\phi-\delta) - \sin\phi\cos\delta(1-\cos H)\} \tag{4.32}$$

one clearly sees the importance of using the cosH signature to determine latitude variations, particularly when the moon is in the same hemisphere as the observing station ($\phi \approx \delta$). An error in station latitude produces a range residual that varies both slowly as the sine of the zenith distance at meridian transit and diurnally as the cosine of the hour angle H.

Herein, lies the difficulty of separating out the latitude information in the residuals from information pertaining to the lunar part of the problem. A quick inspection of equation (4.15) reveals a very close resemblance between the coefficients of $\Delta\phi$ and $\Delta\delta$. Furthermore, consider the analysis of observations gathered over a period of a few days or less and with poor hour-angle distribution. As H approaches zero, so to does the term (1-cosH). This leaves only the slowly varying first term in the derivative to determine the latitude. For periods of a few days or less, $\sin(\phi-\delta)$ is almost constant and this leads to a poor separability of the latitude variation $\Delta\phi$ from both the constant term Δr_r and the declination term $\Delta\delta$ (see equation 4.15). Even with good hour angle coverage the situation is only slightly improved.

Consider a simple case when three observations, made at hour angles -H, 0 and +H, with independent uncertainties of ± 3 cm, are used to determine the corrections $\Delta\phi$, ΔUT0 and Δr_r. One can write the system of equations as

$$\begin{aligned} v_1 = {} & \Delta\rho_1 - r_s\{\cos\phi\cos\delta\sin H\}_1 \Delta UT0 + \\ & r_s\{\sin(\phi-\delta) - \sin\phi\cos\delta(1-\cos H)\}_1 \Delta\phi + \Delta r_r \end{aligned} \tag{4.33}$$

$$v_2 = \Delta\rho_2 + r_s\{\sin(\phi-\delta)\}_2\Delta\phi + \Delta r_r \tag{4.34}$$

$$v_3 = \Delta\rho_3 + r_s\{\cos\phi\cos\delta\sin H\}_3\ \Delta UT0 + \\ + r_s\{\sin(\phi-\delta)-\sin\phi\cos\delta(1-\cos H)\}_3\ \Delta\phi + \Delta r_r \quad . \tag{4.35}$$

The solution is obviously unique (3 equations and 3 unknowns) and so $v_1 = v_2 = v_3 = 0$. Adding equations (4.33) and (4.35), substituting

$$\Delta r_r = -\Delta\rho_2 - r_s\{\sin(\phi-\delta)\}_2\ \Delta\phi \tag{4.36}$$

from equation (4.34), and assuming ϕ and δ are constant over the observation period gives

$$r_s\ \Delta\phi = (\Delta\rho_1+\Delta\rho_3-2\Delta\rho_2)/2\ \sin\phi\cos\delta(1-\cos H) \quad . \tag{4.37}$$

The corresponding variance of the latitude determination, $\sigma^2_{r_s\ \Delta\phi}$ for observation errors which are uncorrelated can be written as

$$\sigma^2_{r_s\ \Delta\phi} = \{\sigma^2_{\Delta\rho_1}+\sigma^2_{\Delta\rho_2}+4\sigma^2_{\Delta\rho_3}\}/4\ \sin^2\phi\cos^2\delta(1-\cos H)^2 \quad . \tag{4.38}$$

Since $\sigma^2_{\Delta\rho_1} = \sigma^2_{\Delta\rho_2} = \sigma^2_{\Delta\rho_3} = 9$ cm, equation (4.38) can be simplified to

$$\sigma_{r_s\ \Delta\phi} = 3\sqrt{6}\ /\ 2\sin\phi\cos\delta(1-\cos H)\ \text{ cm} \tag{4.39}$$

where $\sigma_{r_s\ \Delta\phi}$ is the standard deviation of the latitude determination. For $H = 60°$, $\phi = 30°$ and $\delta = 30°$; $\sigma_{r_s\ \Delta\phi} = 17$ cm. Thus, in this particular example, a 3 cm range uncertainty is mapped into a latitude uncertainty of 17 cm if the diurnal signature (1-cosH) in the derivative is relied on. On the other hand, if $\sin(\phi-\delta)$ is the main term used to determine $\Delta\phi$ and Δr_r is not included as a solution parameter then errors in r_r will contribute an uncertainty of $\sigma_{r_r}/\sin(\phi-\delta)$ to the total uncertainty for $\Delta\phi$. The system of equations becomes

$$v_1 = \Delta\rho_1 - r_s\cos\phi\cos\delta\sin H\ \Delta UT0 \\ + r_s\{\sin(\phi-\delta) - \sin\phi\cos\delta(1-\cos H)\}\ \Delta\phi + \Delta r_r \tag{4.40}$$

$$v_2 = \Delta\rho_2 + r_s\cos\phi\cos\delta\sin H\ \Delta UT0 + r_s\{\sin(\phi-\delta) - \sin\phi\cos\delta(1-\cos H)\}\ \Delta\phi + \Delta r_r \quad . \tag{4.41}$$

Clearly, a unique solution for $\Delta\phi$ and $\Delta UT0$ is obtained by assuming $\Delta r_r = 0$. The uncertainties in $\Delta UT0$ and $\Delta\phi$, taking into account an error in the assumption $\Delta r_r = 0$ and assuming uncorrelated observation errors, can be written as

$$\sigma_{r_s\ \Delta\phi} = \frac{1}{2}\{\sigma^2_{\Delta\rho_1}+\sigma^2_{\Delta\rho_2}+4\sigma^2_{\Delta r_r}\}^{\frac{1}{2}}/\{\sin(\phi-\delta)-\sin\phi\cos\delta(1-\cos H)\} \tag{4.42}$$

and

$$\sigma_{r_s\ \Delta UT0} = \frac{1}{2}\{\sigma^2_{\Delta\rho_1}+\sigma^2_{\Delta\rho_2}\}^{\frac{1}{2}}/\cos\phi\cos\delta\sin H \quad . \tag{4.43}$$

It is clear from equation (4.43) that for observations symmetric about meridian passage the solution for UT0 is completely decoupled from the parameters ϕ and r_r. The uncertainty in UT0 is determined only from the measurement uncertainties. Errors in r_r do not contribute at all. For observations that are not symmetric about the meridian the effect of errors in r_r will have to be considered if Δr_r is not included as a solution parameter. Also, as H approaches zero, the range becomes insensitive to variations in UT0. Equation (4.42), however, shows the contribution an error in r_r makes to the error estimate of a latitude determination. Assume, for example, that $\sigma_{\Delta\rho_1} = \sigma_{\Delta\rho_2} = 3$ cm, $H = 0°$, $(\phi-\delta) = 60°$ and $\sigma_{\Delta r_r} = 20$ cm, then

$$\sigma_{r_s\ \Delta\phi} = 23 \text{ cm} \quad .$$

For $\sigma_{\Delta r_r} = 0$,

$$\sigma_{r_s\ \Delta\phi} = 2.5 \text{ cm} \quad .$$

Of course, this example represents one of the more favourable geometric cases in LLR, that is, when the moon is in the opposite hemisphere to

the observing station. However, when both the moon and the station are in the same hemisphere, $\sin(\phi-\delta) \to 0$ and $\sigma_{r_s \Delta\phi} \to \infty$.

Because of this inescapable geometrical limitation, there is the possibility that the accuracy of polar motion results from an LLR network may not be adequate at specific times during a lunation if all the observing stations are located in the same hemisphere. The present geographical distribution of stations comes perilously close to satisfying this condition and so the polar motion issue is examined further in the next chapter. For UT1, the problem is not as serious. The determination of UT1 depends on a good determination of the sinH term (see equation 4.20) at two or more geographically well dispersed stations. This should be achieved relatively easily. Numerical calculations are carried out in the next chapter to ascertain which LLR station combinations give the best results.

CHAPTER 5

EARTH ROTATION SENSITIVITY STUDIES

5.1 Introduction

In 1974, a COSPAR resolution referring to LLR recommended "...the establishment of a coordinated international program to determine variations in the Earth's rotation...". This led to the planning of an initial observing campaign called EROLD (Earth Rotation by Lunar Distance) which began in 1978 and lasted for one year. While the objectives of the campaign were very commendable, several operational problems at many of the observatories expecting to participate prevented some of the goals from being realized (Calame and Guinot 1979). In all, only the McDonald, and to a lesser extent, the Orroral station contributed data. This meant that no clear-cut statement could be made on the suitability of LLR for monitoring polar motion and Universal time on a very accurate and continuous basis.

Therefore, using the theory presented in Section 3.3.1 and Chapter 4, a series of numerical experiments are carried out in this chapter to study this question. The dependence of the results on station location, lunar declination, averaging interval, data loss due to weather, hour angle coverage and other such factors is examined. The first group of experiments are undertaken with the specific purpose of simulating the likely outcome of future 'EROLD-type' analyses given that more observing stations are able to participate. Factors considered relevant to the outcome include (1) the measurement uncertainty at each station, (2) the network constituency, (3) the length of the averaging interval and (4) the long-period variation in the lunar declination. The second group of experiments are merely carried out for optimization purposes to investigate the strengths and weaknesses of the LLR network geometry and the importance of hour angle coverage.

A detailed description of the 'EROLD-type' analyses undertaken in this work is given in Section 5.3. However, before they are discussed

some comments on the observation selection procedure and the computational approach for these analyses seem appropriate.

5.2 Creating the Simulated Environment

The final uncertainties for polar motion and UT1 will depend partly on the measurement uncertainty and partly on the strength of the statistical determination of these quantities. While the pulse length is the main contributor to the measurement uncertainty, the strength of the statistical determination is a function of the station geometry, the position of the Moon in its orbit, and the number of observations obtainable during a predetermined averaging interval.

The network constituency for the numerical experiments to be reported in this chapter is essentially the one that was expected to be operational when this study was initiated. Of the seven possible stations that either could range or plan to range to the moon (see Sec. 3.4), only five are considered. These stations, together with their latitude and longitude, are listed in Table 5.1. The number of observations obtainable, however, depends on the observing schedule, the adopted averaging interval, the maximum allowable zenith distance, the new Moon effect and the weather. In the next section, the conditions of observability that are imposed for this study are discussed.

5.2.1 Conditions of Observability

5.2.1.1 Basic Limitations

In order for the simulated results to have a reasonable semblance to what might be expected in reality, there are several basic observing restrictions that must be acknowledged when creating the simulated environment. Most of these limitations are determined by the physical constraints of the problem, however, the observing schedule is essentially determined by the amount of telescope time that has been allocated to the LLR experiment.

a) Observing Schedule for Participating Stations. One of the more desirable features of the lunar motion for observing purposes is its slow orbital velocity. Besides the obvious tracking advantages, this

Table 5.1 LLR Station Locations

Station	Latitude	Longitude
	degrees	degrees
Orroral, Australia	-35.5	148.9
Calern, France	43.6	6.9
Dodaira, Japan	35.8	139.2
McDonald, Texas, U.S.A.	30.5	256.0
Haleakala, Hawaii	20.6	203.7

feature not only reduces the observing time needed to obtain acceptable statistics for normal point determinations but also prolongs the length of the orbital pass sufficiently to permit a good determination of the diurnal signatures in hour angle (see Sec. 4.4 for further discussion).

At the McDonald Observatory there are usually three 45 minute observation periods during the course of a day. These are (1) when the moon is approximately three hours east of the meridian, (2) when the moon is approximately on the meridian and (3) when the moon is approximately three hours west of the meridian. While this observing schedule may not be completely satisfactory to determine latitude variations at McDonald, it is basically a compromise between what is theoretically desirable and what is feasible on a time sharing system.

For this study, however, it is assumed that the observing schedule at McDonald can be modified to satisfy a tighter schedule which the other participating stations expect to achieve as dedicated laser ranging facilities. Rather than expecting a success rate of three ranges per day, it is anticipated that a maximum of five normal points can be obtained from any given station on any given day. These are assumed to occur when (1) the moon is four hours east of the station meridian, (2) the moon is two hours east of the station meridian, (3) the moon is on the meridian, (4) the moon is two hours west of the meridian, and (5) the moon is four hours west of the meridian. When all five stations are ranging, a total of 25 observations are possible from the network on any given day but clearly, the other boundary conditions will serve to reduce the number actually considered.

b) Restriction on Allowable Zenith Distance. Because of the possible danger to aircraft the laser at McDonald cannot be fired at zenith distances greater than 70°. Above this limit there is also the problem of modelling the refractive effects at the sub-centimetre level for a photon travel path which skirts the horizon (see e.g. Hopfield 1976).

The effect of this constraint is to reduce the available hour angle coverage when the moon is in the opposite hemisphere to the station. When terms of the order r_s/ρ are neglected, the zenith distance Z is

readily computed as a function of the station latitude, the lunar declination and the lunar hour angle, using the expression

$$\cos Z = \cos \delta \cos \phi \cos H + \sin \delta \sin \phi \quad . \tag{5.1}$$

Clearly, when the moon is on the meridian (H = 0) equation (5.1) reduces to

$$\cos Z = \cos(\phi - \delta) \quad . \tag{5.2}$$

If the LLR stations are located at moderate to high latitudes ($\phi \geq \pm 45°$), the zenith distance restriction has a profound effect. Loumos et al. (1975) estimate that roughly 50% of the observations from their adopted observing schedule are eliminated by a $Z > 70°$ criterion. Fortunately, the effect at the fixed stations is not nearly as severe. Of the five stations used in this study, the greatest loss will occur at the French site where, at southern declinations exceeding -27 degrees, even meridian transit observations may not be possible. However, as Morgan (1977) points out, advances forthcoming from remote atmospheric sensing in specific bands offer the possibility of providing sufficient information to extend the working zenith angle to 75-80 degrees. This would then allow the French site to observe the moon at $\delta = -27$ degrees.

For the purposes of this study, a rather conservative attitude is adopted regarding the zenith distance restriction. Instead of trying to re-schedule an observation that fails the zenith distance criterion closer to the meridian, it is simply excluded from the analysis.

c) Data Loss Around New Moon. One frequent hindrance to LLR data acquisition is the lack of contrast that occurs at new moon between the lunar surface features and the sky background. Experience at McDonald indicates that observations are generally not possible during a 5 to 6 day period centred on new moon, or equivalently, when the sun-moon angle (angle subtended at the geocentre by the solar and lunar position vectors) is less than about 45° (Silverberg 1974). Using conventional trigonometric relations, one can express the sun-moon angle, ψ_{sm} as

$$\cos \psi_{sm} = \cos \beta_m \cos \lambda_m \cos L' + \cos \beta_m \sin \lambda_m \sin L' \tag{5.3}$$

where λ_m and β_m are defined by equations (4.23) and (4.24), respectively and L', the mean longitude of the sun. The expression for L' has the

form (Explanatory Supplement 1961)

$$L' = 279.^{0}696678 + 0.^{0}9856473354\ (d_{MJD} - 15019.5) \quad . \qquad (5.4)$$

In Kaula's (1973) analysis, it is assumed that ranges are made to the moon when $\psi_{sm} \geq 60°$. Although this constraint was a realistic representation of the problem then, there is now hope that the contrast of the television image of the lunar surface can be enhanced electronically and thus permit more daytime observing. As a compromise between present reality and future expectations, it was decided that all observations in the time interval when $\psi_{sm} \leq 40°$ be excluded from the analysis. No attempt has been made to model the short interruptions that occur at the observing stations for telescope maintenance. Hopefully, this work can be accomplished around the time of new moon.

5.2.1.2 Weather Modelling

Optical experiments such as lunar laser ranging are invariably interrupted by overcast weather or atmospheric turbulence. At McDonald the laser is not fired unless there are lunar images that are equivalent to having about 75% of the light from any star located within a 5 asec circle of the photon path (Silverberg 1974). Consequently, the effect of this limitation is to reduce the strength of the statistical determination of the parameters of interest by weakening the network geometry when one or a group of stations are not ranging, and by reducing the number of observations possible during a given averaging interval.

To allow for data loss due to weather in a plausible way, a model based on climatological data and probability theory is constructed. A detailed derivation of the statistical model is given by Ross (1972). The model assumes that the day-to-day weather pattern at any station in the network follows a two-state Markov chain whose transition probability matrix [T] is given by

$$[T] = \begin{bmatrix} T_{00} & T_{01} \\ T_{10} & T_{11} \end{bmatrix} = \begin{bmatrix} 1-b & b \\ 1-a & a \end{bmatrix} \qquad (5.5)$$

where a is the probability that given fine weather on day i it will also be fine on day i+1 and b is the probability that given cloudy weather on

day i it will be fine on day i+1. The subscripts 0 and 1 in equation (5.6) are thus the two states of the Markov chain. Clearly, when the process is in state 0 it is cloudy and when in state 1 it is fine.

An important property of the two-state Markov chain is that the conditional distribution of any future state F_{i+1} given the past states $F_0, F_1, \ldots, F_{i-1}$ and the present state F_i, is independent of the past states and depends only on the present state F_i. Moreover, if F_i is the stochastic ensemble which defines the above weather prediction model then

$$F_{i+1} = \begin{cases} 1 & \text{if } F_i = 1 \text{ and } e_{i+1} < a \\ 1 & \text{if } F_i = 0 \text{ and } e_{i+1} < b \\ 0 & \text{, otherwise} \end{cases} \qquad (5.6)$$

where e_{i+1} are independent random variables uniformly distributed over the interval 0 to 1. The evaluation of the probabilities a and b is accomplished using the general rules of conditional probability and expectation. Let μ be the probability that F_i will be a fine day, that is,

$$\text{Prob}\{F_i=1\} = \mu \quad . \qquad (5.7)$$

Because F_i is a Bernoulli random variable, its expected value can be written as (Ross 1972, p. 30)

$$\begin{aligned} \langle F \rangle \equiv \langle F_i \rangle &= \text{Prob}\{F_i=1\}\, 1 + \text{Prob}\{F_i=0\}\, 0 \\ &= \mu\, 1 + (1-\mu)\, 0 \\ &= \mu \quad . \end{aligned} \qquad (5.8)$$

Given the above conditions of equation (5.7), the probability that F_{i+1} is a fine day is given as

$$\begin{aligned} \text{Prob}\{F_{i+1}=1\} &= \text{Prob}\{F_i=1\}\ \text{Prob}\{e_{i+1}<a\} + \text{Prob}\{F_i=0\}\ \text{Prob}\{e_{i+1}<b\} \\ &= \mu\, a + (1-\mu)\, b \quad . \end{aligned} \qquad (5.9)$$

From the form of equation (5.8) and the result of equation (5.9), one can express the expected value of F_{i+1} as

$$\langle F_{i+1} \rangle = \mu\, a + (1-\mu)\, b \quad . \qquad (5.10)$$

Given the stationary quality of the expected value one can equate equations (5.8) and (5.10) and write

$$\begin{aligned} \langle F_{i+1} \rangle &= \mu\, a + (1-\mu)\, b \\ &\equiv \langle F \rangle = \mu \quad . \end{aligned} \tag{5.11}$$

To complete the evaluation of a and b use is made of the rules of conditional expectation to compute the correlation between F_i and F_{i+1}. In particular, the variance of F_i is defined as (Ross 1972, p. 34)

$$\mathrm{Var}(F_i) = \langle (F_i - \mu)^2 \rangle \quad . \tag{5.12}$$

Expanding equation (5.12) gives (Ross 1972, p. 37)

$$\mathrm{Var}(F_i) = \mu(1-\mu) \quad . \tag{5.13}$$

In a similar fashion, the covariance between F_i and F_{i+1} can be written as (Ross 1972, p. 41)

$$\mathrm{Cov}(F_i, F_{i+1}) = \langle (F_{i+1} - \mu)(F_i - \mu) \rangle \quad . \tag{5.14}$$

Expanding equation (5.14) gives

$$\mathrm{Cov}(F_i, F_{i+1}) = \mu(a-\mu) \quad . \tag{5.15}$$

Using equations (5.13) and (5.15), one can write the correlation c between F_i and F_{i+1} as

$$\begin{aligned} c &= \frac{\mathrm{Cov}(F_i, F_{i+1})}{\mathrm{Var}(F_i)} \\ &= \frac{a-\mu}{1-\mu} \end{aligned} \tag{5.16}$$

Rearranging terms in equation (5.16) gives

$$a = c(1-\mu) + \mu \tag{5.17}$$

and substituting this result into equation (5.11) for b yields

$$b = \mu(1-c) \quad . \tag{5.18}$$

In order to calculate a and b it is necessary to assign reliable values to μ and c based on the available climatological records at each site. For this study, values of what are considered to be indicators of

observability have been compiled on a monthly basis for each station using data from H.M.S.O. (1965), Landsberg (1970), Loumos et al. (1975), Luck et al. (1973) and Orton (1969). These indicators, as listed in Tables 5.2, 5.3 and 5.4, respectively, are: W1, the percentage of days completely clear per month; W2, the percentage of days completely cloudy per month; and W3, a visibility factor, also expressed in percent, which describes the average amount of usable sky per month.

In deriving the monthly weather factors for Orroral, Calern, Dodaira and McDonald a normalization procedure was employed so that the annual average data loss at these stations, as predicted by the weather model, agreed closely with a reliable long-term average of cloud cover for the region in which each station is located. The weather factors for Orroral were taken directly from the reconnaissance study undertaken by the Division of National Mapping, Canberra, Australia (Luck et al. 1973). However, since the study covered a two-year period only, the factors W1, W2 and W3 for this site were normalized so that their annual average agreed with the appropriate regional estimates given by Landsberg (1970).

Values for Calern and Dodaira were obtained solely from the previous reference source and, therefore, are regional estimates only. The W1 factors for both stations are deduced from the number of sunshine hours per month and on some occasions the seasonal values for the number of clear days. Values for W2 are based on estimates for the number of days with precipitation, thunderstorms, gales and fog while W3 values are based on the long-term monthly averages of mean cloudiness.

Values of W1 and W2 for McDonald were obtained directly from Orton (1969) and normalized, according to Landsberg (1970), to give annual averages of 40% and 25% respectively. Values for W3, like those of Calern and Dodaira, are based on the long-term monthly averages of mean cloudiness listed in Landsberg (1970).

Care was taken in deducing the values for the Haleakala site because it was pointed out that it would be risky to use regional weather statistics to describe the sky behaviour at a site situated above the inversion level (Bender, private communication, 1976). The observatory

Table 5.2 Estimated Percentage Number of Completely Clear Days per Month (W1) at LLR Sites

Month	Observatory (Clear Days, %)				
	Orroral	Calern	Dodaira	McDonald	Haleakala
Jan	19	18	37	32	25
Feb	19	19	34	37	30
Mar	25	22	27	32	35
Apr	35	26	22	39	40
May	30	29	19	47	45
June	43	32	13	52	45
July	38	36	13	26	40
Aug	23	33	17	32	35
Sept	34	28	18	49	30
Oct	33	22	29	50	25
Nov	27	18	33	46	25
Dec	33	17	39	38	20

Table 5.3 Estimated Percentage Number of Cloudy Days per Month (W2) at LLR Sites

Month	Observatory (Cloudy Days, %)				
	Orroral	Calern	Dodaira	McDonald	Haleakala
Jan	51	51	45	36	38
Feb	50	45	55	31	33
Mar	43	51	66	36	35
Apr	32	52	79	25	33
May	37	44	75	16	29
June	27	34	57	12	33
July	29	24	61	23	38
Aug	41	34	64	20	35
Sept	32	47	64	21	36
Oct	31	50	57	20	35
Nov	39	46	48	28	36
Dec	31	50	48	32	40

Table 5.4 Estimated Percentage Amount of Visible Sky per Month (W3) at LLR Sites

Month	Observatory (Visibility Factor, %)				
	Orroral	Calern	Dodaira	McDonald	Haleakala
Jan	54	37	63	52	65
Feb	52	35	51	55	75
Mar	52	29	42	54	65
Apr	49	35	36	60	65
May	47	34	31	65	60
June	43	41	19	68	50
July	47	65	25	52	45
Aug	49	57	34	57	50
Sept	52	46	25	68	55
Oct	48	40	32	65	55
Nov	48	32	44	66	60
Dec	53	35	60	57	65

on Mt. Haleakala is at an elevation of approximately 3000 meters above sea level. For this reason, the weather factors for Haleakala were normalized so that the average annual data loss predicted by the model was about 40%. This is the estimate obtained at the site by the LURE team before the station was erected. The monthly values for W1 and W2 were estimated using data from H.M.S.O. (1965) while the values for W3 were deduced from the seasonal weather maps published by Loumos et al. (1975).

Since monthly values of weather data were available, the probabilities a and b were calculated for each station every month. To calculate the value of μ, it seemed logical to use the factor W2, that is,

$$\mu = 1 - 0.01\ W2 \tag{5.19}$$

because the probability that ranging is attempted on any given day in any month is simply a function of the number of completely cloudy days for that month. Choosing a value for the correlation c between F_i and F_{i+1} was extremely difficult because the task of obtaining daily values of W2 at each station in order to compute the covariance function was clearly outside the scope of this work and, more than likely, not warranted. Instead, a compromise was made by setting c equal to 0.5. By invoking this assumption, one not only avoids the time consuming work involved with the alternate method but at the same time has an estimate of c which, given the stochastic properties of the weather, seems reasonable.

After determining whether it is possible to range on day i+1, the next step is to calculate how many ranges should be accepted within a given day. This is accomplished using a random number generator and empirical formulae based on W1 and W3. Clearly, if the weather model allows ranging on day i+1 then the probability of obtaining one range on that day will be very close to unity. A small margin is left to account for the fact that atmospheric seeing may cause acquisition problems even when there is no cloud in the sky. The probability of obtaining one or more ranges is taken to be

$$P_{\geq 1} = 0.001\ W3 + 0.9 \quad . \tag{5.20}$$

Similarly, the probability of obtaining four or more ranges is defined as the number of completely clear days during a month divided by the expected number of days on which ranging is possible during that month, that is,

$$P_{\geq 4} = \frac{W1}{100-W2} \quad . \tag{5.21}$$

The probabilities for getting two or more, three or more and five ranges are obtained by interpolating and extrapolating the values derived from equations (5.20) and (5.21). Once all probabilities have been determined, a random number is compared with these values to settle on the number of ranges actually obtained on that day.

In view of the nature of this study, there did not appear to be anything to gain by incorporating a correlation between observing windows on any day as did Loumos et al. (1975) in their study of the accuracy of site coordinates obtainable with a mobile lunar ranging station. Instead, when less than five ranges are predicted by the weather model the selection procedure (see schedule) tends to place the ranges nearer the meridian as it is less likely to be cloudy towards the zenith. Note, the initial number of accepted ranges is chosen merely on the basis of the weather model. Each range is then checked for compliance with the zenith distance and sun-moon angle constraints (see next section).

The percentage data loss for each month of the year at the LLR sites, as predicted by the weather model, is shown in Table 5.5. Three points are interesting to note. The first is the good agreement ($\leq 5\%$ in all cases) between the annual average data loss indicated by the statistical model and the weather records. Also, the periods of bad weather at Dodaira as mentioned by Kozai (1975) and at Calern as mentioned by Kovalevsky (1975) have been reproduced by this model. However, the expected loss of data at McDonald during the wetter periods in July and sometimes August are barely distinguishable. Nevertheless, the model does conform with McDonald's general weather patterns which permit an average to good availability of observing time throughout the year, but with considerable scatter (Evans 1977).

Schedule for Observation Selection Procedure after Weather Considerations

Number of Accepted Ranges	Placement in Hour Angle, hours				
	-4	-2	0	+2	+4
1				X	
2	X			X	
3	X		X	X	
4	X	X	X	X	
5	X	X	X	X	X

Table 5.5 Data Loss Due to Weather at LLR Sites

Month	Observatory				
	Orroral	Calern	Dodaira	McDonald	Haleakala
	Data Loss, %				
Jan	64	64	76	51	49
Feb	66	61	32	31	29
Mar	54	62	58	50	41
Apr	44	40	73	38	39
May	38	69	85	55	46
June	47	62	79	35	35
July	33	64	68	43	37
Aug	62	49	67	29	45
Sept	43	37	81	28	50
Oct	43	55	41	25	68
Nov	58	72	55	41	48
Dec	64	42	60	47	50
Annual Average					
Weather Model	51	56	65	39	45
Weather Records*	53	60	64	38	40†

*Based on long-term averages of mean cloudiness (Landsberg 1970).

†Value communicated by Bender (private communication, 1976).

5.2.2 Computation Procedure for the Analyses

After the initialization of all respective arrays, the read-in of all necessary input, and the computation of all appropriate conversions, the starting time d_o(MJD) for the analysis is set at the specified date (the beginning of the year) and a calculation begins over two nested 'DO' loops: the outer loop for all days within the specified sampling interval and the inner loop over all stations contributing to the analysis. In the numerical experiments carried out in this study, the sampling interval is either chosen as one, two or five days while the number of contributing stations varies from three to five. The analyses extend over a period of one year (see Section 5.3).

At the beginning d_x(MJD) of each day within the sampling interval, the corresponding Greenwich sidereal time θ_x and the right ascension of the moon α_x are computed using $d_{MJD} = d_x(MJD)$ in equations (4.21) and (4.22). From this information, the time of the lunar meridian transit d_c(MJD) at each station is calculated by

$$d_c(MJD) = (\dot{\theta}-\dot{\alpha})^{-1} \bmod\{(\alpha_x-\theta_x-\lambda),\ 2\pi\} + d_x(MJD) \qquad (5.22)$$

where λ is the station longitude. A check is made every day to ensure that the simulated observations do not overlap those of the previous day.

Once the time of meridian transit is established at each participating station it is a straightforward matter to set up the observing schedule. To do this, the weather model is called for each station to see if ranging is possible on the specified day and to decide on how many ranges are permitted on that day. The initial conditions for the weather station, that is, does $F_{i=1}$ equal 0 or 1 are chosen at random. If it is a fine day ($F_{i=1} = 1$), then the number of ranges permitted by the weather model are placed in their respective 'positions' according to the prescribed placement procedure (see previous section). The values of F_i for each station are stored in an array for the subsequent calculation of F_{i+1} on the next day. For each observation that has been accepted, a determination is made to see whether the Moon is within the maximum allowable zenith distance and beyond the minimum sun-moon angle [see equations (5.1) and (5.3), respectively].

Table 5.6 Effect of Weather, $Z_{max} = 70°$ and New Moon on the Number of Observations Obtainable for a Two-Day Sampling Interval During 1977

Number of Observations Obtained	Occurrence, %
0-5	17
6-10	5
11-15	12
16-20	21
21-25	21
26-30	16
31-35	6
36-40	2
41-45	0
46-50	0

For each of the available observation times that are not eliminated by these constraints, the coefficients of the observation equation (4.20) are evaluated using the appropriate time argument d_{MJD} and written onto tape. In the evaluation, the hour angle for off-meridian observations is calculated from the equation

$$d_{MJD} = d_c(MJD) \pm (\dot{\theta}-\dot{\alpha})^{-1} \cos^{-1} H \qquad (5.23)$$

where d_{MJD} is the specified time of the observation in MJD. Obviously, the observing schedule adopted in this work only allows the quantity $\{d_{MJD} - d_c(MJD)\}$ to have specific values. A typical frequency distribution of the number of accepted ranges after the imposition of all observational constraints is shown in Table 5.6 for a two-day sampling period. Clearly, the significant percentage in the interval range 0-5 is due entirely to the sun-moon angle restriction. For a two-day period, a maximum of 50 observations are possible from a network of five stations.

At the end of the sampling period, the coefficients are read back off the tape and, together with an appropriate [G] matrix for the observation variances, are analyzed according to equations [(3.33) to (3.38)] to obtain the final variance-covariance matrix for the parameters. The standard deviations σ_x, σ_y and σ_{UT1} for the unknown parametric corrections Δx, Δy and $\Delta UT1$ are obtained by taking the square root of the appropriate diagonal elements of the variance-covariance matrix. With the exception of the initial steps, the procedure just outlined is repeated as many times as there are sampling intervals in one year. For a sampling period of 5 days this will mean 73 times.

5.3 Description of the Numerical Experiments

Based on the theory outlined in Chapters 3 and 4, and the previous sections of this chapter, a series of numerical experiments are carried out to ascertain whether LLR can provide frequent earth rotation information accurate to 5 cm given all the observational constraints previously discussed. This accuracy level is a realistic estimate that ultimately should be obtained by the space techniques. No attempt is made in these analyses to correct the observations for errors in the

lunar orbit and rotation. It is assumed that the only contribution to the residual is caused by errors in x, y and UT1 [see eq. (4.20)]. In this context, the results obtained are likely to be slightly more optimistic than pessimistic. This section gives a brief description of the numerical studies undertaken.

The experiments are divided into three major categories according to the measurement uncertainty schedule adopted for each experiment (see Table 5.7). At first glance, the schedule for Experiment 1 appears overly pessimistic with regard to the measurement uncertainties for the Orroral, Calern and Dodaira stations. On the other hand, if the Calern and Dodaira stations were to begin ranging immediately, then the schedule would be a fairly close representation of reality.

Experience has shown, however, that the refinements in the operation and performance of a sophisticated LLR facility takes years to achieve. The schedule for Experiment 2 is thus an optimistic budget that could be achieved within a reasonable time frame if the current developmental and updating programs at each LLR station go according to plan. Finally, the schedule for Experiment 3 is included with the hope that the ± 3 cm accuracy goal of the Hawaiian station can also be realized in the future by every station in the LLR network. Obviously, the results obtained from Experiment 3 will be premature for the present. However, since all observations in Experiment 3 contribute equally to a solution, the results can be scaled accordingly if the measurement uncertainty happens to be uniformly worse at each station.

The purpose of each simulation is to investigate what the likely outcome of a typical 'EROLD-type' experiment would be given the measurement uncertainty schedule discussed above. Of course, interest is mainly focussed on the results obtainable when all five stations, that is, Orroral, Calern, Dodaira, Haleakala and McDonald are participating. However, there is the possibility that less than this number will be operational in the near future and so the results obtainable from likely combinations of three stations and four stations are also presented. Each simulation lasts for a period of one year. The observations are sampled so that accuracies are obtained for one-day, two-day and five-day

Table 5.7 Measurement Uncertainty Schedule

Experiment Number	Stations*				
	A	F	J	T	H
	Measurement Uncertainty σ_1, cm				
1	50	50	50	10	3
2	10	10	10	3	3
3	3	3	3	3	3

*A = Australia, F = France, J = Japan, T = Texas, H = Hawaii.

averages only. The one-day sampling interval is chosen on the basis that the previously described observing schedule is unlikely to produce better than daily values of polar motion and UT1. Two-day and five-day values are currently being obtained by the DMA and BIH agencies and are, therefore, considered for this purpose.

Experiment 3 is also repeated for subsequent years in order to determine what effect the changing declination bandwidth in latitude has on the outcome of the results. During 1977, the declination varies between $\sim \pm 19°$. However, by 1986 the limits have changed to approximately $\pm 28°$ and this could have an effect on the results for polar motion and UT1. The effect is manifest two ways. Firstly, the zenith distance restriction will have a more profound effect on the elimination of off-meridian observations when the moon occupies its orbital positions of maximum declination and secondly, the latitude dependent $\sin(\phi-\delta)$ term is, on the average, much smaller when the declination is $\pm 28°$ than when $\pm 19°$. This means that because of the bias towards north hemisphere stations in the present LLR network, the ranges made at northern declination times will be less sensitive to polar motion variations during 1986. The UT1 determination is dependent, to a certain extent, on the $\cos\delta$ term in its partial derivative. This term, however, is nowhere near as sensitive to declination changes as is the $\sin(\phi-\delta)$ term. Thus, the effect on UT1 determinations will probably be due to a combination of geometry and the impact of the zenith distance constraint.

In the following section the results of these experiments are presented together with some optimization calculations that have been carried out to further explore the dependency of earth rotation results on station location, lunar declination and hour angle coverage.

5.4 Polar Motion and UT1 Results

5.4.1 Outcome of 'EROLD-type' Analyses

Summaries of the simulations for the 'EROLD-type' analyses are presented in Tables 5.8 to 5.14. In all cases, the percentage number of sampling intervals for which uncertainties in x, y and UT1 are better than or equal to 5 cm are given. While expressing the uncertainty of these parameters in units of distance is contrary to normal astronomical

conventions, it does help in the assessment of the results when comparisons are made with the basic measurement uncertainties. Even so, one can easily make the necessary conversions by assuming 1 cm at the earth's surface is equivalent to approximately 3×10^{-4} asecs in x and y and 0.02 msecs in UT1 for an earth radius of 6371 km.

Table 5.8 illustrates fairly conclusively that an LLR network of five stations or less will have great difficulty in consistently providing daily values of UT1, x and y good to ±5 cm. In particular, the measurement uncertainty schedules for Experiments 1 and 2 are clearly unacceptable if these goals are to be achieved. The results for Experiment 3, however, are somewhat more encouraging. The fact that approximately 17% of the daily sampling intervals are eliminated by the sun-moon angle restriction means that of the remaining 83%, approximately 80% have solution uncertainties for x, y and UT1 good to ±5 cm when five stations are ranging. This would seem to indicate that a network of at least seven or eight stations would be required to produce continuous daily values of Universal time and polar motion at the 5 cm level. Of course, this conclusion depends critically on each station attaining a measurement uncertainty level of ±3 cm and the assumption that the lunar orbit and rotation are perfectly known. Also, if the problem around new moon cannot be resolved then users will have to look to other techniques for daily values over this period. However, all these factors are reduced in significance if two-day and five-day averages are considered.

Results for a sampling interval of two days are shown in Table 5.9. As expected, there is no marked improvement in the outcome of Experiment 1 and the fact that there are still no solutions for y with uncertainties less than or equal to ±5 cm is not considered significant. A closer inspection of the computer output for Experiment 1 showed that about 15% of the sampling intervals gave solution uncertainties for y in the range $5 \text{ cm} < \sigma_y \leq 10 \text{ cm}$. The reason for this is due to the fact that the Hawaiian station, which contributes more to the solution for the x component of polar motion, has a measurement uncertainty about a factor of three smaller than the Texan station; the latter station is located near the meridian that defines the y coordinate of the pole. An interesting

Table 5.8 Simulated Outcome of 'EROLD-type' Campaign for Single Day Sampling. The measurement uncertainty schedule of Table 5.7 is used. The first, second, and third value in each column refers to the results for the x, y and UT1 parameters, respectively. The analysis period is one year and extends through 1977.

Stations*					Percentage Number of 1-Day Solution Uncertainties ≤5 cm		
A	F	J	T	H	Experiment 1	Experiment 2	Experiment 3
					x, y and UT1; %		
5 Stations							
o	o	o	o	o	1,0,7	19,32,54	67,66,72
4 Stations							
o		o	o	o	0,0,7	18,27,41	52,47,61
o	o		o	o	1,0,6	17,31,49	60,61,66
	o	o	o	o	0,0,6	16,27,44	54,55,58
3 Stations							
		o	o	o	0,0,6	16,19,29	33,28,40
	o		o	o	0,0,6	15,23,39	42,46,50
o			o	o	0,0,6	15,25,35	38,40,50

*A = Australia, F = France, J = Japan, T = Texas, H = Hawaii.

Table 5.9 Simulated Outcome of 'EROLD-type' Campaign for Two Day Sampling. The measurement uncertainty schedule of Table 5.7 is used. The first, second, and third value in each column refers to the results for the x, y and UT1 parameters, respectively. The analysis period is one year and extends through 1977.

Stations*					Percentage Number of 2-Day Solution Uncertainties ≤5 cm		
A	F	J	T	H	Experiment 1	Experiment 2	Experiment 3
					x, y and UT1, %		
5 Stations							
o	o	o	o	o	14,0,24	53,54,77	79,79,82
4 Stations							
o		o	o	o	14,0,24	42,47,66	71,68,75
o	o		o	o	13,0,24	45,54,75	76,77,79
	o	o	o	o	13,0,24	40,53,69	71,73,75
3 Stations							
		o	o	o	11,0,24	31,40,53	52,51,62
	o		o	o	11,0,23	32,51,66	65,69,71
o			o	o	13,0,24	36,46,58	59,60,67

*A = Australia, F = France, J = Japan, T = Texas, H = Hawaii.

observation on the outcome of Experiment 1 is the number of intervals (≈25%) for which the determination of UT1 has an uncertainty better than or equal to ±5 cm. It was noted that these solutions were obtained only when the Hawaiian and Texan stations were ranging.

Clearly, when the measurement uncertainties for all stations become more balanced, so to do the results for two-day sampling (see results for Experiments 2 and 3, Table 5.9). Once again, the most impressive results are obtained when five stations are ranging and their measurement uncertainties are ±3 cm. This time, however, practically all the two-day solutions for x, y and UT1 outside the new Moon period have uncertainties better than ±5 cm. Even the four station combinations appear capable of providing equivalent results about 70% or more of the time.

Two more points concerning the results of Table 5.9 should be mentioned. The first is the reasonably high percentage of two-day solutions for x, y and particularly UT1 obtained by the five station configuration during Experiment 2 that are good to ±5 cm. This is very encouraging considering the Orroral, Calern and Dodaira stations ranged with measurement uncertainties of ±10 cm. It is also interesting to note that there is not much difference between the UT1 uncertainties as obtained from Experiments 2 and 3. Changing the measurement uncertainties at Orroral, Calern and Dodaira from ±3 cm to ±10 cm has only a marginal effect (≈5-10%) on UT1 uncertainties and a noticeable effect (≈20-30%) on the polar motion uncertainties if two-day sampling is considered. This result suggests that if a network of seven or eight stations were to exist then it would not be compulsory for all stations to achieve a measurement uncertainty of ±3 cm if only two-day values of polar motion and UT1 are needed at the ±5 cm level.

Table 5.10 indicates that five-day values of x, y and UT1 with uncertainties better than 5 cm can almost always be achieved from the five station configuration if the measurement uncertainty schedule for Experiment 2 or 3 is assumed. Even the four station combinations would be adequate if all stations ranged with a measurement uncertainty of ±3 cm. It is unfortunate, however, that there are still times when it is not possible

Table 5.10 Simulated Outcome of 'EROLD-type' Campaign for Five Day Sampling. The measurement uncertainty schedule of Table 5.7 is used. The first, second, and third value in each column refers to the results for the x, y and UT1 parameters, respectively. The analysis period is one year and extends through 1977.

Stations*					Percentage Number of 5-Day Solution Uncertainties ≤5 cm		
A	F	J	T	H	Experiment 1	Experiment 2	Experiment 3
					x, y and UT1, %		
5 Stations							
o	o	o	o	o	35,11,54	85,88,89	93,93,93
4 Stations							
o		o	o	o	34,11,51	77,80,86	90,91,93
o	o		o	o	34,10,53	83,87,87	90,92,92
	o	o	o	o	34,10,50	77,83,88	86,88,89
3 Stations							
		o	o	o	34, 8,47	59,63,80	72,78,87
	o		o	o	33, 9,50	70,82,85	83,87,87
o			o	o	34,10,51	70,77,83	82,84,89

*A = Australia, F = France, J = Japan, T = Texas, H = Hawaii.

to obtain a solution around the new Moon period. Of course, this difficulty could be overcome by spacing the five day periods so that the changeover occurred near new Moon. In particular, the results from the five station configuration for Experiment 3 indicate that some overlapping did occur around this time period. On this occasion, solutions for x, y and UT1 to better than ±5 cm were obtained 93% of the time as opposed to 83%. This latter value would have been the result had the five day sampling intervals coincided exactly with all the new Moon periods that occurred throughout the year. Once again, the results from Experiment 1 are not satisfactory. It is interesting to note, however, that about 50% of the solutions for UT1 had uncertainties better than ±5 cm even with the poor measurement uncertainties.

The percentage number of successful solutions for x, y and UT1, irrespective of whether or not the parameter uncertainties satisfy the ±5 cm limit, are listed in Table 5.11. These results are identical for Experiments 1, 2 and 3 and are for 1977 only. It is emphasized that the percentages for any given station combination will not equal 100 because of the effect of data loss generally, which is to say, that cases where too few observations are available to invert the normal equation matrix [N] are excluded, as is the effect of data loss due to new Moon.

The effect of a change in lunar declination bandwidth on the outcome of the results is shown in Figure 5.1 and summarized in Tables 5.12, 5.13 and 5.14. The results for 1977 are listed again for comparison. In general, the results for single-day and two-day sampling are about 10% worse during 1986 than they are for 1977. This is a consequence of the declination bandwidth changing from ±19° to ±28° for these years and the subsequent effect it has on the zenith distance restriction and the range sensitivity to variations in x, y and UT1. For five-day averages, only the results from the three station configurations change by 10%. For all other years, the results are essentially the same to within 5%. This suggests that this phenomenon should not seriously affect the outcome of LLR earth rotation experiments.

Table 5.11 Percentage Number of Successful Solutions for x, y and UT1 using a One, Two and Five Day Sampling Interval.

Stations*					Sampling		
A	F	J	T	H	Single Day	Two Day	Five Day
					Number of Intervals, %		
5 Stations							
o	o	o	o	o	77	83	93
4 Stations							
o		o	o	o	67	80	93
o	o		o	o	73	81	93
	o	o	o	o	65	78	89
3 Stations							
		o	o	o	51	69	87
	o		o	o	58	74	88
o			o	o	60	74	90

*A = Australia, F = France, J = Japan, T = Texas, H = Hawaii.

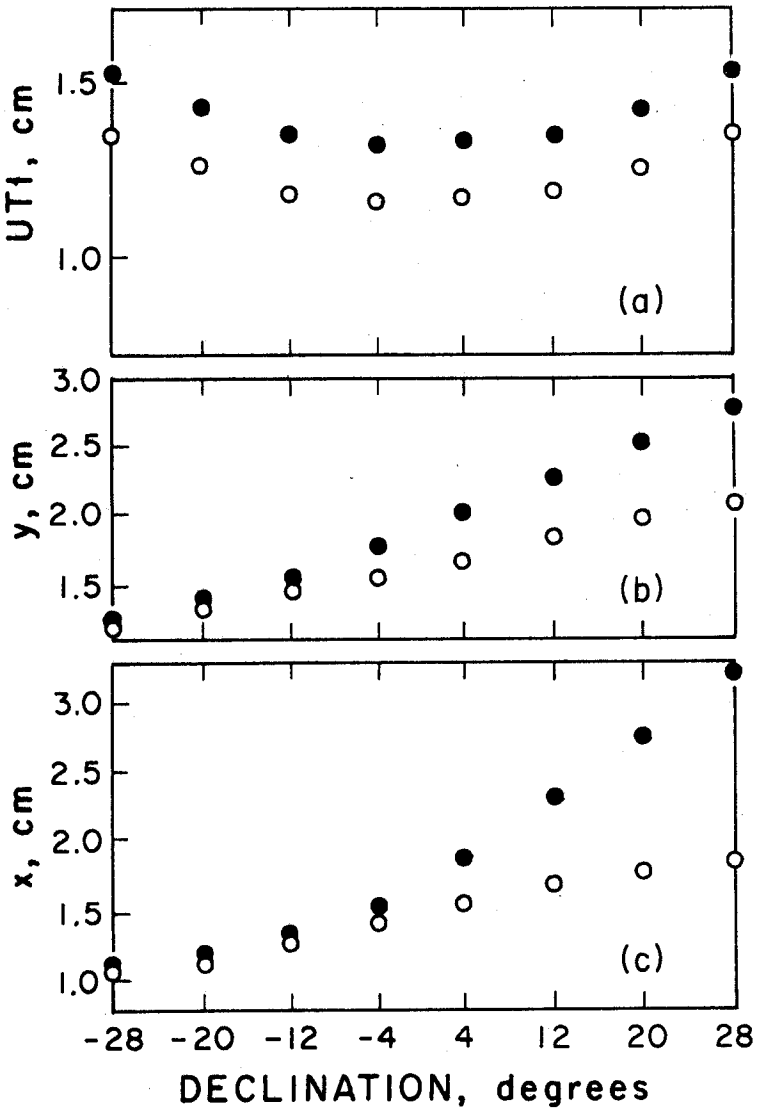

Figure 5.1 (a) Uncertainty for UT1. Open circles: All five stations ranging. Solid circles: Orroral excluded. (b) Same, except for y coordinate of the pole. (c) Same, except for the x coordinate of the pole.

Table 5.12 Simulated Outcome of 'EROLD-type' Campaign for Subsequent Years with Single Day Sampling and ±3 cm Ranging. The first, second, and third value in each column refers to the results for the x, y and UT1 parameters, respectively. The analysis period is one year and the 1977 results are listed again for comparison (Experiment 3 only).

Stations*					Percentage Number of 1-Day Solution Uncertainties ≤5 cm				
A	F	J	T	H	1977	1980	1983	1986	1989
					x, y and UT1, %				
5 Stations									
o	o	o	o	o	67,66,72	66,65,70	64,61,66	60,57,64	63,60,67
4 Stations									
o		o	o	o	52,47,61	50,47,59	47,47,56	47,44,55	49,47,59
o	o		o	o	60,61,66	57,58,63	54,51,58	50,46,55	52,49,58
	o	o	o	o	54,55,58	54,53,59	49,47,54	45,42,49	49,48,54
3 Stations									
		o	o	o	33,28,40	35,26,41	30,25,39	28,23,35	31,28,37
	o		o	o	42,46,50	41,46,48	36,39,41	33,34,35	35,37,40
o			o	o	38,40,50	33,37,47	31,34,45	31,33,45	34,35,48

*A = Australia, F = France, J = Japan, T = Texas, H = Hawaii.

Table 5.13 Simulated Outcome of 'EROLD-type' Campaign for Subsequent Years with Two Day Sampling and ±3 cm Ranging. The first, second, and third value in each column refers to the results for the x, y and UT1 parameters, respectively. The analysis period is one year and the 1977 results are listed again for comparison (Experiment 3 only).

Stations*					Percentage Number of 2-Day Solution Uncertainties ≤5 cm				
A	F	J	T	H	1977	1980	1983	1986	1989
					x, y and UT1, %				
5 Stations									
o	o	o	o	o	79,79,82	80,78,81	81,78,81	77,74,79	79,78,80
4 Stations									
o		o	o	o	71,68,75	72,66,77	72,67,77	68,68,76	72,71,75
o	o		o	o	76,77,79	76,75,78	76,73,79	69,70,73	74,72,74
	o	o	o	o	71,73,75	72,71,74	73,70,74	68,63,68	70,67,71
3 Stations									
		o	o	o	52,51,62	55,47,64	56,45,61	50,40,58	52,45,56
	o		o	o	65,69,71	65,67,69	62,65,66	56,58,58	59,61,62
o			o	o	59,60,67	59,58,68	57,58,67	55,59,67	61,60,68

*A = Australia, F = France, J = Japan, T = Texas, H = Hawaii.

Table 5.14 Simulated Outcome of 'EROLD-type' Campaign for Subsequent Years with Five Day Sampling and ±3 cm Ranging. The first, second, and third value in each column refers to the results for the x, y and UT1 parameters, respectively. The analysis period is one year and the 1977 results are listed again for comparison (Experiment 3 only).

Stations*					Percentage Number of 5-Day Solution Uncertainties ≤5 cm				
A	F	J	T	H	1977	1980	1983	1986	1989
					x, y and UT1, %				
5 Stations									
o	o	o	o	o	93,93,93	92,90,92	89,90,90	91,91,92	89,89,91
4 Stations									
o		o	o	o	90,91,93	86,85,89	85,84,88	89,91,92	86,85,89
o	o		o	o	90,92,92	86,88,89	86,88,89	84,85,88	86,85,89
	o	o	o	o	86,88,89	89,88,89	88,86,88	89,82,89	86,84,88
3 Stations									
		o	o	o	72,78,87	77,74,82	76,69,80	73,68,76	74,68,81
	o		o	o	83,87,87	82,85,85	82,84,85	78,77,82	77,80,84
o			o	o	82,84,89	78,81,85	77,80,86	81,84,88	84,81,89

*A = Australia, F = France, J = Japan, T = Texas, H = Hawaii.

In all the analyses undertaken thus far, no attempt has been made to discuss the correlations between the parameters. The parameter correlations c_{ij}, are a good indicator of the separability of all the parameters that form the mathematical model. They can be obtained almost directly from the variance-covariance matrix [Q] for the adjusted parameters, using the expression

$$c_{ij} = \frac{\sigma_{ij}}{\sigma_i \sigma_j} \quad . \tag{5.24}$$

For the majority of solutions from the previously discussed analyses, the correlations between x, y and UT1 are less than 0.5 which indicates good separability. However, on some occasions the separability was not good and, as expected, a strong dependence of the results on the station location, lunar declination and hour angle coverage was evident. A series of optimization calculations are undertaken in the following two sections in order to investigate the influence of these factors more closely and isolate their effects from those of the weather, the zenith distance restriction, averaging interval and new Moon.

5.4.2 Effect of Lunar Declination and Station Location

Studying the effect of lunar declination and station location is accomplished by assuming the hour angle coverage at each station in the network on any given day is in accordance with the optimum observing schedule (see Section 5.2.1.1). Only daily solutions are considered. This means that for a solution based on the five station combination, the maximum number of observations is 25. Similarly, for a two station combination the number of observations is 10.

The range of values obtainable from all the possible combinations of two or more stations is shown in Table 5.15. As expected, the uncertainties for x and y are smaller when the moon is at southern declination and are worst when the Moon is at northern declination. This is due to the significant bias in the number of northern hemisphere stations. For UT1, the distinction is not nearly as great. The exception to this occurs when the Australian station and one in the northern hemisphere are ranging, and can be best explained by considering the results from the Orroral-McDonald combination. Clearly, at southern declinations

Table 5.15 Dependence of Universal Time and Polar Motion on Station Location and Lunar Declination Using Single Day Sampling with ±3 cm ranging. All stations achieve full hour angle coverage during the course of the day's ranging (i.e. measurements are made at H = ±4, ±2, and 0 hours). Results are for 1977 only and where two values appear in a column the first corresponds to when the moon is at maximum southern declination and the second when the moon is at maximum northern declination.

Stations* A F J T H	Parameter Uncertainty, cm			Correlation, $\lvert c_{ij} \rvert$		
	x	y	UT1	$c_{x,y}$	$c_{x,UT1}$	$c_{y,UT1}$
5 Stations						
o o o o o	1,2	1,2	1	0.1,0.3	0.1,0.2	0.05,0.1
4 Stations						
o o o o	2	2	1,2	0.3,0.6	0.2,0.5	0.1,0.5
o o o o	1,2	2	1	0.05,0.3	0.02	0.1
o o o o	1,2	2	1	0.05,0.3	0.1,0.2	0.2,0.3
o o o o	2	2	1	0.1,0.3	0.2	0.1
o o o o	1,3	2	1	0.05	0.1	0.1,0.2
3 Stations						
o o o	2,3	2,3	2	0.5,0.6	0.5	0.2,0.3
o o o	2	2,3	2	0.3,0.5	0.1,0.4	0.4,0.5
o o o	2	2	2	0.1,0.3	0.2	0.02
o o o	2,3	2,4	2,3	0.1,0.7	0.2,0.7	0.4,0.8
o o o	2	2	1	0.1,0.3	0.02	0.1,0.2
o o o	2	2	2	0.1,0.3	0.02	0.3
o o o	2,4	2,3	1,2	0.3	0.2,0.5	0.02,0.2
o o o	2,4	2,7	1,3	0.05,0.4	0.1,0.5	0.3,0.8
o o o	1,3	2	1,2	0.05	0.1,0.2	0.1
o o o	1,3	2	2	0.05	0.05	0.02
2 Stations						
o o	3	4,3	2	0.5,0.6	0.3,0.4	0.1,0.3
o o	3,10	2,13	2,6	0.6,0.7	0.6,0.9	0.5,0.9
o o	2	2	2	0.4,0.3	0.05	0.05
o o	2,4	8,7	6	0.3,0.9	0.2,0.8	0.9
o o	2,4	2,4	2,3	0.2,0.5	0.2,0.6	0.2,0.6
o o	2,4	2,7	2,3	0.2,0.4	0.05,0.4	0.3,0.8
o o	2,4	3	2	0.3,0.2	0.05,0.2	0.2
o o	6,4	2,5	3	0.4,0.8	0.8	0.2,0.8
o o	2,5	3,9	2,4	0.3,0.05	0.2,0.1	0.6,0.9
o o	2,4	2,3	2	0.2,0.3	0.2,0.5	0.1,0.3

*A = Australia, F = France, J = Japan, T = Texas, H = Hawaii.

the ranges from the McDonald station are far more sensitive to polar motion variations through the sin (ϕ-δ) term than are the ranges from the Orroral station. Since McDonald is close to the meridian that defines y, this explains why the uncertainty for y at southern declinations is a factor of 3 smaller than the uncertainty for x. On the other hand, at north declinations the reverse applies. This time it is the Orroral station that is the main contributor but because its longitude is nearer the meridian that defines x, the uncertainty for this component is slightly better.

Station combinations where parameter separability is a problem are identified by the high correlations. For example, the difference in latitude and longitude between the Haleakala and McDonald stations is not sufficient to permit a precise separation of the earth rotation parameters even when the moon is at southern declinations. The values in Table 5.15 do suggest, however, that better results are obtained from a pair of northern hemisphere stations that are well separated in longitude (e.g. Calern and Haleakala) and, that for a pair containing Orroral, the results are best when the longitude difference is small (e.g. Orroral and Dodaira). These findings are substantiated further in Tables 5.16 and 5.17 and are in agreement with the limited analytical studies carried out by Arnold (1974) and Stolz (1975).

The results obtainable from McDonald (λ = 256°E, ϕ = 30.5°) and a floating station on the same parallel of latitude are summarized in Table 5.16. The values are obtained by assuming the optimum observing schedule with daily averaging and a ±3 cm ranging uncertainty for both stations. They refer specifically to when the Moon is at a northern declination of 28°, that is, at a time when the effect of declination is quite adverse. Clearly, the results are best when the two stations differ in longitude by 180 degrees. It is also interesting to note that when the floating station is situated near the meridian that defines the y component of polar motion, it is in fact the x component of the pole that is best determined. This rather unique case can be explained simply in terms of the observing schedule and its related effect on the partial derivatives. All of the contribution to the solution for x comes from the observations at wide hour angle, that is, ±4 hours. The

Table 5.16 Effect of Longitude on the Results Obtainable from two Northern Hemisphere Stations. The values are obtained using the McDonald Observatory (λ = 256°E, ϕ = 30.5°) and a floating station on the same parallel of latitude (see text for other basic assumptions).

Longitude* Degrees	Parameter Uncertainty, cm		
	x	y	UT1
235	64	31	41
215	30	21	20
195	18	18	12
175	12	16	9
155	9	15	7
135	7	14	5
115	5	13	4
95	5	13	3
75	6	12	3

*Longitude of floating station.

solution for y is essentially determined by the polar motion variations seen by each station in their own meridian. However, in this case δ=+28° and so the sensitivity of the range to a variation in y is smaller compared to x because $\sin(\phi-\delta)$ is small. As the floating station approaches the McDonald Observatory it becomes increasingly difficult to separate x, y and UT1 because, in the limit, this would be identical to the geometry for a single station. As mentioned previously, data from a single station cannot separate the component of polar motion perpendicular to its meridian (in this case, x) from UT1.

Results from Orroral (λ = 148.9°E, ϕ = -35.5°) and a floating station in the northern hemisphere are depicted in Table 5.17 where values for both extremes of declination are given. In carrying out these calculations, no attempt is made to impose the zenith distance condition which may not generally be satisfied for off-meridian observations when the floating station approaches the upper middle latitudes. Clearly, the solutions are best when the floating station is on or near the same meridian as Orroral and is well separated in latitude. Dodaira (λ = 139.2°E, ϕ = 35.8°) fits the description admirably. The other interesting aspect of Table 5.17 is the poor results obtained when the floating station is roughly symmetric about the equator with the Orroral station and differs in longitude by 180 degrees. Arnold (1974) has shown analytically that there is a singularity problem in a two-station solution when the angle subtended at the geocentre by the two station vectors is 180 degrees. In this case, it would occur if the floating station were located at λ = 328.9°E and ϕ = 35.5°. The results for λ = 330°E and ϕ = 40° begin to confirm this particular effect.

The importance of the Orroral station for earth rotation studies when the moon is at northern declinations is shown back in Figure 5.1. In these diagrams, the results obtainable for x, y and UT1 are depicted when all five stations are ranging and also when the Orroral station is excluded. The declination is varied between ±28° and only one-day averages with complete hour angle coverage from each station are considered. The improvement at north declination is most noticeable for x and y; the improvement in the determination of UT1 being attributable entirely to the effect of averaging.

Table 5.17 Effect of Latitude and Longitude on the Parameter Uncertainties for Polar Motion and Universal Time. Where two values appear in a column, the first corresponds to when the Moon is at 28°N declination and the second corresponds to when the Moon is at 28°S declination. The values are obtained by assuming the optimum observing schedule with daily averaging and a ranging uncertainty of ±3 cm for each station.

Longitude† Degrees	$\phi^{\dagger}$ = 40°N			$\phi^{\dagger}$ = 20°N			$\phi^{\dagger}$ = 0°		
	Parameter Uncertainty, cm								
	x	y	UT1	x	y	UT1	x	y	UT1
148.9	2	2	2	2	3	2	3,4	5	2
170	2	2	2	2	4	2	2,3	4,6	2
210	3,2	3	2	2,3	3,5	2	2,6	3,8	2
250	4,6	5,2	4	3,11	4	3,4	2,12	2,6	2
290	8,12	13,5	11,9	4,14	6,5	4,7	3,7	3	2
330	18	30	27	6	10	6	3	5	2

†Latitude and longitude of the floating station.

5.4.3 Significance of Hour Angle Coverage

In this section, an investigation of how differing hour angle coverages at different stations can influence the quality of the earth rotation results is undertaken. The study consists of three basic experiments that have been designed to (1) assess the dependence of the parameter uncertainties on the hour angle coverage obtained at each station and (2) see whether there is any appreciable reduction in the correlations between the earth rotation and lunar orbit parameters when the hour angle coverage is varied at each station. For these analyses, the observation equation is written as

$$\begin{aligned} v_i = \Delta\rho_i + r_s \big[&\{\sin\phi\cos\delta\cos(\lambda-H) - \cos\lambda\sin\delta\cos\phi\}_i \,\Delta x \\ &- \{\sin\phi\cos\delta\sin(\lambda-H) - \sin\lambda\sin\delta\cos\phi\}_i \,\Delta y \\ &+ \{\cos\phi\cos\delta\sin H\}_i \,\Delta UT1 \\ &- \{\sin(\phi-\delta) + \cos\phi\sin\delta(1-\cos H)\}_i \,\Delta\delta\big] + \Delta r_r \quad . \end{aligned} \tag{5.25}$$

It is important to emphasize once again that errors in UT1 and the lunar right ascension α cannot be separated unless they occur at different frequencies. Equation (5.25) assumes that α is perfectly known.

The first of the three experiments examines the improvement and degradation in the parameter uncertainties and correlations when the hour angle coverage at each station is varied from 2 to 8 hours while the remaining stations in the network achieve 2 hour coverage. In this and the other two hour angle experiments, the following common assumptions are made: (1) the solution averaging interval is one day, (2) three ranges are scheduled at each station per day, (3) each station has a range uncertainty of ± 3 cm, (4) the conditions of observability have been waived and (5) all five stations are ranging.

The modified observing schedule is introduced to simplify the calculations. For a station that achieves a 2 hour coverage in hour angle, the ranges are placed at $H = \pm 1$ and 0 hours. Likewise, for a station that achieves an 8 hour coverage in hour angle, the ranges are placed at $H = \pm 4$ and 0 hours and so on. With this observing schedule a total of 15 observations are obtained for each daily solution.

Parameter uncertainties and correlations associated with the first hour angle experiment are summarized in Table 5.18a and b, respectively. Only correlations greater than or equal to 0.5 are listed in Table 5.18b. The values without brackets in both tables are the results obtained when all five stations achieve an hour angle coverage of 2 hours. The bracketed values are the best results that occur for the parameter uncertainties and largest values for the correlations when the hour angle coverage at each specific station is varied from 2 to 8 hours while the remaining four stations in the network achieve 2 hour coverage. Only the most significant changes and salient points are discussed. They are;

(1) the strong dependency of the results for x, y and δ on lunar declination due to the inclusion of only one southern hemisphere station in the network,

(2) the virtual independence of the results for UT1 and r_r on lunar declination,

(3) the significant decrease in the uncertainty for y at northern declination when the Calern station has a wider coverage in hour angle compared to the remaining stations. Off-meridian observations at Calern with large hour angles contribute very strongly to a determination of y at northern declinations.

(4) the significant decrease in the uncertainty for UT1 at all declinations when any one of the stations has a wide coverage in hour angle,

and (5) the high correlation between r_r and δ at southern declination and the moderately high correlations, c_{14} and c_{25}, at northern declination.

Table 5.18a Parameter Uncertainties for Hour Angle Experiment No. 1 as a Function of Lunar Declination

Declination Degrees	Parameter Uncertainty, cm				
	x=1	y=2	UT1=3	r_r=4	δ=5
-28	1	2	(3),5	1	2
0	2	2	(2),5	1	2
28	5	(5),8	(3),5	1	4

Table 5.18b Parameter Correlations for Hour Angle Experiment No. 1 as a Function of Lunar Declination

Declination Degrees	Correlation, $\|c_{ij}\|$	
	0.5-0.7	>0.7
-28		c_{45}
0	c_{45}	
28	c_{14}, c_{25}	(c_{15})

The results of the second hour angle experiment are summarized in Tables 5.19a and b. The values without brackets are the results obtained when all five stations achieve an hour angle coverage of 8 hours. There is, however, no change in the results when the hour angle coverage at individual stations is reduced from 8 to 2 hours. This indicates that when a majority of stations in the network obtain a maximum coverage in hour angle, the results are not degraded if poorer coverage is obtained by one or perhaps even two of the remaining stations. Likewise, no significant changes occur in the correlations. In fact, the results look remarkably similar to those obtained from the first experiment. Reducing the hour angle coverage at the Calern station does, however, increase the correlation between y and δ when the moon is at north declination.

The third and final hour angle experiment is carried out to see what effect a variation in the hour angle coverage at every station in the network has on earth rotation results. Interest is focussed on the changes in parameter uncertainties and correlations when all stations achieve 8, 6, 4 and 2 hour coverages, respectively. Results for the 2 and 8 hour cases can be extracted from the information in Tables 5.18 and 5.19, respectively. The 4 and 6 hour cases are summarized in Tables 5.20a and b. The values without brackets are the results obtained when all five stations achieve 6 hours of hour angle coverage. Bracketed values are the corresponding results for the 4 hour case. Note, that there is no change in the correlations between the 4 and 6 hour cases. Comparing these results to those in Tables 5.18 and 5.19 allows the following conclusions to be drawn;

(1) there is no large difference in the uncertainties and correlations for the 4, 6 and 8 hour cases.

Table 5.19a Parameter Uncertainties for Hour Angle Experiment No. 2 as a Function of Lunar Declination

Declination Degrees	Parameter Uncertainty, cm				
	x=1	y=2	UT1=3	r_r=4	δ=5
-28	1	2	2	1	2
0	2	2	1	1	2
28	4	3	2	1	3

Table 5.19b Parameter Correlations for Hour Angle Experiment No. 2 as a Function of Lunar Declination

Declination Degrees	Correlation, $\|c_{ij}\|$	
	0.5-0.7	>0.7
-28		c_{45}
0	c_{45}	
28	$c_{14}, c_{15}, (c_{25}), c_{45}$	

Table 5.20a Parameter Uncertainties for Hour Angle Experiment No. 3 as a Function of Lunar Declination

Declination Degrees	Parameter Uncertainty, cm				
	x=1	y=2	UT1=3	r_r=4	δ=5
-28	1	2	2,(3)	1	2
0	2	2	2	1	2
28	4	3,(4)	2,(3)	1	3,(4)

Table 5.20b Parameter Correlations for Hour Angle Experiment No. 3 as a Function of Lunar Declination

Declination Degrees	Correlation, $\lvert c_{ij} \rvert$	
	0.5-0.7	>0.7
-28		c_{45}
0	c_{45}	
28	c_{14}	c_{15}

(2) if hour angle coverage continues to be poor (≤2 hours) at most of the stations in the network, then every effort should be made to obtain wide hour angle coverage at Calern, particularly when the moon is at north declinations. This will ensure a good determination of both y and UT1. Poor hour angle coverage at all stations will degrade UT1 determinations at all declinations. Only one station needs a wide hour angle coverage to ensure a good determination of UT1.

(3) there is a slight tendency for the network to determine the x component of the pole better than y and UT1 when the hour angle coverage is poor at all stations.

(4) for better determinations of x and y when the moon is at northern declination it is important to have wide hour angle coverage at a majority of stations. At southern declinations the effect of hour angle coverage is less significant.

(5) when wide hour angle coverage is obtained at all stations, the strength of the x and y determinations is almost identical. UT1 results appear to be better by about a factor of 2.

and (6) in general, most of the parameter correlations are less than 0.5 for all declinations. The exception occurs for the correlations between x and the lunar orbit parameters r_r and δ which are high at northern declinations. The introduction of an additional southern hemisphere station would probably reduce these correlations substantially.

In order to assess how much the uncertainties in x, y and UT1 are reduced when the lunar orbit parameters r_r and δ are not included in the solution, the 8 hour case was repeated with the orbital parameters excluded. The results are shown in Table 5.21 and comparing these values with those in Table 5.19a allows the following conclusions to be drawn:

Table 5.21 Parameter Uncertainties for x, y and UT1 when the Lunar Orbital Parameters are Excluded as Solution Parameters (8 hour case only).

Declination Degrees	Parameter Uncertainty, cm		
	x	y	UT1
-28	1	2	1
0	2	2	1
28	2	2	1

(1) while there is no reduction whatsoever in the uncertainties for the x and y parameters at southern declinations, the improvement at northern declinations is quite significant. Once again, this result is intimately related to the unavoidable imbalance that exists in the LLR network geometry and the subsequent effect this has on the parameter uncertainties and correlations at northern declinations, particularly when the lunar parameters are also included in the model.

(2) there is no large difference in the uncertainties for UT1. This is not entirely unexpected because solutions for UT1 are uniquely decoupled from r_r and δ when off-meridian observations are symmetric about the meridian.

5.5 Summary Remarks

Numerous analyses have been undertaken in this chapter to investigate the suitability of the LLR technique for monitoring the earth's rotation. To summarize all the individual results would only be repetitous, particularly when most of them are self-explanatory. However, it would be beneficial to re-emphasize the basic assumptions made and view the general conclusions within this context.

The fairly low percentage of one-day periods for which polar motion and Universal Time are obtained to better than 5 cm from the five station network, and the fact that this percentage rises significantly when the sampling interval is two days suggests that a five station LLR network can provide accurate earth rotation information if the sampling interval is greater than or equal to two days. Clearly, the addition of a southern hemisphere station in South America and one in South Africa would not only improve the frequency of one-day values but also help alleviate many of the geometrical limitations discussed in this chapter.

The two basic assumptions critical to the validity of these results are that a uniform measuring uncertainty of ± 3 cm will be attained by all the participating stations and that systematic errors in the measurements are negligible. While there is no reason to doubt that the accuracy goal of the Haleakala station ultimately can be realized by the other

stations, one could certainly expect that some systematic errors will be present in the data. The extent to which plate motion and seasonal variations in station position due to surface mass loading contaminate earth rotation results obtained at the 5 cm level is considered in Chapters 6 and 7, respectively.

To estimate the effect of systematic errors on the determination of the parameters in the Earth-Mercury system, Ashby et al. (1981) carry out a modified worst-case analysis that closely follows the theoretical work of Hauser (1974) for the Earth-Moon distance. In brief, the theory predicts the time-dependent systematic error which results in the maximum uncertainty for each parameter of the mathematical model subject to the condition that only the total rms magnitude of the error is known. Hauser (1974) derives a formula which is equivalent to (Ashby et al.1981) the worst-case systematic error σ_p^s in each parameter being larger by a factor of $i^{1/2}$ than its random error, that is,

$$\sigma_p^s = \sigma_p^r (i)^{1/2} \tag{5.26}$$

where i represents the number of observations used for the solution and σ_p^r the random error for the p-th parameter. Since the resulting uncertainty is linear in the estimated total rms error, the final results can also be scaled accordingly to any estimate of the total rms systematic error.

Ashby et al. (1981) point out, however, that it is inconsistent to expect every parameter in the model to have a worst-case uncertainty associated with its determination and so they introduce a factor k to modify the worst-case results in order to give a more reasonable estimate for the final parametric uncertainties, that is,

$$\sigma_p^s = k\, \sigma_p^r (i)^{1/2} \quad . \tag{5.27}$$

If there are a reasonably small number of parameters in the mathematical model, and if the derivatives of the range with respect to these parameters are roughly orthogonal, Bender(private communication, 1980) suggests that a rough rule of thumb is that

$$k < n^{-1/2} \tag{5.28}$$

where n is the number of solution parameters. For the EROLD-type studies undertaken here, k would thus be < 0.58. However, a substantial fraction of the systematic error may occur at frequencies which don't affect the results appreciably. Thus, a value of k = 0.4 is chosen for the present analysis. Ashby et al. (1981) choose a value of 0.25 in their model for the Earth-Mercury distance, for which there are 18 parameters, but some of the parameters of main interest have quite similar partial derivatives of the range.

In applying the theory to the results presented in this chapter, consider the two-day solutions for x, y and UT1 from a five station network achieving a uniform ranging uncertainty of 3 cm. Stolz and Larden (1977) have shown that the random uncertainty in x, y and UT1 for the majority of these solutions is generally less than or equal to 3 cm. If the average number of observations per solution is taken to be 25 (see Table 5.6) then the modified worst-case systematic contribution to the total uncertainty for x, y and UT1, assuming an rms systematic error of 2 cm is achieved in the future (Bender, private communication, 1980), and using the appropriate scalar, is

$$\sigma^{s}_{x,y,UT1} \leq 4.0 \text{ cm} \quad .$$

Writing the total uncertainty σ^{t}_{p} for each parameter as the root sum of squares of the systematic and random contributions gives

$$\sigma^{t}_{x,y,UT1} \leq (3^2 + 4^2)^{1/2} \leq 5 \text{ cm} \quad .$$

Thus, when systematic effects and two-day averages are considered, the uncertainties for x, y and UT1 will generally be about 5 cm.

The results from Tables 5.19a and 5.21 also indicate that solving for the lunar orbit parameters r_r and δ only has a marginal effect on the uncertainties for two-day values of x, y, and UT1. It is, however, very important to have available a good physical model for the orbit before reliable values of x, y and UT1 are obtained. Until this is achieved it may be wise to include the orbit parameters in the analysis model.

CHAPTER 6
PLATE MOTION EFFECTS ON EARTH ROTATION RESULTS FROM LLR

6.1. Introduction

For stations undergoing relative and absolute motions induced by geophysical processes, additional parameters must be included in the distance equation (4.20) so that variations in the distance due to these processes will not be interpreted in the analysis as corrections to x, y and UT1. Over very short time intervals, some of these effects will not be detectable. But as the ranging uncertainties of the space techniques approach the 1-3 cm level, this statement is bound to be reappraised.

One process that will cause changes in the latitude and longitude of LLR observatories is global plate tectonics, the modern-day counterpart for the theory of continental drift. Attempts to deduce these changes from astronomical data (see e.g. Proverbio and Poma 1976) have been seriously limited by the accuracy of the results. Also, many of the stations are located close to plate boundaries in regions of high seismic activity and this can lead to doubtful results. The other alternative for deducing these changes is to adopt an absolute plate velocity model based on geological and seismic evidence and compute the changes in station coordinates and, hence, the time-scales over which these motions become significant in high-precision geodetic experiments. Studies based on the latter approach have been done for the ILS, BIH, VLBI and SLR networks (see e.g. Mueller and Schwarz 1972, Dickman 1977, Soler and Mueller 1978) but a detailed analysis has yet to be carried out for the LLR network.

The purpose of this chapter is to carry out such an analysis. In the first instance, the changes in latitude and longitude of each individual station in the LLR network are computed from the recent absolute plate velocity models constructed by Minster et al. (1974), Kaula (1975) and Solomon et al (1975). The assumptions underlying these models are discussed. The contribution that these changes make to polar

motion and Universal time results obtained by the LLR technique is then calculated. All computations are carried out in the geographic reference system (see Section 2.2.2.1).

6.2. Plate Motion Kinematics

6.2.1. Concept of Global Plate Tectonics

The concept that the earth is made up a relatively small number of rigid lithospheric plates which are in motion with respect to one another is the central hypothesis of global plate tectonics. The theory implies the transportation of mass as the plates move about the earth's surface, material rises from the asthenosphere and cools to generate new oceanic lithosphere, and lithospheric slabs descend to displace asthenospheric material. Chapple and Tullis (1977) discuss the various mechanisms that can cause or impede this process and while mantle convection is a leading contender it is still not clear whether the extent of the convection is confined to the upper mantle or is mantle-wide (O'Connell 1977).

The distinction between lithosphere and asthenosphere is based on rigidity and to a large extent reflects differences in temperature. The depth of the boundary between these two regions is about 100 km (Isacks et al. 1968), however, this value can vary substantially from one seismic region to another (Walcott 1970). As the lithospheric plates slowly move about, some carry oceanic crust, others carry continental crust or both. Their boundaries are generally of three types (Cox 1973): (i) mid-ocean ridges (e.g. mid-Atlantic ridge) where sea-floor spreading processes are operating to add new material to the lithospheric plates,(ii) subduction zones (e.g. Aleutian trench) where one lithospheric plate plunges under another and is reabsorbed back into the mantle, and (iii) transform faults (e.g. San Andreas fault) where two plates move tangentially to one another avoiding both the creation and destruction of the lithosphere.

The actual number of plates, their boundaries and their velocities differ from model to model, although there is consistent agreement with

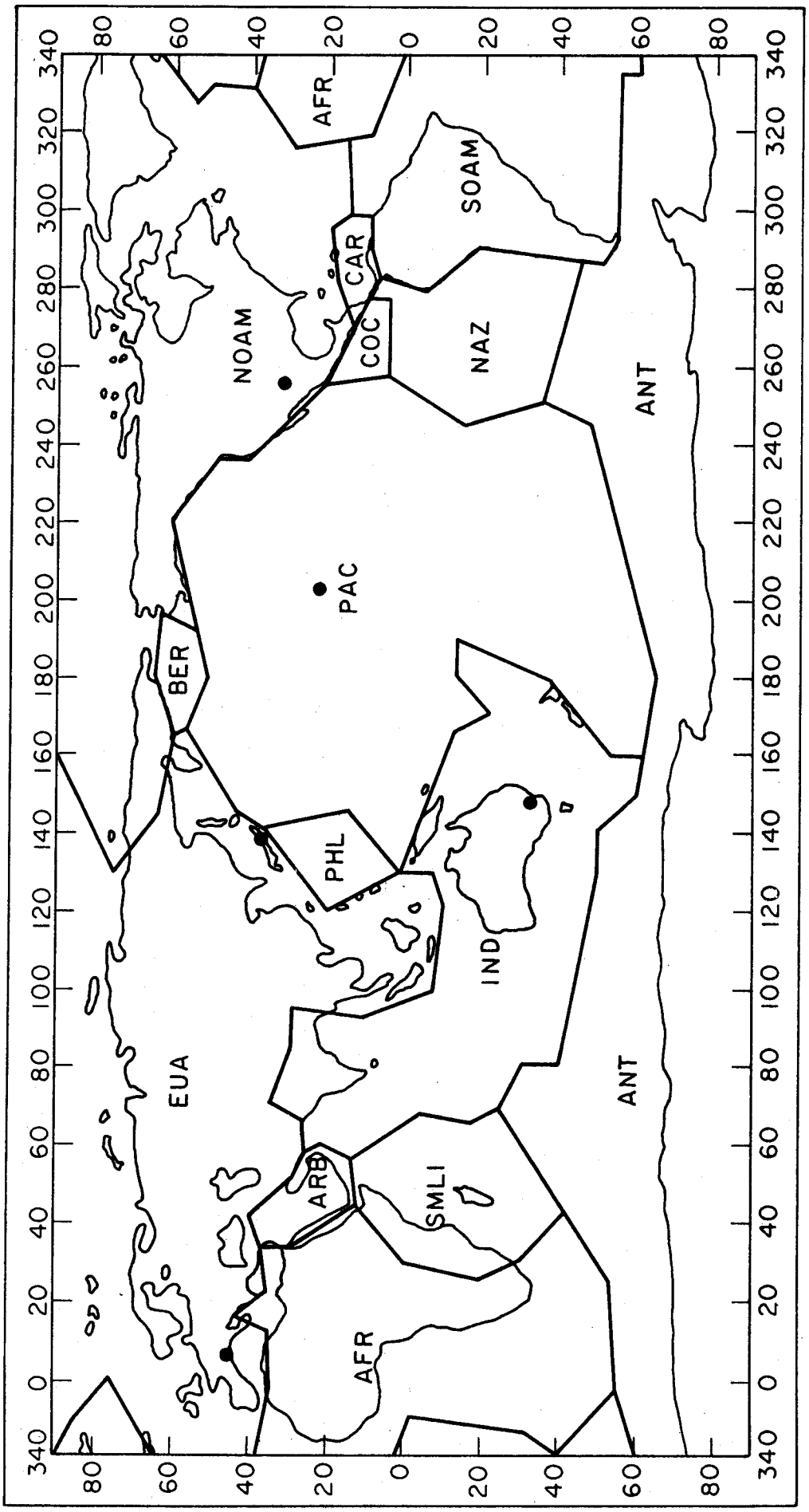

Figure 6.1 Outline of Tectonic Plates. Solid circles indicate the location of the LLR observatories.

regard to the macroplates. Viewed microscopically, the lithospheric plate boundaries are indeed fairly complex with deformation zones extending over quite large regions that often become smaller plates. Even so, one important aspect of the plate tectonic model is that over geological time scales, the plates are assumed to be rigid away from the margins. This assumption implies that the relative geometry of points on the same plate remains unchanged and its verification is one of the primary tasks of NASA's geodynamics program (NASA 1979). The major tectonic plates are shown in Figure 6.1.

An essential aspect of the plate tectonic model is that it represents a time-averaged situation (Lambeck 1980). The primary type of data that forms the basis of all current models is the marine magnetic anomalies which exist in mid-ocean ridge areas (see e.g. McElhinny 1973). This information, together with the geometry of transform faults and earthquake slip vectors, is used to determine the average relative motion between the plates over periods exceeding 10^6 years. Additional constraints are needed if these motions are to be established in an absolute reference frame. Such models and their underlying assumptions are discussed in the next section. Further details on the global tectonic model may be found in the texts by Le Pichon, Francheteau and Bonnin (1973) and Cox (1973).

6.2.2. Absolute Plate Velocity Models

As mentioned in Section 6.1, the changes in the latitude and longitude of the stations in the LLR network due to the drift of the continents can be calculated using the absolute plate velocity models of Minster *et al.* (1974), Kaula (1975) and Solomon *et al.* (1975). However, before outlining the computational procedure and presenting the results of the calculations, several preliminary comments concerning the assumptions upon which these models are based seem in order.

The model of Minster *et al.* consists of eleven major lithospheric plates; included are the Cocos, Nazca and Arabian plates as well as the

six large plates considered by Le Pichon (1968). Recognition is also given to evidence which suggests that the continents of North and South America lie on two separate plates whose motions are resolvable and that internal deformation within the North American plate has resulted in the formation of the Bering plate which is bounded geographically by the eastern end of Siberia, the Bering Sea, and the western part of Alaska.

In Minster et al.'s model the poles of rotation and relative velocities of the plates are obtained by inverting 68 sea-floor spreading rates, 62 fracture zone trends and 106 earthquake slip vectors using a self-consistent maximum likelihood theory. However, no attempt was made to determine the velocity of the Bering plate because the data along its perimeter were not reliable. The model is designated as RM1. The absolute velocities, designated model AM1, are then determined using the hypotheses that the "hotspots" are fixed with respect to each other and that they define a reference frame related to the underlying mantle. Minster et al. believe there has not been any significant relative motion between the hotspots during the last 10^7 years but this assertion has been challenged (see e.g. Molnar and Francheteau 1975). It appears that when time periods of 5×10^7 years are considered, hotspots appear to show relative velocities averaging 1-2 cm/year (see e.g. Molnar and Atwater 1973).

Hotspots are regions of volcanic activity, presumably surface manifestations of deep, upwelling "plumes", that are usually located in the plate interiors. It was first proposed by Wilson (1963) that plate motions over these regions were responsible for the genesis of various island chains (e.g. the Hawaiian Islands in the Pacific) and aseismic ocean ridges. Morgan (1972) extended Wilson's list of hotspots and constructed a model for the lithospheric plate motions with respect to the underlying mantle that was compatible with the directions of the hotspot traces on the plates.

Minster et al. (1974) invert the trends of 20 linear island chains and aseismic ocean ridges, located on eight of the lithospheric plates, to determine their absolute plate velocity model. The data, which include 16 of the traces used by Morgan (1972), fit the model quite

well. That only one of the computed trace azimuths deviates from its measured value by more than its observational uncertainty speaks strongly in favour of the Wilson-Morgan hotspot hypothesis.

Kaula (1975), on the other hand, approaches the absolute plate motion problem from a slightly different viewpoint and explores solutions that minimize the translational motion of the mid-ocean ridges and, hence, their motion with respect to convective upstreams. Kaula also applies a condition which minimizes the motions for the overthrust plates in zones of subduction and had all the hotspot traces in Minster et al.'s (1974) model been close to these zones, the two models would probably be very similar. As it turns out, the results between both models agree to within 1 cm/year.

The basis of Kaula's boundary velocity minimization model is the plate system and the relative velocities of Minster et al. (1974). In addition, Kaula includes the Philippine and Somali plates and determines a minimum velocity for the Bering plate by least squares fitting the data from four adjacent aseismic regions. Every plate boundary segment is given a tectonic description (e.g. mid-ocean ridge, ocean plate subducted under ocean plate, etc.) and results are presented for five solutions, each based on a different selection of the boundary types for which the absolute velocities are minimized.

Kaula's solution number 5, designated here as K5, is the most comprehensive and, as such, is chosen as one of the models for the calculations undertaken in this chapter. In this solution, the overthrusting plate velocities are minimized at all types of subduction zones and the transverse velocities are minimized for all other boundary types considered. The results indicate that oceanic plates move at rates of the order of 5 cm/year, about a factor of 3 or 4 greater than continental plates. The minimum boundary velocities are consistent with the results obtained by Solomon et al. (1975) and are of the order 1-2 cm/year. These results may suggest a possible interaction between the lithosphere and the convective flow scheme and a rather temporary existence of the so-called absolute global reference frame.

Solomon et al. (1975), using a modified version of the relative velocity model of Minster et al. (1974), determine the absolute plate velocities after postulating that the lithosphere as a whole is in mechanical equilibrium. This assumption was originally discussed by Solomon and Sleep (1974) and is equivalent to stating that the lithosphere is not accelerating. By conservation of angular momentum, the torques exerted on the lithosphere by bouyancy forces at plate boundaries and by viscous drag forces beneath the plates must sum to zero. Therefore, if some fraction of the torque exerted on the lithosphere is produced by forces which depend on the velocity of the plates with respect to the underlying mantle, then the no net torque condition provides a framework for determining the absolute velocities.

The basic plate boundary and relative velocity model used by Solomon et al., although similar in most respects to the models of Minster et al. and Kaula, does have some obvious differences. Included in the plate schedule are the Philippine and Caribbean plates, however, the model does not recognize either the Bering plate or the division of the American plate into separate North and South American plates. The Bering plate is judged simply as an artifact of the systematic errors believed present in the slip vectors of the Aleutian earthquakes while the division of the American plate produces relative motions between the Caribbean and South American plates that conflict with the geological and seismic evidence for that region. All authors have avoided the small controversial plates (e.g. Gorda, Fiji, Iran etc.).

A total of eight absolute plate velocity models are presented by Solomon et al. To determine the absolute velocities, various torque balances on the plates (e.g. the viscous drag on continental plates is a factor of three larger than that experienced by oceanic plates) are assumed subject to a further condition that the asthenospheric drag exerted on the lithosphere acts to resist the plate motions. On the other hand, should mantle-wide, non-passive convection be a reality, it

would invalidate the torque-balancing models because the lithosphere-mantle interaction would change from resisting to a driving nature.

Table 6.1 lists the models considered in this study together with their appropriate designation and a brief description of the basic assumptions upon which they are based. All of Solomon et al.'s (1975) plate models are included since all have been constrained to physically plausible properties. The rotation poles and angular velocities for the absolute motions of the tectonic plates appropriate to the LLR network are listed in Table 6.2. Moreover, Orroral is taken to be on the Indian plate, Calern and Dodaira to be on the Eurasian plate, Haleakala to be on the Pacific plate and McDonald to be on the American plate. The triplet of values for the n-th plate denotes the latitude (ϕ_n) and east longitude (λ_n) of the rotation pole, in degrees, and the angular velocity (w_n) in 10^{-8} radians/year, respectively. The rate of rotation is taken to be positive in a right-handed sense, or expressed differently, the plate rotation is positive if the plate moves in an anticlockwise direction as viewed by an observer standing on the pole of rotation and looking down the rotation axis of the plate.

With the exception of the Japanese site, there is no reason to expect the uncertainties in the predicted plate motions to exceed 1 cm/year. All of the plate motion models agree to within 1 cm per year for the velocities of the major plates and the Orroral, Calern, Haleakala and McDonald Observatories are safely located away from the plate boundaries in reasonably stable regions (see Figure 6.1). However, because Dodaira is situated very close to the Japan trench, one of the most tectonically active regions of the globe (Isacks and Molnar 1969) and the Eurasian plate is relatively slow moving, it would not be unreasonable to expect the error in the predicted motion at Dodaira to be as large as the motion itself. Such errors would arise if substantial local and regional motions were to exist and not be taken into account (see Dickman (1977) and Morgan (1977) for a brief discussion of these phenomena). It is also informative to mention that there is no concensus among geophysicists as to whether the present-day relative plate velocities are the same as the 5×10^6 year averages

Table 6.1. Schedule of Absolute Plate Velocity Models*

Plate Model Designation	Description	Literature Source
AM1	Fixed hotspots	Minster et al. (1974)
K5	Boundary velocity minimizations	Kaula (1975)
A3	Uniform drag coefficient beneath all plates	Solomon et al. (1975)
B3	Drag beneath continents only	Solomon et al. (1975)
B4	Continents have three times more drag than oceans	Solomon et al. (1975)
C3	Drag opposing horizontal translation of slabs, oceanic subduction zones only	Solomon et al. (1975)
C4	Same as C3, but including the Arabian and Himalayan trenches	Solomon et al. (1975)
D1	Maximum pull by slabs plus plate drag	Solomon et al. (1975)
E2	Drag beneath 8 mid-plate hotspots of Morgan (1971)	Solomon et al. (1975)
E3	Drag beneath 19 hotspots of Morgan (1971)	Solomon et al. (1975)

*See Minster et al. (1974), Kaula (1975) and Solomon et al. (1975) for further details.

Table 6.2. Plate Rotation Poles and Angular Velocities. Each triplet of values denotes the latitude and east longitude of the rotation pole, in degrees, and the angular velocity in 10^{-8} radians/year, respectively. The rate of rotation is taken to be positive in a right-handed sense.

Plate Model Designation	Plate Name											
	Pacific			American*			Eurasian			Indian		
	ϕ_n,	λ_n,	w_n	ϕ_n,	λ_n,	w_n	ϕ_n,	λ_n,	w_n	ϕ_n,	λ_n,	w_n
AM1	-67.3,	120.6,	1.45	-48.1,	-82.1,	0.42	38.1,	-110.5,	0.21	31.6,	29.6,	1.06
K5	-65.6,	124.0,	1.38	-38.8,	-89.4,	0.37	48.3,	-138.3,	0.31	36.2,	30.2,	1.08
A3	-66.4,	121.7,	1.24	-33.8,	-96.0,	0.25	56.5,	-98.7,	0.37	39.6,	24.3,	1.20
B3	-64.4,	117.8,	1.56	-78.5,	-155.5,	0.42	23.9,	-162.1,	0.10	27.2,	35.1,	1.09
B4	-65.2,	119.2,	1.37	-62.0,	-108.2,	0.29	56.2,	-112.8,	0.24	34.6,	29.3,	1.15
C3	-67.2,	121.1,	1.16	-18.2,	-88.7,	0.26	57.4,	-90.8,	0.44	41.4,	21.7,	1.25
C4	-66.5,	119.1,	1.22	-30.9,	-89.5,	0.24	58.6,	-92.0,	0.38	39.5,	23.9,	1.23
D1	-60.0,	110.6,	1.32	-86.1,	-61.3,	0.16	69.2,	-153.4,	0.30	35.7,	33.7,	1.29
E2	-69.7,	107.1,	1.30	-44.6,	-62.1,	0.32	46.2,	-63.2,	0.31	33.1,	21.9,	1.25
E3	-66.0,	112.7,	1.44	-74.2,	-81.9,	0.34	56.7,	-87.2,	0.15	30.0,	29.6,	1.17

*For models AM1 and K5 the rotationl poles and angular velocities refer specifically to the North American plate.

inferred from the geological and seismic evidence. These factors must always be borne in mind in theoretical studies of this nature.

6.2.3 Changes in LLR Station Coordinates Due to Plate Motion

Once the absolute angular velocity vector $\vec{w}_n$ for each plate is known (see Table 6.2), the time variations $\delta\phi_{nk}$ and $\delta\lambda_{nk}$ in latitude and longitude of the k-th station belonging to a particular plate P_n can be computed. The required formulation for evaluating the differential changes is based on the well-known theorem due to Euler which states that the instantaneous motion of a rigid plate constrained to lie on the surface of a sphere can be completely and uniquely described by an axial rotation. Since the length of the station vector is invariant under this type of rotation, the velocity field of a mosaic of n plates is simply determined by specifying the absolute angular velocity vector of each plate, referenced to some fixed frame whose origin is at the centre of the sphere. The geographic reference system described in Section 2.2.2.1 is used throughout these calculations. With respect to this reference frame, the velocity v(r) of a point r belonging to plate P_n, in vector format, is (Minster et al. 1974)

$$\vec{v}(r) = \vec{w}_n \times \vec{r} \tag{6.1}$$

where $\vec{w}_n$ has been defined previously. From Figure 6.2, the Cartesian components of these vectors are

$$\vec{r} = \begin{bmatrix} r_s \cos\phi_k \cos\lambda_k \\ r_s \cos\phi_k \sin\lambda_k \\ r_s \sin\phi_k \end{bmatrix} \qquad \vec{w}_n = \begin{bmatrix} w_n \cos\phi_n \cos\lambda_n \\ w_n \cos\phi_n \sin\lambda_n \\ w_n \sin\phi_n \end{bmatrix} \tag{6.2}$$

where all quantities have been defined previously. Since the velocity vector is always tangent to the sphere, it can be expressed in terms of its latitudinal component, v^{ϕ}_{nk} and its longitudinal component, v^{λ}_{nk}.

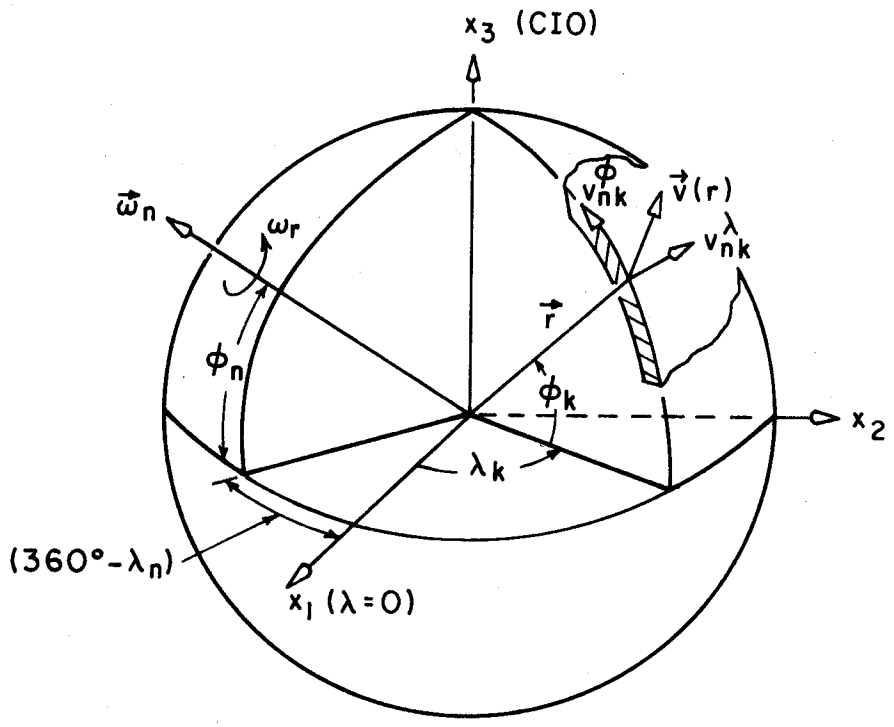

Figure 6.2 Geometry of Plate Motion Kinematics

From equations (6.1) and (6.2), the Cartesian components of v(r) can be written as

$$v_{x_1} = r_s w_n \{\sin\phi_k \cos\phi_n \sin\lambda_n - \cos\phi_k \sin\lambda_k \sin\phi_n\}$$

$$v_{x_2} = r_s w_n \{\cos\phi_k \cos\lambda_k \sin\phi_n - \sin\phi_k \cos\phi_n \cos\lambda_n\}$$

$$v_{x_3} = r_s w_n \{\cos\phi_k \cos\phi_n \sin(\lambda_k - \lambda_n)\} \quad . \tag{6.3}$$

Taking the inner product of v(r) with the unit tangents to the meridian of longitude and the parallel of latitude passing through r gives

$$v^{\phi}_{nk} = -\sin\lambda_k v_{x_1} + \cos\lambda_k v_{x_2}$$

$$v^{\lambda}_{nk} = -\sin\phi_k \{\cos\lambda_k v_{x_1} + \sin\lambda_k v_{x_2}\} + \cos\phi_k v_{x_3} \quad . \tag{6.4}$$

Substituting equation (6.3) into equation (6.4) gives

$$v^{\phi}_{nk} = r_s w_n \cos\phi_n \sin(\lambda_k - \lambda_n)$$

$$v^{\lambda}_{nk} = r_s w_n \{\cos\phi_k \sin\phi_n - \sin\phi_k \cos\phi_n \cos(\lambda_k - \lambda_n)\} \quad . \tag{6.5}$$

In equation (6.5), v^{ϕ}_{nk} and v^{λ}_{nk} are given in linear units. To express these quantities in their angular measure equivalents, $\delta\phi_{nk}$ and $\delta\lambda_{nk}$, one may write

$$\delta\phi_{nk} = v^{\phi}_{nk}/r_s = w_n \cos\phi_n \sin(\lambda_k - \lambda_n)$$

$$\delta\lambda_{nk} = v^{\lambda}_{nk}/r_s \cos\phi_k = w_n \{\sin\phi_n - \tan\phi_k \cos\phi_n \cos(\lambda_k - \lambda_n)\} \quad . \tag{6.6}$$

The predicted secular changes in the latitude and longitude of the LLR observatories due to absolute plate motions are shown in Table 6.3. These values are expressed in milliarcsecs yr^{-1} and are obtained from a direct evaluation of equation (6.6), assuming appropriate conversions have been made. The most obvious comment about these

Table 6.3. Secular Changes in LLR Station Coordinates due to Plate Motion

Plate Model Designation	Observatory									
	Orroral		Calern		Dodaira		McDonald		Haleakala	
	$\delta\phi$	$\delta\lambda$	$\delta\phi$	$\delta\lambda$	$\delta\phi$	$\delta\lambda$	$\delta\phi$	$\delta\lambda$	$\delta\phi$	$\delta\lambda$
	Change in Station Coordinates, $0.''001\ yr^{-1}$									
AM1	1.6,	0.5	0.3,	0.5	-0.3,	0.3	-0.2,	-0.9	1.1,	-2.8
K5	1.6,	0.7	0.2,	0.8	-0.4,	0.4	-0.1,	-0.8	1.1,	-2.6
A3	1.6,	0.8	0.4,	0.7	-0.4,	0.8	-0.1,	-0.5	1.0,	-2.4
B3	1.8,	0.4	0.0,	0.3	-0.2,	0.0	0.1,	-0.9	1.4,	-2.9
B4	1.7,	0.6	0.2,	0.5	-0.3,	0.5	0.0,	-0.7	1.2,	-2.6
C3	1.5,	0.9	0.5,	0.8	-0.4,	1.0	-0.1,	-0.4	0.9,	-2.2
C4	1.6,	0.8	0.4,	0.7	-0.3,	0.8	-0.1,	-0.5	1.0,	-2.3
D1	1.9,	0.9	0.0,	0.6	0.0,	0.6	0.0,	-0.3	1.3,	-2.3
E2	1.7,	0.5	0.4,	0.3	-0.2,	0.8	-0.3,	-0.7	0.9,	-2.4
E3	1.8,	0.5	0.2,	0.3	-0.1,	0.3	-0.1,	-0.8	1.2,	-2.7

results is the good agreement for the drifts in latitude and longitude as predicted by the ten different models. Expressed as a linear rate, the largest discrepancy is 2.5 cm/year. This occurs for the longitude drift at Dodaira as predicted by Models B3 and C3 of Solomon et al. (1975). However, the largest discrepancy between the more favoured models AM1, K5 and B4 (Dickman 1977) occurs for the longitude drift at Calern but only amounts to 7 mm/year. Overall, the Orroral and Haleakala observatories have the largest velocities; they are of the order 6 cm/year and 8 cm/year, respectively. The velocities of the North American plate upon which McDonald is located and the Eurasian plate upon which Calern and Dodaira are located are much smaller by comparison. Stations on these plates do not move faster than ~3 cm/year.

It is important to note that the direction of the station drift plays a significant role with regard to the extent plate motions will contaminate earth rotation results. From equation (4.18) it follows that changes in latitude will have a first order effect on polar motion while the changes in longitude enter the equation through the sine and cosine terms and, as such, have only a second-order effect. Nevertheless, equations (4.13) and (4.19) clearly show that changes in longitude will affect UT1 results directly.

The extent of the corrections to LLR earth rotation results caused by the drift of the network is examined in the next section. A least squares procedure is used to arrive at these results and so the magnitude of the corrections will depend on the degree to which the individual station drifts cancel each other in an average sense.

6.3 Apparent Variations in Polar Motion and Universal Time Due to LLR Station Drifts

If the changes $\delta\phi$ and $\delta\lambda$ in LLR station coordinates are known then their effects δx, δy and $\delta UT1$ on the determination of polar motion and Universal time can be computed from expressions similar to equations (4.18) and (4.19), that is, (Stolz and Larden 1977)

$$\delta\phi = \delta x \cos\lambda - \delta\lambda \sin\lambda$$

$$\delta\lambda = \tan\phi(\delta x \sin\lambda + \delta y \cos\lambda) + \delta UT1 \quad . \tag{6.7}$$

Stated differently, the problem reduces to determining three small angles $\delta\alpha_i$ $i = 1,2,3$ that will transform the geographic reference system x_i, as defined by the LLR station coordinates at time t_0, to the new apparent system $\tilde{x}_i$ at time t_1 after the plate motions have been applied. The Cartesian coordinates of the two systems are related by the known transformation

$$[\tilde{x}_i] = R_3(\delta\alpha_3)R_1(\delta\alpha_2)R_2(\delta\alpha_1)[x_i] \quad . \tag{6.8}$$

Consequently, if δx, δy and $\delta UT1$ are given in linear units, then $\sin \delta\alpha_1 = \delta x/r_s$, $\sin \delta\alpha_2 = \delta y/r_s$ and $\sin \delta\alpha_3 = \delta UT1/r_s$.

It is clear from equation (6.7) that if δx, δy and $\delta UT1$, are determined by the least squares method, they represent the apparent changes in the spin axis coordinates and the position of the zero meridian needed to produce, in an average sense only, the drift of the LLR network due to plate motion. Equations (6.7) thus form the observation equations which contribute to a least squares solution for the unknowns δx, δy and $\delta UT1$ given the coordinate changes $\delta\phi$ and $\delta\lambda$. Note, also that values of $\delta\phi$ and $\delta\lambda$ from more than one observatory are required to determine these unknowns. Therefore, if $\{x,y,UT1\}_{LLR}$ are the LLR solutions for polar motion and Universal time made in ignorance of the plate motion effect and $\{x,y,UT1\}_{COR}$ are the correct solutions, which take into account the changes in latitude and longitude due to plate motion, then the relation between these two solution sets follows as (see e.g. Okuda 1972)

$$x_{COR} = x_{LLR} - \delta x$$

$$y_{COR} = y_{LLR} - \delta y$$

$$UT1_{COR} = UT1_{LLR} - \delta UT1 \quad . \tag{6.9}$$

Values for δx, δy and $\delta UT1$ are shown in Tables 6.4 to 6.7, in cm/year, for the five station network and selected two, three and four-station combinations. The value for $\delta UT1$ is given in the equatorial plane and if positive indicates that the average displacement of the zero meridian for the LLR network is in an eastward direction.

The following trends are evident from the results listed in Tables 6.3 to 6.7:

(a) As the number of stations in the LLR network increases, the effect of plate motion on earth rotation results over short time periods tends to be less significant. The calculations indicate that plate motions will contaminate determinations of x, y and UT1, accurate to 5 cm, if a five station network is constantly in operation after about four or five years. For two station combinations the timescale for contamination can be shorter by anywhere up to a factor of 8, depending on which parameter and station combination is under consideration. The results for three and four station combinations generally lie somewhere in between these limits. In the previous study by Stolz and Larden (1977), substantially shorter time intervals for the five station case were given. However, these earlier results were based on the relative velocity model given by Solomon and Sleep (1974) in which the Pacific plate was held fixed. By using the actual absolute motions it is clear that the effect of plate motion on earth rotation results can be viewed in a more appropriate perspective.

(b) In general, the absolute plate velocity models considered in this study predict changes in the LLR station coordinates that are in good agreement. With the exception of the latitude change at McDonald predicted by Model B3 (drag beneath continents only), all other coordinate changes are consistent. For this particular model, McDonald has a slow drift northward whereas the majority of the models predict a slow drift southward but since the meridianal motion at McDonald is about 1 cm/year, which is the level of

Table 6.4. Effect of Secular Changes in LLR Station Coordinates on Polar Motion and Universal Time Determinations for the Five-Station Network.

Plate Model Designation	δx	δy	δ_{UT1}
		cm yr^{-1}	
AM1	-0.9	1.3	-1.7
K5	-0.8	1.7	-1.2
A3	-0.6	1.3	-0.5
B3	-1.7	1.6	-2.2
B4	-1.2	1.4	-1.3
C3	-0.4	1.1	-0.2
C4	-0.7	1.1	-0.4
D1	-1.9	1.1	-0.6
E2	-0.7	0.5	-1.1
E3	-1.4	1.1	-1.7

Table 6.5. Effect of Secular Changes in LLR Station Coordinates on Polar Motion and Universal Time Determinations for Selected Four-Station Combinations.

Plate Model Designation	Four-Station Combinations*								
	FJTH			AJTH			AFTH		
	δx, δy, δ_{UT1}; cm yr^{-1}								
AM1	0.8,	1.8,	-2.2	-1.8,	0.6,	-2.4	-2.1,	2.4,	-3.3
K5	0.8,	2.3,	-1.6	-1.7,	0.8,	-2.0	-2.0,	2.7,	-2.7
A3	1.0,	1.9,	-1.0	-1.5,	0.6,	-1.2	-1.8,	2.4,	-2.1
B3	-0.1,	2.2,	-2.7	-2.6,	1.0,	-2.9	-2.9,	2.7,	-3.8
B4	0.5,	2.0,	-1.7	-2.1,	0.8,	-1.9	-2.3,	2.5,	-2.8
C3	1.2,	1.7,	-0.6	-1.3,	0.5,	-0.8	-1.6,	2.2,	-1.8
C4	1.0,	1.7,	-0.9	-1.6,	0.5,	-1.1	-1.9,	2.2,	-2.0
D1	-0.3,	1.7,	-1.1	-2.8,	0.5,	-1.3	-3.1,	2.2,	-2.2
E2	0.9,	1.0,	-1.5	-1.6,	-0.2,	-1.7	-1.9,	1.6,	-2.7
E3	0.3,	1.6,	-2.1	-2.3,	0.4,	-2.3	-2.6,	2.2,	-3.3

*A = Orroral, Australia; F = Calern, France; J = Dodaira, Japan

T = McDonald, Texas; H = Haleakala, Hawaii

Table 6.6. Effect of Secular Changes in LLR Station Coordinates on Polar Motion and Universal Time Determinations for Selected Three-Station Combinations.

Plate Model Designation	Three Station Combinations*								
	ATH			FTH			JTH		
	δx, δy, δ_{UT1}; cm yr^{-1}								
AM1	-4.8,	1.0,	-5.1	0.2,	3.7,	-3.2	0.2,	0.4,	-3.3
K5	-4.8,	1.2,	-4.6	0.1,	3.3,	-3.9	0.3,	0.7,	-2.8
A3	-4.6,	1.1,	-3.9	0.3,	3.3,	-2.7	0.5,	0.7,	-1.9
B3	-5.7,	1.5,	-5.6	-0.8,	3.7,	-4.4	-0.6,	1.0,	-3.6
B4	-5.1,	1.3,	-4.6	-0.2,	3.5,	-3.4	-0.1,	0.8,	-2.6
C3	-4.4,	1.0,	-3.5	0.6,	3.2,	-2.3	0.7,	0.5,	-1.5
C4	-4.6,	1.0,	-3.8	0.3,	3.2,	-2.6	0.4,	0.5,	-1.8
D1	-5.8,	1.0,	-4.0	-0.9,	3.2,	-2.8	-0.8,	0.5,	-2.0
E2	-4.6,	0.3,	-4.4	0.3,	2.5,	-3.2	0.4,	-0.1,	-2.4
E3	-5.3,	0.9,	-5.0	-0.4,	3.1,	-3.8	-0.3,	0.5,	-3.0

*See Table 6.5 for notations

Table 6.7. Effect of Secular Changes in LLR station Coordinates on Polar Motion and Universal Time Determinations for Selected Two-Station Combinations.

Plate Model Designation	Two-Station Combinations*								
	AF			AH			TH		
	δx, δy, δ_{UT1}; cm yr^{-1}								
AM1	-0.1,	-7.9,	7.5	-5.3,	3.9,	-5.4	-5.6,	-2.0,	-8.3
K5	-0.2,	-7.2,	7.9	-5.2,	4.2,	-4.9	-5.6,	-1.8,	-7.7
A3	0.2,	-8.1,	8.7	-4.9,	3.7,	-4.2	-4.9,	-1.4,	-6.6
B3	-0.9,	-7.8,	7.0	-6.0,	4.0,	-5.9	-6.0,	-1.0,	-8.3
B4	-0.3,	-8.0,	8.0	-5.4,	3.8,	-4.9	-5.4,	-1.2,	-7.3
C3	0.4,	-8.3,	9.1	-4.7,	3.5,	-3.8	-4.7,	-1.5,	-6.2
C4	0.2,	-8.3,	8.8	-5.0,	3.5,	-4.1	-4.9,	-1.5,	-6.5
D1	-1.1,	-8.3,	8.6	-6.2,	3.5,	-4.3	-6.2,	-1.5,	-6.7
E2	0.1,	-8.9,	8.2	-5.0,	2.9,	-4.7	-5.0,	-2.2,	-7.1
E3	-0.6,	-8.3,	7.5	-5.7,	3.5,	-5.3	-5.7,	-1.6,	-7.7

*See Table 6.5 for notations.

agreement between the plate velocity models, one cannot consider the appearance of this anomaly to be very significant. The fastest drift in latitude occurs at the Orroral station where the rate is about 5 cm/year northward. For longitude, the rate of 8 cm/year at Haleakala is the largest.

(c) It is noticeable from Tables 6.6 and 6.7 that the plate motion effects at Orroral and Haleakala will have a significant impact on earth rotation results after about one year if a two or three-station network which includes these stations is in existence. Also, it must be remembered that even if a five station network is in operation, weather conditions will not always permit a five station solution. For example, if polar motion and UT1 results are obtained using just the Orroral and Haleakala station data, then plate motion effects will need to be considered after one year because both these stations are located on fast moving plates. However, as more stations are added to the LLR network and contribute to the solutions for polar motion and UT1 the plate motion impact becomes less significant due to averaging and cancellation effects.

(d) With the exception of the AF case (see Table 6.7), all plate velocity models produce an apparent westward displacement of the zero meridian for the LLR networks that have been considered. It is also instructive to note that when the apparent drift of the pole is computed after consideration of the LLR station motions, the majority of models give results that are consistent. For the five-station network, all models predict an apparent drift of the CIO at a rate of approximately 1.5 cm/year in a direction bounded by longitudes 20°E and 60°E. The magnitude of this drift is about a factor of 6 smaller than the present astronomically observed secular motion of the pole and in a direction roughly perpendicular to it (see Section 2.4.3.3).

The determination and maintenance of a global geodynamics reference frame for earth rotation and plate tectonic studies is presently the subject of considerable discussion (see e.g. Bender 1981). One of the leading questions to be considered will be whether or not a theoretical model for the plate motions should be adopted and if so, which model? The results of the analyses carried out in this chapter indicate that the currently available absolute plate velocity models appear consistent. Even if these models were not an adequate representation of the present-day relative plate velocities, the data from the space ranging techniques will certainly provide an avenue for their improvement. Although recourse to geophysical hypotheses is necessary to deduce the absolute motions, the wide variety of assumptions upon which the ten models considered in the study are based, and the general agreement between the results indicates that adopting a model for the plate motions is not likely to have serious drawbacks. Since models AM1, K5 and B4 give compatible results for likely four and five-station LLR networks, then it would seem desirable to consider the adoption of any one of these models in the reduction of high-precision LLR data. One must also give due consideration to the recently published absolute plate motion models of Minster and Jordan (1978) and Chase (1978). A close inspection of these models, however, indicates that the velocities of the major plates, upon which the LLR stations are located, are in close agreement with those suggested by models AM1, K5 and B4.

In the next chapter, efforts are made to assess the geodetic consequences of two additional geophysical mechanisms which hitherto have been regarded as sources of observational noise. Specific consideration is given to the seasonal redistribution of air mass and groundwater and the associated elastic deformation of the earth's surface as incorporated in the surface mass loading problem. Since both involve a form of mass transfer, the extent and nature of geocentre motion is also examined. The significance of the results is discussed within the context of the expected 1 to 3 cm measurement accuracy level for the space ranging techniques.

CHAPTER 7

GEODETIC CONSEQUENCES OF SEASONAL ATMOSPHERIC AND GROUNDWATER LOADING

7.1. Introduction

As the measurement uncertainties at LLR, SLR and VLBI observing stations approach the 3 cm level (see Chapter 2) and new data types from the next generation of geodetic measuring systems are used to densify regional survey networks with expected relative point positioning accuracies of 1 to 2 cm (see e.g. Anderle 1979, Faller et al. 1979, MacDoran 1979, Larden and Bender 1981), one can query whether there exist other time-dependent geophysical phenomena, apart from global plate tectonic activity, that hitherto have been considered as sources of observational noise in the space ranging techniques but could now produce measurable displacements within the context of centimetre geodesy.

Identification of these processes ahead of time using geophysical data and knowing the significance of their effect on geodetic observations serves a two-fold purpose. Firstly, such information will give valuable insight on what effects deserve parameterization in reduction programs for high-precision data and secondly, is particularly useful when the data contain signatures of spectral similarity that require separation before experimental results on, say, the earth's rotation and crustal motions, can be correctly interpreted.

As discussed in Chapter 2, there are many geophysical mechanisms that contribute to the spectrum of the earth's rotation. What has not been studied as thoroughly, though, are their effects on the position of the geocentre and the geometrical shape of the earth's surface. Such studies are extremely important because three-dimensional position measurements to the LAGEOS satellite and the moon are sensitive to distortions in the shape of the earth's surface as well as to the movement of the geocentre. As pointed out in Chapter 2, the term geocentre is used in

this study to mean the centre of mass of the solid earth which is deemed to include the core. In the surface mass loading problem (see e.g. Farrell 1972), mass transfer outside the earth's surface causes the geocentre, along with the solid earth, to shift in inertial space so that the centre of mass of the whole system (earth plus load) is not displaced. It is in this context that the concept of geocentre motion is discussed.

Some geodesists use the term geocentre rather loosely and state that it is the centre of mass of the earth when they really mean the centre of mass of the combined solid earth, oceans and atmosphere. While this definition has a fundamental basis in satellite orbital dynamics (in this context, the geocentre is located at the focus of the orbital ellipse) it does, however, invalidate the concept of a movement of the geocentre as discussed above. It should be emphasized that the definition in the preceding paragraph is chosen for conceptual reasons only and that it is not the author's intention to advocate which definition should be applied to the origin of the geographic reference system. Such a decision is not critical to the interpretation of the results in this chapter.

Among the mechanisms that have to be considered, in addition to plate tectonic activity, are the earth and ocean tides, changes in sea-level associated with the melting of the polar ice caps, atmospheric pressure and groundwater variations, and earthquakes. The geodetic consequences of some of these effects have been discussed many times (see e.g. Melchior 1978, Walsh and Rice 1979, Goad 1980, Peltier 1980). In this chapter, specific consideration is given to the combined seasonal effects of atmospheric-groundwater loading which until recently had not received much attention in the geodetic literature. Since this mechanism involves a form of mass transfer, the magnitude of geocentre motion is calculated together with the associated radial deformation of the earth's surface as the latter responds elastically under the action of the variable load. The corresponding tangential displacements for seasonal atmospheric-groundwater loading turn out to be very small and, therefore, are not computed (Stolz and Larden 1980).

Previous calculations for the radial deformations of the earth by the atmosphere have only been done for regions of limited extent and then in

connection with gravimetric and tiltmeter studies (see e.g. Urmantsev 1971, 1975; Trubytsyn and Makalkin 1976, Warburton and Goodkind 1977). Theoretical solutions for the distortions of a model earth by a radial stress which is uniformly distributed over equal antipodal caps have also been reported by Slichter and Caputo (1960). While the calculated displacements are of the order 1 cm, it is difficult to reconcile these purely theoretical results with reality. The first global solution for the seasonal distortions in the shape of the earth's surface due solely to atmospheric loading was carried out by Stolz and Larden (1979). A comprehensive account of this study is given in this chapter.

Studies on the geodetic implications of groundwater variations have mainly dealt with the impact of variations in water table levels on the interpretation of crustal movements as deduced by gravimeter and classical leveling methods. Like the atmospheric studies, analyses were only carried out for regional areas (see e.g. Lambert and Beaumont 1977, Hein 1980) and no attempt was made to investigate the time-dependent effects of moisture stored on the surface in the form of snow, ice and vegetation as well as water stored between the surface and the water table.

Ever since the introduction of the Kimura term in the wobble equation for latitude variations by the ILS, researchers have used the existence of this term as likely evidence for geocentre motion (see e.g. Schumann 1903, Munk and McDonald 1960, Sugawa et al. 1973). Initial estimates for the component of the term attributable to a shift of the geocentre were made by Naito and Sugawa (1973), using seasonal data of atmospheric pressure and oceanic mass transports across the 39th parallel of latitude on which the ILS network is located. While it seems possible that oceanic mass transports can explain the term, the overwhelming number of observational, geophysical and astronomical factors that can contribute to the term are still not known well enough to warrant definite conclusions about the results (Lambeck 1980). Recent studies show that the atmospheric tides (E. Groten, unpublished manuscript 1976) and the M_2 ocean tide (Brosche and Sunderman 1977) displace the geocentre in space by less than 1 and 2 cm, respectively. Using three of the plate tectonic mass transfer models constructed by Mather and Larden (1978),

Larden (1980) has shown that for realistic models, the displacement of the geocentre relative to the earth's surface due to plate tectonic activity probably isn't more than 5 mm/century.

Stolz (1976a,b) has estimated the contributions from seasonal variations in air-mass, groundwater and sea level, and concludes that together they amount to a seasonal shift in the geocentre of less than 5 millimetres. However, the atmospheric data used in this study were quite old and only extended to latitude 40°S where, by the form of the integrals which have to be evaluated, a maximum effect is expected. Also, an algebraic error was made by Stolz (1976a) when allowing for the oceanic response to atmospheric pressure changes and like many previous studies, the dynamical nature of the calculated geocentre motion was not specified. Stolz and Larden (1979) corrected these oversights in their recent calculation of the seasonal displacement and deformation of the earth by the atmosphere, using newer and more complete data. However, the unresolved issues in this more recent study are the effect of deformation on the displacement of the earth in space and the magnitude of the surface distortions produced by seasonal groundwater variations, for which fairly reliable data can be obtained. No attempt is made here to evaluate the contributions due to seasonal fluctuations in sea level since reliable data are not available (Lambeck 1980). Gill (1978, private communication) believes it will be a decade or two before a reliable ocean mass transport model becomes available.

In the following sections, the theory of the elastic deformations of the earth is reviewed to provide the necessary mathematical platform from which the geodetic consequences of seasonal atmospheric-groundwater loading and the unresolved aspects of Stolz and Larden (1979) can be explored. Specific consideration is given to the interpretation of the low-degree Love numbers as they apply to the surface mass loading problem, the data used and its manipulation, and the errors introduced by the assumptions made in the calculation. Above all, however, efforts are made to explain the nature of the calculated displacements and assess the significance of the results on LLR, SLR and VLBI geodetic networks.

7.2. Load Deformation Theory

7.2.1. Development of the theory

The equilibrium response of an elastic earth, subject to surface mass loading (see e.g. Longman 1962, 1963; Farrell 1972, Dahlen 1974), is an established topic of geophysics which has now attracted the interest of geodesists who are involved with the analyses of high-precision measurements made on the earth's surface and from it to extra-terrestrial sources. The computation of ocean loading effects on measured geodetic quantities is a typical example (see e.g. Farrell 1973, Bretreger and Mather 1978, Chiaruttini and Livieratos 1978, Goad 1980). Since the theory has been discussed in numerous texts and papers, only a brief account of the more general aspects is given here.

For an elastic earth that is radially stratified, spherically symmetric and in hydrostatic equilibrium before the surface load is applied, the linearized equations of motion for small deformations can be written as (Lambeck 1980)

$$\vec{\nabla}\cdot T - \vec{\nabla}(\rho g \vec{d}\cdot\vec{i}_r) - \rho\vec{\nabla}U + g\vec{\nabla}\cdot(\rho\vec{d})\vec{i}_r - \rho\partial^2\vec{d}/\partial t^2 = 0 \qquad (7.1)$$

where T is the non-hydrostatic stress tensor, ρ is the density and g is the gravitational acceleration in the equilibrium state, $\vec{d}$ is the displacement vector, $\vec{i}$ is a unit vector with radial and tangential components $\vec{i}_r$ and $\vec{i}_t$, respectively, and $\vec{\nabla}$ is the gradient operator defined as

$$\vec{\nabla} = \frac{\partial}{\partial x_j}\vec{j} \quad .$$

The perturbation in gravitational potential U has two components U_1 and U_2 which are, respectively, the perturbation in potential due to the deformation and the potential of the applied mass load. Inside the earth, U satisfies Poisson's equation, that is, (see e.g. Heiskanen and Moritz 1967)

$$\vec{\nabla}^2 U = -4\pi G\vec{\nabla}\cdot(\rho\vec{d}) \qquad (7.2)$$

where G is the gravitational constant. Since equations (7.1) and (7.2) are to be solved for spherically symmetric earth models with elastic

properties that are functions of radius (r) alone, one can obtain solutions for these equations if U is harmonic, that is,

$$U = \sum_n U'_n(r) S_n \tag{7.3}$$

where $U'_n(r)$ are the radially dependent functions defining the potential perturbation and S_n is a surface harmonic of degree n. The solution to equations (7.1) and (7.2) for this case is also harmonic and can be written in the form

$$\vec{d} = \sum_n \{V_n(r) S_n \vec{i}_r + W_n(r) \vec{\nabla} S_n \vec{i}_t\} \tag{7.4}$$

where $V_n(r)$ and $W_n(r)$ are the radially dependent functions for the radial displacement and tangential displacement in the direction of the load, respectively. To facilitate further solution, equation (7.1) is transformed with (7.2) and (7.4) to reduce the equations of motion to six coupled first-order differential equations of the form

$$\underset{i\times 1}{dY_i/dr} = \underset{i\times j}{[H]}\ \underset{j\times 1}{[Y]} \qquad i, j = 1,....6 \tag{7.5}$$

where [H] is a 6 x 6 coefficient matrix whose elements are functions of the Lamé parameters λ and μ, the density ρ, the gravitational acceleration g, the harmonic degree n, and the frequency σ of the deformation. The Y_i's denote the following quantities;

i = 1; radial displacement, $Y_1 = V_n(r)$

i = 2; radial stress

i = 3; tangential displacement, $Y_3 = W_n(r)$

i = 4; tangential stress

i = 5; potential perturbation, $Y_5 = U'_n(r)$

i = 6; The derivative of $U'_n(r)$ less the radial displacement contribution; $Y_6 = \partial U'_n(r)/\partial r - 4\pi G\rho V_n(r)$.

Equation (7.5) is completely general and, in addition to the surface mass loading problem, can be applied to studies of the earth's free oscillations and the deformations accompanying earth tides. Subject to appropriate boundary conditions, equation (7.5) can be solved by numerically integrating this set of differential equations to obtain values of the Y_i's (see e.g. Farrell 1972 for integration techniques).

For example, the boundary conditions relevant to the surface loading problem are different from those of the earth tide problem in that the load exerts a normal stress on the loaded surface that is missing in the other case. Nevertheless, the conditions of (1) regularity at the origin, (2) continuity of deformation and stress across internal surfaces of discontinuity, and (3) internal and external gravitational potentials and their respective gradients must be equal at free surfaces and across surfaces of discontinuity, still apply (see e.g. Alterman et al. 1959).

7.2. The Load Love Numbers

In the surface mass loading problem which is of concern here, it is conventional to discuss the deformation of an elastic sphere, due to an applied potential U_2 of the form (7.3), in terms of the dimensionless load Love numbers $h'_n(r)$, $\ell'_n(r)$ and $k'_n(r)$ (Munk and MacDonald 1960). For

$$U_2 = \sum_n U_{2,n} = \sum_n U'_{2,n}(r) S_n \quad , \tag{7.6}$$

the displacement functions $V_n(r)$ and $W_n(r)$, and the potential perturbation $U'_{1,n}(r)$ due to deformation are related to the load Love numbers by (see, e.g. Farrell 1972)

$$\begin{bmatrix} V_n(r) \\ W_n(r) \\ U'_{1,n}(r) \end{bmatrix} = U'_{2,n}(r) \begin{bmatrix} h'_n(r)/g(r) \\ \ell'_n(r)/g(r) \\ k'_n(r) \end{bmatrix} \tag{7.7}$$

In terms of the Y_i's of equation (7.5)

$$\begin{aligned} Y_1(r) &= h'_n(r) U'_{2,n}(r)/g(r) \\ Y_3(r) &= \ell'_n(r) U'_{2,n}(r)/g(r) \\ Y_5(r) &= [1 + k'_n(r)] U'_{2,n}(r) \end{aligned} \tag{7.8}$$

Of geodetic interest, are the radial, $\vec{d}_r$, and tangential, $\vec{d}_t$, displacements in position and the perturbation in potential, U, at the earth's surface (r = a, where a is the earth's radius). Dropping the radial argument

when r = a and using equations (7.3) and (7.4) together with equations (7.7) and (7.8) gives

$$\vec{d}_r = \sum_n Y_1 S_n \vec{i}_r = \sum_n [h'_n U_{2,n}/g]\vec{i}_r \tag{7.9a}$$

$$\vec{d}_t = \sum_n Y_3(\vec{\nabla}S_n)\vec{i}_t = \sum_n [\ell'_n \vec{\nabla}U_{2,n}/g]\vec{i}_t \tag{7.9b}$$

$$U = \sum_n Y_5 S_n = \sum_n (1+k'_n)U_{2,n} \tag{7.9c}$$

Implicit in these equations is the combined effect of loading and attraction. The deformation is due to two opposing effects. While the major component is the surface depression caused by the load, there is also a smaller component which is due to the attraction by the load. The combined effect is described by equations (7.9a,b). The additional potential due to the distortion alone is given by $k'_n U_{2,n}$ (see equation 7.9c). Similar equations can be employed to study the effect of surface mass loading on gravimeter and tiltmeter measurements (see e.g. Goad 1980).

An important aspect of the load Love number formulation that should be discussed here is the dependence of the calculated load Love numbers on the frequency of the load. In most calculations of these numbers (see e.g. Longman 1963, 1966; Dahlen 1976) it is customary to assume the elastic response behaves statically. The concept of purely static deformation is based on zero frequency response (σ=0) which implies that when the load is applied, the elastic deformation occurs instantaneously and follows a linear pattern. This assumption nullifies the contribution of the frequency dependent terms in the [H] matrix of equation (7.5) and leads to expressions for the Y_i's and the load Love numbers, h'_n, ℓ'_n and k'_n that are merely functions of the Lamé parameters λ and μ, the density ρ, gravitational acceleration g, and the harmonic degree n. Values of h'_n, ℓ'_n and k'_n deduced in this manner are often referred to as static load Love numbers (see e.g. Dahlen 1974).

For cases where the frequency σ of the applied load potential U_2 is close to $\sigma_0 \approx 26$ cycles/day, that is, the frequency of the fundamental mode of free oscillation (see Stacey 1977 for a discussion of these

modes), the static response approximation is unreliable for load Love number calculations and the dynamic approach is necessary in order to account for resonant effects. This is accomplished by retaining the frequency dependent terms in the [H] matrix of equation (7.5) (see Farrell 1972).

In deciding whether the static approximation can be used in practice, Jeffreys and Vicente (1966) offer the following general rule. They suggest that the fractional difference in the static Love numbers (σ=0) and the values for frequency σ should be of the order of σ^2/σ_0^2 where σ_0 is defined above. This order of magnitude has been substantiated by the studies of Pekeris and Accad (1972). For loads that vary annually (σ=1/365 cycles per day), such as the seasonal redistribution of atmospheric mass and groundwater, the differences are infinitesimal. This clearly indicates that the static equilibrium response approximation is more than adequate for the calculations in this chapter. Even at the semi-diurnal tidal frequency (σ=2 cycles/day) the static approximation is, at least, good to 1%. There is, however, some controversy on how to treat the fluid core response in static deformation problems (see e.g. Dahlen 1974, Crossley and Gubbins 1975) but this issue does not seem to affect the results for the response at the surface of the earth (Dahlen 1974).

Values of the load Love number h_n', as deduced by various authors, are listed in Table 7.1 for all harmonics up to and including degree 36. It did not seem necessary to list the companion values ℓ_n' and k_n' since the tangential displacements are very small for seasonal atmospheric-groundwater loading (Stolz and Larden 1980) and the perturbations in gravitational potential are not considered in this study. Consequently, an evaluation of equations (7.9b,c) was not undertaken.

Longman's (1966) results have been derived for a Gutenberg earth model with an Adams-Williamson core using the static response approximation. The properties of this model are described by Alterman et al. (1961) and Longman (1963). In his extension and review of Longman's work, Farrell (1972) calculates h_n' for the same earth model but uses the dynamic approach and chooses the loading frequency σ as the M_2

Table 7.1. Values of Load Love Number ($-h'_n$) for Radial Deformation Calculations

Degree n	Longman (1966)	Farrell (1972)*	Dahlen (1976)
0 (19)	0.134 (1.949)	--- (*)	0.135 (2.016)
1 (20)	--- (1.994)	0.290 (*)	0.292 (2.064)
2 (21)	1.007 (2.037)	1.001 (*)	1.010 (2.110)
3 (22)	1.059 (2.078)	1.052 (*)	1.074 (2.154)
4 (23)	1.059 (2.117)	1.053 (*)	1.080 (2.196)
5 (24)	1.093 (2.156)	1.088 (*)	1.116 (2.235)
6 (25)	1.152 (2.194)	1.147 (*)	1.177 (2.273)
7 (26)	1.223 (2.223)	* (*)	1.250 (2.309)
8 (27)	1.296 (2.257)	1.291 (*)	1.326 (2.343)
9 (28)	1.369 (2.291)	* (*)	1.401 (2.376)
10 (29)	1.439 (2.322)	1.433 (*)	1.475 (2.407)
11 (30)	1.506 (2.351)	* (*)	1.545 (2.437)
12 (31)	1.572 (2.380)	* (*)	1.613 (2.465)
13 (32)	1.631 (2.408)	* (2.379)	1.679 (2.492)
14 (33)	1.691 (2.429)	* (*)	1.741 (2.518)
15 (34)	1.747 (2.455)	* (*)	1.801 (2.543)
16 (35)	1.798 (2.470)	* (*)	1.859 (2.566)
17 (36)	1.852 (2.497)	* (*)	1.914 (2.589)
18	1.902	1.892	1.966

*Values not listed by Farrell (1972).

semi-diurnal ocean tide frequency because he is primarily interested in the loading effect of this constituent. The differences between these results and Longman's are at the 1% level as predicted by Jeffreys and Vicente (1966).

Farrell, however, does not bother to list all the load Love numbers since these are merely intermediaries for the solution of the point-mass ocean loading problem where local effects may dominate. For some point-mass problems it is more convenient to use Green's functions, since the load Love number approach outlined in equations (7.9a,b,c) involves the use of a large number of parameters. One of the simplifying aspects of the seasonal atmospheric and groundwater load is that its energy is concentrated in the low degree spherical harmonics which makes the load Love number approach far more attractive.

Dahlen (1976) has computed static load Love numbers for the more recent earth models 1066A and 1066B of Gilbert and Dziewonski (1975). The discrepancy between these values and those of Longman and Farrell are at the 5% level. This can mainly be attributed to the differences in the earth models, particularly the detailed structure of the mantle. Tests also revealed that the difference between radial displacement results using h_n' values for model 1066A and 1066B in areas where atmospheric-groundwater deformations were the largest did not exceed a few tenths of a millimetre at the most. Therefore, only values for model 1066A are listed in Table 7.1.

Whereas Dahlen (1976) derives all values of h_n' up to and including degree 36, Longman (1966) ignores the first degree term (h_1') and Farrell (1972) sets the zero degree term (h_0') equal to zero. Both the zero and first degree terms are needed in this study for reasons given in the following section. Since the static approximation is more than adequate at the annual frequency and the load Love numbers of Dahlen (1976) are complete, his values for model 1066A are used throughout this study.

7.2.3. Interpretation of Low-Degree Load Love Numbers

The significance of the load Love numbers of degree 0 and 1 deserves a special word of mention. A zero degree term is introduced to

model the earth's response to a load whose mass is not conserved and characterizes a load component that is uniformly distributed over the entire earth's surface. Since the earth is compressible this component causes a radial displacement which is accompanied neither by a tangential displacement nor by a perturbation in the gravitational potential. If mass is conserved then the zero degree term will vanish (Rochester and Smylie 1974), but not if the radial deformations due to seasonal air-mass and groundwater variations are calculated without considering the oceans (Stolz and Larden 1980).

An estimate of the zero degree contribution for both these constituents can be obtained by examining the results of Stolz and Larden (1979) and Lambeck (1980). According to Stolz and Larden (1979), the seasonal variation in mean atmospheric load $q_E^A(t)$ over the whole earth, in grams per centimetre squared (g cm^{-2}), is

$$q_E^A(t) = -0.11 \cos\Theta - 0.06 \sin\Theta \text{ g cm}^{-2} \qquad (7.10)$$

where Θ is the longitude of the sun measured from the beginning of the year. Mean groundwater storage also varies in a similar manner but is slightly out of phase. From Van Hylckama's (1956) groundwater data, which are used in this work, Munk and MacDonald (1960) estimate

$$q_E^G(t) = 0.19 \cos\Theta + 0.77 \sin\Theta \text{ g cm}^{-2} \quad . \qquad (7.11)$$

The total seasonal variation in the combined atmospheric-groundwater load is obtained simply by adding equations (7.10) and (7.11), that is,

$$q_E^{AG}(t) = 0.08 \cos\Theta + 0.71 \sin\Theta \text{ g cm}^{-2} \quad . \qquad (7.12)$$

Clearly, the combined mass within these two constituents is not conserved on a seasonal basis otherwise the right hand side of equation (7.12) would be zero. Equation (7.12) is thus an indicator of the zero degree contribution.

At any particular location on the globe, the zero degree contribution of the combined atmospheric-groundwater load will not exceed $(0.71^2 + 0.08^2)^{1/2} = 0.72$ g cm^{-2}. In areas of geodetic importance, that is, on land where the space ranging networks are located and the deformations

are a maximum, this value is about 10% of the observed seasonal load departures. This conclusion was reached by comparing the value 0.72 g cm^{-2} with the local seasonal variations at strategic sites as indicated by the atmospheric dataset of Schutz and Gates (1971, 1972, 1973, 1974) and the groundwater dataset of van Hylckama (1956). Since no attempt has been made to conserve mass in these calculations, one would expect the deformation results to contain a zero degree contribution of about 10%. This clearly will not affect the general conclusions that can be drawn from the results presented in section 7.4.

Lambeck (1980) has estimated $q_E^G(t)$ using a scaled version of Van Hylckama's (1956) groundwater data set (Van Hylckama 1970) which leads to a smaller estimate for the seasonal change in total groundwater storage of

$$q_E^G(t) = 0.02 \cos\Theta + 0.60 \sin\Theta \text{ g cm}^{-2} \quad . \tag{7.13}$$

Adding equations (7.10) and (7.13) for the total seasonal variation in the combined atmospheric-groundwater load gives

$$q_E^{AG}(t) = -0.09 \cos\Theta + 0.54 \sin\Theta \text{ g cm}^{-2} \tag{7.14}$$

which is not significantly different from equation (7.12) and, therefore, does not alter the previous statement concerning the zero degree contribution to the deformation results.

Terms of degree 1 were omitted from earlier sets of the load Love numbers because their inclusion implied a displacement of the whole earth in space which to a geophysicist was of no direct consequence. Cathles (1971) realized this was incorrect for the surface loading problem and noted that the earth responded to a first degree load in two ways. Firstly, there is a displacement of the earth's surface in space and secondly, the earth is deformed. The displacement of the solid part of the earth in space follows directly from the equations of motion, which show that the position of the centre of mass of the earth plus load remains stationary. As the load is redistributed, the solid earth moves to keep the whole system in equilibrium. The geocentre thus moves, along with the solid earth, in space. It will be shown in section

7.5.1 that the magnitude of the displacement is, for all intents and purposes, the same irrespective of whether the earth is treated as a rigid or elastic body. Farrell (1972) and Dahlen (1976) assume this shift has already taken place and compute the load Love numbers accordingly. Equation(7.9a) thus gives the deformations relative to the position of the earth's surface after the load is redistributed but before any deformation has taken place. The first degree component of the deformation is simply accounted for by the h_1' term (see Table 7.1). Assuming the shift of the geocentre in space has already taken place permits the load Love numbers to be determined independently of the load magnitude (Cathles 1975). However, the satellite geodesist requires that this shift be monitored because it is one of the many phenomena that can affect the measurements.

In section 7.4, both the radial deformations and shift of the geocentre that accompany the seasonal redistribution of atmospheric and groundwater mass are evaluated. These calculations are preceded in section 7.3 by a discussion of the data and followed in section 7.5 by a discussion of the results, their accuracy and their significance within the context of centimetre geodesy.

7.3. Data

7.3.1. Atmospheric Pressure

To estimate the seasonal variations in geodetic position (see section 7.4), global datasets of atmospheric pressure and groundwater storage are needed. For the atmospheric calculations the January, April, July and October averages of sea-level pressure compiled by Schutz and Gates (1971, 1972, 1973, 1974) from the atlases of Taljaard et al. (1969) and Crutcher and Meserve (1970) are used. These data are given at grid-points spaced every 4° of latitude and 5° of longitude over the entire earth but need to be adjusted back to station elevation before the evaluation of equations (7.6), (7.9a) and the geocentre motion integrals of equation (7.37) (Munk and MacDonald 1960). Ideally, the pressure should refer to the mean elevation of the area for which the grid value is assumed to be representative. However, since the method

of estimating sea-level pressure from station level data varies from station to station it is only possible to perform this adjustment approximately.

In this study, Laplace's formula as modified by Siderenkov and Stekhnovskiy (1971) is used to make the correction. Assuming that the atmosphere is polytropic up to the maximum height on land one can write the surface pressure P as

$$P = P_0 \left(\frac{T}{T_0}\right)^{\frac{\bar{g}}{R\gamma}} \cdot \frac{g}{g_{45°}} \qquad (7.15)$$

where P_0 is the pressure at sea-level, T is the surface temperature in degrees Kelvin, $T_0 = T + \gamma\bar{h}$ is the temperature at sea-level, $\bar{g} = 980.618$ cm sec^{-2} is the value of gravity averaged over the earth, $R = 0.287 \times 10^7$ ergs g^{-1} deg^{-1} is the gas constant, $\gamma = 6°$ km^{-1} is the mean temperature gradient, g is the local acceleration of gravity, and $g_{45°}$ is the sea-level value of g at latitude 45°. The surface temperatures for January, April, July and October at the grid-points were obtained from Schutz and Gates (1971, 1972, 1973, 1974) and an averaging process was used to determine the mean elevation $\bar{h}$ of each 4° × 5° compartment from the 1° × 1° height data of Lee and Kaula (1967). A conversion factor of 1 millibar = 1.02 g cm^{-2} is used to convert the pressure values given, in millibars, by Schutz and Gates, to the equivalent load units of g cm^{-2} via the hydrostatic approximation (see Munk and MacDonald 1960, p. 108).

7.3.2. Groundwater

For seasonal departures in groundwater storage, the dataset of Van Hylckama (1956) has been used. This monthly compilation lists estimates of the total amount of water stored in the ground, in units of 10^{16} cubic centimetres, for 10° × 10° areas of the earth's surface. As mentioned in Chapter 2, the definition for groundwater includes moisture stored on the surface (snow, vegetation, lakes) as well as in the upper regions of the crust. In particular, the seasonal variation in the amount of water stored between the earth's surface and the shallowest position of the water table is an important consideration

(Munk and MacDonald 1960). Data beyond latitudes 70°N and 70°S, in areas that are comparatively small and where moisture changes are slight and information is sparse, have not been included in the dataset. Used in this work are the volume estimates for the months of January, April, July and October. Noting that 1 cubic centimetre of water weighs 1 gram, the values for each 10° × 10° compartment were divided by the area of the compartment to yield the surface load in g cm^{-2}.

The reliability of the method used by Van Hylckama to deduce the amount of water stored on and in the ground hinges primarily on how adequately the empirical expression developed by Thornthwaite (1948) can estimate the evapotranspiration term in the water balance equation as a function of air temperature and latitude. The problem has been discussed by Lambeck (1980) together with a brief summary of the other viable methods that can be used to estimate the change in groundwater storage. For global calculations, Thornthwaite's method appears to be the most versatile.

A discussion of the effect of errors in the groundwater and atmospheric data on the results is left until section 7.5.

7.4. Seasonal Variations in Geodetic Position

As a matter of convenience, the vector joining the geocentre and an observing station on the earth's crust shall be referred to as the geocentric station vector. Changes in the length of this vector can be caused by a shift of the geocentre with respect to the earth's surface or surface deformations. A shift of the geocentric station vector in space will not alter its length in any way but will be detected by measurements to artificial satellites and the moon. It, therefore, must be considered. The VLBI technique, for example, is insensitive to movements of the geocentre.

In this section, consideration is given to the movements of the geocentric station vector caused by seasonal atmospheric-groundwater loading. In the first instance, the surface deformations are calculated individually for the atmospheric and groundwater loads. The results are presented in contour form on global maps for each of the four

seasons. Secondly, the nature and extent of the accompanying motion of the geocentre is investigated. The approach here will be to solve the problem for a rigid earth and then, if necessary, correct the solution for the effects of load deformation. Details of the basic assumptions invoked for these calculations are given in section 7.5.

7.4.1. Seasonal Departures in Radial Position

The radial displacements d_r are calculated directly from equation (7.9a). The potential U_2 at the surface arising from seasonal departures in surface load $q(\phi,\lambda,t)$ g cm^{-2} may be written as (Munk and MacDonald 1960, p. 29)

$$U_2 = \sum_n U_{2,n} = 4\pi Ga \sum_n \frac{q_n}{2n+1} \tag{7.16}$$

where q_n is the nth degree surface spherical harmonic representation of $q(\phi,\lambda,t)$ at a particular point on the globe (see e.g. Heiskanen and Moritz 1967, p. 30), a is the earth's radius, and G is the gravitational constant. Substituting (7.16) into (7.9a) gives

$$d_r = |\vec{d}_r| = \frac{4\pi Ga}{g} \sum_n \frac{h'_n q_n}{2n+1} \quad . \tag{7.17}$$

q_n may be determined in two ways (Heiskanen and Moritz 1967 p. 29). The easiest method is to expand the load in terms of spherical harmonic coefficients but this approach is not very convenient if, as is done in this study, the errors introduced by solution truncations are to be investigated. Thus, the direct approach is chosen, namely

$$q_n = \frac{2n+1}{4\pi} \int_S q(\phi,\lambda;t) P_n(\cos\psi) dS \tag{7.18}$$

where $P_n(\cos\psi)$ is the Legendre polynomial, ψ is the angle between the radius vector at the computation point and the radius vector at the location (ϕ,λ) of the disturbing load, $dS = \cos\phi d\phi d\lambda$ is a surface element on a unit sphere and S is the surface of the earth. Substituting (7.18) into (7.17) gives

$$d_r = \frac{Ga}{g} \sum_n h'_n \int_S q(\phi,\lambda;t) P_n(\cos\psi) dS \quad . \tag{7.19}$$

Equation (7.19) is used extensively to compute the radial displacements caused by the seasonal departures in the atmospheric and groundwater load from an annual average value.

7.4.1.1. Deformation due to Atmospheric Loading

Departures in radial position from an annual average position due to atmospheric loading are shown in Figures 7.1, 7.2, 7.3 and 7.4, that is, for each of the four seasons. The response of the oceans to seasonal changes in atmospheric pressure is assumed to follow the inverted barometer rule on a global basis (see Munk and MacDonald 1960, and sections 7.4.2 and 7.5 for further discussion). The oceans thus yield so as to annul horizontal pressure gradients. The seasonal departures in load on the ocean floor, at any particular instant, are thus everywhere the same but varying in time because of the seasonal variation $q_0(t)$ in the mean atmospheric load that lies above the oceans. Following Jeffreys (1916) one can write

$$q_0(t) = \frac{1}{4\pi a_0^0} \int_{\text{Oceans}} q(\phi,\lambda;t) dS \tag{7.20}$$

as

$$q_0(t) = \frac{1}{4\pi a_0^0} \int_{\text{Oceans}} [-\frac{1}{2} m \sin(\Theta-\alpha) + \frac{1}{2} m' \cos(\Theta-\alpha)] dS \tag{7.21}$$

where m and m' are the January minus July and April minus October load differences, respectively; a_0^0 is the fraction of the earth covered by oceans, $\alpha = 104°.2$ is the longitude of the sun on April 15 and Θ has been defined previously. From the oceanic pressure data of Schutz and Gates (1971, 1972, 1973, 1974) and using $a_0^0 = 0.697$ from Balmino et al. (1973), Stolz and Larden (1979) find

$$q_0(t) = -0.73 \cos\Theta - 0.19 \sin\Theta \text{ g cm}^{-2} \tag{7.22}$$

while Siderenkov (1973), assuming zero phase lag, gets

$$q_0(t) = -0.82 \cos\Theta \text{ g cm}^{-2} \tag{7.23}$$

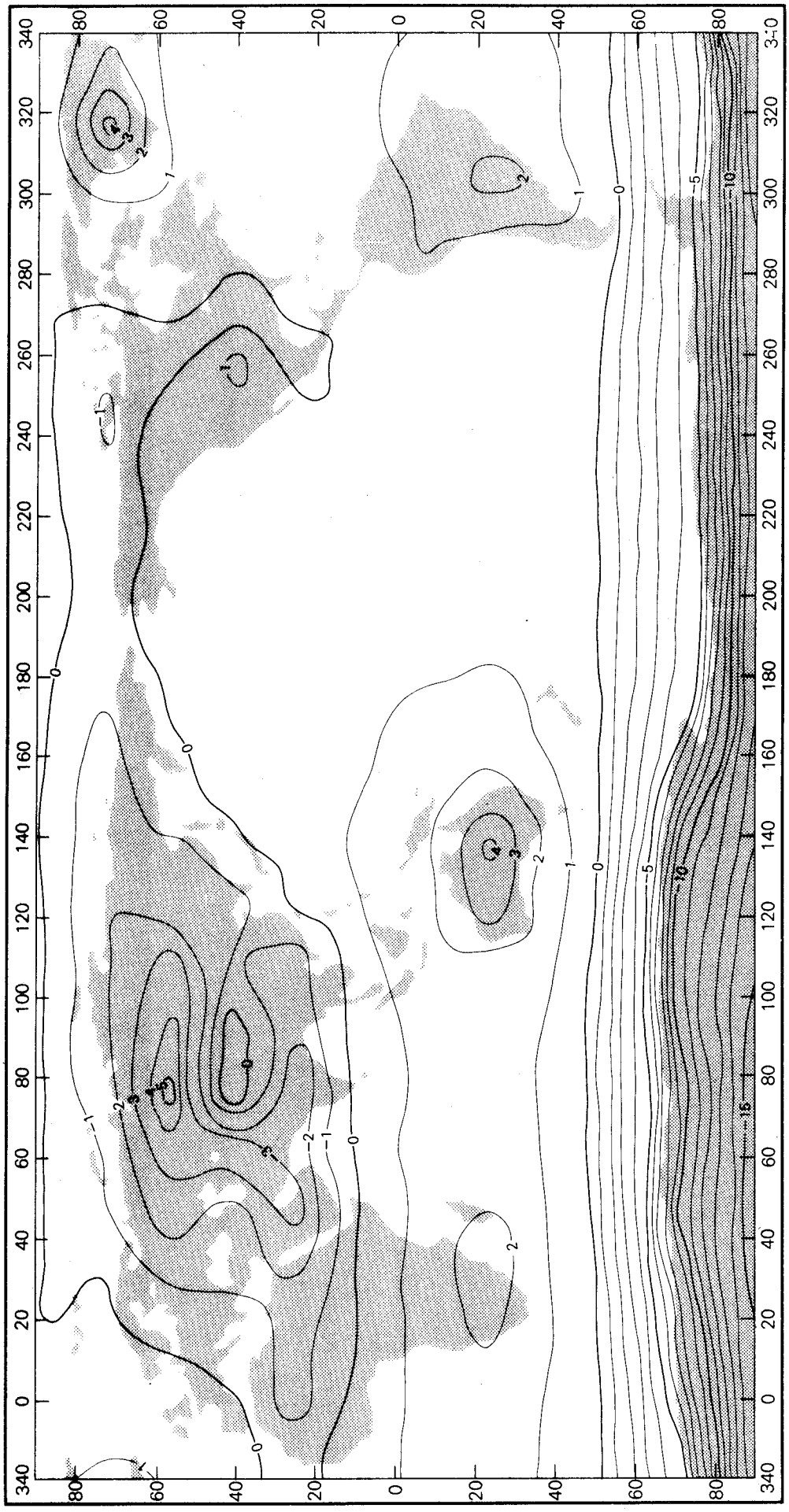

Figure 7.1 Departures in Radial Position due to Atmospheric Loading, in millimetres, for January
(taken from Stolz and Larden 1979)

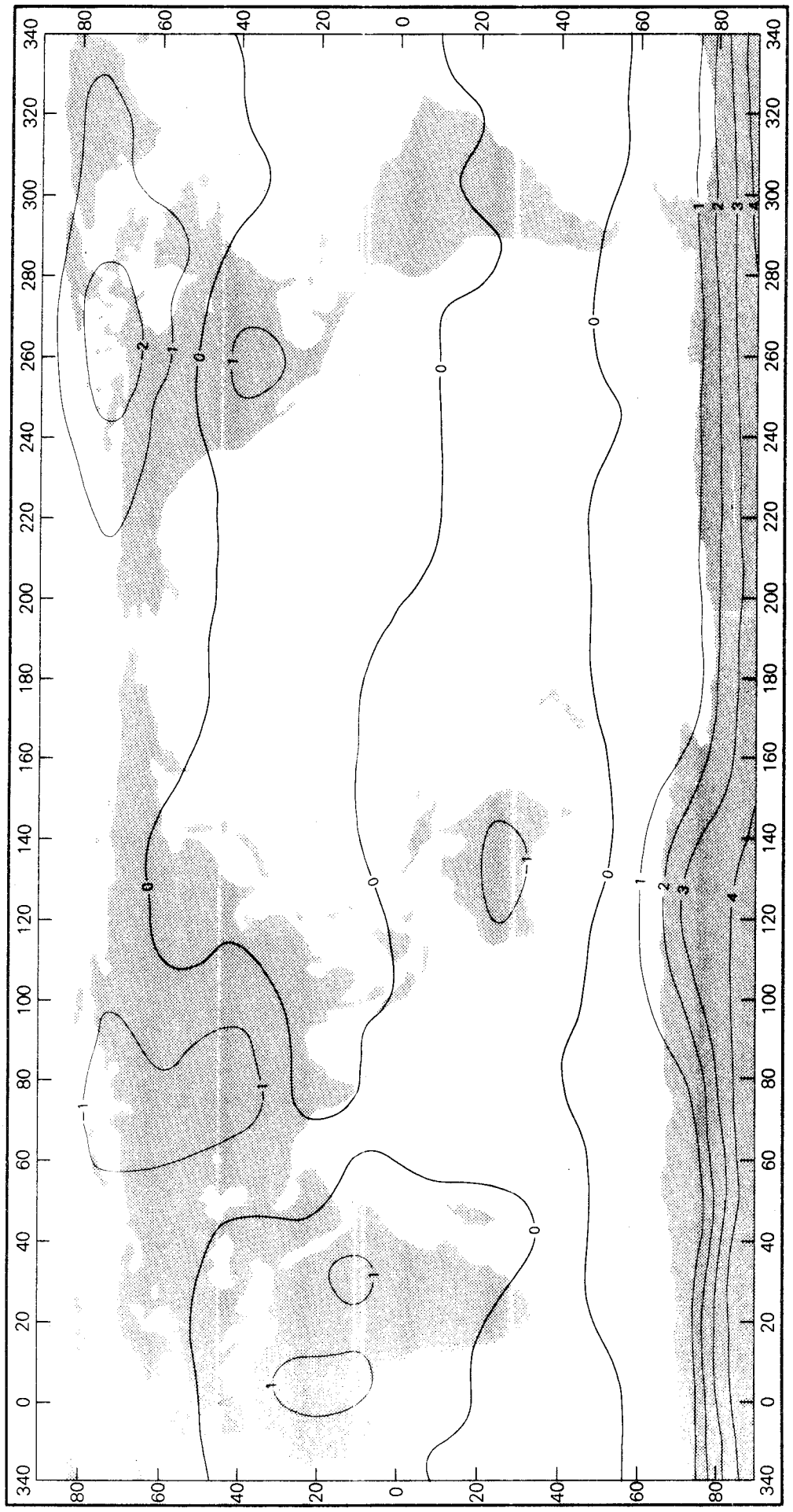

Figure 7.2 Same as Figure 7.1, for April

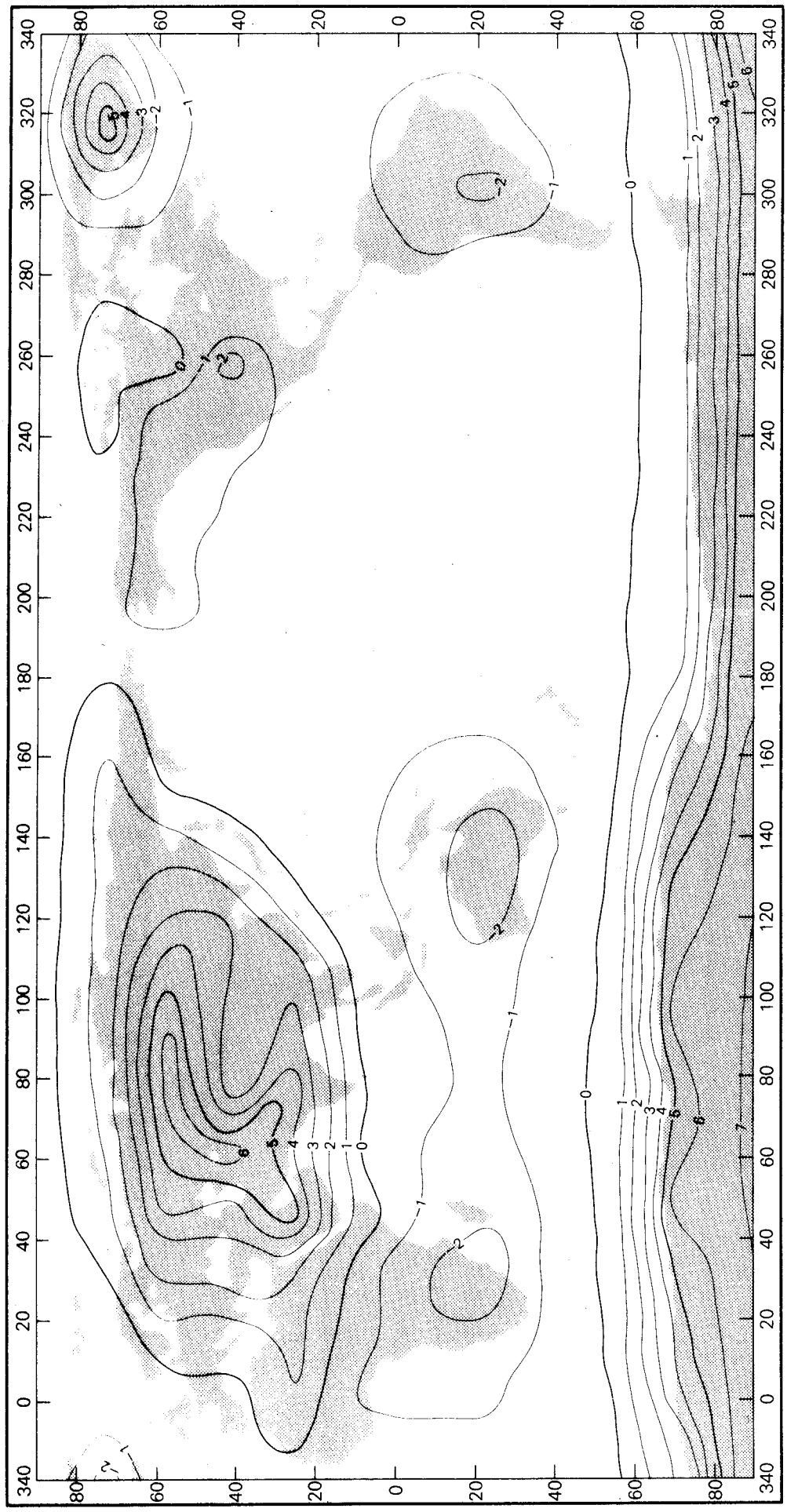

Figure 7.3 Same as Figure 7.1, for July

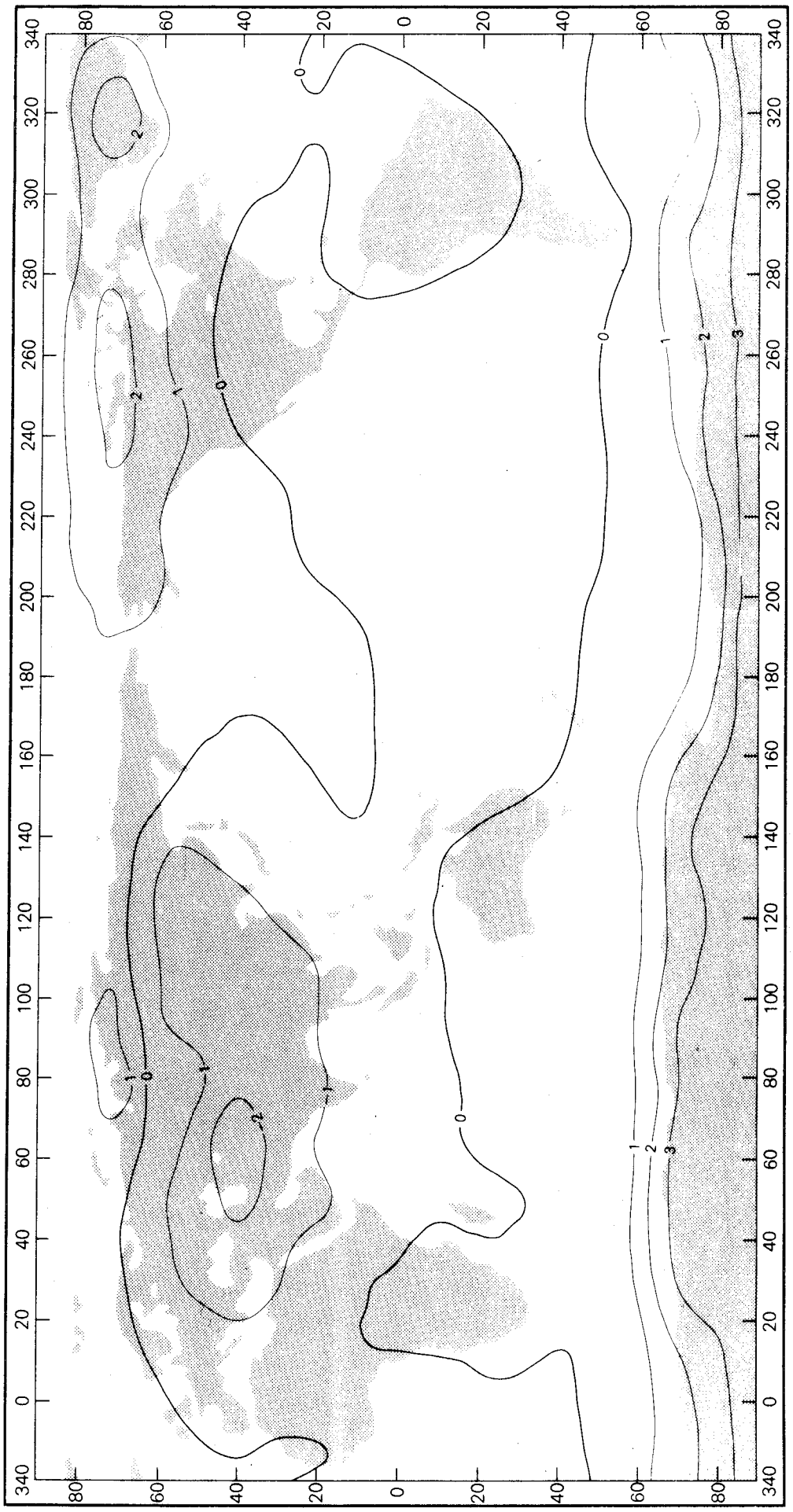

Figure 7.4 Same as Figure 7.1, for October

using the data from Siderenkov and Stekhnovskiy (1971). An alternate method of evaluating $q_0(t)$ is given in section 7.4.2, however, the difference in results is insignificant.

Lines of equal deformation in Figures 7.1, 7.2, 7.3 and 7.4 were drawn using computed values of d_r at grid points spaced every 16° in latitude and 15° in longitude. Values of d_r were computed with the complete (n=36) load Love number dataset of Dahlen (1976), however, the spacing used to prepare the global maps was chosen because the harmonics of the atmospheric pressure field up to an including degree 12 contribute nearly all the power in the seasonal radial deformations (see Figure 7.5). Note, a negative contour interval represents a depression of the earth's surface from an annual average position whereas a positive value indicates a relaxation or lengthening of the geocentric station vector.

The most striking aspects of these maps are the dominant cells located over Australia, Greenland, Antartica and near Central Russia in January, the absence of any significant departures in radial position for April, the reappearance of dominant cells over Central Asia, Greenland and Antartica in July, and the disappearance, once again, of major departures during October. In general, the peak-to-peak annual variations in radial position over parts of Asia, Europe and Greenland approach 1 cm and are larger by a factor of 2 in Antartica. Over the Australian and American continents, the peak-to-peak amplitudes are only of the order 0.5 cm.

These general trends correlate well with the seasonal pattern of pressure systems. For example, the 5 mm depression over Central Russia in January (see Figure 7.1) is caused by the high pressures which prevail over the Eurasian continent during winter. The shift in air-mass associated with this broad high pressure cell also contributes significantly to the observed annual term in polar motion (see Munk and MacDonald 1960, Lambeck 1980). In the northwestern hemisphere, the Icelandic low pressure system dominates during winter and is responsible for the 4 mm departure in radial position over parts of Greenland. The maximum seasonal departure occurs in Antartica where there is a 1.5 cm

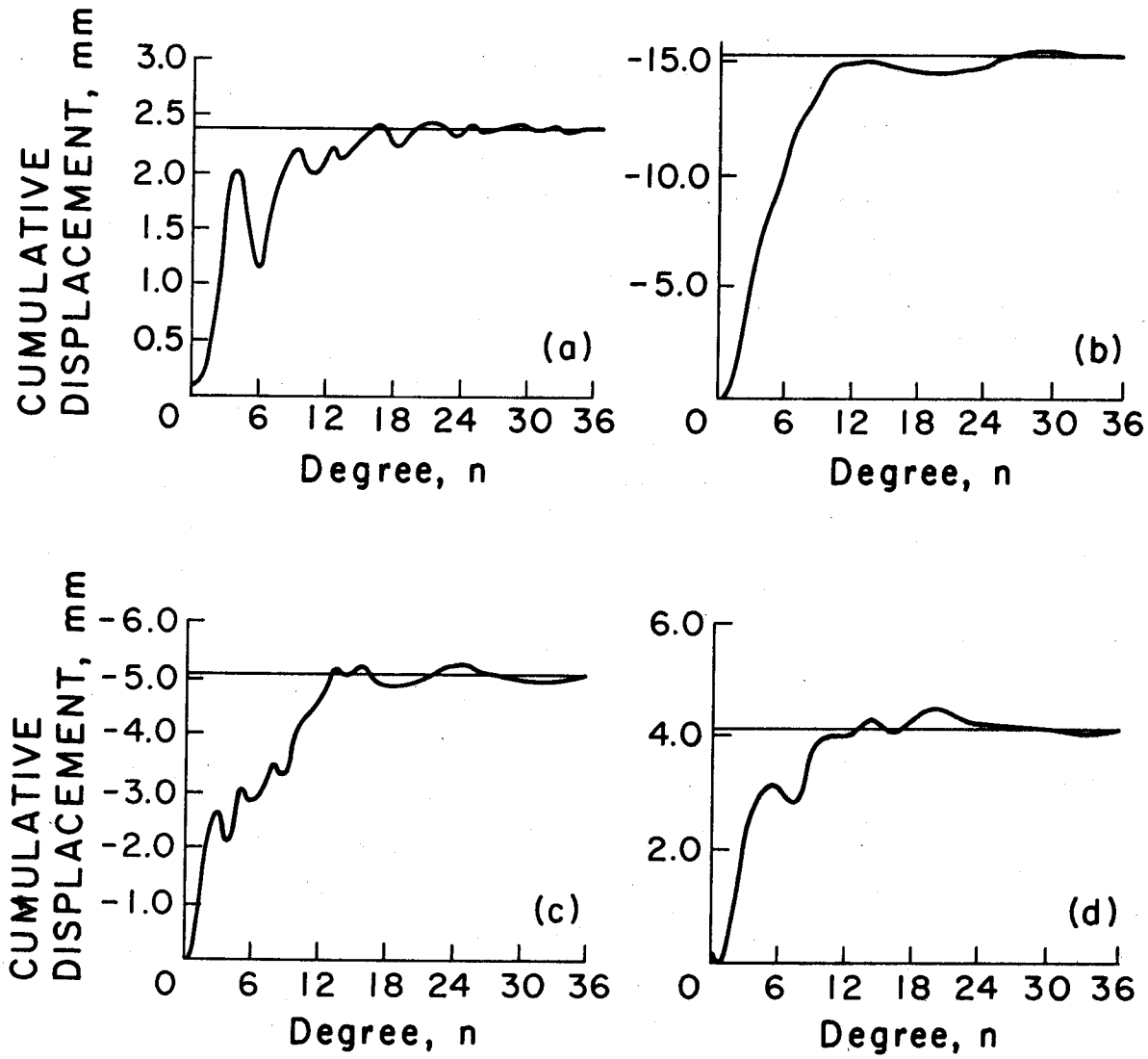

Figure 7.5 Cumulative Degree Contribution to Radial Displacement Due to Atmospheric Loading for January Departures at Selected Global Locations (a) South America, (b) Antartica, (c) Eurasia, (d) Australia

depression caused by the summer high pressures which, in some local areas, deviate up to 25 mb from the mean annual value. By July, the atmospheric loading process has reversed and corresponding departures are opposite in sign. During the months of April and October the seasonal departures in radial position due to atmospheric loading are of the order 2 mm for most parts of the globe. However, this is not necessarily true for groundwater loading as is discussed in the next section.

7.4.1.2. Deformation due to Groundwater Loading

Seasonal departures in radial position from an annual average position due to groundwater loading are shown in Figures 7.6, 7.7, 7.8 and 7.9. The global maps were prepared from values of d_r calculated on a 10° × 10° grid. Because the groundwater data are spaced on a similar grid network, only load Love numbers up to and including degree 18 were used to calculate d_r. Calculating the contribution of the higher harmonics through degree 36 requires data on, at least, a 5° × 5° grid. However, the experience gained from the atmospheric calculations indicates that higher degree terms make only minor contributions to the total deformation.

The most obvious difference between Figures 7.6 to 7.9 and their atmospheric counterparts is the phase shift between the maximum and minimum departures. Maximum groundwater storage usually occurs in late winter and the middle of spring whereas the minimum storage occurs during the late summer and early fall. In temperate climates, the evapotranspiration mechanism hardly operates during the periods of cold weather while precipitation and snowfalls continue. During the summer the reverse applies; the snow melts and runs off, soil moisture evaporates, plants transpire and rainfall activity reduces. Of course, the exception to this trend occurs in the monsoon areas of the tropics where in India, for example, the wet and dry seasons coincide with summer and winter, respectively. Atmospheric effects are generally more predictable and are most pronounced during summer and winter.

In general, the maximum peak-to-peak annual variations in radial position due to groundwater loading occur over parts of South-East Asia,

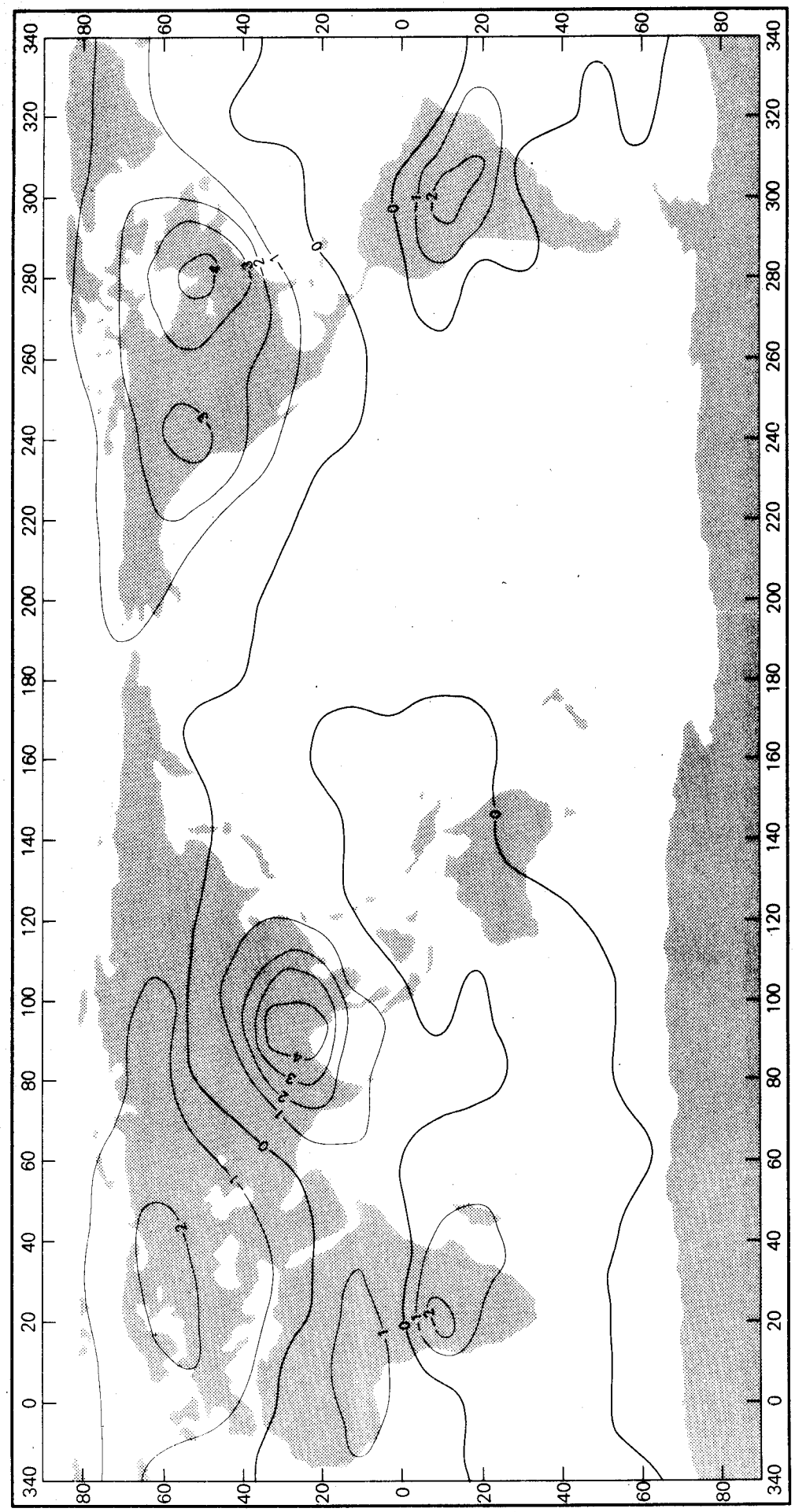

Figure 7.6 Departures in Radial Position Due to Groundwater Loading, in millimetres, for January

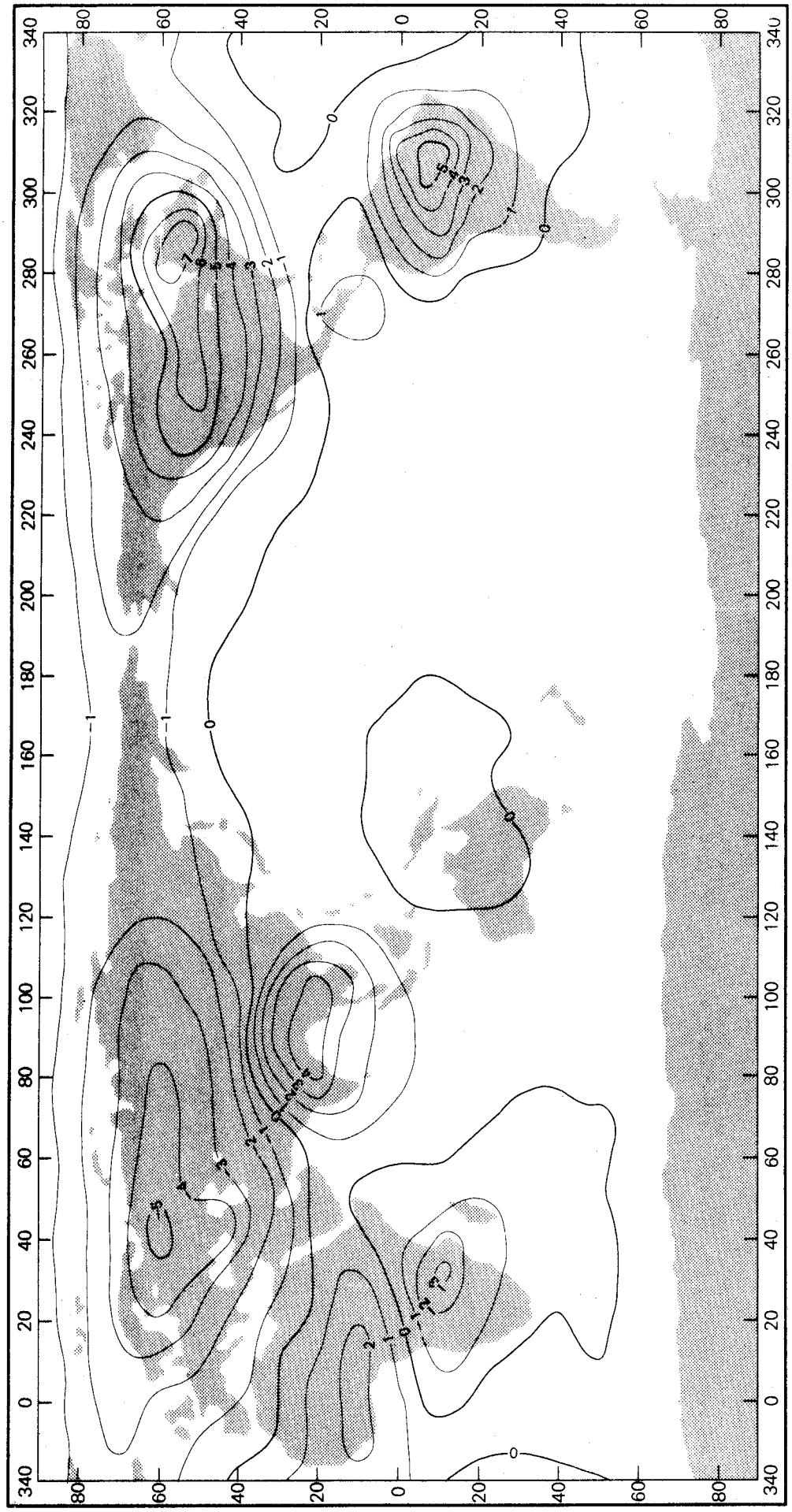

Figure 7.7 Same as Figure 7.6, for April

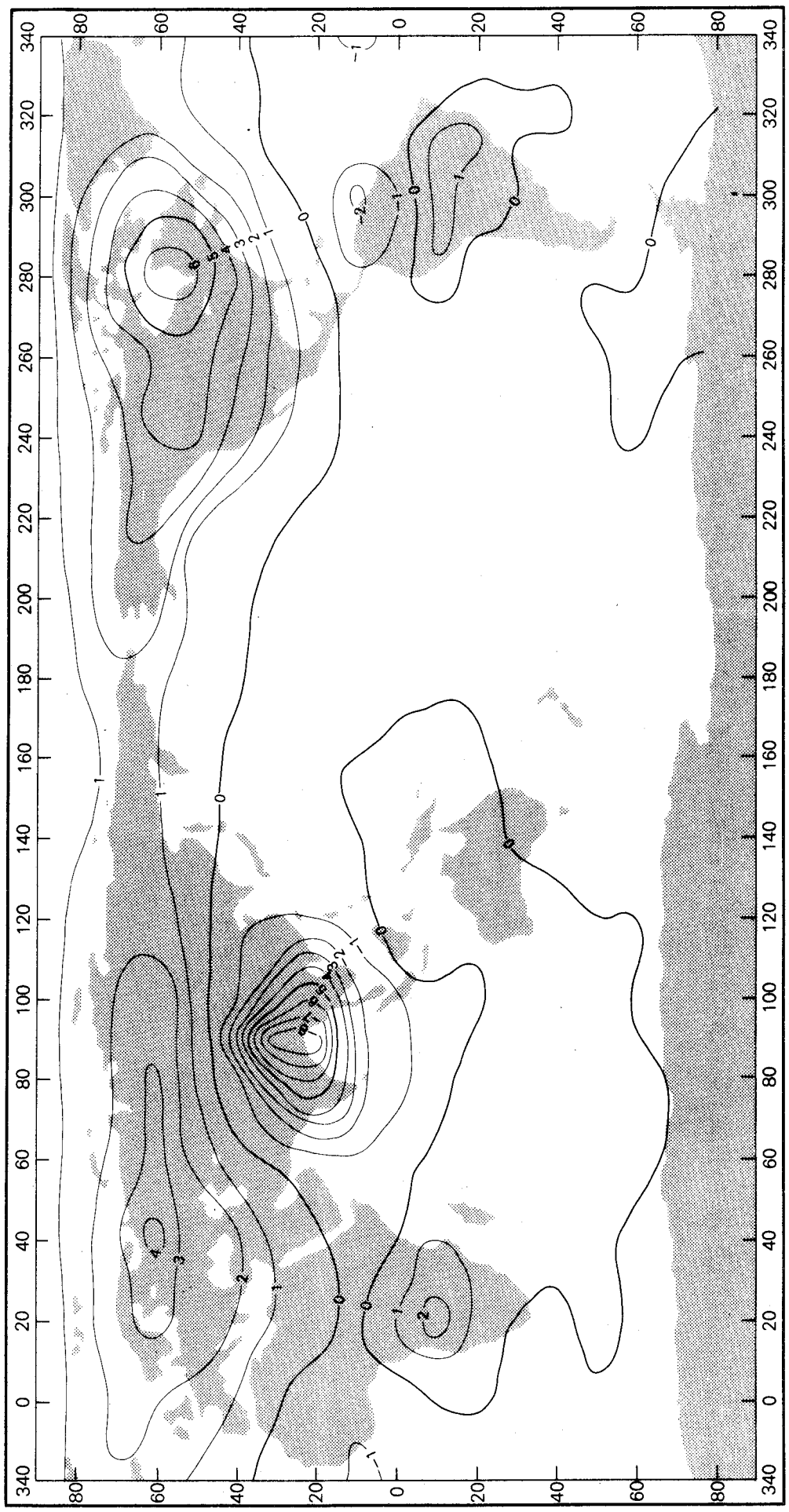

Figure 7.8 Same as Figure 7.6, for July

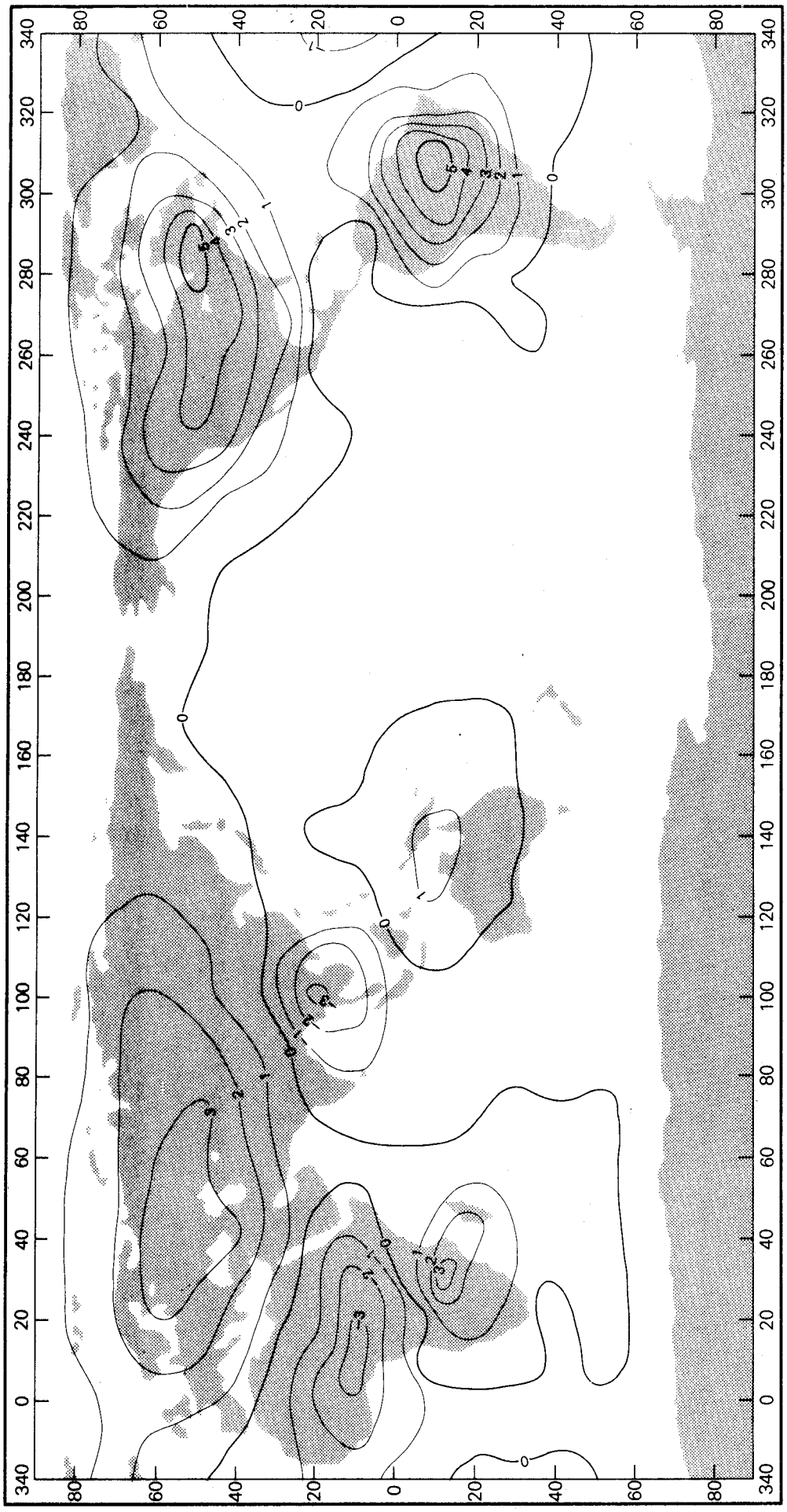

Figure 7.9 Same as Figure 7.6, for October

Table 7.2. Global Trends for Combined Seasonal Atmospheric-Groundwater Loading Effects on Radial Position

Country/ Continent	Annual Radial Deformation	
	Amplitude, mm	Phase, deg
Europe	9	211
Asia	5.5	60
North America	7	255
Greenland	4.5	334
South America	5	291
Australia	3	6
South Africa	3	285
North Africa	3	96
Antartica*	11	192

*Results are for atmospheric loading only since groundwater data were not available.

Canada, Europe and South America and are of the order 1 to 1.5 cm. In Africa and the United States the peak-to-peak variations are less by about a factor of two while in Australia they are virtually negligible.

It is clear from the above results and those presented in section 7.4.1.1 that when the radial surface deformations caused by the seasonal departures in atmospheric pressure and groundwater storage are combined algebraically, the results become marginally significant at the expected 1 to 3 cm accuracy level for new geodetic measuring techniques. The likelihood and influence of errors in the geophysical data and year-to-year fluctuations in the annual components of atmospheric pressure and groundwater, therefore, must be considered (see discussion in section 7.5).

The major global trends are summarized in Table 7.2. The results are given for regions within each country or continent where the deformations are largest and are expressed in functional form using the relation

$$d_r = A \cos(\Theta - \beta) \qquad (7.24)$$

where A and β are the amplitude and phase of the annual radial deformation, respectively. Peak-to-peak variations (2A) exceed 1 cm in Asia, North America and South America, and approach 2 cm in Europe and Antartica. Appropriate corrections may need to be made, particularly if a Transportable Laser Ranging Station (TLRS) visits a site in a region of maximum deformation. Most dedicated geodetic observatories are not located in such regions and so the loading effects are not as significant. These results are summarized in the next section.

7.4.1.3 Deformations at LLR, SLR and VLBI Stations

Two recent studies by Stolz and Larden (1980) and Larden (1980) addressed the question of whether variations in radial position due to seasonal atmospheric-groundwater loading were significant at VLBI sites and over the North American continent. The results of these studies form the basis of a more comprehensive summary presented here that

incorporates SLR and LLR stations as well. Table 7.3 lists the annual radial deformations at a selection of sites that either are actively involved in or might be of interest for LLR, SLR and VLBI experiments. Results for Dodaira (SLR/LLR), Japan; Haleakala (SLR/LLR), Hawaii; Papeete (SLR), Tahiti and Madrid (VLBI), Spain have not been listed because the amplitudes are negligible. Stations in close proximity to those listed have also been omitted to avoid duplication of results.

The most significant variation in radial position occurs at Novosibirsk, USSR where the peak-to-peak amplitude is 1.4 cm. Annual variations of about 1 cm peak-to-peak amplitude are also evident at Duluth, Minnesota; McMurdo Sd, Antartica; Greenbelt, Maryland; Westford, Massachusetts and Brazil, South America. The peak-to-peak amplitudes at LLR sites are of the order 5 mm or less and are not considered significant.

Many of the stations listed in Table 7.3 will form the terminals of geodetic baselines whose lengths will be monitored as part of the global plate tectonics program (National Academy of Sciences, 1978). It is, therefore, worthwhile to investigate whether the radial deformations, d_r^A and d_r^B, at two sites A and B might compound to produce larger motions of the baseline AB. If A and B are located on the surface of a sphere then the change Δb_{AB} in baseline length due to the motions d_r^A and d_r^B follows as

$$\Delta b_{AB} = (d_r^A + d_r^B)\{(1 - \cos \psi_{AB})/2\}^{1/2} \qquad (7.25)$$

where

$$\cos \psi_{AB} = \cos \phi_A \cos \phi_B \cos(\lambda_A - \lambda_B) + \sin \phi_A \sin \phi_B \quad , \qquad (7.26)$$

is the cosine of the angle ψ_{AB} subtended at the geocentre by the geocentric station vectors A and B.

Table 7.4 lists the annual variation in length for a selection of possible SLR baselines whose peak-to-peak amplitudes exceed 1 cm. The results were obtained by a direct evaluation of equation (7.25) using the information given in Table 7.3. The peak-to-peak annual

Table 7.3. Annual Radial Deformations at LLR, SLR and VLBI Sites Due to Seasonal Atmospheric-Groundwater Loading

Station Location	Latitude deg	Longitude deg	Amplitude mm	Phase deg	Station Designation
Arequipa, Peru	-16	289	1	298	SLR
ESO, Chile	-29	289	1.5	310	SLR
Nairobi, Kenya	-1	37	1	355	SLR
Grasse, France	44	7	2	232	SLR,LLR
Wettzel, Germany	49	13	3	234	SLR,LLR
Bangalore, India	13	78	2.5	59	SLR
Novosibirsk, U.S.S.R.	55	83	7	223	SLR
Kootwijk, Netherlands	52	6	3	239	SLR,VLBI
Duluth, MN; USA	47	268	6.5	244	SLR
McMurdo Sd, Antartica	-78	167	6	196	SLR
Athens, Greece	38	24	3	212	SLR
Bonn, Germany	51	7	3	236	VLBI
Greenbelt, MD; USA	39	283	4.5	243	SLR
Geraldton, Australia	-29	115	2	0	SLR
Canberra, Australia	-36	149	2	5	SLR,VLBI,LLR
Fort Davis, TX; USA	31	256	2	248	SLR,VLBI,LLR
Westford, MA: USA	43	289	5	251	VLBI
Owens Valley, CA; USA	37	242	2	265	VLBI
Onsala, Sweden	57	12	3.5	240	VLBI
Brazil, S. America	-15	310	4.5	284	VLBI

Table 7.4. Annual Baseline Variations

Baseline	Amplitude mm	Phase deg
Novosibirsk - McMurdo	12	211
Minnesota - McMurdo	10.5	221
Minnesota - Novosibirsk	8.5	233
Minnesota - Geraldton	5.5	262

variation of baselines formed by LLR stations is below 1 cm. Similar conclusions have also been reached for VLBI baselines (Stolz and Larden 1980).

7.4.2. Geocentre Motion

Up to this point, the discussion has concentrated on the deformations of the earth relative to the displaced position of the whole earth in inertial space. In other words, no attempt has been made to compute the annual oscillation of the whole earth produced by the first degree (P_1) component of the combined seasonal departures in atmospheric-groundwater load. It will be shown that the above-mentioned shift corresponds to one of the solid earth, including the geocentre, in inertial space and that the magnitude of the shift will be the same irrespective of whether the earth is treated as a rigid or elastic body. The mathematical formulation presented here follows essentially that of Stolz (1976a) and begins by assuming that the solid parts of the earth are rigid.

For a redistribution of matter loading the earth's surface, the changes $\Delta x_i(t) = [x_i(t_o) - x_i(t)]$ in the coordinates of the geocentre with time are (Stolz 1976a)

$$\Delta x_1(t) = \frac{a^3}{M} \int_S q(\phi,\lambda;t)\cos\phi\cos\lambda \, dS$$

$$\Delta x_2(t) = \frac{a^3}{M} \int_S q(\phi,\lambda;t)\cos\phi\sin\lambda \, dS$$

$$\Delta x_3(t) = \frac{a^3}{M} \int_S q(\phi,\lambda;t)\sin\phi \, dS \qquad (7.27)$$

where ϕ and λ are the latitude and longitude of the seasonal load departures, M is the mass of the earth, S is the surface of the earth, and a, $q(\phi,\lambda;t)$ and dS have been defined previously. As was the case for the deformation calculations, the effect of the seasonal redistribution of the atmospheric and groundwater loads on $\Delta x_1(t)$, $\Delta x_2(t)$ and $\Delta x_3(t)$ will be discussed separately and then combined algebraically.

Since Jeffrey's work in 1916, it has been customary to treat the effects of the atmosphere and the ocean response to pressure changes together. For studies involving seasonal variations, the usual approach is to assume the oceans respond to atmospheric pressure changes like an inverted barometer (see e.g. Lambeck 1980). The increase in the atmospheric pressure, over and above the mean pressure over the total ocean surface, depresses the local ocean surface by about 1 cm for every millibar of pressure. As the sea surface responds, a flow pattern is set up between the various oceans of the world so as to annul the horizontal pressure gradients on the sea floor.

Since the inverted barometer rule implies that the seasonal departures of the total load on the sea floor are constant at any instant, but vary with time according to the variable fraction of the atmosphere that lies above the oceans, one can express equations (7.27) as (Munk and MacDonald 1960, p. 109)

$$\Delta x_1(t) = \frac{a^3}{M}\left[\int_{\text{Land}} q(\phi,\lambda;t)\cos\phi\cos\lambda dS + q_0(t)\int_{\text{Oceans}} \cos\phi\cos\lambda dS\right]$$

$$\Delta x_2(t) = \frac{a^3}{M}\left[\int_{\text{Land}} q(\phi,\lambda;t)\cos\phi\sin\lambda dS + q_0(t)\int_{\text{Oceans}} \cos\phi\sin\lambda dS\right]$$

$$\Delta x_3(t) = \frac{a^3}{M}\left[\int_{\text{Land}} q(\phi,\lambda;t)\sin\phi dS + q_0(t)\int_{\text{Oceans}} \sin\phi dS\right] \qquad (7.28)$$

where $q_0(t)$ is the mean value of $q(\phi,\lambda;t)$ over the ocean areas [see equation (7.21) for the evaluation of $q_0(t)$]. It should be emphasized that oceanic mass must be conserved for these equations to be valid. Using the fact that

$$\int_S \cos\phi\cos\lambda dS = \int_{\text{Land}} \cos\phi\cos\lambda dS + \int_{\text{Oceans}} \cos\phi\cos\lambda dS = 0 \quad ,$$

$$\int_S \cos\phi\sin\lambda dS = \int_{\text{Land}} \cos\phi\sin\lambda dS + \int_{\text{Oceans}} \cos\phi\sin\lambda dS = 0$$

and

$$\int_S \sin\phi dS = \int_{Land} \sin\phi dS + \int_{Ocean} \sin\phi dS = 0$$

one can express equations (7.28) as

$$\Delta x_1(t) = \frac{a^3}{M} \int_{Land} \{q(\phi,\lambda;t) - q_0(t)\} \cos\phi\cos\lambda dS$$

$$\Delta x_2(t) = \frac{a^3}{M} \int_{Land} \{q(\phi,\lambda;t) - q_0(t)\} \cos\phi\sin\lambda dS$$

$$\Delta x_3(t) = \frac{a^3}{M} \int_{Land} \{q(\phi,\lambda;t) - q_0(t)\} \sin\phi dS \quad . \tag{7.29}$$

In section 7.4.1.1, $q_0(t)$ was evaluated using the oceanic pressure data of Schutz and Gates (1971, 1972, 1973, 1974). However, since pressure data are more plentiful over continents, and the seasonal variation in mean atmospheric load $q_E^A(t)$ can be calculated from seasonal compilations of atmospheric water vapour one can alternatively deduce $q_0(t)$ from the relation (Munk and MacDonald 1960)

$$q_0(t) = \frac{1}{a_0^0} q_E^A(t) - \frac{(1-a_0^0)}{a_0^0} q_L(t) \tag{7.30}$$

where $q_L(t)$ is the mean value of $q(\phi,\lambda;t)$ over land and all other quantities have been previously defined. The validity of equation (7.30) rests on the assumption that mass and the amount of dry air in the atmosphere are conserved. From a monthly compilation of precipitable atmospheric water vapour by Tuller (1968), Stolz and Larden (1979) find [see also equation (7.10)]

$$q_E^A(t) = \frac{1}{4\pi}\int_S q(\phi,\lambda;t)dS$$

$$= \frac{1}{4\pi}\int_S \left[-\frac{1}{2}\,m\,\sin(\Theta-\alpha) + \frac{1}{2}\,m'\,\cos(\Theta-\alpha)\right]dS$$

$$= -0.11\,\cos\Theta - 0.06\,\sin\Theta \text{ g cm}^{-2} \qquad (7.31)$$

where m and m' are the January minus July and April minus October load differences, respectively. Data spaced on a grid 10° in latitude and 15° in longitude were used to evaluate the integral in equation (7.31) and a conversion factor of 1 inch of water = 2.54 g cm^{-2} was used to convert Tuller's values of precipitable water, in inches, to the load equivalent of g cm^{-2}. Munk and MacDonald's (1960) comparable estimate for $q_E^A(t)$ using the data of Bannon and Steele (1957), which are only available between latitudes 70°N and 52°S, is

$$q_E^A(t) = -0.17\,\cos\Theta - 0.08\,\sin\Theta \text{ g cm}^{-2} \quad . \qquad (7.32)$$

The annual variation $q_L(t)$ in mean atmospheric load over land is given, in analogy to equation (7.21), by

$$q_L(t) = \frac{1}{4\pi(1-a_0^0)}\int_{\text{Land}}\left[-\frac{1}{2}\,m\,\sin(\Theta-\alpha) + \frac{1}{2}\,m'\,\cos(\Theta-\alpha)\right]dS \qquad (7.33)$$

where this time m and m' are the January minus July and April minus October load differences computed from the pressure data of Schutz and Gates (1971, 1972, 1973, 1974) over land after their adjustment back to station elevation using equation (7.15). With these data and procedures, Stolz and Larden (1979) find

$$q_L(t) = 1.30\,\cos\Theta + 0.31\,\sin\Theta \text{ g cm}^{-2} \quad . \qquad (7.34)$$

Substituting equations (7.31) and (7.34) into equation (7.30) gives

$$q_0(t) = -0.73\,\cos\Theta - 0.22\,\sin\Theta \text{ g cm}^{-2} \quad . \qquad (7.35)$$

Stolz and Larden (1979) also calculate $q_0(t)$ by the above method using a value for $q_E^A(t)$ based on seasonal averages of precipitable water vapour rather than mid-season values as are used in equation (7.31). This procedure gives

$$q_0(t) = -0.75 \cos\Theta - 0.20 \sin\Theta \text{ g cm}^{-2} \quad . \tag{7.36}$$

Clearly, the difference between the results from equations (7.35) and (7.36) and the result from equation (7.21) using oceanic pressure data alone is hardly significant. In making a choice for the evaluation of equations (7.29), the value of $q_0(t)$ deduced from oceanic pressures is judged to be superior since the stations used to produce these data are more abundant and their geographic distribution is more representative than the stations used to produce Tuller's (1968) maps. Substituting (Jeffreys 1916)

$$q(\phi,\lambda;t) = -\frac{1}{2} m \sin(\Theta-\alpha) + \frac{1}{2} m' \cos(\Theta-\alpha)$$

and equation (7.22) into the integrals of equation (7.29) and expanding terms for $\alpha = 104°.2$ gives

$$\Delta x_1(\Theta) = \frac{a^3}{M} \int_{\text{Land}} q(\Theta) \cos\phi\cos\lambda dS$$

$$\Delta x_2(\Theta) = \frac{a^3}{M} \int_{\text{Land}} q(\Theta) \cos\phi\sin\lambda dS$$

$$\Delta x_3(\Theta) = \frac{a^3}{M} \int_{\text{Land}} q(\Theta) \sin\phi dS \tag{7.37}$$

where

$$q(\Theta) = (0.12\ m + 0.48\ m' + 0.19) \sin\Theta$$
$$+ (0.48\ m - 0.12\ m' + 0.73) \cos\Theta \quad .$$

The evaluation of $q(\Theta)$ is equivalent to the procedure adopted by Rosenhead (1929) in his study of the annual component for polar motion where atmospheric load values are amended to allow for the response of the oceans.

Equations (7.37) are based on formulae for the centre of mass of continuous matter occupying a closed region of inertial space. This region is taken to be bounded by the surface of the earth and the atmosphere is considered as a load exterior to this surface. The loads $q(\Theta)$ may thus be thought of as a series of point masses acting radially on this surface. The terms $q(\Theta)\cos\phi\cos\lambda$, $q(\Theta)\cos\phi\sin\lambda$ and $q(\Theta)\sin\phi$ are then the Cartesian components of $q(\Theta)$ and integration over the earth's surface is equivalent to compounding the loads at the geocentre. Accordingly, for the total system (solid earth plus load) to remain in equilibrium, the quantities $\Delta x_1(\Theta)$, $\Delta x_2(\Theta)$ and $\Delta x_3(\Theta)$ must represent the Cartesian components of an oscillation of the solid earth in space with respect to the centre of mass of the system. Evaluation of equation (7.37) for the motion of the geocentre due to atmospheric loading using the appropriate adjusted data of Schutz and Gates gives (Stolz and Larden 1979)

$$\Delta x_1(\Theta) = 0.6\cos\Theta - 0.1\sin\Theta$$

$$\Delta x_2(\Theta) = 1.5\cos\Theta + 0.1\sin\Theta$$

$$\Delta x_3(\Theta) = -0.1\cos\Theta - 0.2\sin\Theta \qquad (7.38)$$

where the units are millimetres and, the values 6.371×10^9 mm and 5.977×10^{27} g are used for the earth's radius and mass, respectively.

A comparison of the above result with the previous estimate by Stolz (1976a) based on Rosenhead's (1929) data indicates that the Δx_3 motion is smaller. However, this can be attributed to the influence of the additional data in the polar regions that were not listed in Rosenhead's earlier compilation. For reasons given in the next section, no attempt has been made to recompute the earlier estimate by Stolz (1976a) for the seasonal motion of the geocentre due to groundwater loading. Using the groundwater data of Van Hylckama (1956), Stolz (1976a) obtains

$$\Delta x_1'(\Theta) = 0.1\cos\Theta + 0.8\sin\Theta \text{ mm}$$

$$\Delta x_2'(\Theta) = -0.6 \cos\Theta - 1.2 \sin\Theta \text{ mm}$$

$$\Delta x_3'(\Theta) = 1.0 \cos\Theta + 2.8 \sin\Theta \text{ mm} \quad . \qquad (7.39)$$

Addition of equations (7.38) and (7.39) gives the combined annual variation in the motion of the geocentre due to seasonal atmospheric-groundwater loading expressed in Cartesian form as

$$\Delta x_1 = 0.7 \cos\Theta + 0.7 \sin\Theta \text{ mm}$$

$$\Delta x_2 = 0.9 \cos\Theta + 1.1 \sin\Theta \text{ mm}$$

$$\Delta x_3 = 0.9 \cos\Theta + 2.6 \sin\Theta \text{ mm} \qquad (7.40)$$

where Δx_1, Δx_2 and Δx_3 are the changes in the components of the geocentre with respect to the centre of mass of the earth plus the atmospheric-groundwater load. The motion is an elliptical oscillation with the major and minor axes being 5.8 and 1.4 mm, respectively. The magnitude is very small indeed and well below the detection level of future dynamic satellite and also gravimetric measuring techniques.

7.5. Discussion of the Results

During the execution of the calculations just described in the previous sections, several assumptions were invoked that deserve some justification. In this section, a discussion on the impact of these assumptions is given together with some concluding remarks concerning the geodetic significance of the results.

7.5.1 Basic Assumptions and Result Accuracy

1. No attempt has been made to evaluate the small corrections to the atmospheric results arising from the changes in sea-level caused by the deformation of the crust beneath the oceans and by the mutual attraction between the oceans and atmosphere. Another minor defect is that by accepting the inverted barometer rule, the sea surface does not end up being an equipotential surface. A systematic development to the problem was considered by Munk and MacDonald (1960) and the

general theory which permits the static equilibrium response of the oceans to be determined rather than presumed has been developed by Dahlen (1976) and Farrell and Clark (1976). While this theory incorporates the gravitational self attraction of the oceans and the elastic-gravitational response of the earth model to both the applied potential and the equilibrium oceanic tidal load, its application to the atmospheric loading problem requires a complete coverage of actual pressure data over the oceans. The oceanic data of Schutz and Gates (1971, 1972, 1973, 1974) hardly qualify since they were compiled from a mere sprinkling of coastal and island stations around the globe. Since the results obtained here are already small, it is unlikely that a more rigorous approach using other atmospheric pressure datasets will achieve much.

2. The premise that oceanic mass is conserved, which is implicit in the inverted barometer rule, is not strictly valid and thus requires further investigation. A complication arises due to the fact that there is a seasonal net transfer of water between the earth, atmosphere and oceans. From equation (7.14), the total seasonal change in atmospheric moisture and groundwater is

$$q_E^{AG}(t) = -0.09 \cos\Theta + 0.54 \sin\Theta \text{ g cm}^{-2} \quad ,$$

which must be redistributed over the oceans. Thus sea level will be uniformly modified by $-q_E^{AG}(t)/a_0^0$, or

$$\xi = 0.13 \cos\Theta - 0.77 \sin\Theta \text{ cm} \quad .$$

This corresponds to a uniform tide of about 8 mm in amplitude and an additional load $q_0'(t)$ on the ocean floor of about 0.8 g cm^{-2}. It is because this effect is small that no attempt is made to ensure that sea level remains an equipotential surface (Lambeck 1980).

From equations (7.19) and (7.28), the changes in the computed deformations and displacement of the earth due to the additional load can be written as

$$\delta d_r = \frac{Ga}{g} \sum_n h'_n \int_S q'_0(t) P_n(\cos\psi) dS$$

and

$$\delta\{\Delta x_1(t)\} = \frac{a^3}{M} q'_0(t) \int_{\text{Oceans}} \cos\phi\cos\lambda \, dS$$

$$\delta\{\Delta x_2(t)\} = \frac{a^3}{M} q'_0(t) \int_{\text{Oceans}} \cos\phi\sin\lambda \, dS$$

$$\delta\{\Delta x_3(t)\} = \frac{a^3}{M} q'_0(t) \int_{\text{Oceans}} \sin\phi \, dS \quad ,$$

respectively. Substituting $q'_0(t) < 0.8$ g cm^{-2} into these equations gives δd_r, and

$$\delta s = \left[\delta\{\Delta x_1(t)\}^2 + \delta\{\Delta x_2(t)\}^2 + \delta\{\Delta x_3(t)\}^2\right]^{1/2}$$

less than 0.4 mm. The effect is clearly insignificant for these calculations.

3. In the expression for the load deformation potential [equation (7.18)], the angle ψ should be assigned all values in the range 0° to 180° when calculating the nth degree surface spherical harmonic representation of the load at the point of computation. This tends to make the calculations rather time-consuming and costly and so in order to improve the efficiency in computation time and at the same time achieve a reasonable trade-off between cost and accuracy, several tests were conducted to see whether data beyond a certain value of ψ could be truncated from the solution without seriously affecting the results. Test points on each continent were chosen in areas where maximum deformation occurred. Areas beyond ψ = 30, 60, 90, 120, and 150, respectively were assumed to have zero contribution to the solution and the approximate result for d_r was compared with the

result from the full global calculation. The optimum angle for ψ that produced acceptable truncation errors was 90°. Table 7.5 shows that by excluding data beyond $\psi = 90°$ the results will not be in error by more than 0.2 mm. More detailed results on the effect of truncating the atmospheric load are given by Stolz and Larden (1979).

4. It was shown in section 7.4.2 that the shift of the geocentre in space due to seasonal atmospheric-groundwater loading did not exceed 6 mm. To obtain this result, the earth was assumed to respond to the redistributed load as if it were a rigid body. In other words, no attempt was made to calculate the additional shift of the geocentre caused by the further redistribution of mass as the earth deforms under the action of a P_1 load. The significance of this omission can be assessed intuitively as follows. It is clear (Cathles 1975) that a load component of form P_1 is characteristic of the transfer of mass from one side of the earth to the other. The effective amount of mass transferred can be estimated using an expression similar in form to equation (7.27), that is,

$$\Delta M = \frac{\Delta S \, M}{S'} \qquad (7.41)$$

where ΔM is the total amount of mass transferred, ΔS is the rigid body value for the peak-to-peak shift of the geocentre in space due to atmospheric-groundwater loading and M is the mass of the earth. S', the average distance over which all the mass is transferred, can be obtained from the expression

$$S' = a \int_0^{\pi/2} \sin^2\phi\cos\phi d\phi = \frac{4a}{3}$$

where a is the earth's radius. Substituting $\Delta S = 5.8$ mm from equation (7.40), $M = 5.98 \times 10^{27}$ g and $S' = 8.49 \times 10^9$ mm into equation (7.41) gives

$$\Delta M = 4.1 \times 10^{18} \text{ g} \quad .$$

What then are the consequences of moving this amount of mass from one side of the earth to the other and allowing the earth to deform?

Table 7.5. Truncation Errors for Atmospheric and Groundwater Calculation with Zero Contribution from Data Beyond $\psi = 90°$.

Continent	Error, mm	
	Atmosphere†	Groundwater*
Europe	0.2	0.1
Asia	0.2	0.1
Antartica	0	No data
North America	0.2	0
South America	0	0.2
Australia	0.2	0.2
Africa	0.2	0.2

†Results obtained from January departures.

*Results obtained from July departures

To approach the problem simply but not affect the conclusions, let's assume the mass is moved from the southern hemisphere to the northern hemisphere and that the pole of maximum deformation coincides with the north pole. Since the redistributed mass must characterize a first degree load to produce a shift in the geocentre, one can write the total amount ΔM of mass transferred to the northern hemisphere as a function of the load q_1 at the pole of maximum deformation as

$$\Delta M = a^2 \int_{\lambda=0}^{2\pi} \int_{\phi=0}^{\pi/2} q_1 \sin\phi\cos\phi d\phi \cdot d\lambda \tag{7.42}$$

Evaluating equation (7.42) gives $q_1 = 3.2$ g cm^{-2}. From equation (7.19), the accompanying radial deformation at the north pole caused by the redistributed mass can be written as

$$d_{r_1} = \frac{Gah_1'}{g} \left[\int_{\lambda=0}^{2\pi} \int_{\phi=\pi/2}^{0} q_1 \sin\phi\cos\phi d\phi \cdot d\lambda + \int_{\lambda=0}^{2\pi} \int_{\phi=0}^{-\pi/2} -q_1 \sin\phi\cos\phi d\phi \cdot d\lambda \right]$$

or after evaluation of the integrals

$$d_{r_1} = - \frac{2\pi Gah_1' q_1}{g} \quad .$$

Making the relevant substitutions gives

$$d_{r_1} = 0.25 \text{ cm}$$

which can be used to estimate the volume ΔV of the depression over the northern hemisphere as

$$\Delta V = a^2 \int_{\lambda=0}^{2\pi} \int_{\phi=\pi/2}^{0} d_{r_1} \sin\phi\cos\phi d\phi \cdot d\lambda = \pi a^2 d_{r_1}$$

$$= 3.2 \times 10^{17} \text{ cm}^3 \quad .$$

If the volume created by the depression is filled with water ($\rho_w = 1$ g cm^{-3}) then the additional redistribution of mass $\Delta M'$

accompanying the deformation is

$$\Delta M' = \rho_w \Delta V$$
$$= 3.2 \times 10^{17} \text{ g} \quad .$$

When the redistribution occurs globally (S' = 4a/3), the correction to the rigid-body value for the peak-to-peak shift of the geocentre in space is

$$\Delta S' = \frac{\Delta M' \, S'}{M} = 0.46\text{mm} \quad .$$

Alternatively, if the volume is filled with water from nearby regions, say S' < 100 km, then the value for $\Delta S'$ will be considerably less. Note, however, that the above process is an iterative one. Substituting $\Delta S' = \Delta S$ back into equation (7.41) for the second iteration gives an iterative correction to $\Delta S'$ of 0.04mm. After the third iteration the correction is 0.003 mm which, for all intents and purposes, is negligible. The maximum additional shift of the geocentre due to seasonal atmospheric-groundwater loading is of the order 0.5 mm, that is, about 8% of the calculated rigid-body value. This conclusion holds true for any location of the pole of maximum deformation. If the redistribution of matter accompanying the deformation occurs locally then this percentage will be at least an order of magnitude smaller. Farrell (1972) makes the assumption in his calculation of the load Love numbers that the centre of mass of the undeformed earth and the centre of mass of the deformed earth coincide in the reference frame which he adopts for the integrations. This gives a zero value for the potential term k_1'.

5. Radial deformation calculations were also carried out using the load Love numbers of Longman (1966) and Farrell (1972). The rms differences between these results and the results presented in figures 7.1 to 7.4 were of the order 0.2 and 0.1mm, respectively,while the maximum differences of 0.9 and 0.3,respectively, occurred near the south pole. Similar tests showed that these statistics are also valid for the groundwater loading effects. The calculations agree because the h_0' and h_1'

coefficients which are omitted from Longman (1966) and Farrell (1972) are about an order of magnitude smaller than the remaining coefficients and, because the harmonics of degree 2 through 12 for which the corresponding coefficients are essentially identical in all three data-sets, contain nearly all the power in the radial deformations (see e.g. figure 7.5).

6. The theoretical results of Slichter and Caputo (1960) mentioned in the introduction to this chapter are in reasonable agreement with those presented here. Any differences that do occur are primarily due to the fact that (1) the mutual attraction of the earth's surface by the load is not taken into account by these authors and (2) the finer features of the atmospheric-groundwater load are difficult to include in their simplified theoretical development.

7. A previous study by Urmantsev (1971) on the seasonal atmospheric loading over a 2000 km leveling traverse in the U.S.S.R. indicated that radial deformations due to air-mass variations alone could be as large as 3.6 cm peak-to-peak. Based on the results presented in figures 7.1 to 7.4, Stolz and Larden (1979) believe this value is too large by about a factor of two and suggest that Urmantsev's choice of sea-level pressures and severe truncation limit of $\psi = 30^{\circ}$ is responsible for the discrepancy. For accurate results, surface pressures must be used together with a more realistic truncation limit. Table 7.5 clearly shows that choosing $\psi = 90^{\circ}$ for the truncation limit is more than satis-factory.

8. The effect of errors in the atmospheric and groundwater data on the accuracy of the results is difficult to evaluate precisely because the compilation of the global datasets involves an extensive amount of extrapolation. For example, the distribution of stations reporting atmospheric pressure is fairly uniform over most continents. The exceptions are Antartica, Greenland and Central Asia where the coverage is either sparse or non-existent. Over the oceans there is also a lack of actual pressure data but this only becomes a problem

insofar as it affects the determination of $q_0(t)$. The independent estimates of this quantity, however, are in good agreement. Lack of actual pressure data over the abovementioned continents is indeed a problem because it is in these regions where the computed seasonal departures in radial position are a maximum. A constant error of about 10 mb in the seasonal departure of atmospheric pressure over a continent the size of Antartica produces an error in the corresponding departure in radial position of about 1 cm. Fortunately, most space ranging networks have their stations located in other regions of the globe but if a TLRS should visit the abovementioned areas then clearly regional climatological factors need to be considered.

Similar problems are encountered with regard to the groundwater data. Runoff data, in particular, are very hard to obtain on a global basis (Stolz and Larden 1979) and Thornthwaite's method tends to overestimate the evapotranspiration rate (Lambeck 1980). In retrospect, it would seem desirable to divide the groundwater deformation calculations for geodetic sites where measurable distortions occur into two separate parts as is done with the computation of geoid heights by gravimetric methods (see e.g. Heiskanen and Moritz 1967). The inner zone contribution (say, $\psi < 20°$) could be evaluated with groundwater data based on a more precise method for estimating the evapotranspiration rate, like Penman's method (see e.g. Lambeck 1980), while the outer zone contribution could simply be evaluated using a global data set. On the other hand, it is interesting to note that Thornthwaite's method is remarkably accurate for North America (Munk and MacDonald 1960) which is where many of the space ranging stations are located. Another encouraging aspect is that even if Van Hylckama's (1956) data were in error by 25%, the error in the peak-to-peak variation in radial position due to groundwater variations would only be about 3 mm over south-east Asia where the maximum distortion occurs. In other areas the error would be considerably less.

The difference between the results of Stolz (1976a) and Stolz and Larden (1979) for the shift of the geocentre due to the seasonal redistribution of air-mass can be attributed to two factors; (1) the algebraic error made by Stolz (1976a) and (2) differences between the two atmospheric

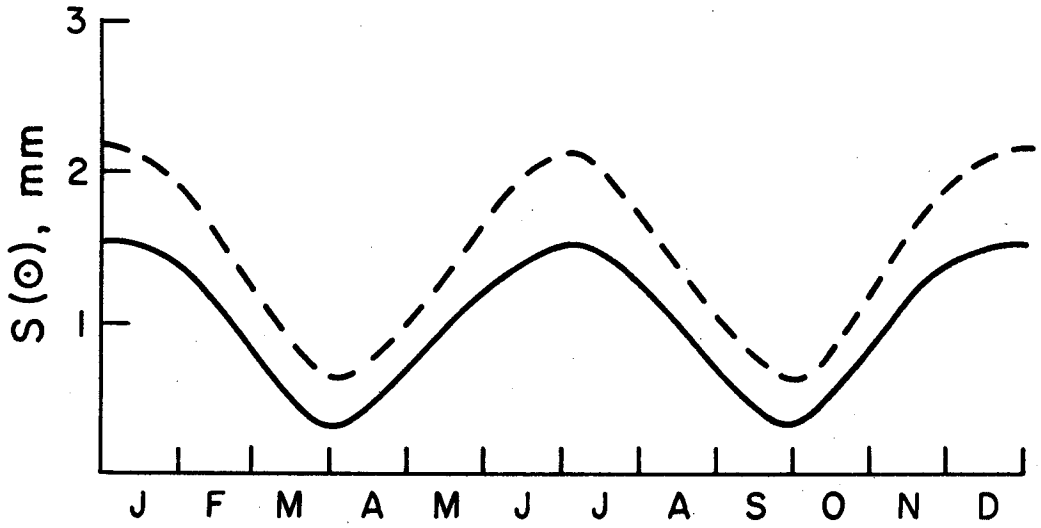

Figure 7.10 Geocentre Motion Due to Seasonal Atmospheric Loading
Broken line, Stolz (1976a); Solid line, Stolz and Larden (1979)

datasets. Figure 7.10, which is a plot of the function $S(\theta) = \{\Delta x_1(\theta)^2 + \Delta x_2(\theta)^2 + \Delta x_3(\theta)^2\}^{1/2}$ against time, shows that the difference is of the order 0.6 mm. A recomputation of the groundwater contribution using newer data is still in progress (Stolz, private communication, 1980).

7.5.2. Summary

An attempt has been made in this chapter to give some insight on the geodetic consequences of seasonal atmospheric-groundwater loading. In reviewing the various aspects of the problem, it was pointed out that the pioneering efforts of Stolz (1976a) indicated that the shift of the geocentre brought on by the seasonal redistribution of air mass and groundwater was very small. However, the data (Rosenhead 1929, Van Hylckama 1956) used to obtain this result were quite old and so, in an extension of this work, Stolz and Larden (1979) recomputed the atmospheric contribution to the motion of the geocentre as well as the accompanying radial surface deformations caused by the atmospheric load using the more recent pressure data of Schutz and Gates (1971, 1972, 1973, 1974). At the time, it was concluded that better values of soil moisture storage were not available in most parts of the world and so the groundwater calculations in Stolz (1976a) were not redone. Nevertheless, it did seem desirable to carry out an order of magnitude study on the surface deformations caused by seasonal groundwater loading using Van Hylckama's data and combine them with the results of Stolz and Larden (1979). This work is documented in this chapter.

The results here indicate that the radial surface deformations caused by the combined seasonal variation in atmospheric pressure and groundwater are significant in some parts of the world at the 1 to 2 cm level (see Tables 7.2, 7.3 and 7.4). Since all future satellite and gravimetric measuring techniques are likely to detect deformation at this accuracy level (Bender et al. 1979, Faller et al 1979), steps must be taken to make the appropriate measurement corrections for these effects before the results are used to gain a better understanding of the forces that drive the tectonic plates and the subsurface density and strain changes that occur in active seismic zones. From equation (4.15) it is

easy to show that radial surface deformations will affect an LLR measurement accordingly as

$$\Delta\rho = \{\cos(\phi-\delta) - \cos\phi\cos\delta(1-\cos H)\}\Delta r_s \qquad (7.41)$$

where from equation (7.24)

$$\Delta r_s \equiv d_r = A\cos(\Theta-\beta) \quad .$$

Clearly, the effect of radial surface deformations on measurements from LLR sites is geometry dependent. Equation (7.41) indicates that the maximum contributions will come at times of the year when the distortions are largest and when the moon is toward the zenith of the observing station. Tangential displacements will enter the range equation through the $\Delta\phi$ and $\Delta\lambda$ terms but these are negligible for seasonal atmospheric-groundwater loading.

Since the LLR range equation (4.15) has been formulated in a geocentric frame based on the centre of mass of the solid earth, oscillations of this point in space will be manifest as apparent variations in the coordinates (r_r, δ, α) of the reflector. On the other hand, if the range equation were formulated in a frame whose origin coincided with the centre of mass of the solid earth, oceans and atmosphere, the motion of the geocentre in space would produce variations in station positions with respect to this point. In any case, the shift of the geocentre in space due to the combined seasonal redistribution of air-mass and groundwater is very small and well below the detection level of future dynamic satellite and gravimetric measuring techniques. The partials needed to evaluate the effect of geocentre motion on the range measurement are given in equation (4.16), however, equation (7.40) must be transformed to its spherical coordinate equivalent before performing the substitution. The evaluation is not carried out here because the effects are extremely small. Once again, the maximum contribution will occur at specific times during the year and will be geometry dependent. At most times, the peak-to-peak contribution will be considerably less than the 6 mm indicated by equation (7.40).

To substantially reduce the effect of seasonal variations during crustal motion re-observing programs employing transportable systems

(see e.g. NASA 1979), one could schedule the times of site occupancy during the same season. If this strategy is not practical then corrections for seasonal effects must be considered. It is also important to remember than the results presented here are based on average seasonal values for air pressure and groundwater and that year-to-year fluctuations in these quantities cannot be dismissed (Lambeck 1980). To estimate the magnitude of year-to-year fluctuations, it is necessary to repeat the calculations here using geophysical data gathered over a different time span (see e.g. Kurihara et al. 1968; Y. Kurihara, unpublished data, 1977). A major study has already started (Stolz, private communication, 1980) in which the wobble excitation functions [see equations (2.13)], the displacement, and the deformations of the earth are being recomputed using the latest groundwater dataset obtained from the atlases of the world water balance published by the UNESCO Press, Paris (see e.g. Korzoun 1979). Comparison of these results with those presented here will help give some insight into the extent of year-to-year variations.

The possibility that large short-period displacement will occur cannot be ruled out either. For example, Trubytsyn and Makalkin (1976) proved that the crustal deformations resulting from cyclones may be larger than 2 cm. While it is unlikely that observations will be attempted at times of extreme meteorological activity, it is clear that the regional response of the earth to such events needs to be considered before the new space ranging data can be used to provide further detailed knowledge on the earth's interior.

CHAPTER 8

CONCLUSIONS

Recognizing the importance of continuous, high-accuracy determinations of Universal time (UT1) and polar motion for the analysis of observational data acquired by the space techniques and as a tool for geophysical research, a series of extensive numerical analyses were undertaken to assess some of the potentialities and problems of monitoring these rotational modes by lunar laser ranging. In what eventually became a rather lengthy but, nevertheless, fruitful and instructive exercise, efforts were made in the review Chapters 2 and 3 to introduce the reader to the complexities of the earth's rotation and give a broad account of the lunar laser ranging technique. From thereon, the study was directed toward answering three basic questions of motivation:

1) Can a future LLR station network determine the earth's polar motion and UT1 at the desired 5 cm accuracy level on a continuous daily basis?
2) What are the consequences of the outcome of these results if the shift of the observatories due to lithospheric plate motions are neglected?

and

3) Is it possible that seasonal atmospheric-groundwater loading can produce measurable displacements and deformations of the earth's surface at the expected 1 to 3 cm measurement accuracy level for the space techniques?

An idealized model for the topocentric distance from an observatory on the earth's surface to a reflector package on the lunar surface was constructed and a least squares formulation used to estimate the expected parametric uncertainties for polar motion and Universal time as measured relative to the lunar orbit. For simplicity, polar motion was defined as the movement of the spin axis in the geographic reference

system with the forced diurnal terms removed. Problems of parameter separability were discussed, the chief ones being the linear dependence of UT1 on the correction to the lunar right ascension and the insensitivity of the range to station latitude variations when the moon is at the station zenith.

The model, in its most basic form, assumes that the range residual is entirely due to errors in polar motion and UT1. The distance is assumed corrected for such effects as planetary perturbations, tidal deformation (including ocean loading), precession and nutation. Errors in the lunar orbit and libration, and in the definition of the terrestrial reference frame are also assumed to be negligible. Thus, given the adequacy of the weather model and the remaining conditions of observability, the earth rotation results presented in Chapter 5 are probably indicative of the ultimate one can hope to achieve with the lunar laser ranging technique. At best, it appears that a high percentage ($\approx$70-80%) of two-day values of polar motion and UT1 can be obtained to better than 5 cm when four or five LLR stations are ranging with $\pm$3 cm measurement uncertainties. Including the geocentric distance and declination of the reflector as solution parameters and allowing for the effect of systematic range errors, does not seem to change this conclusion significantly. It must be noted, however, that the present status of the LLR network is still far from meeting the above requirements. The analyses undertaken in this study confirm that less optimistic measurement uncertainty schedules do not give satisfactory results.

Two other interesting points concerning the results presented in Chapter 5 are worth emphasizing once again. These are the obvious lack of southern hemisphere stations which are so important in earth rotation experiments when the moon is at northern declination (see Figure 5.1) and the fact that there is no significant difference in the uncertainties for polar motion and UT1 or their correlation with the lunar orbital parameters r and δ when hour angle coverage is varied uniformly at each LLR station. If additional stations with dual capabilities of ranging to the LAGEOS satellite and the moon are contemplated then it is strongly recommended that they be placed in the southern hemisphere, and

near the meridians and in equatorial symmetry with existing northern hemisphere stations. Should the most cost-effective scenario for lunar laser ranging, regarding its contribution to the determination of earth rotation information, include a combination of resources and detailed coordination with complementary methods as suggested by Silverberg (1979), then it would appear from the analyses undertaken here that hour angle coverage is not likely to be a critical factor in the design of a joint observing schedule involving both LAGEOS and the moon. The results presented in Chapter 5, where further conclusions on this subject can be found, form the basis of this conclusion.

Estimates of the changes in LLR station coordinates due to plate motion have been presented in Chapter 6 in order to assess the allowable time period before these effects begin to contaminate polar motion and UT1 results at the 5 cm accuracy level. For a network of five stations, the movement of the lithospheric plates, in principle, might not contaminate polar motion and UT1 results until after about 4 or 5 years. However, as was pointed out in Chapter 6, weather conditions will not always permit a five station solution and if polar motion and UT1 results are obtained using the two station combination of Orroral and Haleakala, then plate motion effects will be significant after about 1 year because both these stations are located on fast moving plates.

In order to avoid the inconvenience of making corrections to polar motion and UT1 results for plate motion which are dependent on the particular station combination that contributed to the solution, it would seem more desirable to model the station motions using a reliable absolute plate velocity model. The station motions predicted by model AM1 of Minster et al. (1974), K5 of Kaula (1975) and B4 of Solomon et al. (1975) as listed in Table 6.3, are all in good agreement. This is very encouraging, particularly in view of the fact that each model is based on widely differing yet physically plausible assumptions. If episodic plate motions were to cause the present-day station motions to depart from their 5×10^6 year average inferred by the plate models above, then the results for polar motion and UT1 would start to

appear noiser than one would expect from the space ranging techniques. This would indicate that a new solution for the station coordinates would be needed in order to improve the plate velocity model and, hence, the earth rotation results.

An attempt was also made to estimate the combined effect of seasonal atmospheric-groundwater loading on geodetic position using atmospheric pressure and groundwater storage data. In contrast to the ocean loading problem, it was shown that for this type of load the conventional load Love number approach could be used to calculate such effects because most of the deformational power in the atmospheric-groundwater load is concentrated in the lower degree harmonics. While this approach has often been criticized as an uneconomic procedure on the computer, it was also shown that truncating the solution to $\psi = 90°$ to reduce the computer time did not produce adverse errors (see Table 7.5). The results indicate that the peak-to-peak radial surface deformations caused by the combined seasonal variations in atmospheric pressure and groundwater are of the order of 1 to 2 cm at several strategic geodetic locations around the world and, therefore, will be marginally significant in high precision geodetic experiments. The results do, however, contradict Urmantsev's (1971) previous assertion that the radial deformations over Europe due to seasonal variations in atmospheric pressure alone could be as large as 3.6 cm. Reasons for the differences are clearly stated in Section 7.5.

It was also shown that the peak-to-peak variations in radial position at LLR and VLBI observatories, and the associated motion of the geocentre in space due to the first degree component of the atmospheric-groundwater load were below 1 cm and probably not detectable by the future dynamic satellite or gravimeter measuring techniques. On the other hand, it should be mentioned, that the validity of these results depends heavily on the reliability of Van Hylckama's (1956) groundwater data which are very old. The recomputations presently being undertaken by Stolz (1980, private communication) using more recently published groundwater data should resolve this issue.

REFERENCES

Abbot, R. I., P. J. Shelus, J. D. Mulholland and E. C. Silverberg (1973). Laser observations of the Moon: Identification and construction of normal points for 1969-1971, Astron. J., 78, 784-793.

Alley, C. O. and P. L. Bender (1968). Information obtainable from laser range measurements to a lunar corner reflector, in Continental Drift, Secular Motion of the Pole, and Rotation of the Earth, (ed. W. Markowitz and B. Guinot), IAU Symp., 32, 86-90, D. Reidel, Dordrecht, Holland.

Alterman, Z., H. Jarosch and C. L. Pekeris (1959). Oscillations of the Earth, Proc. Roy. Soc. Lond. A, 252, 80-95.

Alterman, Z., H. Jarosch and C. L. Pekeris (1961). Propagation of Rayleigh waves in the Earth, Geophys. J. R. astr. Soc., 4, 219-241.

Anderle, R. J. (1973). Determination of polar motion from satellite observations, Geophys. Surv., 1, 147-161.

Anderle, R. J. (1976). Polar motion determined by Doppler satellite observations, Bull. Geod., 50, 377-390.

Anderle, R. J. (1977). Earth's rotational rate, in National Geodetic Satellite Program, (ed. S. W. Henriksen), U.S. Government Printing Office, Washington, D.C.

Anderle, R. J. (1979). Accuracy of geodetic solutions based on Doppler measurements of the NAVSTAR global positioning system satellites, Bull. Geod., 53, 109-116.

Anderle, R. J. and L. K. Beuglass (1970). Doppler satellite observations of polar motion, Bull. Geod., 96, 125-141.

Anderson, D. L. and J. B. Minster (1979). The frequency dependence of Q in the Earth and implications for mantle rheology and Chandler wobble, Geophys. J. R. astr. Soc., 58, 431-440.

Aoki, S. and C. Kakuta (1971). The excess secular change in the obliquity of the ecliptic and its relation to the internal motion of the Earth, Celestial Mech., 4, 171-181.

Arnold, K. (1974). Geodetic aspects of laser distance measurements to the Moon and radio-interference measurements to quasars, Gerlands Beitr. Geophysik, 83, 249-269.

Ashby, N., P. L. Bender and J. M. Wahr (1981). Accuracy of gravitational physics tests and of the solar quadrupole moment from ranging to a Mercury orbiter, in preparation.

Asteriadas, G. (1977). Determination of precession and galactic rotation from the proper motions of the AGK3, Astron. Astrophys., 56, 25-38.

Atkinson, R. d'E (1973). On the "dynamical variations" of latitude and time, Astron. J., 78, 147-151.

Atkinson, R. d'E (1975). On the Earth's axes of rotation and figure, Mon. Not. R. astr. Soc., 71, 381-386.

Balmino, G., K. Lambeck and W. M. Kaula (1973). A spherical harmonic analysis of the Earth's topography, J. Geophys. Res., 78, 478-481.

Bannon, J. K. and L. P. Steele (1957). Average water-vapour content of the air, Air Ministry, Meteorological Res. Comm., London, 1075.

Bender, P. L. (1975). Applications of PTTI to new techniques for determining crustal movements, polar motion, and the rotation of the Earth, in Proc. of the Sixth Annual Precise Time and Time Interval (PTTI) Planning Meeting, Goddard Space Flight Centre Rep., X-814-75-117, Greenbelt, Maryland.

Bender, P. L. (1981). Establishment of terrestrial reference frames by new observational techniques, in On Reference Coordinate Systems for Earth Dynamics, IAU Colloq., 56, D. Reidel, Dordrecht, Holland, in press.

Bender, P. L., D. G. Currie, R. H. Dicke, D. H. Eckhardt, J. E. Faller, W. M. Kaula, J. D. Mulholland, H. H. Plotkin, S. K. Poultney, E. C. Silverberg, D. T. Wilkinson, J. G. Williams and C. O. Alley (1973). The lunar laser ranging experiment, Science, 182, 229-238.

Bender, P. L., J. E. Faller, J. Levine, S. Moody, M. R. Pearlman and E. C. Silverberg (1979). Possible high-mobility LAGEOS ranging station, Tectonophysics, 52, 69-73.

Bender, P. L. and C. C. Goad (1979). Probable LAGEOS contributions to a worldwide geodynamics control network, in The Use of Artificial Satellites for Geodesy and Geodynamics, 2, 145-161, (ed. G. Veis and E. Livieratos), National Technical University, Athens, Greece.

Berger, A. L. (1977). Support for the astronomical theory of climatic change, Nature, 269, 44-45.

BIH (1975). Annual Report for 1974, Bureau International de l'Heure, Paris, France.

BIH (1978). Annual Report for 1977, Bureau International de l'Heure, Paris, France.

Böhme, S. and W. Fricke (1965). Astronomical Constants. A survey of determined values, Bull. Astron., 25, 269-293.

Brans, C. and R. H. Dicke (1961). Mach's principle and a relativistic theory of gravitation, Phys. Rev., 124, 925-935.

Breedlove, W. J., Jr. (1977). A numerical study of the effects of fourth degree terms in the Earth-Moon mutual potential on lunar physical librations, in Scientific Applications of Lunar Laser Ranging, (ed. J. D. Mulholland), Astrophys. Space Sci. Lib. Ser., 62, 65-77, D. Reidel, Dordrecht, Holland.

Bretreger, K. and R. S. Mather (1978). Modelling ocean-loading effects on tidal gravity in Australia, Geophys. J. R. astr. Soc., 52, 241-257.

Brosche, P. and J. Sündermann (1977). Effects of oceanic tides on the rotation of the Earth, in Scientific Applications of Lunar Laser Ranging, (ed. J. D. Mulholland), Astrophys. Space Sci. Lib. Ser., 62, 133-141, D. Reidel, Dordrecht, Holland.

Brown, E. W. (1908). Theory of the motion of the Moon, Mem. R. Astron. Soc., 59, 1-103.

Busse, F. H. (1970). The dynamical coupling between inner core and mantle of the Earth and the 24-year libration of the pole, in Earthquake Displacement Fields and the Rotation of the Earth, (ed. L. Mansinha, D. E. Smylie and A. E. Beck), Astrophys. Space Sci. Lib. Ser., 20, 88-98, D. Reidel, Dordrecht, Holland.

Calame, O. (1975). Etude des Mouvements Libratoires Lunaires et Localisation des Stations Terrestres, a partir des Mesures Laser de Distances, Ph.D. Thesis, University of Paris, France, 152 pp.

Calame, O. (1976). Description des mouvements Terre-Lune dans le cadre de l'analyse des mesures par laser, Manuscripta Geod., 1, 173-259.

Calame, O. (1977). Free librations of the Moon from lunar laser ranging, in Scientific Applications of Lunar Laser Ranging, (ed. J. D. Mulholland), Astrophys. Space Sci. Lib. Ser., 62, 53-63, D. Reidel, Dordrecht, Holland.

Calame, O. and B. Guinot (1979). Earth rotation by lunar distances (EROLD): Preliminary determination of universal time by lunar laser ranging (from observations of McDonald Observatory), in Bureau International de l'Heure Annual Report for 1978, D27-D48, Paris, France.

Calame, O. and J. D. Mulholland (1978). Lunar tidal acceleration determined from lunar range measures, Science, 199, 977-978.

Cappallo, R. J. (1980). The Rotation of the Moon, Ph.D. Thesis, Mass. Int. Technol., Cambridge, Massachusetts, 104 pp.

Carter, W. E. (1980). Project POLARIS: A status report, in Radio Interferometry Techniques for Geodesy, NASA Conf. Pub. 2115, 455-460, Washington, D.C.

Carter, W. E., E. Berg and S. Laurila (1977). The University of Hawaii lunar ranging experiment geodetic-geophysics support programme, Phil. Trans. R. Soc. Lond. A, 284, 451-456.

Carter, W. E., A. E. E. Rogers, C. C. Counselman and I. I. Shapiro (1980). Comparison of geodetic and radio interferometric measurements of the Haystack-Westford baseline vector, J. Geophys. Res., 85, 2685-2687.

Cathles, L. M. (1971). The Viscosity of the Earth's Mantle, Ph.D. Thesis, Princeton University, Princeton, New Jersey.

Cathles, L. M. (1975). The Viscosity of the Earth's Mantle, Princeton University Press, Princeton, New Jersey, 386 pp.

Cazenave, A. (1975). Interactions Entre les Irregularites de la Vitesse de Rotation de la Terre et les Phenomenes Meteorologiques et Climatiques, Ph.D. Thesis, Universite Paul Sabatier, Toulouse, France, 258 pp.

Chandler, S. C. (1891). On the variation of latitude, Astron. J., 11, 83.

Chapple, W. M. and T. E. Tullis (1977). Evaluation of the forces that drive the plates, J. Geophys. Res., 82, 1967-1984.

Chase, C. G. (1978). Plate kinematics: The Americas, East Africa, and the rest of the world, Earth Planet. Sci. Lett., 37, 353-368.

Chiaruttini, C. and E. Livieratos (1978). Oceanic loading on European laser-ranging sites, Geophys. J. R. astr. Soc., 54, 593-600.

Chollet, F. C. (1970). Mouvements de l'axe instantane de rotation de la Terre deduits des mesures laser de distance Terre-Lune, Astron. Astrophys., 9, 110-124.

Chollet, F. C. and S. Debarbat (1972). Analyse des observations de latitude effectuees a l'astrolabe Danjon de l'Observatoire de Paris de 1956.5 a 1970.8, Astron. Astrophys., 18, 133-142.

Counselman, C. C. (1976). Radio astrometry, Ann. Rev. Astron. Astrophys., 14, 197-214.

Counselman, C. C., H. F. Hinteregger, R. W. King and I. I. Shapiro (1973). Lunar baselines and libration from differential VLBI observations of Alseps, The Moon, 8, 484-489.

Cox, A., Editor (1973). Plate Tectonics and Geomagnetic Reversals, W. H. Freeman and Co., San Francisco, 702 pp.

Crossley, D. J. and D. Gubbins (1975). Static deformation of the Earth's liquid core, Geophys. Res. Lett., 2, 1-4.

Crutcher, H. and J. Meserve (1970). Selected level heights, temperatures, and dew points for the northern hemisphere, NAVAIR 50-IC-52, Nav. Weather Serv. Command, Washington, D.C.

Currie, R. G. (1975). Period, Q_p and amplitude of the pole tide, Geophys. J. R. astr. Soc., 43, 73-86.

Currie, R. G. (1976). The spectrum of sea level from 4 to 40 years, Geophys. J. R. astr. Soc., 46, 513-520.

Currie, R. G. (1979). Distribution of solar cycle signal in surface air temperature over North America, J. Geophys. Res., 84, 753-761.

Currie, R. G. (1980). Detection of the 11-year sunspot cycle signal in Earth rotation, Geophys. J. R. astr. Soc., 61, 131-140.

Currie, R. G. (1981). Solar cycle signal in Earth rotation: Non-stationary behaviour, Science, 211, 386-389.

Dahlen, F. A. (1971). The excitation of the Chandler wobble by earthquakes, Geophys. J. R. astr. Soc., 25, 157-206.

Dahlen, F. A. (1973). A correction to the excitation of the Chandler wobble by earthquakes, Geophys. J. R. astr. Soc., 32, 203-217.

Dahlen, F. A. (1974). On the static deformation of an Earth model with a fluid core, Geophys. J. R. astr. Soc., 36, 461-485.

Dahlen, F. A. (1976). The passive influence of the oceans upon the rotation of the Earth, Geophys. J. R. astr. Soc., 46, 363-406.

Daillet, S. (1979). Secular variation of pole tide: Correlation with Chandler wobble ellipticity, preprint.

Dartt, D. G. and A. D. Belmont (1964). Periodic features of the 50-millibar zonal winds in the tropics, J. Geophys. Res., 69, 2887-2893.

Darwin, G. (1877). On the influence of geological changes on the Earth's axis of rotation, Phil. Trans. R. Soc. Lond. A, 167, 271-312.

Dickey, J. O., J. G. Williams and C. F. Yoder (1980). Results from lunar laser ranging, EOS Trans. Am. Geophys. Un., 61, 939 (abstract).

Dickman, S. R. (1977). Secular trend of the Earth's rotation pole: Consideration of motion of the latitude observatories, Geophys. J. R. astr. Soc., 51, 229-244.

Dickman, S. R. (1979a). Consequences of an enhanced pole tide, J. Geophys. Res., 84, 5447-5456.

Dickman, S. R. (1979b). Continental drift and true polar wandering, Geophys. J. R. astr. Soc., 57, 41-50.

Duncombe, R. L. (1958). Motion of Venus 1750-1949, Astron. Pap. Am. Ephem. Naut. Alm., 16, 1-258.

Duncombe, R. L. and T. C. van Flandern (1976). Secular variation of the obliquity of the ecliptic, Astron. J., 81, 281-284.

Dunn, P. J., D. E. Smith and R. Kolenkiewicz (1977). The measurement of latitude, time and height variations at a single laser tracking station, J. Geophys. Res., 82, 895-897.

Eckert, W. J., M. J. Walker and D. Eckert (1966). Transformations of the lunar coordinates and orbital parameters, Astron. J., 71, 314-332.

Eckhardt, D. H. (1965). Computer solutions of the forced physical librations of the Moon, Astron. J., 70, 466-471.

Eckhardt, D. H. (1970). Lunar libration tables, The Moon, 1, 264-275.

Eckhardt, D. H. (1973). Physical librations due to the third and fourth degree harmonics of the lunar gravity potential, The Moon, 6, 127-134.

Elsmore, B. (1976). Methods for the determination of lunisolar precession from observations of extragalactic radio sources, Mon. Not. R. astr. Soc., 177, 291-298.

Evans, D. S. (1977). Discussion, in Scientific Applications of Lunar Laser Ranging, (ed. J. D. Mulholland), Astrophys. Space Sci. Lib. Ser., 62, 216, D. Reidel, Dordrecht, Holland.

Explanatory Supplement (1961). Explanatory Supplement to the Astronomical Ephemeris, Her Majesty's Stationery Office, London.

Fajemirokun, F. A. (1971). Applications of laser ranging and VLBI observations for selenodetic control, Dept. of Geod. Sci. Rep., 157, The Ohio State University, Columbus, Ohio, 230 pp.

Faller, J. E., P. L. Bender, C. O. Alley, D. G. Currie, R. H. Dicke, W. M. Kaula, G. J. F. MacDonald, J. D. Mulholland, H. H. Plotkin, E. C. Silverberg and D. T. Wilkinson (1972). Geodesy results obtainable with lunar retroreflectors, in The Use of Artificial Satellites for Geodesy, (ed. S. W. Henriksen, A. Mancini and B. H. Chovitz), Geophys. Mono. Ser., 15, 261-264, Washington, D.C.

Faller, J. E., R. L. Rinker and M. A. Zumberge (1979). Plans for the development of a portable absolute gravimeter with a few parts in 10^9 accuracy, Tectonophysics, 52, 107-116.

Fanselow, J. L., J. B. Thomas, E. J. Cohen, P. F. MacDoran, W. G. Melbourne, B. D. Mulhall, G. H. Purcell, D. H. Rogstad, L. J. Skjerve, D. J. Spitzmesser, J. Urech and G. Nicholson (1979). Determination of UT1 and polar motion by the Deep Space Network using very long baseline interferometry, in Time and the Earth's Rotation, (ed. D. D. McCarthy and J. D. Pilkington), IAU Symp., 82, 199-209, D. Reidel, Dordrecht, Holland.

Farrell, W. E. (1972). Deformation of the Earth by surface loads, Rev. Geophys. Space Phys., 10, 761-797.

Farrell, W. E. (1973). Earth tides, ocean tides and tidal loading, Phil. Trans. R. Soc. Lond. A, 274, 253-259.

Farrell, W. E. and J. A. Clark (1976). On postglacial sea level, Geophys. J. R. astr. Soc., 46, 647-667.

Fedorov, E. P. (1963). Nutation and Forced Motion of the Earth's Pole, MacMillan, New York, 152 pp.

Fedorov, E. P., M. L. Smith and P. L. Bender, Editors (1980). Nutation and the Earth's Rotation, IAU Symp., 78, D. Reidel, Dordrecht, Holland, 266 pp.

Felsentreger, T. L., J. G. Marsh and R. G. Williamson (1978). Tidal perturbations on the satellite 1967-92A, J. Geophys. Res., 83, 1837-1842.

Felsentreger, T. L., J. G. Marsh and R. G. Williamson (1979). M_2 ocean tide parameters and the deceleration of the Moon's mean longitude from satellite orbit data, J. Geophys. Res., 84, 4675-4679.

Ferrari, A. J., W. S. Sinclair, W. L. Sjogren, J. G. Williams and C. F. Yoder (1980). Geophysical parameters of the Earth-Moon system, J. Geophys. Res., 85, 3939-3951.

Fricke, W. (1971). A rediscussion of Newcomb's determination of precession, Astron. Astrophys., 13, 298-303.

Fricke, W. (1972). Fundamental constants of position and proper motions, Ann. Rev. Astron. Astrophys., 10, 101-128.

Gaposchkin, E. M. (1972). Analysis of pole position from 1846 to 1970, in Rotation of the Earth, (ed. P. Melchior and S. Yumi), IAU Symp., 48, 19-32, D. Reidel, Dordrecht, Holland.

Garthwaite, K., D. B. Holdridge and J. D. Mulholland (1970). A preliminary special perturbation theory for the lunar motion, Astron. J., 75, 1133-1139.

Gilbert, F. and A. M. Dziewonski (1975). An application of normal mode theory to the retrieval of structural parameters and source mechanisms from seismic spectra, Phil. Trans. R. Soc. Lond. A, 278, 187-269.

Goad, C. C. (1980). The computation of tidal loading effects with integrated Green's functions, in Proc. Second Int. Symp. On Problems Related to the Definition of North American Vertical Geodetic Networks, Canadian Institute of Surveying, 587-601, 26-30 May, 1980, Ottawa, Canada.

Goad, C. C. and B. C. Douglas (1978). Lunar tidal acceleration obtained from satellite-derived ocean tide parameters, J. Geophys. Res., 83, 2306-2310.

Gold, T. (1967). Radio method for the precise measurement of the rotation period of the Earth, Science, 157, 302-304.

Goldreich, P. and A. Toomre (1969). Some remarks on polar wandering, J. Geophys. Res., 74, 2555-2567.

Goldstein, H. (1950). Celestial Mechanics, Addison-Wesley, Reading, Massachusetts, 399 pp.

Graber, M. A. (1976). Polar motion spectra based on Doppler, IPMS and BIH data, Geophys. J. R. astr. Soc., 46, 75-85.

Grafarend, E. W. (1977). Space-time differential geodesy, in The Changing World of Geodetic Science, (ed. U. A. Uotila), Dept. of Geod. Sci., Rep., 250, The Ohio State University, Columbus, Ohio.

Groten, E. (1976). On variations of geocentric positions with time, unpublished manuscript.

Guinot, B. (1970). Work of the Bureau International de l'Heure on the rotation of the Earth, in Earthquake Displacement Fields and the Rotation of the Earth, (ed. L. Mansinha, D. E. Smylie and A. E. Beck), Astrophys. Space Sci. Lib. Ser., 20, 54-62, D. Reidel, Dordrecht, Holland.

Guinot, B. and M. Feissel (1968). Nouvelles methodes de calcul du Bureau International de l'Heure, in Continential Drift, Secular Motion of the Pole, and Rotation of the Earth, (ed. W. Markowitz and B. Guinot), IAU Symp., 32, 63-70, D. Reidel, Dordrecht, Holland.

Guinot, B., M. Feissel and M. Granveaud (1971). Annual Report for 1970, Bureau International de l'Heure, Paris, France.

Harris, A. W. and J. G. Williams (1977). Earth rotation study using lunar laser ranging data, in Scientific Applications of Lunar Laser Ranging, (ed. J. D. Mulholland), Astrophys. Space Sci. Lib. Ser., 62, 179-190, D. Reidel, Dordrecht, Holland.

Haubrich, R. A. (1970). An examination of the data relating pole motion to earthquakes, in Earthquake Displacement Fields and the Rotation of the Earth, (ed. L. Mansinha, D. E. Smylie and A. E. Beck), Astrophys. Space Sci. Lib. Ser., 20, 149-158, D. Reidel, Dordrecht, Holland.

Haubrich, R. and W. Munk (1959). The pole tide, J. Geophys. Res., 64, 2373-2388.

Hauser, J. P. (1974). An Analysis of the Effects of Systematic Errors in the Lunar Laser Ranging Experiment, Ph.D. Thesis, University of Colorado, Boulder, Colorado, 85 pp.

Hein, G. W. (1980). The influence of ground water variations on re-levelling data, in Proc. Second Int. Symp. On Problems Related to the Redefinition of North American Vertical Geodetic Networks, Canadian Institute of Surveying, 603-622, 26-30 May, 1980, Ottawa, Canada.

Heiskanen, W. A. and H. Moritz (1967). Physical Geodesy, W. H. Freeman and Co., San Francisco, 364 pp.

Hide, R. (1977). Towards a theory of irregular variations in the length of the day and core-mantle coupling, Phil. Trans. R. Soc. Lond. A, 284, 547-554.

Hide, R., N. T. Birch, L. V. Morrison, D. J. Shea and A. A. White (1980). Atmospheric angular momentum fluctuations and changes in the length of the day, Nature, 286, 114-117.

Hinteregger, H. F., I. I. Shapiro, D. S. Robertson, C. A. Knight, R. A. Ergas, A. R. Whitney, A. E. E. Rogers, J. M. Moran, T. A. Clark and B. F. Burke (1972). Precision geodesy via radio interferometry, Science, 178, 396-398.

H.M.S.O. (1965). Tables of Temperature, Relative Humidity and Precipitation for the World, Part 1, North America, Greenland and the North Pacific, Her Majesty's Stationery Office, London.

Holdridge, D. B. (1967). An alternate expression for light time using general relativity, JPL Space Program Summary 37-48, 3, 2-4.

Hopfield, H. S. (1976). Tropospheric effects on signals at very low elevation angles, APL/JHU, TG 1291, Silver Spring, Maryland.

Hosoyama, K., I. Naito and N. Sato (1976). Tidal admittance of pole tide, J. Phys. Earth, 24, 51-62.

Hough, S. S. (1895). The oscillations of a rotating ellipsoidal shell containing fluid, Phil. Trans. R. Soc. Lond. A, 186, 469-506.

IAU (1980). Resolution No. 11(b), International Astronomical Union, Information Bulletin, 43, 24-25, D. Reidel, Dordrecht, Holland.

Iijima, S. and S. Okazaki (1966). On the biennial component in the rate of rotation of the Earth, J. Geod. Soc. Japan, 12, 91.

Inglis, D. (1957). Shifting of the Earth's axis of rotation, Rev. Mod. Phys., 29, 9-19.

Isacks, B. and P. Molnar (1969). Mantle earthquake mechanisms and the sinking of the lithosphere, Nature, 223, 1121-1124.

Isacks, B., J. Oliver and L. R. Sykes (1968). Seismology and the new global tectonics, J. Geophys. Res., 73, 5855-5899.

IUGG (1980). Resolutions of the XVII General Assembly of the International Union of Geodesy and Geophysics, Canberra, Australia, December 1979, Bull. Geod., in press.

Jeffreys, H. (1916). Causes contributory to the annual variation of latitude, Mon. Not. R. astr. Soc., 76, 499-525.

Jeffreys, H. (1956). The damping of the variation of latitude, Mon. Not. R. astr. Soc., 116, 362-364.

Jeffreys, H. (1972). The variation of latitude, in Rotation of the Earth, (ed. P. Melchior and S. Yumi), IAU Symp., 48, 39-42, D. Reidel, Dordrecht, Holland.

Jeffreys, H. (1978). On imperfections of elasticity in the Earth's interior, Geophys. J. R. astr. Soc., 55, 273-281.

Jeffreys, H. (1980). Some difficulties in the theory of nutation, in Nutation and the Earth's Rotation, (ed. E. P. Fedorov, M. L. Smith and P. L. Bender), IAU Symp., 78, 9-11, D. Reidel, Dordrecht, Holland.

Jeffreys, H. and R. O. Vicente (1957a). The theory of nutation and the variation of latitude, Mon. Not. R. astr. Soc., 117, 142-161.

Jeffreys, H. and R. O. Vicente (1957b). The theory of nutation and the variation of latitude: The Roche core model, Mon. Not. R. astr. Soc., 117, 162-173.

Jeffreys, H. and R. O. Vicente (1966). Comparison of forms of the elastic equations for the Earth, Mem. Acad. R. Belgique, 37, 3-30.

Jochmann, H. (1976). Der einfluss von luftmassenbewegungen in der Atmosphäre auf die polbewegung, Veroeff Zentralinst. Phys. Erde, Akad. Wiss. DDR, 35, 5-38.

Johnson, T. S. (1977). GSFC Laser DME, in National Geodetic Satellite Program, (ed. S. W. Henriksen), U.S. Government Printing Office, Washington, D.C.

Jurdy, D. M. (1981). True polar wander, in Quantitative Methods of Assessing Plate Motions, (eds. S. C. Solomon, R. van der Voo and M. A. Chinnery), Tectonophysics, 74, 1-16.

Jurdy, D. M. and R. van der Voo (1974). A method for the separation of true polar wander and continental drift, including results for the last 55 m.y., J. Geophys. Res., 79, 2945-2952.

Kanamori, H. and J. J. Cipar (1974). Focal process of the great Chilean earthquake May 22, 1960, Phys. Earth Planet. Inter., 9, 128-136.

Kaula, W. M. (1966). Introduction to Satellite Geodesy, Blaisdell, Waltham, Massachusetts, 124 pp.

Kaula, W. M. (1973). Potentialities of lunar laser ranging for measuring tectonic motions, Phil. Trans. R. Soc. Lond. A, 274, 185-193.

Kaula, W. M. (1975). Absolute plate motions by boundary velocity minimizations, J. Geophys. Res., 80, 244-248.

Kaula, W. M. and P. A. Baxa (1973). The physical librations of the Moon, including higher harmonic effects, The Moon, 8, 287-307.

Kikuchi, N. (1975). On the excitation of polar motion due to the variation of the atmospheric pressure, J. Geod. Soc. Japan, 21, 170-178.

King, R. W., C. C. Counselman and I. I. Shapiro (1976). Lunar dynamics and selenodesy: Results from analysis of VLBI and laser data, J. Geophys. Res., 81, 6251-6256.

King, R. W., C. C. Counselman and I. I. Shapiro (1978). Universal time: Results from lunar laser ranging, J. Geophys. Res., 83, 3377-3381.

Kinoshita, H. (1977). Theory of the rotation of the rigid Earth, Celestial Mech., 15, 277-326.

Kinoshita, H., K. Nakajima, Y. Kubo, I. Nakagawa, T. Sasao and K. Yokoyama (1979). Note on nutation in ephemerides, Publ. Int. Lat. Obs., Mizusawa, 12, 71-108.

Klein, F. and A. Sommerfeld (1903). Theorie des Kreisels, 3, Teubner, Leipzig.

Kolaczek, B. (1977). On the problems of the astrometric methods and of the lunar laser ranging in the study of the Earth's rotation, in Scientific Applications of Lunar Laser Ranging, (ed. J. D. Mulholland), Astrophys. Space Sci. Lib. Ser., 62, 171-178, D. Reidel, Dordrecht, Holland.

Kolaczek, B. and G. Weiffenbach, Editors (1975). On Reference Coordinate Systems for Earth Dynamics, IAU Colloq., 26, Polish Academy of Science, Warsaw, Poland, 478 pp.

Kolenkiewicz, R., D. E. Smith, D. P. Rubincam, P. J. Dunn and M. H. Torrence (1977). Polar motion and Earth tides from laser tracking, Phil. Trans. R. Soc. Lond. A, 284, 485-494.

Korzoun, V. I., Editor-in-Chief (1979). Atlas of World Water Balance, Hydrometeorological Publishing House, UNESCO Press, Paris, France.

Kovalevsky, J. (1975), in minutes of the EROLD Steering Committee, 21 August, Grenoble, France.

Kovalevsky, J. (1977). Scientific expectations in the selenosciences, in Scientific Applications of Lunar Laser Ranging, (ed. J. D. Mulholland), Astrophys. Space Sci. Lib. Ser., 62, 21-36, D. Reidel, Dordrecht, Holland.

Kozai, Y. (1975), in minutes of the EROLD Steering Committee, 21 August, Grenoble, France.

Koziel, K. (1948). The Moon's libration and figure as derived from Hartwig's Dorpat heliometric observations, Acta Astronomica, 4, 61-193.

Koziel, K. (1967). The constants of the Moon's physical libration derived on the basis of four series of heliometric observations from the years 1877-1915, Icarus, 7, 1-28.

Krasinsky, C. A. (1975). On constructing the inertial system of high accuracy by VLBI methods, in On Reference Coordinate Systems for Earth Dynamics, (ed. B. Kolaczek and G. Weiffenbach), IAU Colloq., 26, 381-393, Polish Academy of Science, Warsaw, Poland.

Kurihara, Y., H. Shinoda and T. Sakurai (1968). Normals of monthly mean sea-level pressure for the northern and southern hemispheres, Tech. Rep., 61, Japan Meteorol. Agency, Tokyo.

Lambeck, K. (1977). Tidal dissipation in the oceans: Astronomical, geophysical and oceanographic consequences, Phil. Trans. R. Soc. Lond. A, 287, 545-594.

Lambeck, K. (1979). Methods and geophysical applications of satellite geodesy, Rep. Prog. Phys., 42, 547-628.

Lambeck, K. (1980). The Earth's Variable Rotation: Geophysical Causes and Consequences, Cambridge University Press, 449 pp.

Lambeck, K. and A. Cazenave (1973). The Earth's rotation and atmospheric circulation. I. Seasonal variations, Geophys. J. R. astr. Soc., 32, 79-93.

Lambeck, K. and A. Cazenave (1974). The Earth's rotation and atmospheric circulation. II. The continuum, Geophys. J. R. astr. Soc., 38, 49-61.

Lambeck, K. and A. Cazenave (1976). Long term variations in length of day and climatic change, Geophys. J. R. astr. Soc., 46, 555-573.

Lambeck, K. and A. Cazenave (1977). The Earth's variable rate of rotation: A discussion of some meteorological and oceanic causes and consequences, Phil. Trans. R. Soc. Lond. A, 284, 495-506.

Lambeck, K. and P. Hopgood (1979). New results for the angular momentum exchange between the solid Earth and atmosphere, 1963-1973, Symp. 6, Int. Union Geod. Geophys., Canberra, Australia, December 1979.

Lambert, A. and C. Beaumont (1977). Nano variations in gravity due to seasonal groundwater movements: Implications for the gravitational detection of tectonic movements, J. Geophys. Res., 82, 297-306.

Lambert, W. D. (1922). The interpretation of apparent changes in mean latitude at the International Latitude Stations, Astron. J., 34, 103-110.

Lambert, W., F. Schlesinger and E. Brown (1931). The variation of latitude, Bulletin 78 of the National Research Council, 16, 245.

Landsberg, H. E., Editor-in-Chief (1970). World Survey of Climatology, Vols. 5, 8, 11, 13, Elsevier, New York.

Langley, R. B., R. W. King and I. I. Shapiro (1981). Earth rotation from lunar laser ranging, J. Geophys. Res., submitted.

Larden, D. R. (1980). Some geophysical effects on geodetic levelling networks, in Proc Second Int. Symp. On Problems Related to the Definition of North American Vertical Geodetic Networks, Canadian Institute of Surveying, 151-167, 26-30 May, 1980, Ottawa, Canada.

Larden, D. R. (1981). A search for irregularities in the Earth's polar motion during 1974 using lunar ranging data, in preparation.

Larden, D. R. and P. L. Bender (1981). Expected accuracy of geodetic baseline determinations using the GPS reconstructed carrier phase method, Bull. Géod., in preparation.

Laubscher, R. E. (1972). A determination of the motion of the ecliptic, Astron. Astrophys., 20, 407-414.

Laubscher, R. E. (1976). Dynamical determinations of the general precession in longitude, Astron. Astrophys., 51, 9-20.

Lee, W. H. K. and W. M. Kaula (1967). A spherical harmonic analysis of the Earth's topography, J. Geophys. Res., 72, 753-758.

Leick, A. (1980). Potentialities of lunar laser range-differencing for measuring the Earth's orientation, Bull. Géod., 54, 55-68.

Le Pichon, X. (1968). Sea-floor spreading and continental drift, J. Geophys. Res., 73, 3661-3697.

Le Pichon, X., J. Francheteau and J. Bonnin (1973). Plate Tectonics, Elsevier, Amsterdam, 300 pp.

Liu, H. S., L. Carpenter and R. W. Agreen (1974). Plate motion and the secular shift of the mean pole, J. Geophys. Res., 79, 4379-4382.

Longman, I. M. (1962). A Green's function for determining the deformation of the Earth under surface mass loads 1. Theory, J. Geophys. Res., 67, 845-850.

Longman, I. M. (1963). A Green's function for determining the deformation of the Earth under surface mass loading 2. Computations and numerical results, J. Geophys. Res., 68, 485-496.

Longman, I. M. (1966). Computation of Love numbers and load deformation coefficients for a model Earth, Geophys. J. R. astr. Soc., 11, 133-137.

Loumos, G. L., J. D. Mulholland, P. J. Shelus and E. C. Silverberg (1975). Accuracy of site coordinates obtainable by a mobile lunar laser station: Final report, Res. Mem. in Astron., 75-007, University of Texas, Austin.

Luck, J. Mck., M. J. Miller and P. J. Morgan (1973). The National Mapping lunar laser program, in Earth's Gravitational Field and Secular Variations in Position, (ed. R. S. Mather and P. V. Angus-Leppan), School of Surveying, University of New South Wales, Sydney, Australia.

MacDoran, P. F. (1973). Very long baseline interferometry (VLBI) applications to secular geodynamics and Earth strain measurement, in Earth's Gravitational Field and Secular Variations in Position, (ed. R. S. Mather and P. V. Angus-Leppan), School of Surveying, University of New South Wales, Sydney, Australia.

MacDoran, P. F. (1979). Satellite emission radio interferometric earth surveying SERIES -- GPS geodetic system, Bull. Géod., 53, 117-138.

Manabe, S. (1969). Climate and the ocean circulation, 1, The atmospheric circulation and the hydrology of the Earth's surface, Mon. Weather Rev., 97, 739-774.

Mansinha, L. and D. E. Smylie (1967). Effect of earthquakes on the Chandler wobble and the secular polar shift, J. Geophys. Res., 72, 4731-4743.

Mansinha, L., D. E. Smylie and C. H. Chapman (1979). Seismic excitation of the Chandler wobble revisited, Geophys. J. R. astr. Soc., 59, 1-17.

Markowitz, W. (1968). Concurrent astronomical observations for studying continental drift, polar motion, and the rotation of the Earth, in Continental Drift, Secular Motion of the Pole, and Rotation of the Earth, (ed. W. Markowitz and B. Guinot), IAU Symp., 32, 25-32, D. Reidel, Dordrecht, Holland.

Markowitz, W. (1970). Sudden changes in rotational acceleration of the Earth and secular motion of the pole, in Earthquake Displacement Fields and the Rotation of the Earth, (ed. L. Mansinha, D. E. Smylie and A. E. Beck), Astrophys. Space Sci. Lib. Ser., 20, 69-81, D. Reidel, Dordrecht, Holland.

Mather, R. S. and D. R. Larden (1978). On the recovery of geodynamic information from secular gravity changes, Unisurv G, 29, 11-22.

McCarthy, D. D., P. K. Seidelmann and T. C. van Flandern (1980). On the adoption of empirical corrections to Woolard's nutation theory, in Nutation and the Earth's Rotation, (ed. E. P. Fedorov, M. L. Smith and P. L. Bender), IAU Symp., 78, 117-124, D. Reidel, Dordrecht, Holland.

McClure, P. (1973). Diurnal polar motion, Goddard Space Flight Centre, Report X-592-73-259, Greenbelt, Maryland, 109 pp.

McElhinny, M. W. (1973). Palaeomagnetism and Plate Tectonics, Cambridge University Press, 358 pp.

Melbourne, W. G., J. D. Mulholland, W. L. Sjogren and F. M. Sturms (1968). Constants and related information for astrodynamic calculations, 1968, JPL Tech. Rep., 32-1306, Pasadena, California.

Melchior, P. (1971). Precession-nutations and tidal potential, Celestial Mech., 4, 190-212.

Melchior, P. (1978). The Tides of the Planet Earth, Pergamon Press, Oxford, 609 pp.

Merriam, J. B. and K. Lambeck (1979). Comments on the Chandler wobble Q, Geophys. J. R. astr. Soc., 59, 281-286.

Migus, A. (1980). Analytical lunar libration tables, The Moon and the Planets, 23, 391-427.

Miller, S. P. and C. Wunsch (1973). The pole tide, Nature, 246, 97-102.

Milne, J. (1906). Bakerian Lecture, Proc. Roy. Soc. Lond Ser. A, 77, 365-376.

Minster, J. B. and T. H. Jordan (1978). Present-day plate motions, J. Geophys. Res., 83, 5331-5354.

Minster, J. B., T. H. Jordan, P. Molnar and E. Haines (1974). Numerical modelling of instantaneous plate tectonics, Geophys. J. R. astr. Soc., 36, 541-576.

Misner, C. W., K. S. Thorne and J. A. Wheeler (1973). Gravitation, W. H. Freeman and Co., San Francisco, 1279 pp.

Mitchell, J. (1976). An overview of climatic variability and its causal mechanisms, Quaternary Res., 6, 481-491.

Molnar, P. and T. Atwater (1973). Relative motion of hot spots in the mantle, Nature, 246, 288-291.

Molnar, P. and J. Francheteau (1975). The relative motion of 'hot spots' in Atlantic and Indian Oceans during the Cenozoic, Geophys. J. R. astr. Soc., 43, 763-774.

Molodensky, M. S. (1961). The theory of nutation and diurnal Earth tides, Com. Obs. R. Belgique, 288, 25-56.

Morgan, P. (1977). A review of perturbing parameters which affect the quality of laser distance measurements, in Scientific Applications of Lunar Laser Ranging (ed. J. D. Mulholland), Astrophys. Space Sci. Lib. Ser., 62, 223-239, D. Reidel, Dordrecht, Holland.

Morgan, W. J. (1971). Convection plumes in the lower mantle, Nature, 230, 42-43.

Morgan, W. J. (1972). Plate motions and deep mantle convection, Geol. Soc. Am. Mem., 132, 7-22.

Morrison, L. V. and C. G. Ward (1975). The analysis of the transits of Mercury, Mon. Not. R. Astron. Soc., 173, 183-206.

Moyer, T. D. (1976). Transformation from proper time on Earth to coordinate time in solar system barycentric space-time frame of reference, JPL Tech. Mem., 33-786, Pasadena, California.

Mueller, I. I. (1969). Spherical and Practical Astronomy as Applied to Geodesy, Frederick Ungar, New York, 615 pp.

Mueller, I. I. and C. R. Schwarz (1972). Separating the secular motion of the pole from continental drift where and what to observe?, in Rotation of the Earth, (ed. P. Melchior and S. Yumi), IAU Symp., 48, 68-77, D. Reidel, Dordrecht, Holland.

Mulholland, J. D. (1972). Measures of time in astronomy, Publ. astr. Soc. Pacific, 84, 357-364.

Mulholland, J. D. (1975). Coordinate systems in lunar ranging, in On Reference Coordinate Systems for Earth Dynamics, (ed. B. Kolaczek and G. Weiffenbach), IAU Colloq., 26, 433-443, Polish Academy of Science, Warsaw, Poland.

Mulholland, J. D. (1977). Mathematical modelling of lunar laser measures and their application to improvement of physical parameters, in Scientific Applications of Lunar Laser Ranging, (ed. J. D. Mulholland), Astrophys. Space Sci. Lib. Ser., 62, 1-8, D. Reidel, Dordrecht, Holland.

Mulholland, J. D. (1980). Scientific achievements from ten years of lunar laser ranging, Rev. Geophys. Space Phys., 18, 549-564.

Muller, P. M. (1976). Determination of the cosmological rate of change of G and the tidal accelerations of Earth and Moon from ancient and modern astronomical data, Rep. SP 43-36, Jet Propulsion Laboratory, Pasadena, California, 24 pp.

Munk, W. H. and E. M. Hassan (1961). Atmospheric excitation of the Earth's wobble, Geophys. J. R. astr. Soc., 4, 339-358.

Munk, W. H. and G. J. F. MacDonald (1960). The Rotation of the Earth, Cambridge University Press, 323 pp.

Munk, W. H. and R. Miller (1950). Variations in the Earth's angular velocity resulting from fluctuations in atmospheric and oceanic circulation, Tellus, 2, 93-101.

Naito, I. (1977). Secular variation of pole tide, J. Phys. Earth, 25, 221-231.

Naito, I. and C. Sugawa (1973). On the relation between the meridionally asymmetric mass distribution of the Earth and the z-term in the latitude variation, Proc. Int. Lat. Observ. Mizusawa, 13, 84-95.

Nakiboglu, S. M. and K. Lambeck (1980). Deglaciation effects on the rotation of the Earth, Geophys. J. R. astr. Soc., 62, 49-58.

NASA (1979). Applications of space technology to crustal dynamics and earthquake research, NASA Tech. Paper 1464, Greenbelt, Maryland, 257 pp.

National Academy of Sciences (1978). Geodesy: Trends and Prospects, W. M. Kaula (Chairman), Committee on Geodesy, Washington, D. C.

Newcomb, S. (1897). A new determination of the precessional constant with the resulting precessional motions, Astron. Pap. Am. Ephem., 8 (1).

Niell, A. E., K. M. Ong, P. F. MacDoran, G. M. Resch, D. D. Morabito, E. S. Claflin and J. F. Dracup (1979). Comparison of a radio interferometric differential baseline measurement with conventional geodesy, Tectonophysics, 52, 49-58.

Nordtvedt, K. Jr. (1973). Post-Newtonian gravitational effects in lunar laser ranging, Phys. Rev. D, 7, 2347-2356.

Nordtvedt, K. Jr. and C. M. Will (1972). Conservation laws and preferred frames in relativistic gravity. II. Experimental evidence to rule out preferred-frame theories of gravity, Astrophys. J., 177, 775-792.

O'Connell, R. J. (1977). On the scale of mantle convection, Tectonophysics, 38, 119-136.

O'Connell, R. J. and A. M. Dziewonski (1976). Excitation of the Chandler wobble by large earthquakes, Nature, 262, 259-262.

Oesterwinter, C. (1979). Polar motion through 1977 from Doppler satellite observations, in Time and the Earth's Rotation, (ed. D. D. McCarthy and J. D. Pilkington), IAU Symp., 82, 263-278, D. Reidel, Dordrecht, Holland.

Okuda, T. (1972). An interpretation of the ambiguity between annual terms obtained by time and latitude observations, in Rotation of the Earth, (ed. P. Melchior and S. Yumi), IAU Symp., 48, 49-55, D. Reidel, Dordrecht, Holland.

Ong, K. M., P. F. MacDoran, J. B. Thomas, H. F. Fliegel, L. J. Skjerve, D. J. Spitzmesser, P. D. Batelaan and S. R. Paine (1976). A demonstration of a transportable radio interferometric surveying system with a 3-cm accuracy on a 307-m base line, J. Geophys. Res., 81, 3587-3593.

Ooe, M. (1978). An optimal complex AR.MA model of the Chandler wobble, Geophys. J. R. astr. Soc., 53, 445-457.

Ooe, M. (1979). Private communication.

Ooe, M. and T. Sasao (1974). Polar wobble, sway and astronomical latitude-longitude observations, Publ. Int. Lat. Observ. Mizusawa, 9, 223-233.

Oppolzer, T. R. V. (1880). Bahnbestimmung der Kometen und Planeteen, Englemann, Leipzig Union, 2nd edition, 1, 154-155.

Orton, R. B. (1969). Climatography of the U.S., U. S. Department of Commerce, ESSA/EDS, Washington, D. C.

Peale, S. J. (1975). Dynamical consequences of meteorite impacts on the Moon, J. Geophys. Res., 80, 4939-4946.

Peale, S. J. (1976). Excitation and relaxation of the wobble, precession and libration of the Moon, J. Geophys. Res., 81, 1813-1827.

Pease, G. E. (1977). Estimates of precession and polar motion errors from planetary encounter station location solutions, in The Deep Space Network Progress Report, 42-43, 29-49, Jet Propulsion Laboratory, Pasadena, California.

Pedersen, G. P. H. and M. G. Rochester (1972). Spectral analysis of the Chandler wobble, in Rotation of the Earth, (ed. P. Melchior and S. Yumi), IAU Symp., 48, 33-38, D. Reidel, Dordrecht, Holland.

Pekeris, C. L. and Y. Accad (1972). Dynamics of the liquid core of the Earth, Phil. Trans. R. Soc. Lond. A, 273, 237-260.

Peltier, W. R. (1980). Slow changes in the Earth's shape and gravitational field: Signatures of glacial isostasy, in Proc. Second Int. Symp. On Problems Related to the Definition of North American Vertical Geodetic Networks, Canadian Institute of Surveying, 133-150, 26-30, May, 1980, Ottawa, Canada.

Peltier, W. R., D. A. Yuen and P. Wu (1980). Postglacial rebound and transient rheology, Geophys. Res. Lett., 7, 733-736.

Poincaré, H. (1910). Sur la précession des corps deformables, Bull. Astron., 27, 321-356.

Poma, A. and E. Proverbio (1976). The secular motion of the pole from BIH results, Astron. Astrophys., 47, 105-111.

Popov, N. A. (1963). Determination of diurnal nutation from observations of bright zenith stars at Poltava, Sov. Astron., 7, 422-423.

Press, F. (1965). Displacements, strains and tilts at teleseismic distances, J. Geophys. Res., 70, 2395-2412.

Proverbio, E. and A. Poma (1976). Astronomical evidence of change in the rate of the Earth's rotation and continental motion, in Growth Rhythms and the History of the Earth's Rotation, (ed. G. D. Rosenberg and S. K. Runcorn), John Wiley, New York.

Reasenberg, R. D., I. I. Shapiro, P. E. MacNeil, R. B. Goldstein, J. C. Breidenthal, J. P. Brenkle, D. L. Cain, T. M. Kaufman, T. A. Komarek and A. I. Zygielbaum (1979). Viking relativity experiment: Verification of signal retardation by solar gravity, Astrophys. J., 234, L219-L221.

Resch, G. M. and E. S. Claflin (1980). Microwave radiometry as a tool to calibrate tropospheric water-vapor delay, in Radio Interferometry Techniques for Geodesy, NASA Conf. Pub. 2115, 377-384, Washington, D. C.

Robertson, D. S. (1975). Geodetic and Astrometric Measurements with Very-Long-Baseline Interferometry, Ph.D. thesis, Mass. Int. Technol., Cambridge, Massachusetts.

Robertson, D. S., W. E. Carter, B. E. Corey, W. D. Cotton, C. C. Counselman, I. I. Shapiro, J. J. Wittels, H. F. Hinteregger, C. A. Knight, A. E. E. Rogers, A. R. Whitney, J. W. Ryan, T. A. Clark, R. J. Coates, C. Ma and J. M. Moran (1979). Recent results of radio interferometric determinations of a transcontinental baseline, polar motion, and Earth rotation, in Time and the Earth's Rotation, (ed. D. D. McCarthy and J. D. Pilkington), IAU Symp., 82, 217-224, D. Reidel, Dordrecht, Holland.

Robertson, D. S., T. A. Clark, R. J. Coates, C. Ma, J. W. Ryan, B. E. Corey, C. C. Counselman, R. W. King, I. I. Shapiro, H. F. Hinteregger, C. A. Knight, A. E. E. Rogers, A. R. Whitney, J. C. Pigg and B. R. Schupler (1980). Polar motion and UT1: Comparison of VLBI, lunar laser, satellite laser, satellite doppler, and conventional astrometric determinations, in Radio Interferometry Techniques for Geodesy, NASA Conf. Pub. 2115, 33-44, Washington, D. C.

Rochester, M. G. (1970). Polar wobble and drift: A brief history, in Earthquake Displacement Fields and the Rotation of the Earth, (ed. L. Mansinha, D. E. Smylie and A. E. Beck), Astrophys. Space Sci. Lib. Ser., 20, 3-13, D. Reidel, Dordrecht, Holland.

Rochester, M. G. (1973). The Earth's rotation, EOS, Trans. Am. Geophys. Union, 54, 769-780.

Rochester, M. G. (1974). The effect of the core on the Earth's rotation, Veroeff. Zentralinst. Phys. Erde, Akad. Wiss. DDR, 30, 77-89.

Rochester, M. G. (1976). The secular decrease of obliquity due to dissipative core-mantle coupling, Geophys. J. R. astr. Soc., 46, 109-126.

Rochester, M. G., O. G. Jensen and D. E. Smylie (1974). A search for the Earth's 'nearly diurnal free wobble', Geophys. J. R. astr. Soc., 38, 349-363.

Rochester, M. G. and D. E. Smylie (1974). On changes in the trace of the Earth's inertia tensor, J. Geophys. Res., 79, 4948-4951.

Rogers, A. E. E. (1970). Very long baseline interferometry with large effective bandwidth for phase delay measurements, Radio Sci., 5, 1239-1248.

Rogers, A. E. E., C. A. Knight, H. F. Hinteregger, A. R. Whitney, C. C. Counselman, I. I. Shapiro, S. A. Gourevitch and T. A. Clark (1978). Geodesy by radio interferometry: Determination of a 1.24-km baseline vector with ~5 mm repeatability, J. Geophys. Res., 83, 325-334.

Rosenhead, L. (1929). The annual variation of latitude, Mon. Not. R. astr. Soc., Geophys. Suppl., 2, 140-197.

Ross, S. M. (1972). Introduction to Probability Models, Academic Press, New York, 272 pp.

Sanchez, B. V. (1979). Ocean tidal excitation of polar motion, NASA Tech. Mem. 80243, Goddard Space Flight Centre, Greenbelt, Maryland, 23 pp.

Sasao, T. (1978). How do Earth tides affect astronomers?, in Applications of Geodesy to Geodynamics, (ed. I. I. Mueller), Proc. Ninth GEOP Research Conference, Dept. of Geod. Sci. Rep., 280, 341-343, The Ohio State University, Columbus, Ohio.

Sasao, T., S. Okubo and M. Saito (1980). A simple theory on dynamical effects of stratified fluid core upon nutational motion of the Earth, in Nutation and the Earth's Rotation, (ed. E. P. Fedorov, M. L. Smith and P. L. Bender), IAU Symp., 78, 165-183, D. Reidel, Dordrecht, Holland.

Schumann, R. (1903). Über die Polhöhenschwankung, Astron. Nachr., 162, 197-204.

Schutz, B. E., B. D. Tapley and J. Ries (1979). Polar motion from laser range measurements of GEOS-3, in Time and the Earth's Rotation, (ed. D. D. McCarthy and J. D. Pilkington), IAU Symp., 82, 239-244, D. Reidel, Dordrecht, Holland.

Schutz, C. and W. Gates (1971). Global climatic data for surface, 800 mb, 400 mb: January, ARPA Rep. R-915-ARPA, Rand Corp., Santa Monica, California.

Schutz, C. and W. Gates (1972). Global climatic data for surface, 800 mb, 400 mb: July, ARPA Rep. R-1029-ARPA, Rand Corp., Santa Monica, California.

Schutz, C. and W. Gates (1973). Global climatic data for surface, 800 mb, 400 mb: April, ARPA Rep. R-1317-ARPA, Rand Corp. Santa Monica, California.

Schutz, C. and W. Gates (1974). Global climatic data for surface, 800 mb, 400 mb: October, ARPA Rep. R-1425-ARPA, Rand Corp., Santa Monica, California.

Scrutten, C. T. (1978). Periodic growth features in fossil organisms and the length of the day and month, in Tidal Friction and the Earth's Rotation, (ed. P. Brosche and J. Sunderman), 154-196, Springer-Verlag, New York.

Shapiro, I. I., C. C. Counselman and R. W. King (1976). Verification of the principle of equivalence for massive bodies, Phys. Rev. Lett., 36, 555-558.

Shapiro, I. I., D. S. Robertson, C. A. Knight, C. C. Counselman, A. E. E. Rogers, H. F. Hinteregger, S. Lippincott, A. R. Whitney, T. A. Clark, A. E. Niell and D. J. Spitzmesser (1974). Transcontinental baselines and the rotation of the Earth measured by radio interferometry, Science, 186, 920-922.

Shapiro, I. I., W. B. Smith, M. B. Ash, R. P. Ingalls and G. H. Pettengill (1971). Gravitational constant: Experimental bound on its time variation, Phys. Rev. Lett., 26, 27-30.

Shelus, P. J. (1978). Lunar laser ranging data deposited in the National Space Science Data Centre: Normal points, filtered observations and unfiltered photon detections from 1 April 1977 through 30 September 1977, Res. Mem. in Astron., University of Texas, Austin.

Shelus, P. J., S. W. Evans and J. D. Mulholland (1977). Earth rotation as inferred from McDonald Observatory lunar laser observations during October 1975, in Scientific Applications of Lunar Laser Ranging (ed. J. D. Mulholland), Astrophys. Space Sci. Lib. Ser., 62, 191-200, D. Reidel, Dordrecht, Holland.

Shelus, P. J., P. J. Morgan and J. D. Mulholland (1979). A preliminary Orroral Valley-McDonald Observatory baseline as determined by lunar laser ranging observations, (abstract), EOS Trans. Am. Geophys. Un., 60, 234.

Shen, P. Y. and L. Mansinha (1976). Oscillation, nutation, and wobble of an elliptical rotating Earth with liquid outer core, Geophys. J. R. astr. Soc., 46, 467-496.

Siderenkov, N. S. (1973). The inertia tensor of the atmosphere, the annual variation of its components and the variations of the Earth's rotation, Izv. Acad. Sci. USSR, Atmos. Ocean Phys., 9, 339-351.

Siderenkov, N. S. and A. R. Chvykov (1973). Estimated seasonal redistribution of air masses affecting motion of Earth's poles, Sov. Astron., 17, 285-287.

Siderenkov, N. S. and D. I. Stekhnovskiy (1971). The total mass of the atmosphere and its seasonal redistribution, Izv. Acad. Sci. USSR, Atmos. Ocean Phys., 7, 646-648.

Silverberg, E. C. (1974). Operation and performance of a lunar laser ranging station, Applied Optics, 13, 565-574.

Silverberg, E. C. (1979). On the effective use of lunar ranging for the determination of the Earth's orientation, in Time and the Earth's Rotation, (ed. D. D. McCarthy and J. D. Pilkington), IAU Symp., 82, 247-255, D. Reidel, Dordrecht, Holland.

Silverberg, E. C., P. J. Shelus, J. D. Mulholland and G. L. Loumos (1976). An estimate of the geodetic accuracy attainable with a transportable lunar laser station, Bull. Géod., 50, 331-340.

Slichter, L. B., and M. Caputo (1960). Deformation of an Earth model by surface pressures, J. Geophys. Res., 65, 4151-4156.

Sludskii, F. (1896). De la rotation de la Terre supposée fluid à son intérieur, Bull. Soc. Natur. Moscou, 9, 285-318.

Smith, D. E., R. Kolenkiewicz, P. J. Dunn, H. H. Plotkin and T. S. Johnson (1972). Polar motion from laser tracking of satellites, Science, 178, 405-406.

Smith, D. E., R. Kolenkiewicz, R. W. Agreen and P. J. Dunn (1973). Dynamic techniques for studies of secular variations in position from ranging to satellites, in Earth's Gravitational Field and Secular Variations in Position, (ed. R. S. Mather and P. V. Angus-Leppan), School of Surveying, University of New South Wales, Sydney, Australia.

Smith, D. E., R. Kolenkiewicz, P. J. Dunn and M. H. Torrence (1979). Determination of polar motion and Earth rotation from laser tracking of satellites, in Time and the Earth's Rotation, (ed. D. D. McCarthy and J. D. Pilkington), IAU Symp., 82, 231-238, D. Reidel, Dordrecht, Holland.

Smith, M. L. (1974). The scalar equations of infinitesimal elastic-gravitational motion for a rotating, slightly elliptical Earth, Geophys. J. R. astr. Soc., 37, 491-526.

Smith, M. L. (1976). Translational inner core oscillations of a rotating, slightly elliptical Earth, J. Geophys. Res., 81, 3055-3065.

Smith, M. L. (1977). Wobble and nutation of the Earth, Geophys. J. R. astr. Soc., 50, 103-140.

Smith, M. L. and F. A. Dahlen (1981). The period and Q of the Chandler wobble, Geophys. J. R. astr. Soc., in press.

Smylie, D. E. (1977). Whole Earth dynamics and lunar laser ranging, in Scientific Applications of Lunar Laser Ranging (ed. J. D. Mulholland), Astrophys. Space Sci. Lib. Ser., 62, 105-130, D. Reidel, Dordrecht, Holland.

Smylie, D. E. and L. Mansinha (1971). The elastic theory of dislocations in real Earth models and changes in the rotation of the Earth, Geophys. J. R. astr. Soc., 23, 329-354.

Smylie, D. E., G. K. C. Clarke and T. J. Ulrych (1973). Analysis of irregularities in the Earth's rotation, Methods. Comp. Phys., 13, 391-430.

Soler, T. and I. I. Mueller (1978). Global plate tectonics and the secular motion of the pole, Bull. Géod., 52, 39-57.

Solomon, S. C. and N. H. Sleep (1974). Some simple physical models for absolute plate motions, J. Geophys. Res., 79, 2557-2567.

Solomon, S. C., N. H. Sleep and R. M. Richardson (1975). On the forces driving plate tectonics: Inferences from absolute plate velocities and intraplate stress, Geophys. J. R. astr. Soc., 42, 769-801.

Spitaler, R. (1897). Ursache der breitenschwankungen, Denkschr. Akad. Wiss. Wien, 64, 633-642.

Stacey, F. D. (1977). Physics of the Earth, 2nd edition, John Wiley, New York, 414 pp.

Stolz, A. (1975). Geodetic uses of lunar laser ranging, Bull. Géod., 115, 5-16.

Stolz, A. (1976a). Changes in the position of the geocentre due to seasonal variations in air mass and ground water, Geophys. J. R. astr. Soc., 44, 19-26.

Stolz, A. (1976b). Changes in the position of the geocentre due to variations in sea-level, Bull. Géod., 50, 159-168.

Stolz, A. (1979). Precise modelling aspects of lunar laser measurements and their use for the improvement of geodetic parameters, Bay. Acad. Wiss., Veröff. Deutschen. Geod. Komm. A, 90, 23 pp.

Stolz, A., P. L. Bender, J. E. Faller, E. C. Silverberg, J. D. Mulholland, P. J. Shelus, J. G. Williams, W. E. Carter, D. G. Currie and W. M. Kaula (1976). Earth rotation measured by lunar laser ranging, Science, 193, 997-999.

Stolz, A. and D. Larden (1977). Accuracy obtainable for universal time and polar motion during the EROLD campaign, in Scientific Applications of Lunar Laser Ranging (ed. J. D. Mulholland), Astrophys. Space Sci. Lib. Ser., 62, 201-216, D. Reidel, Dordrecht, Holland.

Stolz, A., and D. R. Larden (1979). Seasonal displacement and deformation of the Earth by the atmosphere, J. Geophys. Res., 84, 6185-6194.

Stolz, A. and D. R. Larden (1980). Crustal deformation at very long baseline interferometry sites due to seasonal air-mass and ground water variations, in Radio Interferometry Techniques for Geodesy, NASA Conf. Pub. 2115, 145-151, Washington, D. C.

Sugawa, C., H. Ishii and I. Naito (1973). On the spectral analysis of z-terms, Publ. Int. Lat. Observ. Mizusawa, 13, 39-53.

Takeuchi, H. and N. Sugi (1972). Polar wandering and mantle convection, in Rotation of the Earth, (ed. P. Melchior and S. Yumi), IAU Symp., 48, 212-214, D. Reidel, Dordrecht, Holland.

Taljaard, J., H. van Loon, H. Crutcher and R. Jenne (1969). Climate of the upper air: Southern hemisphere, Vol. 1, Temperatures, Dew Points and Heights at Selected Pressure Levels, NAVAIR 50-IC-55, Nav. Weather Serv. Command, Washington, D. C.

Tapley, B. D., B. E. Schutz and R. J. Eanes (1981). Polar motion and earth rotation from LAGEOS laser ranging, EOS Trans. Am. Geophys. Un., 62, 259 (abstract).

Thornthwaite, C. (1948). An approach toward a rational classification of climate, Geograph. Rev., 38, 55-94.

Toomre, A. (1966). On the coupling of the Earth's core and mantle during the 26000 year precession, in The Earth-Moon System, (ed. B. G. Marsden and A. G. W. Cameron), 33-45, Plenum Press, New York.

Toomre, A. (1974). On the 'nearly diurnal wobble' of the Earth, Geophys. J. R. astr. Soc., 38, 335-348.

Trubytsyn, A. P. and A. V. Makalkin (1976). Deformations of the Earth's crust due to atmospheric cyclones, Izv. Acad. Sci. USSR, Phys. Solid Earth, 12, 343-344.

Tuller, S. E. (1968). World distribution of mean monthly and annual precipitable water, Mon. Weather Rev., 96, 785-797.

Urmantsev, F. M. (1971). Barometric and thermal surface inclinations and their effect on the determination of contemporary vertical movements of the Earth's crust by geodetic method, Izv. Acad. Sci. USSR, Phys. Solid Earth, 6, 444-447.

Urmantsev, F. M. (1975). An estimate of the effect of diurnal variations of atmospheric pressure on gravimeter and tiltmeter readings, and on precise levelling work, Izv. Acad. Sci. USSR, Phys. Solid Earth, 11, 201-203.

van der Voo, R. (1978). Polar wander analysis from paleomagnetic data, in Applications of Geodesy to Geodynamics, (ed. I. I. Mueller), Proc. Ninth GEOP Research Conference, Dept. of Geod. Sci. Rep., 280, 35-37, The Ohio State University, Columbus, Ohio.

van Hylckama, T. E. A. (1956). The water balance of the Earth, Publ. in Climatology, 9, 59-110, Drexel Inst. of Technol., Philadelphia, Pennsylvania.

van Hylckama, T. E. A. (1970). Water balance and Earth unbalance, in International Association of Scientific Hydrology, Proceedings of the Reading Symposium on World Water Balance, Publication 92, 434-553, AIHS-UNESCO.

Vicente, R. O. and R. G. Currie (1976). Maximum entropy spectrum of long period polar motion, Geophys. J. R. astr. Soc., 46, 67-73.

Wahr, J. M. (1979). The Tidal Motions of a Rotating, Elliptical, Elastic and Oceanless Earth, Ph.D. Thesis, University of Colorado, Boulder, Colorado, 216 pp.

Wahr, J. M. and D. R. Larden, (1981). A search for the 'nearly diurnal free wobble using lunar laser ranging data, EOS Trans. Am. Geophys. Un., 62, 258-259 (abstract).

Walcott, R. I. (1970). Flexural rigidity, thickness, and viscosity of the lithosphere, J. Geophys. Res., 75, 3941-3954.

Walsh, J. B. and J. R. Rice (1979). Local changes in gravity resulting from deformation, J. Geophys. Res., 84, 165-170.

Walter, H. G. (1974). Accuracy estimation of astronomical constants from long baseline interferometer observations (abstract), in New Problems in Astrometry, (ed. W. Gliese, C. A. Murray and R. H. Tucker), IAU Symp., 61, 131, D. Reidel, Dordrecht, Holland.

Warburton, R. J. and J. M. Goodkind (1977). The influence of barometric-pressure variations on gravity, Geophys. J. R. astr. Soc., 48, 281-292.

Wells, F. J. and M. A. Chinnery (1973). On the separation of the spectral components of polar motion, Geophys. J. R. astr. Soc., 34, 179-192.

Williams, J. G. (1970). Very long baseline interferometry and its sensitivity to geophysical and astronomical effects, JPL Space Programs Summary, 2, 37-62, Jet Propulsion Laboratory, Pasadena, California.

Williams, J. G. (1974). A potpourri of corrections to nutations, polar motion and UT1, JPL Eng. Mem., 391-592, Jet Propulsion Laboratory, Pasadena, California.

Williams, J. G. (1977). Present scientific achievements from lunar laser ranging, in Scientific Applications of Lunar Laser Ranging, (ed. J. D. Mulholland), Astrophys. Space Sci. Lib. Ser., 62, 37-50, D. Reidel, Dordrecht, Holland.

Williams, J. G., R. H. Dicke, P. L. Bender, C. O. Alley, W. E. Carter, D. G. Currie, D. H. Eckhardt, J. E. Faller, W. M. Kaula, J. D. Mulholland, H. H. Plotkin, S. K. Poultney, P. J. Shelus, E. C. Silverberg, W. S. Sinclair, M. A. Slade and D. T. Wilkinson (1976). New test of the equivalence principle from lunar laser ranging, Phys. Rev. Lett., 36, 551-554.

Williams, J. G., W. S. Sinclair and C. F. Yoder (1978). Tidal acceleration of the Moon, Geophys. Res Lett., 5, 943-946.

Wilson, C. R. (1979). Estimation of the parameters of the Earth's polar motion, in Time and the Earth's Rotation, (ed. D. D. McCarthy and J. D. Pilkington), IAU Symp., 82, 307-312, D. Reidel, Dordrecht, Holland.

Wilson, C. R. and R. A. Haubrich (1976). Meteorological excitation of the Earth's wobble, Geophys. J. R. astr. Soc., 46, 707-743.

Wilson, C. R. and R. A. Haubrich (1977). Earthquakes, weather and wobble, Geophys. Res. Lett., 4, 283-284.

Wilson, C. R. and R. O. Vicente (1980). An analysis of the homogeneous ILS polar motion series, Geophys. J. R. astr. Soc., 62, 605-616.

Wilson, J. T. (1963). A possible origin of the Hawaiian Islands, Can. J. Phys., 41, 863-870.

Wilson, P., K. Nottarp and H. Seeger (1978). The short-pulse laser-ranging system installed in Wettzell, in Proceedings of the Third International Workshop on Laser Ranging Instrumentation, 58-63, May 23-27, Lagonissi, Greece.

Woolard, E. W. (1953). Theory of the rotation of the Earth around its centre of mass, Astron. Pap. Am. Ephem. Naut. Alm., 15, 3-165.

Woolard, E. W. (1959). Inequalities in mean solar time from tidal variations in the rotation of the Earth, Astron. J., 64, 140-142.

Wu, S. C. (1979). Optimum frequencies of a passive microwave radiometer for tropospheric pathlength correction, IEEE Trans. Ant. Prop., AP-27, 233-239.

Wunsch, C. (1974). Dynamics of the pole tide and the damping of the Chandler wobble, Geophys. J. R. astr. Soc., 39, 539-550.

Yatskiv, Y. S. and T. Sasao (1975). Chandler wobble and viscosity in the Earth's core, Nature, 255, 655.

Yatskiv, Y. S., Y. Wako and Y. Kaneko (1975). Study of the nearly diurnal free nutation based on latitude observations of the ILS stations (I), Publ. Int. Lat. Observ. Mizusawa, 10, 1-31.

Yumi, S. (1970). Polar motion in recent years, in Earthquake Displacement Fields and the Rotation of the Earth, (ed. L. Mansinha, D. E. Smylie and A. E. Beck), Astrophys. Space Sci. Lib. Ser., 20, 45-52, D. Reidel, Dordrecht, Holland.

Yumi, S. (1978). Annual Report of the International Polar Motion Service for the Year 1976, Central Bureau of the International Polar Motion Service, Mizusawa, Japan.

Publications from
THE SCHOOL OF SURVEYING, THE UNIVERSITY OF NEW SOUTH WALES
P.O. Box 1, Kensington, N.S.W. 2033
AUSTRALIA

Reports

1.* G.G. Bennett, "The discrimination of radio time signals in Australia", Uniciv Rep. D1, 88 pp. (G 1)

2.* J.S. Allman, "A comparator for the accurate measurement of differential barometric pressure", Uniciv Rep. D3, 9 pp. (G 2)

3. R.S. Mather, "The establishment of geodetic gravity networks in South Australia", Uniciv Rep. R-17, 26 pp. (G 3)

4.* R.S. Mather, "The extension of the gravity field in South Australia", Uniciv Rep. R-19, 26 pp. (G 4)

5.* J.S. Allman, "An analysis of the reliability of barometric elevations", Unisurv Rep. 5, 335 pp. (S 1)

6.* R.S. Mather, "The free air geoid for South Australia and its relation to the equipotential surfaces of the earth's gravitational field", Unisurv Rep. 6, 491 pp. (S 2)

7.* P.V. Angus-Leppan, (Editor), "Control for mapping" (Proceedings of Conference, May 1967), Unisurv Rep. 7, 329 pp. (G 5)

8.* G.G. Bennett & J.G. Freislich, "The teaching of field astronomy", Unisurv Rep. 8, 30 pp. (G 6)

9.* J.C. Trinder, "Photogrammetric pointing accuracy as a function of properties of the visual image", Unisurv Rep. 9, 64 pp. (G 7)

10.* P.V. Angus-Leppan, "An experimental determination of refraction over an icefield", Unisurv Rep. 10, 23 pp. (G 8)

11.* R.S. Mather, "The non-regularised geoid and its relation to the telluroid and regularised geoids", Unisurv Rep. 11, 49 pp. (G 9)

12.* G.G. Bennett, "The least squares adjustment of gyro-theodolite observations", Unisurv Rep. 12, 53pp. (G 10)

13.* R.S. Mather, "The free air geoid for Australia from gravity data available in 1968", Unisurv Rep. 13, 38 pp. (G 11)

* OUT OF PRINT

14.* R.S. Mather, "Verification of geoidal solutions by the adjustment of control networks using geocentric Cartesian co-ordinate systems", Unisurv Rep. 14, 42 pp. (G 12)

15.* G.G. Bennett, "New methods of observation with the Wild GAKI gyro-theodolite", Unisurv Rep. 15. 68 pp. (G 13)

16.* G.G. Bennett, "Theoretical and practical study of a gyroscopic attachment for a theodolite", Unisurv Rep. 16, 343 pp. (S 3)

17.* J.C. Trinder, "Accuracy of monocular pointing to blurred photogrammetric signals", Unisurv Rep. 17, 231 pp. (S 4)

18. A. Stolz, "The computation of three dimensional Cartesian co-ordinates of terrestrial networks by the use of local astronomic vector systems", Unisurv Rep. 18, 47 pp. (G 14)

19. R.S. Mather, "The Australian geodetic datum in earth space", Unisurv Rep. 19, 130 pp. (G 15)

20.* J.G. Fryer, "The effect of the geoid on the Australian geodetic network", Unisurv Rep. 20, 221 pp. (S 5)

21.* G.F. Toft, "The registration and cadastral survey of native- held rural land in the Territory of Papua and New Guinea", Unisurv Rep. 21, 441 pp. (S 6)

22. R.S. Mather et al, "Communications from Australia to Section V, International Association of Geodesy, XV General Assembly, International Union of Geodesy and Geophysics, Moscow 1971", Unisurv Rep. 22, 72 pp. (G 16)

23.* A.H. Campbell, "The dynamics of temperature in surveying steel and invar measuring bands", Unisurv Rep. S 7, 195 pp.

24. A. Stolz, "Three-D Cartesian co-ordinates of part of the Australian geodetic network by the use of local astronomic vector systems", Unisurv Rep. S 8, 182 pp.

25. Papers by R.S. Mather, H.L. Mitchell & A. Stolz on the following topics:- Four-dimensional geodesy, Network adjustment and Sea surface topography, Unisurv G 17, 73 pp.

26. Papers by L. Berlin, G.J.F. Holden, P.V. Angus-Leppan, H.L. Mitchell & A.H. Campbell on the following topics:- Photogrammetry co-ordinate systems for surveying integration, Geopotential networks and Linear measurement, Unisurv G 18, 80 pp.

27. R.S. Mather, P.V. Angus-Leppan, A. Stolz & I. Lloyd, "Aspects of four-dimensional geodesy", Unisurv G 19, 100 pp.

28. H.L. Mitchell, "Relations between MSL & geodetic levelling in Australia", Unisurv Rep. S 9, 264 pp.

29. A.J. Robinson, "Study of zero error & ground swing of the model MRA101 tellurometer", Unisurv Rep. S 10, 200 pp.

30. Papers by J.S. Allman, R.C. Lister, J.C. Trinder & R.S. Mather on the following topics:- Network adjustments, Photogrammetry, and 4-Dimensional geodesy, Unisurv G 20, 133 pp.

31. G.J.F. Holden, "An evaluation of orthophotography in an integrated mapping system", Unisurv Rep. S 12, 232 pp.

32. G.J. Hoar, "The analysis precision and optimization of control surveys", Unisurv Rep. S 13, 200 pp.

33. Papers by E. Grafarend. R.S. Mather & P.V. Angus-Leppan on the following topics:- Mathematical geodesy, Coastal geodesy and Refraction, Unisurv G 21, 100 pp.

34. Papers by R.S. Mather, J.R. Gilliland, F.K. Brunner, J.C. Trinder, K. Bretreger & G. Halsey on the following topics:- Gravity, Levelling, Refraction, ERTS imagery, Tidal effects on satellite orbits and Photogrammetry, Unisurv G 22, 96 pp.

35. Papers by R.S. Mather, E.G. Anderson, C. Rizos, K. Bretreger, K. Leppert, B.V. Hamon & P.V. Angus-Leppan on the following topics:- Earth tides, Sea surface topography, Atmospheric effects in physical geodesy, Mean sea level and Systematic errors in levelling, Unisurv G 23, 96 pp.

36. Papers by R.C. Patterson, R.S. Mather, R. Coleman, O.L. Colombo, J.C. Trinder, S.U. Nasca, T.L. Duyet & K. Bretreger on the following topics:- Adjustment theory, Sea surface topography determinations, Applications of LANDSAT imagery, Ocean loading of Earth tides, Physical geodesy, Photogrammetry and Oceanographic applications of satellites, Unisurv G 24.

37. E.G. Anderson, "The Effect of Topography on Solutions of Stokes' Problem", Unisurv Rep. S 14, 252 pp.

38. A.H.W. Kearsley, "The Computation of Deflections of the Vertical from Gravity Anomalies", Unisurv Rep. S 15, 181 pp.

39. Papers by S.M. Nakiboglu, B. Ducarme, P. Melchior, R.S. Mather, B.C. Barlow, C. Rizos, B. Hirsch, K. Bretreger, F.K. Brunner & P.V. Angus-Leppan on the following topics:- Hydrostatic equilibrium figures of the Earth, Earth tides, Gravity anomaly data banks for Australia, Recovery of tidal signals from satellite altimetry, Meteorological parameters for modelling terrestrial refraction and Crustal motion studies in Australia, Unisurv G 25.

40. Papers by R.S. Mather, E.G. Masters, R. Coleman, C. Rizos, B. Hirsch, C.S. Fraser, F.K. Brunner, P.V. Angus-Leppan, A.J. McCarthy & C. Wardrop on the following topics:- Four-dimensional geodesy, GEOS-3 altimetry data analysis, Analysis of meteorological measurements for microwave EDM and Meteorological data logging system for geodetic refraction research, Unisurv G 26, 113 pp.

41. Papers by F.K. Brunner, C.S. Fraser, S.U. Nasca, J.C. Trinder, L. Berlin, R.S. Mather, O.L. Colombo & P.V. Angus-Leppan on the following topics:- Micrometeorology in geodetic refraction, LANDSAT imagery in topographic mapping, Adjustment of large systems, GEOS-3 data analysis, Kernel functions and EDM reductions over sea, Unisurv G 27, 101 pp.

42. K. Bretreger, "Earth Tide Effects on Geodetic Observations", Unisurv S 16, 173 pp.

43. Papers by S.M. Nakiboglu, H.L. Mitchell, K. Bretreger, T.A. Herring, J.M. Rueger, K.R. Bullock, R.S. Mather, B.C. Forster, I.P. Williamson & T.S. Morrison on the following topics:- Variations in gravity, Oceanographic and geodetic levelling, Ocean loading effects on Earth tides, Deflections of the vertical, Frequencies of EDM instruments, Land information systems, Sea surface topography, Accuracy of Aerial Triangulation and Questionnaire to Surveyors, Unisurv G 28, 124 pp.

44. Papers by F.L. Clarke, R.S. Mather, D.R. Larden & J.R. Gilliland on the following topics:- Three dimensional network adjustment incorporating ξ, η and N, Geoid determinations with satellite altimetry, Geodynamic information from secular gravity changes and Height and free-air anomaly correlation, Unisurv G 29, 87 pp.

From June 1979 Unisurv G's name was changed to Australian Journal of Geodesy, Photogrammetry and Surveying (Aust.J.Geod.Photo.Surv.).

45. Aust.J.Geod.Photo.Surv. No. 30, (June,1979), 127 pp.:
Bretreger, "Ocean tide models from GEOS-3 altimetry";
Trinder & Smith, "Rectification of LANDSAT data";
Nakiboglu & Lim, "Numerical test of initial value method";
Herring, "The accuracy of deflections of vertical";
Angus-Leppan, "Radiation effects on temperature of metal tape";
Covell, "Errors of short range distance meters", and
Nasca, "Contour lines in engineering".

46.* Aust.J.Geod.Photo.Surv. No. 31, (December 1979) 177 pp.
(contributions to the XVII General Meeting of the IUGG, Canberra, 3-15 December, 1979):
Allman et al., "Readjustment of Australian geodetic survey";
Angus-Leppan, "Ratio method and meteorology" and
"Refraction in levelling",
Berlin, "Adjustment of continental networks",
Brunner, "Limiting factor to geodetic precision";
Coleman et al., "Sea surface slope along NE Australia",
Kahar and Kearsley, "Jawa geoid from altimetry and gravity",
Kearsley & van Gysen, "Outer zone effects on the Australian geoid",
Masters et al., "Tide models from GEOS-3 altimetry", and
Mather & Rizos, "Global mean sea level from altimetry".

47. C. Rizos, "The role of the gravity field in sea surface topography studies", Unisurv S 17 (February,1980), 299 pp.

48. Aust.J.Geod.Photo.Surv. No. 32, (June,1980) 121 pp.:
van Gysen, "Gravimetric deflections of the vertical",
Fraser, "Self calibration of non-metric camera",
Rizos, "Ocean circulation from SST studies",
Trinder, "Film granularity and visual performance".

49. Aust.J.Geod.Photo.Surv. No. 33, (December,1980) 85 pp.:
Burford, "Controlling geodetic networks";
Masters & Stolz, "Crustal motion from LAGEOS";
Fraser, "Variance analysis of adjustments", and
Brunner et al., "Incremental strain near Palmdale".

50. B.C. Forster, "Some measures of urban residual quality from LANDSAT multi-spectral data", Unisurv S 18, (January,1981) 223 pp.

51. Aust.J.Geod.Photo.Surv. No. 34, (June,1981) 94 pp.:
Welsch, "Variances of geodetic observations";
Gilliland, "Outer zones effects on geoid", and
Khalid, "Models of vertical refraction".

52. Richard Coleman, "A Geodetic Basis for recovering Ocean Dynamic Information from Satellite Altimetry", Unisurv S 19, (October,1981) 332 pp.

53. Aust.J.Geod.Photo.Surv. No.35 (December 1981):
Kahar, "Geoid in Indonesia",
Morgan, "Crustal Motion in Papua New Guinea",
Masters et al, "LAGEOS Range Filter",
Stolz et al, "Baseline Values from LAGEOS",
Bishop, "Digital Elevation Models".

54. Aust.J.Geod.Photo.Surv. No.36 (June 1982)
Nakiboglu and Torenberg, "Earth's Gravity and Surface Loading"
Nakiboglu, "Changes in Sea Level and Gravity"
Villanueva, "Geodetic Boundary Value Problem"
Stolz and Harvey, "Australian Geodetic VLBI Experiment"
Gilliland, "Free-air Geoid for South Australia"
Allman, "Geoid for S.E. Asia and S.W. Pacific"
Angus-Leppan, "Gravity Measurements in Levelling"

55. Douglas R. Larden, "Monitoring the Earth's Rotation by Lunar Laser Ranging", Unisurv Report S 20, 280 pp.

56. R. Patterson, "Approximation and Statistical Methods in Physical Geodesy", Unisurv Report S 21, 179 pp.

* Out of print

Proceedings

P.V. Angus-Leppan (Editor), "Proceedings of conference on refraction effects in geodesy & electronic distance measurement", 264 pp.
Price: $10.00

R.S. Mather & P.V. Angus-Leppan (Eds.), "Australian Academy of Science/International Association of Geodesy Symposium on Earth's Gravitational Field & Secular Variations in Position", 740 pp.
Price: $20.00

Monographs

1. R.S. Mather, "The theory and geodetic use of some common projections", (2nd edition), 125 pp. Price: $ 5.00

2. R.S. Mather, "The analysis of the earth's gravity field", 172 pp.
Price: $ 5.00

3. G.G. Bennett, "Tables for prediction of daylight stars", 24 pp.
Price: $ 2.50

4. G.G. Bennett, J.G. Freislich & M. Maughan, "Star prediction tables for the fixing of position", 200 pp. Price: $ 8.00

5. M. Maughan, "Survey computations", 98 pp.
Price: $ 5.00

6. M. Maughan, "Adjustment of Observations by Least Squares", 61 pp.
Price: $ 4.00

7. J.M. Rüeger, "Introduction to Electronic Distance Measurement", (2nd Edition), 140 pp. Price: $ 10.00

Note: Prices do not include postage.

OTHER PRICES for 1982 (Surface Mail Postage Inclusive)

1. **Aust.J.Geod.Photo.Surv.** (formerly Unisurv G), 2 issues annually of approximately 100 pages each issue.

   To Libraries $18
   To Individuals $12

2. **Special Series** (Unisurv S)
   Research reports of 200 to 300 pages, published annually (on average).

   To Libraries $25 per copy
   To Individuals $18 per copy

To order, write to Publications Officer, School of Surveying, U.N.S.W.